

AD-A039 336

GTE LABS INC WALTHAM MASS
SEALED LITHIUM INORGANIC ELECTROLYTE CELL.(U)
APR 77 N MARINCIC, A LOMBARDI

F/G 10/3

UNCLASSIFIED

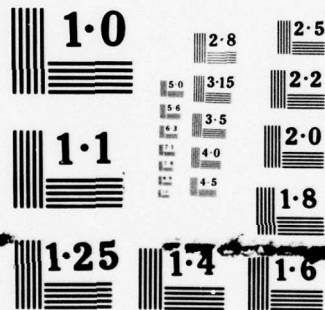
1 OF 3
ADA
039336

ECOM-74-0108-F

DAAB07-74-C-0108

NL





NATIONAL BUREAU OF STANDARDS
MICROCOPY RESOLUTION TEST CHART



AD A 039336

Research and Development Technical Report

ECOM - 74-0108-F

SEALED LITHIUM INORGANIC BATTERY

N. MARINCIC
A. LOMBARDI
GTE LABORATORIES
Waltham, Massachusetts 02154

April 1977

Final Report for Period March, 1974 to October, 1976



DISTRIBUTION STATEMENT

Approved for public release;
distribution unlimited.

DDC FILE COPY

Prepared for
ECOM

US ARMY ELECTRONICS COMMAND FORT MONMOUTH, NEW JERSEY 07703

NOTICES

Disclaimers

The findings in this report are not to be construed as an official Department of the Army position, unless so designated by other authorized documents.

The citation of trade names and names of manufacturers in this report is not to be construed as official Government indorsement or approval of commercial products of services referenced herein.

Disposition

Destroy this report when it is no longer needed. Do not return it to the originator.

UNCLASSIFIED

SECURITY CLASSIFICATION OF THIS PAGE (When Data Entered)

19 REPORT DOCUMENTATION PAGE		READ INSTRUCTIONS BEFORE COMPLETING FORM
1. REPORT NUMBER ECOM 74-0108-F	2. GOVT ACCESSION NO.	3. RECIPIENT'S CATALOG NUMBER
4. TITLE (and Subtitle) Sealed Lithium Inorganic Electrolyte Cell.	5. TYPE OF REPORT & PERIOD COVERED Final Report, March 1974-Oct 76	6. PERFORMING ORG. REPORT NUMBER
7. AUTHOR(s) N./Marincic A./Lombardi	8. CONTRACT OR GRANT NUMBER(s) DAAB-07-74-C-0108	
9. PERFORMING ORGANIZATION NAME AND ADDRESS GTE Laboratories Incorporated 40 Sylvan Road Waltham, Massachusetts 02154	10. PROGRAM ELEMENT, PROJECT, TASK AREA & WORK UNIT NUMBERS 1S762705AH94-P1-213	
11. CONTROLLING OFFICE NAME AND ADDRESS U.S. Army Electronics Command ATTN: AMSEL-TL-PR Fort Monmouth, New Jersey 07703	12. REPORT DATE April 1977	13. NUMBER OF PAGES 221
14. MONITORING AGENCY NAME & ADDRESS (if different from Controlling Office)	15. SECURITY CLASS. (of this report) Unclassified	15a. DECLASSIFICATION/DOWNGRADING SCHEDULE
16. DISTRIBUTION STATEMENT (of this Report) Approved for Public Release; Distribution Unlimited		
17. DISTRIBUTION STATEMENT (of the abstract entered in Block 20, if different from Report)		
18. SUPPLEMENTARY NOTES		
19. KEY WORDS (Continue on reverse side if necessary and identify by block number) Inorganic Electrolyte Battery Carbon Cathode Evaluation Thionyl Chloride Gas Generation Lithium Cell Design Lithium - Aluminum Chloride		
20. ABSTRACT (Continue on reverse side if necessary and identify by block number) This report describes the work carried out at GTE Laboratories and sponsored by US Army ECOM between March 1974 and October 1976 on the development of sealed lithium inorganic batteries. Most of the work was done with the components or subassemblies intended for use in wound electrode structures, i. e. the cells designed for a high rate of discharge, although the Laboratories' models and the low rate cells were used on occasions as the test vehicles in the evaluation of performance parameters of this		

DD FORM 1 JAN 73 1473 EDITION OF 1 NOV 65 IS OBSOLETE

UNCLASSIFIED

SECURITY CLASSIFICATION OF THIS PAGE (When Data Entered)

406462

Jmce

DDC
RECEIVED
MAY 12 1977
RESOLVED

UNCLASSIFIED

SECURITY CLASSIFICATION OF THIS PAGE(When Data Entered)

electrochemical system. The report is arranged chronologically, presenting the characteristics of the system, followed by the design, testing and evaluation of finished, sealed D size cells.

The rate capability of the cell was established, along with the side effects of discharge at extreme rates such as the thermal runaway, gassing at the end of discharge, etc. Protective devices were developed and tested, preventing the discharge at excessive rates (fuses) or opening the cell to the atmosphere (venting) before it reaches critical pressure and temperature that leads to explosion. The procedures were developed for a computer aided design and optimization of electrode structures, enabling the construction of D cell exceeding the energy density of 500 Wh/kg and 17 Wh/in.³

Cum.

UNCLASSIFIED

SECURITY CLASSIFICATION OF THIS PAGE(When Data Entered)

CONTENTS

<u>Section</u>		<u>Page</u>
1	Introduction	1
2	Electrochemical System	3
3	Test Vehicles	5
4	Carbon Cathodes	19
5	Lithium Anodes	23
6	Electrolytes	25
7	Sealed D Cells in Cold Rolled Steel Hardware	29
	7.1 Cell Construction	29
	7.2 Capacity of Fresh Cells	32
	7.3 Shelf Life at Various Temperature	34
	7.4 Voltage Delay After Storage	123
	7.5 Pressure Build Up in Sealed Cells	131
8	Electrolyte Additives	143
	8.1 Ultrapure Electrolytes	143
	8.2 Electrolyte with Excess Chlorine	145
	8.3 Electrolyte with Excess $AlCl_3$	145
	8.4 Electrolyte with SO_2	147
	8.5 Iron Impurities	149
9	Corrosion of Cell Hardware	153
	9.1 Laboratory Tests	153
10	Voltage Delay with Various Hardware Materials	171
11	Optimization of Electrode Structure	189
12	Hermetic Cell Design	191
13	Thermal Effects of Battery Discharge	195

ADDITIONAL

NTIS ☒ Write Section

DIC ☐ Soft Section

UNANNOUNCED ☐

JUSTIFICATION ☐

BY _____

DISTRIBUTION/AVAILABILITY CODES

Dist. ☐ ATAIL ☐ R/L/O/SPECIAL

A

CONTENTS (Cont'd)

<u>Section</u>		<u>Page</u>
14	Safety Devices for High Power Cells	199
14.1	Fusing of D Cell	199
14.2	Venting of D Cells	202
15	Cells Delivered	213
15.1	High Power Cells	213
15.2	High Energy Cells	215
16	References	217

ABSTRACT

This report describes the work carried out at GTE Laboratories and sponsored by US Army ECOM between March 1974 and October 1976 on the development of sealed lithium inorganic batteries.

Most of the work was done with the components or subassemblies intended for use in wound electrode structures, i.e. the cells designed for a high rate of discharge, although the Laboratories' models and the low rate cells were used on occasions as the test vehicles in the evaluation of performance parameters of this electrochemical system. The report is arranged chronologically, presenting the characteristics of the system, followed by the design, testing and evaluation of finished, sealed D size cells.

The rate capability of the cell was established, along with the side effects of discharge at extreme rates such as the thermal runaway, gassing at the end of discharge, etc. Protective devices were developed and tested, preventing the discharge at excessive rates (fuses) or opening the cell to the atmosphere (venting) before it reaches critical pressure and temperature that leads to explosion. The procedures were developed for a computer aided design and optimization of electrode structures, enabling the construction of D cell exceeding the energy density of 500 Wh/kg and 17 Wh/in.³

1. INTRODUCTION

Primary lithium batteries of highest energy density have been under development at GTE Labs for a number of years. Cells designed for low discharge rates are more advanced and have been in production for special applications for almost three years. A steady growth in the demand for these cells in some of the most sensitive applications (cardiac pacemakers) has demonstrated that corrosive and otherwise toxic materials could be used without risks in hermetic cells with a proper choice of hardware materials and with a proven stability of the electrochemical system.

The cells designed for high discharge rates could be abused and can become hazardous under short circuit conditions. The development program at GTE Labs for US Army ECOM was, therefore, undertaken not only with the purpose of achieving high rate discharge of high energy density cells but also for the purpose of establishing the hazards involved and developing various safety devices.

This report attempts to present a brief, up-to-date description of the electrochemical system, based on lithium as the anode material, combined with thionyl chloride electrolyte-depolarizer and a catalytic carbon electrode used as a substrate for reduction of thionyl chloride. The art of making cell components is also presented, along with the methods of evaluation as they were developed through various stages of the program. The test vehicles used in the evaluation program are also described involving purely laboratory set ups as well as standard commercial size cells in more or less finished form. The use of commercial type hardware materials was considered first and special materials were introduced only after the inadequacy of the standard materials was demonstrated. Such was the case with the use of cold rolled steel cans which at the beginning appeared promising if cathodically protected by lithium, but which later proved to be inadequate due to a pronounced effect of small iron impurities in the electrolyte on the passivation of lithium anodes. The tests with the cold rolled steel hardware have been continued throughout a significant portion of the program in spite of an early realization of inadequacy of this material. This reduced significantly the cost of evaluation of fresh cell performance, particularly the evaluation of parameters unaffected by the presence of iron impurities (venting, fusing, gassing etc.)

Some additives to the electrolyte were introduced in an attempt to reduce the passivation of the lithium surface. Some of them, such as Cl_2 , were found to prevent the passivation at the expense of a rapid loss in capacity. The other, such as iron,

caused a rapid passivation of anode surface beyond recovery. This observation dictated a closer look at the hardware corrosion problem and, eventually, elimination of cold rolled steel from the list of usable materials.

The tests with the cold rolled steel hardware were conducted with an unoptimized electrode structure, since there was no sufficient understanding of the materials distribution during discharge. The empirical optimization alone proved to be insufficient, since a significant improvement in the cell capacity was obtained with the development of the optimization procedure that included both the stoichiometric characteristics of the system and the practical performance parameters of active components. This, combined with the development of hermetic closures, resulted in an overall improvement of high rate cells.

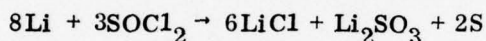
An increase in the cell capacity and in the strength of the closure has increased the hazards associated with the discharge of cells at excessive rates. Crimped cells at a short circuit usually burst under pressure before rapid reaction of SOCl_2 and molten Li begins, while hermetically sealed (welded) cells do not burst until they develop much higher pressure and temperature. The safe operation of hermetic cells under conditions of abuse dictated further development of safety devices such as fuses and vents. Thermal effects of battery discharge were studied in order to define a limiting rate at which a cell could be safely discharged. This resulted in a better understanding of interdependence between the discharge rate, the operating voltage, the rate of increase in cell temperature and the cell explosion. This also enabled us to define more closely the design parameters of the safety devices built either to avoid the cell explosion caused by the external short circuit fuses or to minimize the consequences of cell rupture caused by either internal or external short circuits or by external heating.

The overall improvement in the performance of hermetic cells, whether developed under this or other parallel programs, is demonstrated with the data presented at the end of this report. The state of the art is illustrated by the test results presented and also incorporated in the cell delivered to US Army ECOM at the end of the program.

2. ELECTROCHEMICAL SYSTEM

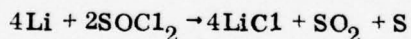
The object of this program was the development of sealed D size cells using Li/SOCl₂ system. The system is unique in that the liquid SOCl₂ serves both as the depolarizer and also as the solvent for the cell electrolyte. The absence of inert solvents contributes to a high energy density of cell, provided that the cell design was made to accommodate specific behavior of active materials during discharge.

Several discharge reactions were postulated in the early stage of the development, none sufficiently supported by experiments. The earliest one came from Auburn, et al.¹ based on a qualitative identification of discharge products and a very good agreement between the predicted and actual cell voltage:



This reaction failed to describe adequately the behavior of the system during discharge for several reasons. It does not allow for formation of gaseous products, in spite of the fact that at higher discharge rates a measurable increase in cell pressure was observed.

The second most quoted reaction was postulated by Dey and Schlaikjer² suggesting the formation of gaseous product:



This mechanism, as presented above, could not be supported by quantitative experimental evidence. The pressure increase during discharge is noticeable only at high discharge rates and only in the magnitude far below that predicted by the above mechanism. In fact, the latest evidence produced^{3, 4, 6} makes the above mechanism totally unacceptable, even if one assumes the formation of some "condensed" form of SO₂. Several other reactions have been postulated, some of them in direct contradiction with the experimental evidence.^{5, 6}

The cell discharge mechanism, although still unresolved, has been sufficiently defined to enable the optimization of the cell. Empirical optimization³ confirmed the predictions of the materials balance study based on the combination of stoichiometric

and performance parameters.⁷⁻¹⁰ Highest energy densities were obtained using this electrochemical system and it is doubtful that the final resolution of the discharge mechanism would contribute further to the energy density obtained. The question of gaseous products, however, is still of interest since it will dictate some design parameters, such as the strength of cell hardware and the type of cell closures.

3. TEST VEHICLES

Three types of test vehicles were used in the preliminary evaluation of cell components, one with the parallel plate electrodes and the other with wound electrode structures.

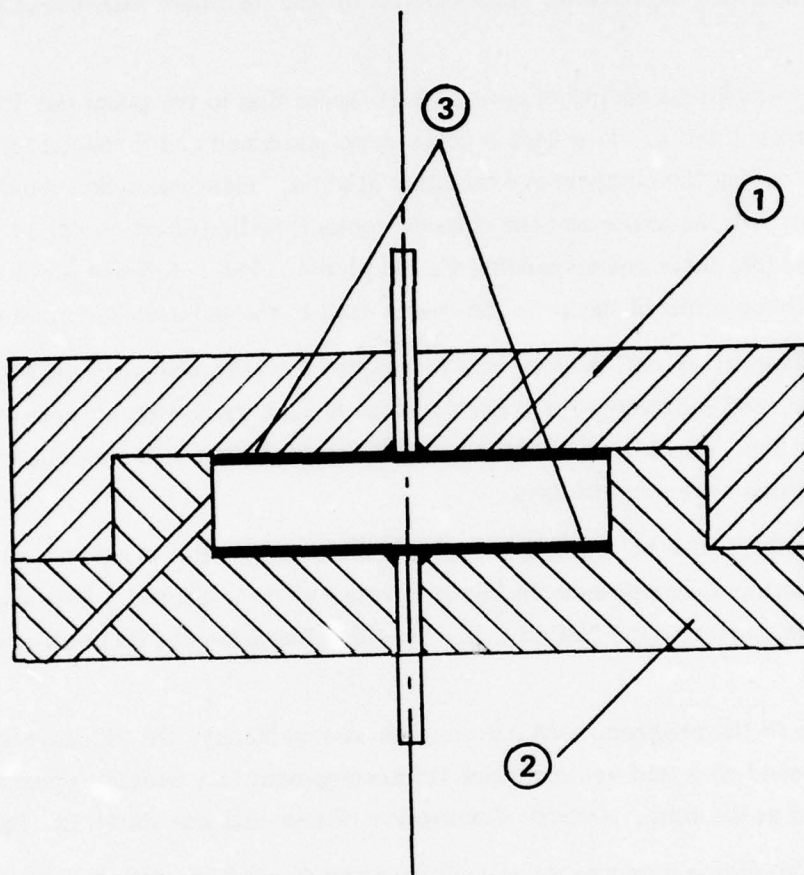
Laboratory cell components were built according to the proposed design, as shown in Figures 1 and 2. Two Teflon parts were machined and threaded for easy reassembling during the component evaluation studies. Identical nickel back plates were made for both the anode and the cathode contact, with welded nickel wire terminals pressure fitted into their corresponding Teflon plates. The reference electrode parts were made only on a few of the cells that were used in the polarization studies.

The laboratory cell prototypes were tested for hermeticity by filling them with the electrolyte, and examining for possible signs of leakage during storage at room temperature. The cell closure seemed tight, since no weight loss was observed at room temperature over several days.

A standard size button cell, developed under a parallel program, has also been used for evaluation of components in this program, since it offered a hermeticity superior to that of the laboratory-type Teflon cell. Outside dimensions of this cell are shown in Figure 3.

Early in the program, and for reasons of expediency, the standard size AA cell was also used as a test vehicle since its development in a parallel program was more advanced at the time. Outside dimensions of this cell are shown in Figure 4.

Cell hardware components are all designed to conform with the overall dimensions of the standard D cell. The component materials were selected on the basis of the preliminary materials compatibility studies, carried out in the last two years, combined with the recent experience gained in the course of a post mortem analysis of aged cell prototypes. The interior components (electrodes, separators and connectors) are designed to provide a high rate capability with energy density as high as possible. The size of the electrodes is not final, and will be altered after the first test results are available and the post mortem is performed on the spent cells. There may be a need for several stepwise alterations in the process of optimizing the cell electrode structure. A brief description of the cell components is given here, as they appear on Figures 5 to 12.



NOTES:

NO. 1, 1 PC., FEP TEFLON
NO. 2, 1 PC., FEP TEFLON
NO. 3, 2 PC., PURE NICKEL

Figure 1. Laboratory Cell, Assembly Drawing

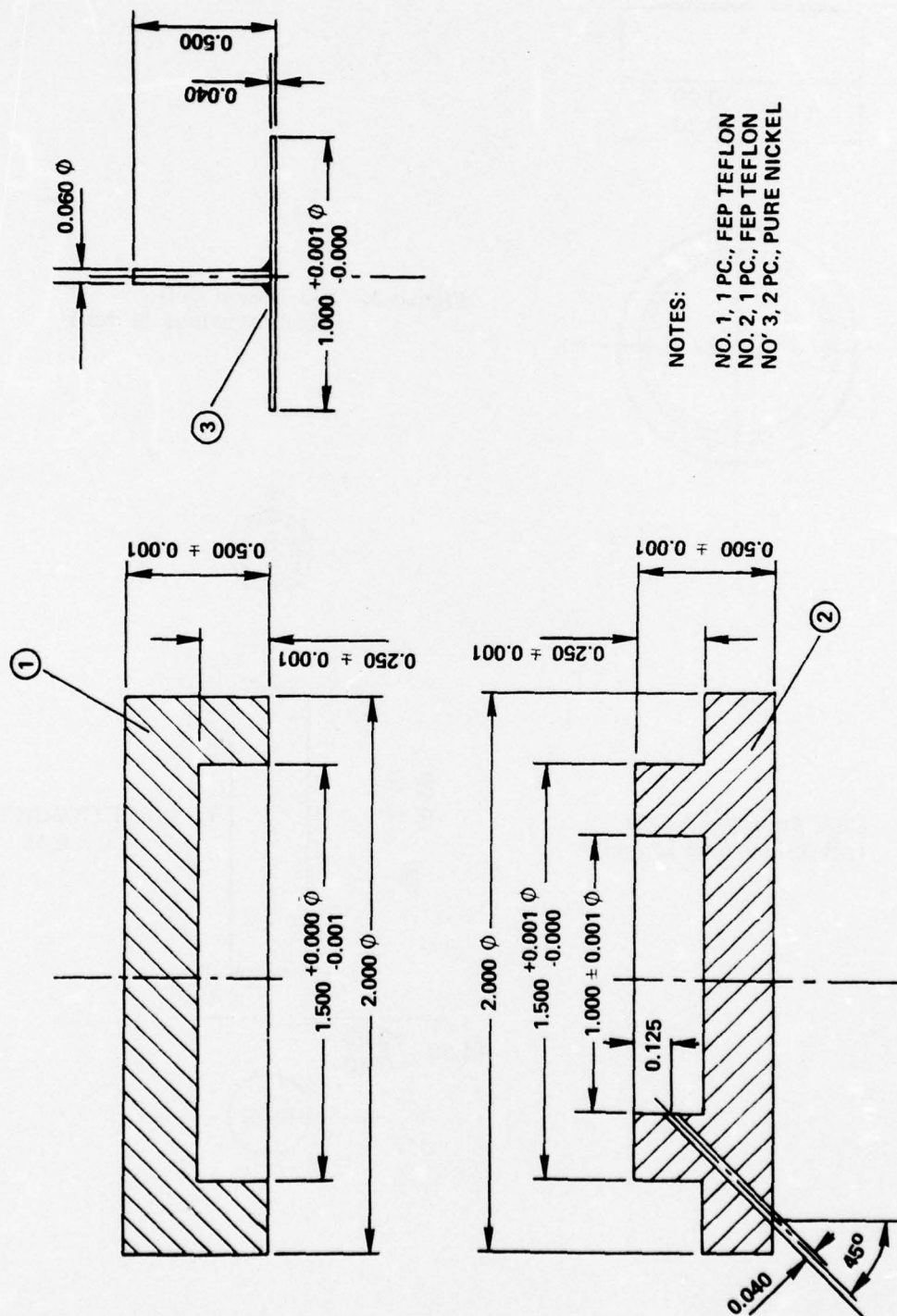


Figure 2. Laboratory Cell Parts

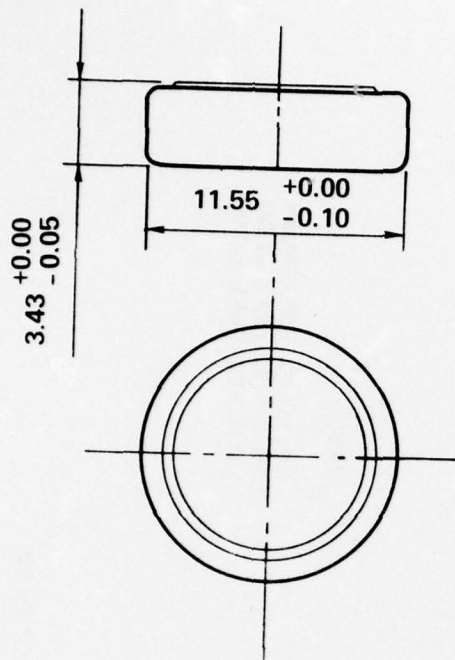
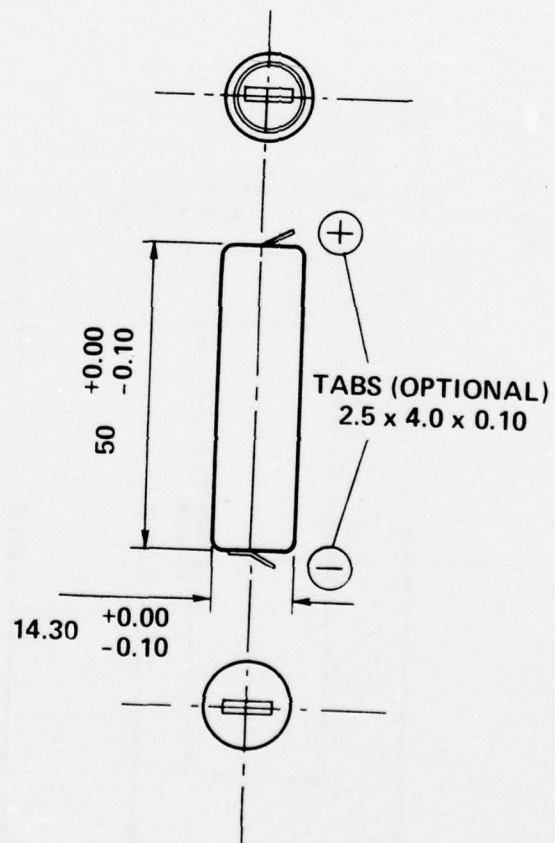
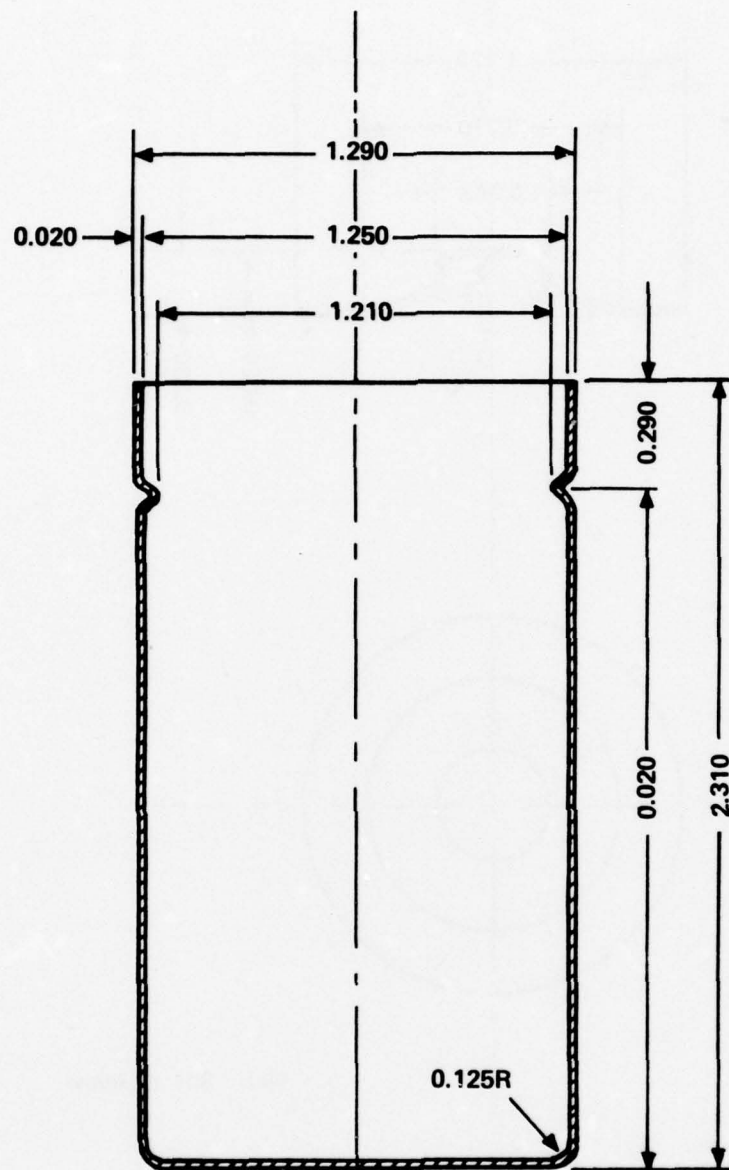


Figure 3. X-1 Button Cell
(All dimensions in mm)

Figure 4. High Energy AA Cell
(All dimensions in mm)





Mat: CRS, Nickel Plated on outside, 3-4 μ

Figure 5. Can

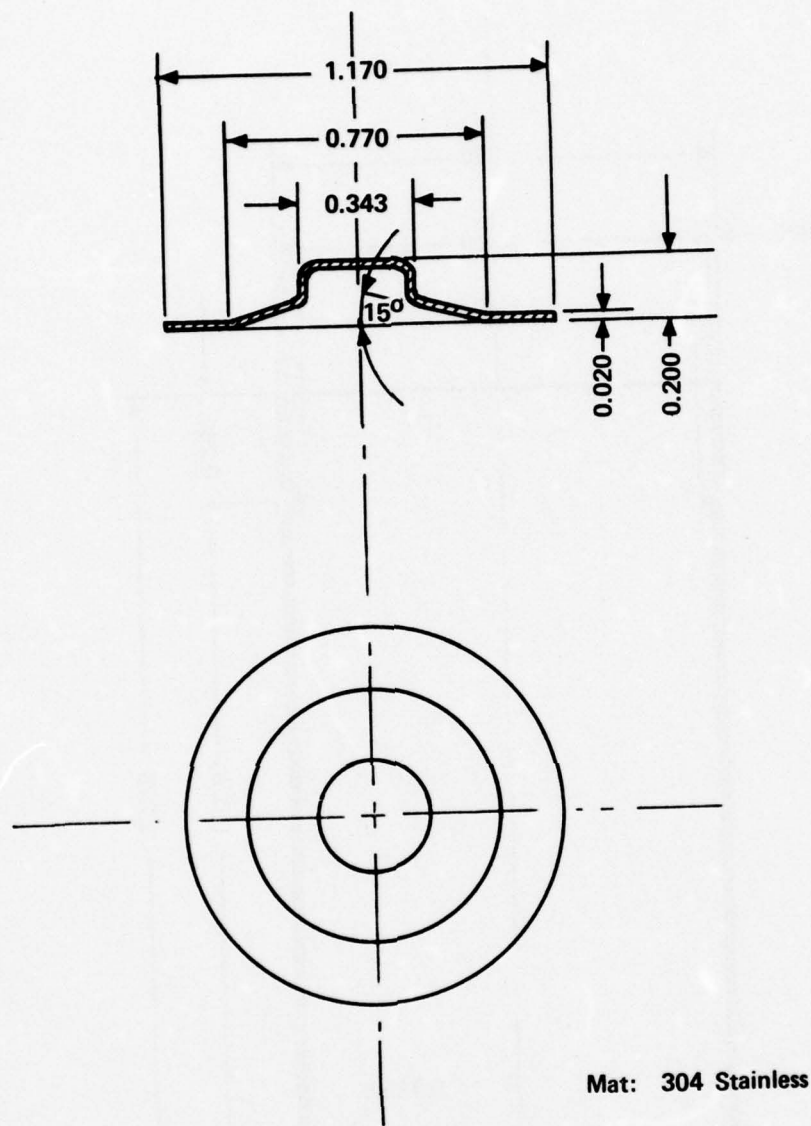


Figure 6. Cover

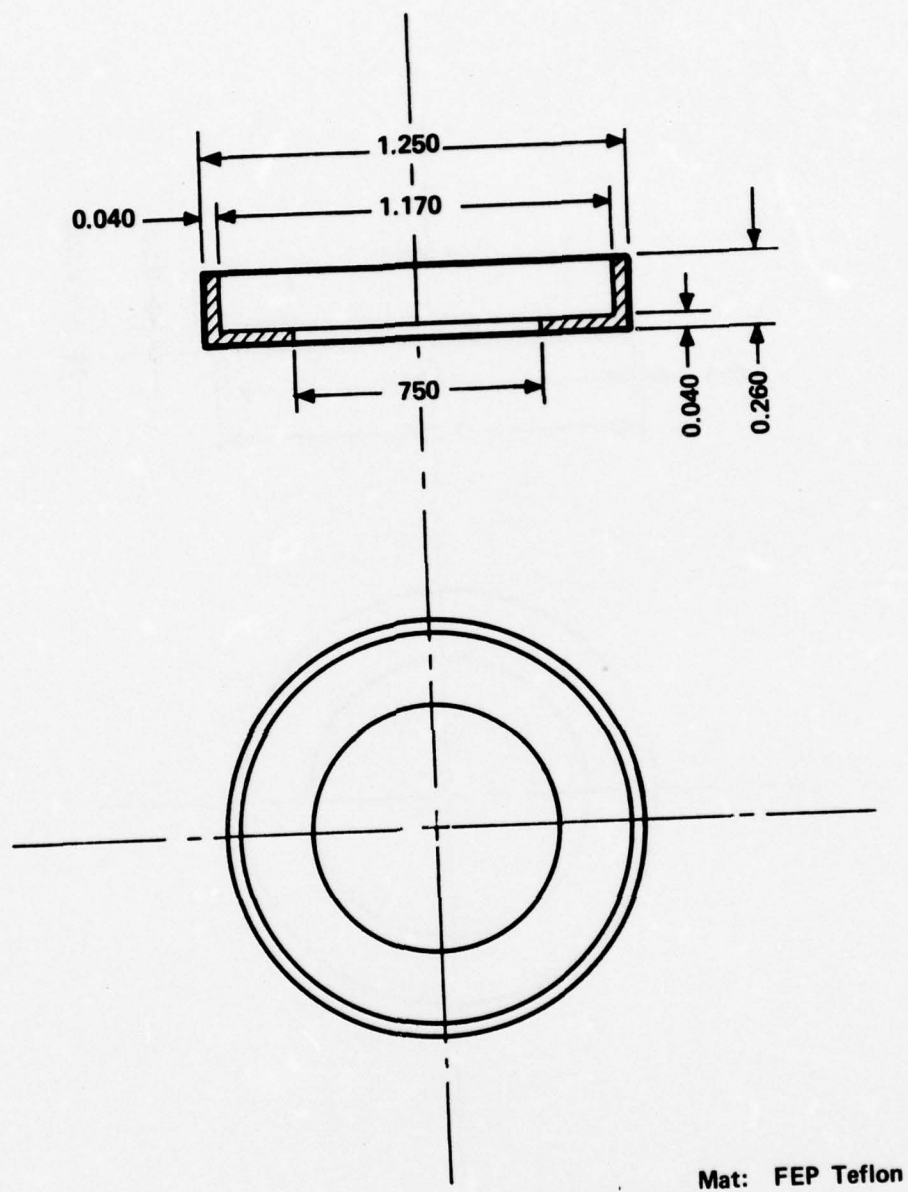


Figure 7. Gasket

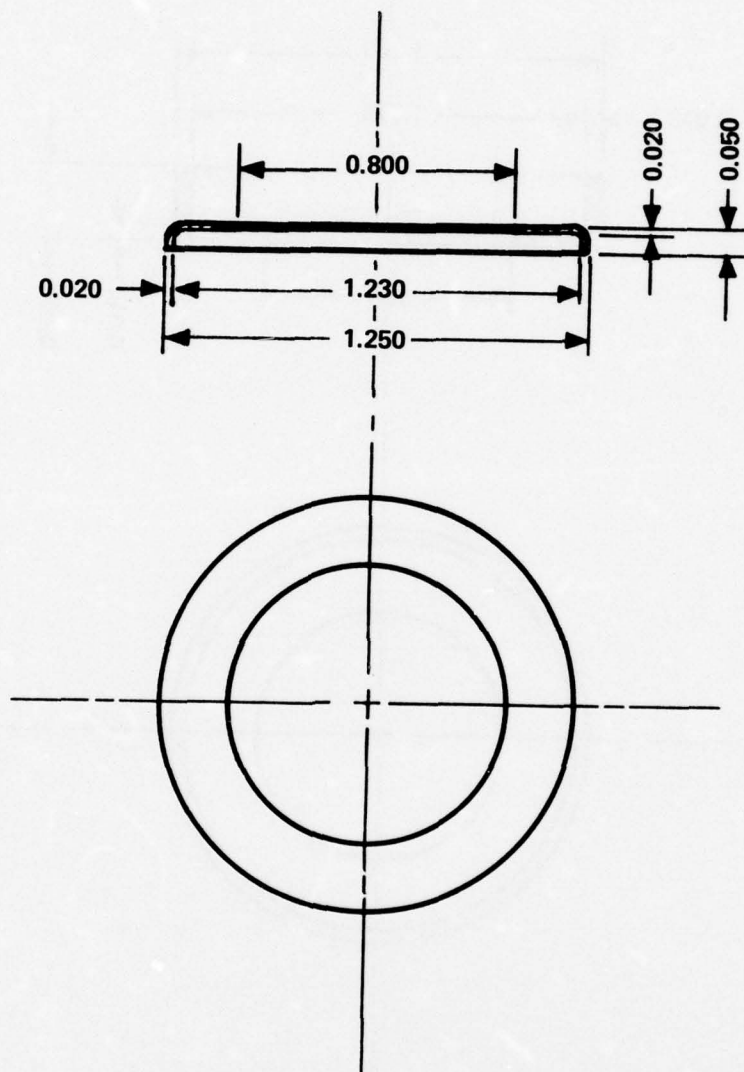


Figure 8. Support Ring

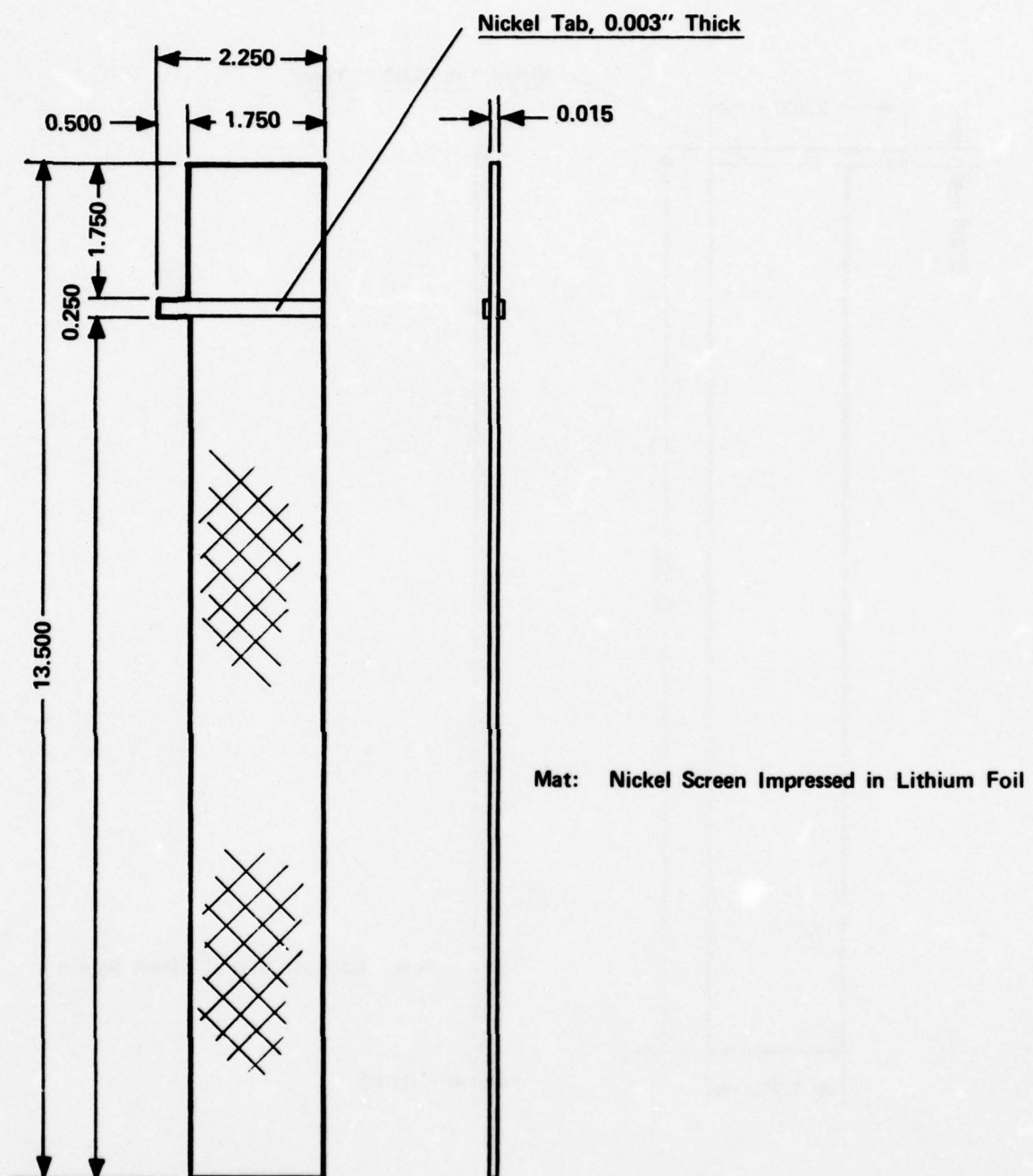


Figure 9. Anode

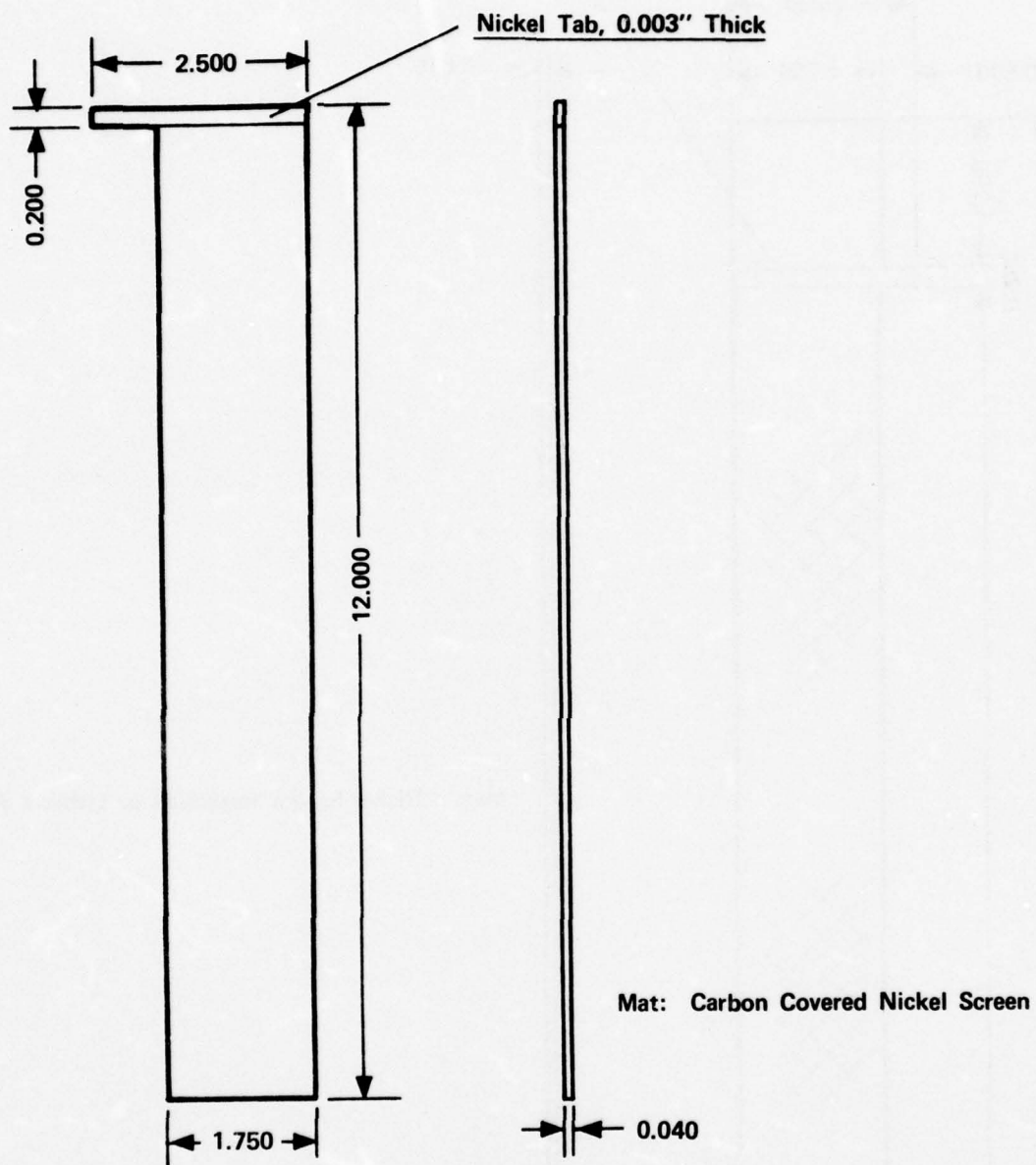
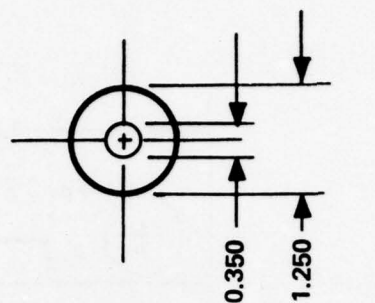
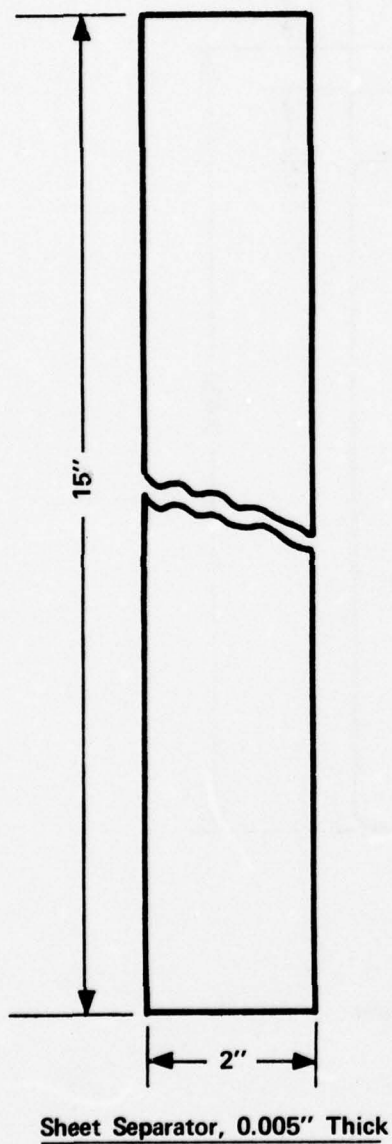
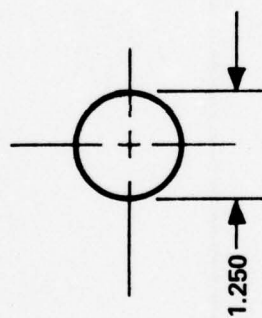


Figure 10. Cathode



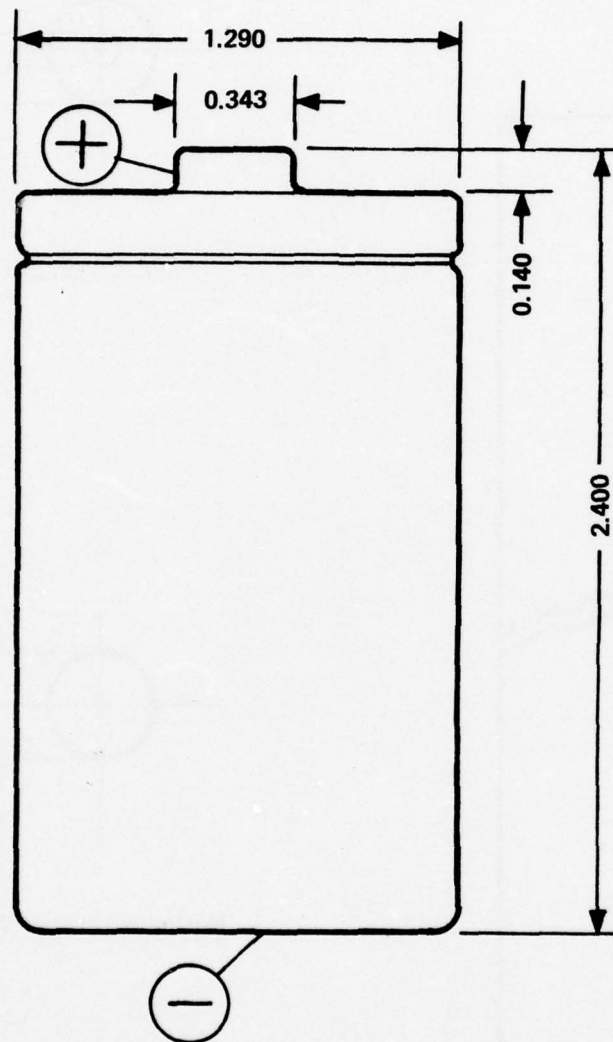
Top Separator, 0.010" Thick



Bottom Separator, 0.010" Thick

Mat: Glass Non-woven

Figure 11. Separators



Add 0.020 to 0.040" to all dimensions
to allow for label and jacket.

Figure 12. Standard Cell

The can is made of cold rolled steel by the multistep deep drawing process, just as in the production of alkaline cells. A 0.020 in. thick wall appears strong enough to form and hold the tension in the crimp type seal. On the outside, the can is nickel plated to protect the cell from the corrosion in a humid environment. Difficulties were experienced in locating a shop that can plate ductile, corrosion-resistant nickel, since it is no longer in demand. Modern nickel-plating procedures are adjusted to yield bright nickel deposits that are not desirable here because of brittleness associated with the inclusions in the deposit. Brittle deposits crack during the crimping operation and expose the most sensitive part of the can to corrosion. For this reason, we have set up our own ductile nickel-plating facility of a small capacity, adequate for the needs of this program. It produces gray deposits that adhere well to the steel substrate, and also follows the mechanical shape changes of the substrate in the assembling of the cell.

The cover is stamped out of stainless steel sheets, 0.020 in. thick. The cathode current collector is in direct contact with the cover, via a connecting tab. In the past, this material did not show any sign of corrosion when exposed to the cell electrolyte under similar conditions.

The gaskets were made and tested to our satisfaction. Cells of different sizes, with a similar type of seal, have been under test at various temperatures. Tooling has been made for the production of these gaskets in limited quantities.

The support ring is made of 0.020 in. thick CRS sheet metal. The tooling and the production of this part was carried out in our own shops.

The anodes were made by impressing an expanded nickel screen into lithium foil. Nickel ribbon was used to make a welded connection between the anode current collector (screen) and the cell can.

The cathodes are produced by pasting the carbon blend on both sides of the expanded nickel screen. All the materials needed for making these thin sheet cathodes have been delivered.

The separator materials are available in several thicknesses and varieties of structure. They have to be evaluated in the finished cell while the optimization of cell electrodes is being carried out.

The finished cell is shown on Figure 12, with the dimensions closely conforming to the established standards for the D size cell.

4. CARBON CATHODES

The best cathode making procedures available in 1974 were used in producing flat electrodes of various thicknesses for evaluating the discharge rate capability. The cathodes used in the first evaluation experiments were of the following dimensions:

- 1.5 in. wide
- 3.75 in. long
- 0.020 in. thick

They were made by rolling the carbon mix onto an expanded nickel screen; this screen was 0.005 in. thick. The resultant electrodes, in the presence of an excess of lithium and electrolyte, delivered a 1.2 Ah capacity, or over 16 mAh/cm², at a typical discharge rate of 4 mA/cm². Lower discharge rates, applied to cathodes this thin, do not result in significantly higher total capacity obtained. Therefore, this could, for all practical solutions, be considered the bottom limit of the thickness for cathodes of this type. At the thickness of 0.040 in. and up, one begins to see a difference in the total capacity obtained with various discharge rates at least in these preliminary types of experiments.

The evaluation of thin cathodes was started using the laboratory type demountable cell as originally proposed. Many difficulties were experienced with those cell, particularly in the experiments that lasted over a long period of time. The main difficulty was the leakage of the electrolyte along the wire contacts, pressure fitted into the Teflon body and leading to the electrode back plates. The fit was tight only for a while, but then relaxed since the flow of Teflon was not restricted in any way. After completing the experiments with various cathodes at high discharge rates, we had to abandon this test vehicle and choose another that would ensure the tight seal throughout the duration of all tests.

The laboratory-type cell fixture was also intended for use with a reference electrode to study the voltage behavior of cell electrodes during discharge. However, these measurements proved to be unnecessary; the issue of the electrode behavior was settled in an independent program. Following are the major findings that resulted from this study:

1. In the operation of fresh cells the polarization of cell electrodes is a minor contribution to the cell overall impedance. The major contribution is the ohmic resistance of the electrolyte, causing a linear dependence of the cell polarization upon current density over a wide range of discharge rates and temperatures.

2. The lithium electrode is solely responsible for the impedance build-up in storage. The cell, made of two identical lithium electrodes, was increasing its internal resistance at twice the rate of increase for the cell with a lithium and a carbon electrode. The same cell built with two carbon electrodes (without lithium) did not show any impedance change with time.

The evaluation of thin cathodes was carried out using our X-1 type button cell as a test vehicle. The thicknesses of the electrodes selected for this study were all below the thickness normally required for the optimal operation of this cell. Our experimental cell was, therefore, cathode limited, which is what was needed for this evaluation. All other parts were the standard parts of this button cell. The geometric surface area of the electrode was used in determining the current density applied in each test. The discharge tests were conducted under constant current conditions on the test set-up equipped with automatic voltage cut-off set at 1.5 V.

Three different thicknesses of electrodes were used in these tests, covering discharge rates of 0.2, 0.5, 1, 2.00, 5 and 10 mA/cm². The dependence of the electrode capacity on the discharge rate is shown in Figure 13 for all three electrode thicknesses tested. The other pertinent data are shown in Table 1.

TABLE 1
MAXIMUM CAPACITIES OBTAINED WITH VARIOUS CATHODES

Cathode Thickness in.	Weight of Carbon Blend mg/cm ²	Maximum Capacity Obtained	
		mAh/cm ²	Ah/g of Carbon Blend
0.023	14	44	3.14
0.034	28	53	1.89
0.052	52	62	1.19

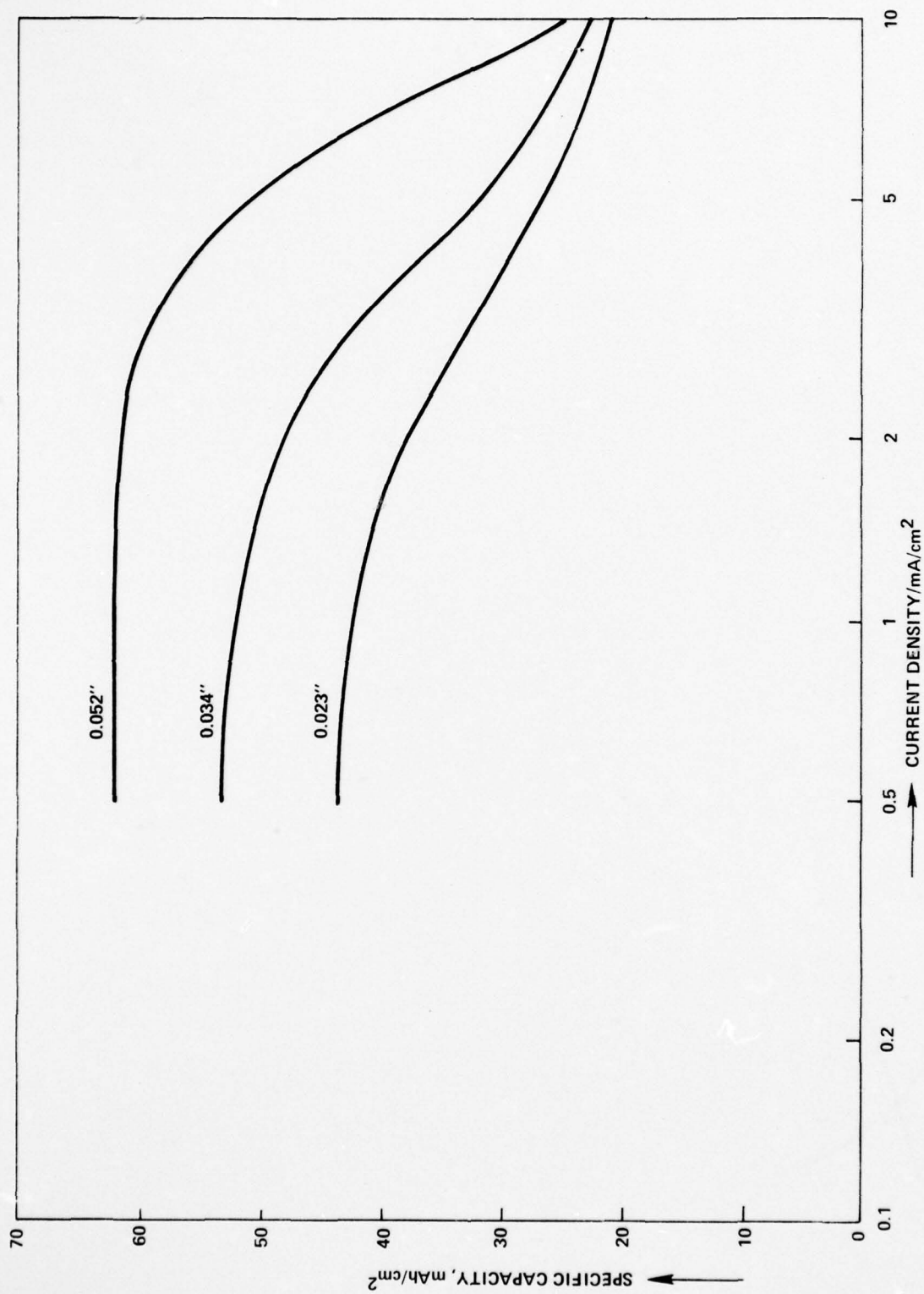


Figure 13. Limiting Specific Cathode Capacity as a Function of Discharge Rate for Various Cathodes

5. LITHIUM ANODES

Simple anode construction was employed in all three test vehicles used in this program. Lithium foil was pressed against a stainless steel screen from one or both sides to form a composite with sufficient mechanical strength and good electrical conductivity. The inert current collector (screen) was required even in the cell construction made with lithium in excess of the capacity of cathode, at least at the beginning of the program, in order to avoid lithium isolation at the end of discharge due to a possible nonuniformity in current distribution over the anode surface. Lithium foil of various thicknesses was available from at least three sources (Foote Mineral, Litco and Kawecki-Berylco). There was no reason to believe at the beginning of the program that lithium from different sources would behave differently, at least as far as the capacity was concerned.

The anodes for wound cells were made by precutting sections of lithium foil and passing the foil and the screen between rollers with preadjusted clearance. A single pass was sufficient in most cases to form the composite, whether it was made with a screen-foil pair or with two layers of foil and a screen in between. Many difficulties were expected, such as the passivation of anodes on storage at elevated temperatures, but it was not clear at this early stage of the program how the anode construction could improve the performance after storage.

6. ELECTROLYTES

We started our electrolyte evaluation using the standard size AA cell with a wound electrode structure, as it was developed under an independent program. This cell appeared to be a suitable test vehicle since a more elaborate sealing technique was available and also since fairly reproducible electrodes could be made using these procedures.

The choice of electrolytes was a limited one since the preliminary work, over a period of several years, clearly indicated the advantage of thionyl chloride and sulfuryl chloride over other oxyhalides available. The higher open circuit voltage obtained with sulfuryl chloride had to be investigated further since the stability of this higher voltage had not been tested under constant current discharge conditions. Both the thionyl chloride and the sulfuryl chloride electrolytes were made using high purity chemicals (Fisher Scientific) in order to eliminate possible effects of low concentrations of impurities commonly found in industrial grade solvents. Solvents were redistilled immediately before use, disregarding the first 10% of the distillate and leaving the last 10% in the distillation flask. Aluminum chloride was freshly sublimed, while lithium chloride was just vacuum dried. The electrolytes were made inside of a dry box in which the cell filling and closing were also carried out. Each electrolyte was made by dissolving 1.8 M each of AlCl_3 and LiCl in the solvents.

Standard AA cells were made using lithium and carbon electrodes of 72 cm^2 surface area each (counting both sides). Polarization curves were obtained of this cell with the sulfuryl chloride electrolyte, and compared with those of the same type cell made with the thionyl chloride electrolyte obtained earlier.¹¹ The polarization behavior of these cells is shown in Figure 14 and Figure 15 for comparison. A wide range of temperatures was covered in order to more fully describe possible differences observed in the performance of cells with different electrolytes.

It was evident from the results in Figure 15 that one could take advantage of the high voltage with sulfuryl chloride electrolyte only in cells made for relatively low rate applications. At room temperature the cells could be discharged at the high voltage only with rates below 100 mA (approximately 1.4 mA/cm^2). Higher rates of discharge could not be sustained at this high voltage, and a very slight increase in the rate would cause the voltage to drop to a value comparable to that obtained with the thionyl chloride

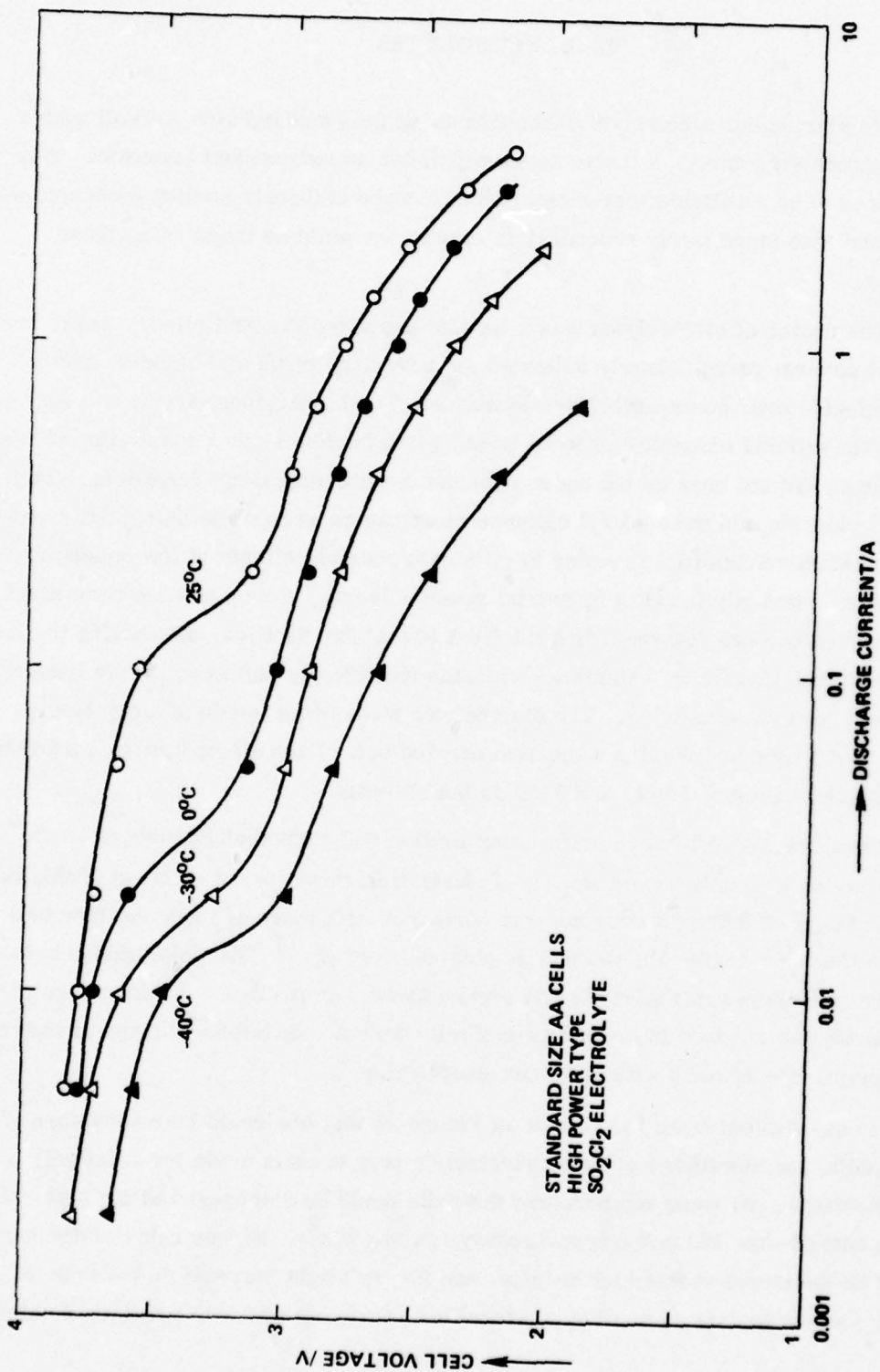


Figure 14. Cell Voltage vs. Discharge Current at Various Temperatures: High Power AA Cell with Sulfuryl Chloride Electrolyte

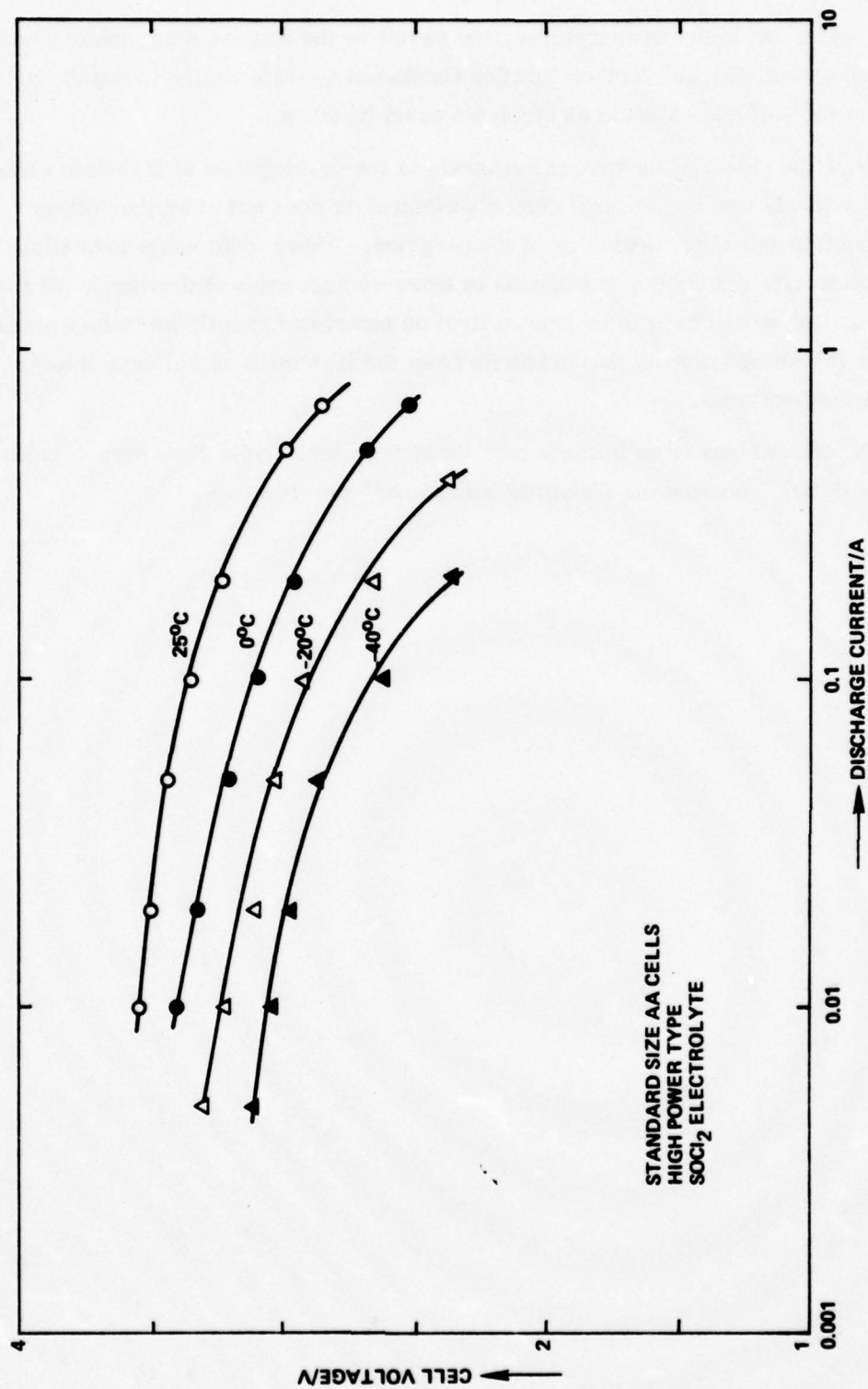


Figure 15. Cell Voltage vs. Discharge Current at Various Temperatures: High Power AA Cell with Thionyl Chloride Electrolyte

type electrolyte. At lower temperatures, the switch to the lower voltage plateau occurred at lower rates of discharge, further limiting the discharge rate region in which full advantage of the sulfuryl chloride electrolytes could be taken.

Since the object of the present program is the development of high rate cells, one has to conclude that the sulfuryl chloride electrolyte does not offer the voltage advantage anticipated at the beginning of the program. There were some indications that this electrolyte might be advantageous at extreme high rates of discharge (20 mA/cm² and higher). These will have to be proven first on completed D cells and then weighed against possible disadvantages that originate from the instability of sulfuryl chloride at elevated temperatures.

The comparison of cells made with these two electrolytes have been carried out in more detail¹² confirming the above preliminary observations.

7. SEALED D CELLS IN COLD ROLLED STEEL HARDWARE

7.1 CELL CONSTRUCTION

The earliest experiments with the standard size D cell were conducted using a demountable cell housing, before the procurement of cell hardware was completed. The interior space of this structure was made to be the same as that of standard cells.

A wound electrode structure was assembled using the components shown in Figures 9 to 11. The effective surface area of the electrodes, facing each other, amounted to 268 cm^2 . The cell was discharged with a constant current of 1 A, or 3.7 mA/cm^2 . The discharge curve is shown in Figure 16. A stable discharge voltage of 3.1 V was maintained throughout most of the 8.4 hours of discharge, delivering about 8.4 Ah capacity to 3.0 V cutoff voltage, or the energy of 26 Wh at this discharge rate. This is strictly a preliminary test, showing only that these electrodes could be made to provide energy at a high rate of discharge.

At the other extreme, the lowest rate was tested using the same demountable setup combined with low surface area (thick) electrodes. The simplest configuration, involving a single layer of lithium next to the can wall and a bobbin type cathode, delivered close to 12 Ah capacity at 150 mA constant current discharge. These two capacities represent the extreme two ends of a region in which many types of cells will fail, depending on the design of the cell structure. Rate capability will be realized at the expense of the energy density, as the surface area of the electrodes is increased. This means that no universal type D cell will be possible if one wishes to realize a maximum energy density. Cells should be tailored according to each individual application for a maximum energy output, at each power output required. Gravimetric energy densities could not have been correctly estimated from this test. The electrode structure was kept unchanged through the next set of tests carried out in the standard D size cell hardware.

Three types of wound D cells were made with characteristics of the electrodes shown in Table 2. A large batch of cells was made for fresh tests and discharged after storage.

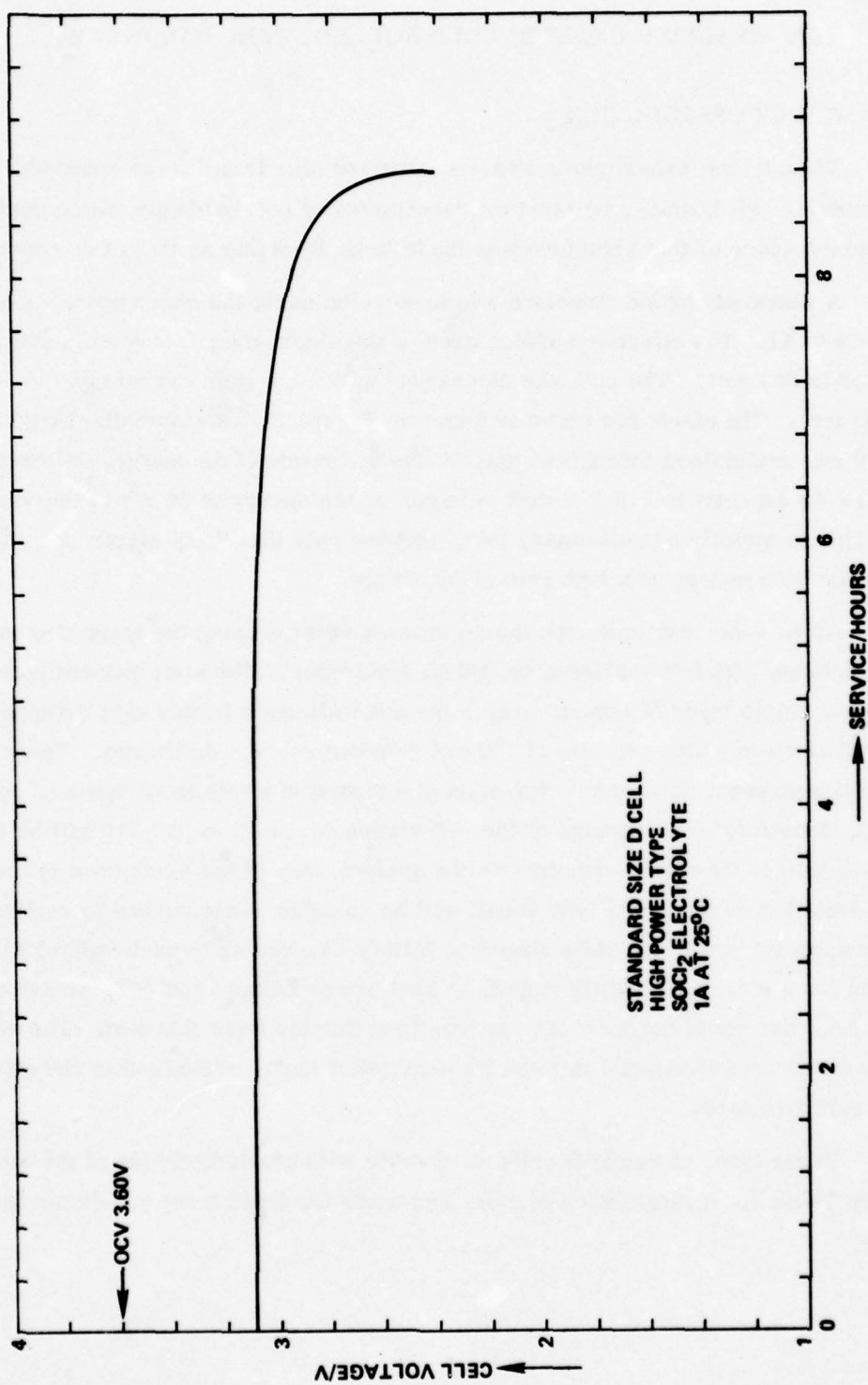


Figure 16. Discharge Curve of a High Power Type D Cell: Thionyl Chloride Electrolyte, 1A, 25°C

TABLE 2
ELECTRODE PARAMETERS

Design/Electrode		Length Inches	Width Inches	Thickness Inches
A	Cathode	16	1.75	0.023
	Anode	18	1.75	0.010
B	Cathode	14	1.75	0.034
	Anode	16	1.75	0.015
C	Cathode	12	1.75	0.052
	Anode	14	1.75	0.022

Nine cells were discharged, three of each type, with one at each selected discharge rate. The discharge conditions and the test results are shown in Table 3. The results clearly indicate the reduction in the cell capacity with an increased rate capability. The cells of design A were made with a maximum surface area of electrodes and are capable of delivering their energy at the highest rate but at the expense of the lower maximum energy obtainable from the package.

On the basis of these preliminary results, design B was chosen for the extensive testing that followed, since it showed a good maximum capacity with a high rate capability.

A total of 224 cells of design B were assembled with close control of all electrode dimensions as well as the assembling conditions. The cathodes were all made from the same batch of carbon blend; under identical drying, curing and storage conditions. The anodes were produced from the same batch of lithium foil that had been previously inspected for possible traces of discoloration that usually indicates a reaction with nitrogen in the presence of small amounts of water. The cells were assembled at 3% relative humidity. The electrolyte dispensing and the cell crimping operations were done within 24 hours of the cell assembling. All cells were kept under observation for several days before they were assigned to their respective tests. During this period the individual cell weights were recorded. The open circuit voltage was checked immediately after closing as well as before the cells were assigned to the tests.

The cells with open circuit voltage below 3.62 V were suspected of internal discharging and were discarded. A few extra cells were stored at each of the three selected temperatures just in case some of the cells failed the storage tests. The initial storage results seemed to indicate the adequacy of the cell sealing technique.

TABLE 3
TEST RESULTS WITH DIFFERENT DESIGNS

Design	Discharge Current A	Current Density mA/cm ²	Time of Discharge Hours	Cell Cap. to 3.0 V Ah
A	1.40	3.90	3.0	4.20
	0.70	1.95	9.5	6.65
	0.35	0.97	21.0	7.35
B	1.20	3.82	7.5	9.00
	0.60	1.91	17.5	10.5
	0.30	0.96	31.5	9.45
C	1.00	3.72	10.0	10.0
	0.50	1.86	26.5	13.25
	0.25	0.93	45.5	11.38

The cells were discharged under constant current conditions using a test set-up equipped with the automatic voltage cutoff device for each test station with an individually adjustable cutoff voltage level. A multichannel recorder (Texas Instrument FMWO6B) was used to monitor the cell voltage during discharge. Parallel with it was a fast chart recorder (Varian-A-25) to monitor the initial voltage drop and the recovery for the cells that were expected to show a voltage delay. The fast monitoring was discontinued when a stable discharge voltage was achieved.

7.2 CAPACITY OF FRESH CELLS

The summary of the fresh cell discharge results is presented in the form of a capacity-rate diagram in Figure 17. Individual discharge curves are represented in

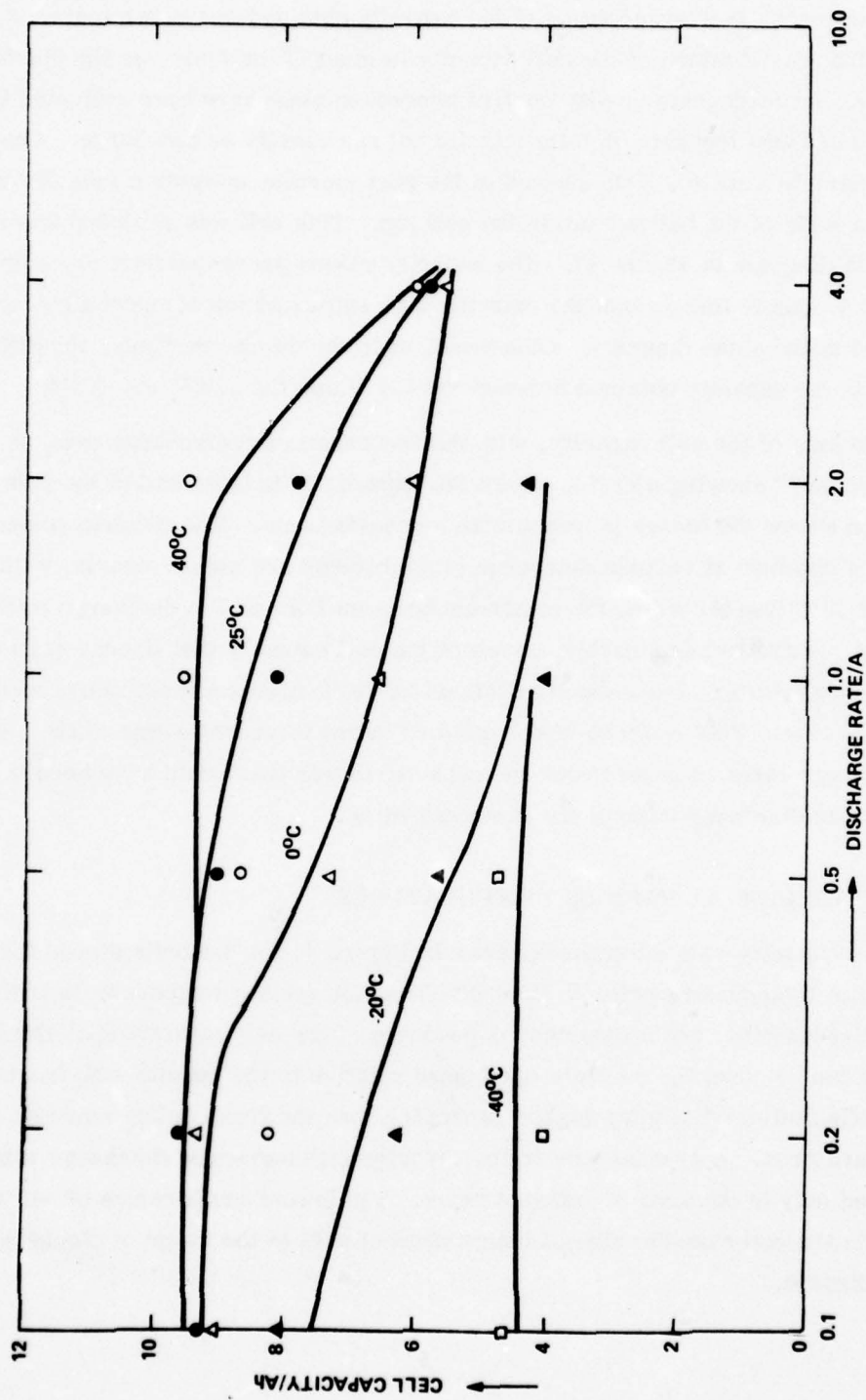


Figure 17. Capacity-Rate Behavior of Fresh Lithium/SOCl₂ D Cells

Figures 18 to 43. Two cells were tested under each set of conditions and the data in Figure 17 represent an average value of the capacity obtained in the two tests. A good reproducibility was obtained of the cell capacity in most of the tests, as the discharge curves show. An inadequate quality control procedure must have been reflected in the performance of those few sets of cells that did not run closely on discharge. One of them, for example Cell No. 209, showed in the post mortem analysis a loss of contact due to a poor weld of the cathode tab to the cell top. This cell was excluded from the capacity-rate diagram in Figure 17. The capacity values presented here were obtained with the 2.0 V cutoff line so that the extreme high rates and low temperatures could be presented in the same diagram. Otherwise, at lower discharge rates, the difference is minimal in the capacity obtained between the 3.0 V and the 2.0 V cutoff line.

The loss of the cell capacity, with the increase in the discharge rate, is a familiar function¹³ showing a region where the capacity is independent of the rate and then a region where the losses increase with increasing rate. The relative positions of the curves obtained at various discharge temperatures are shown clearly, with the exception of 40°C line for which the maximum between 1 A and 2 A discharge could not be explained. A gradual decrease is shown of the cell capacity with decreasing temperature through -20°C. The capacity obtained at -40°C seems almost independent of the discharge rate. This could be best explained by the internal heating of the cell at higher discharge rates, compensating the capacity losses that would have been incurred by the high rate discharge without the heat generation.

7.3 SHELF LIFE AT VARIOUS TEMPERATURES

The capacity-rate diagram is shown in Figure 44 for the cells stored for one month at room temperature prior to their discharge at various temperatures indicated. A better reproducibility and a smoother dependence of the cell capacity upon the discharge rate can be observed on these aged cells relative to the results with fresh cells. All these cells delivered slightly higher capacities than the fresh cells, more so at lower temperatures. A gradual loss in the capacity with increased discharge rates was observed only in the area of extreme rates. The lowest temperature of -40°C showed again the cell capacity almost independent of rate at the range of discharge rates investigated.

Figure 18

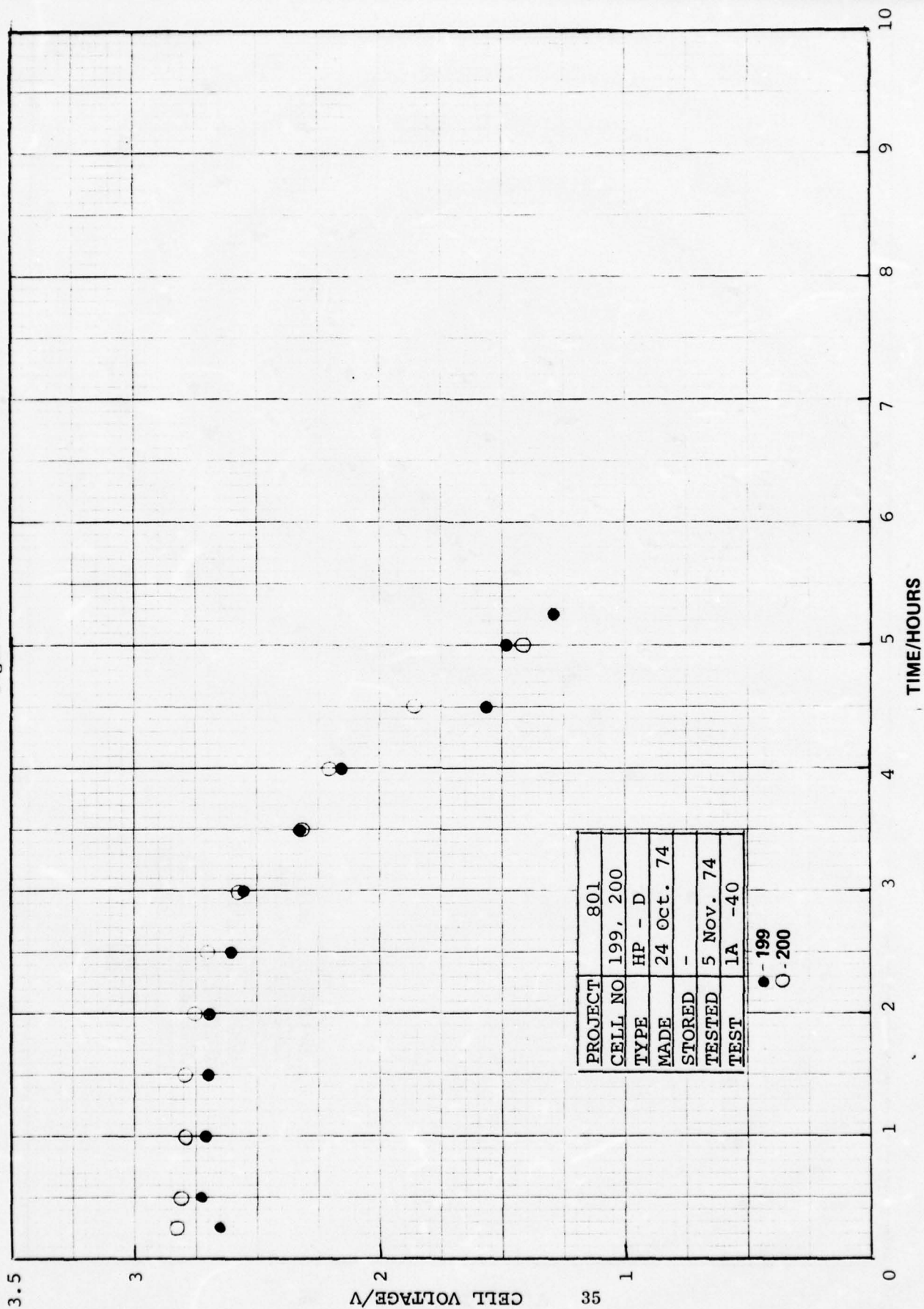


Figure 19

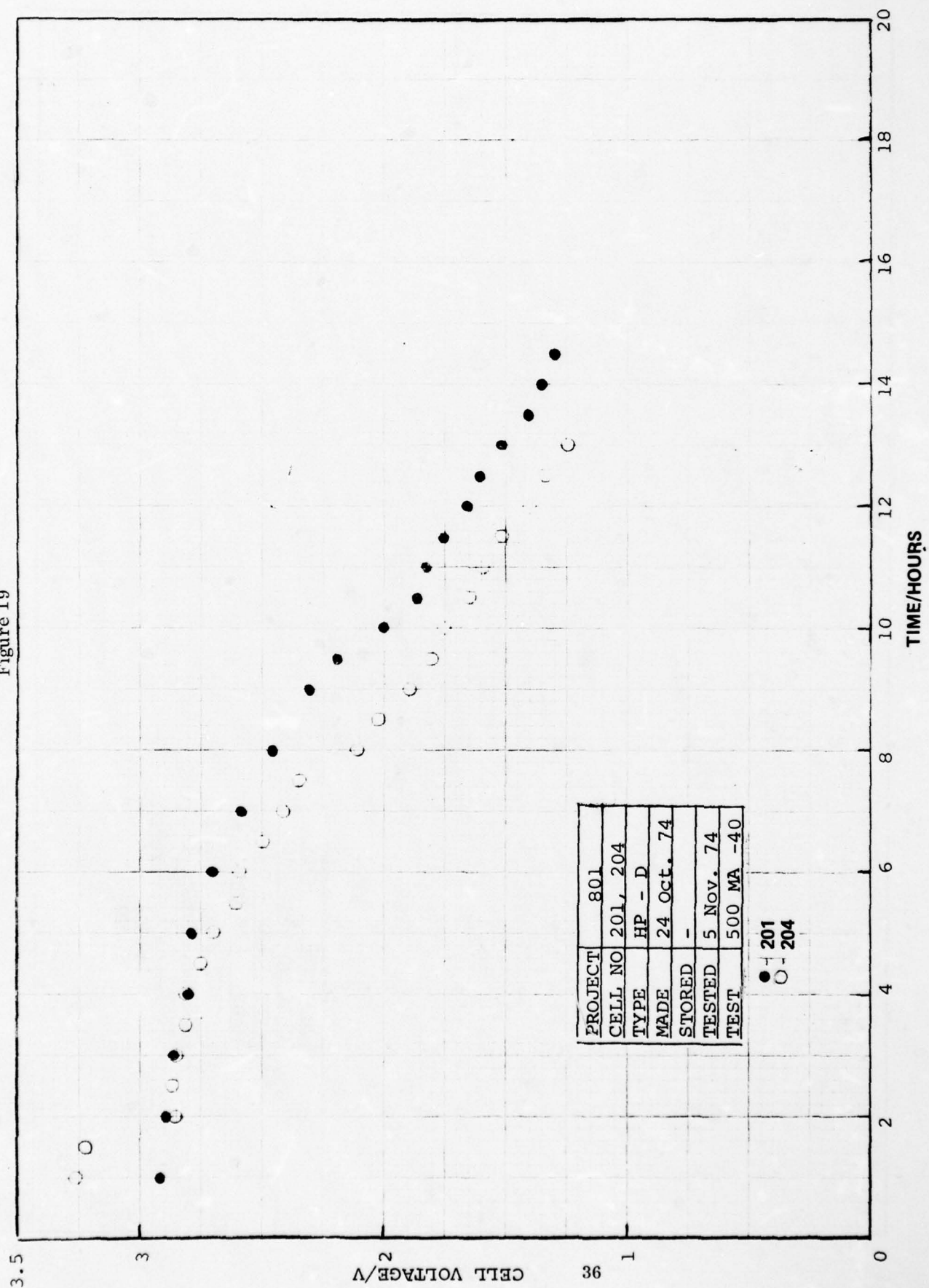
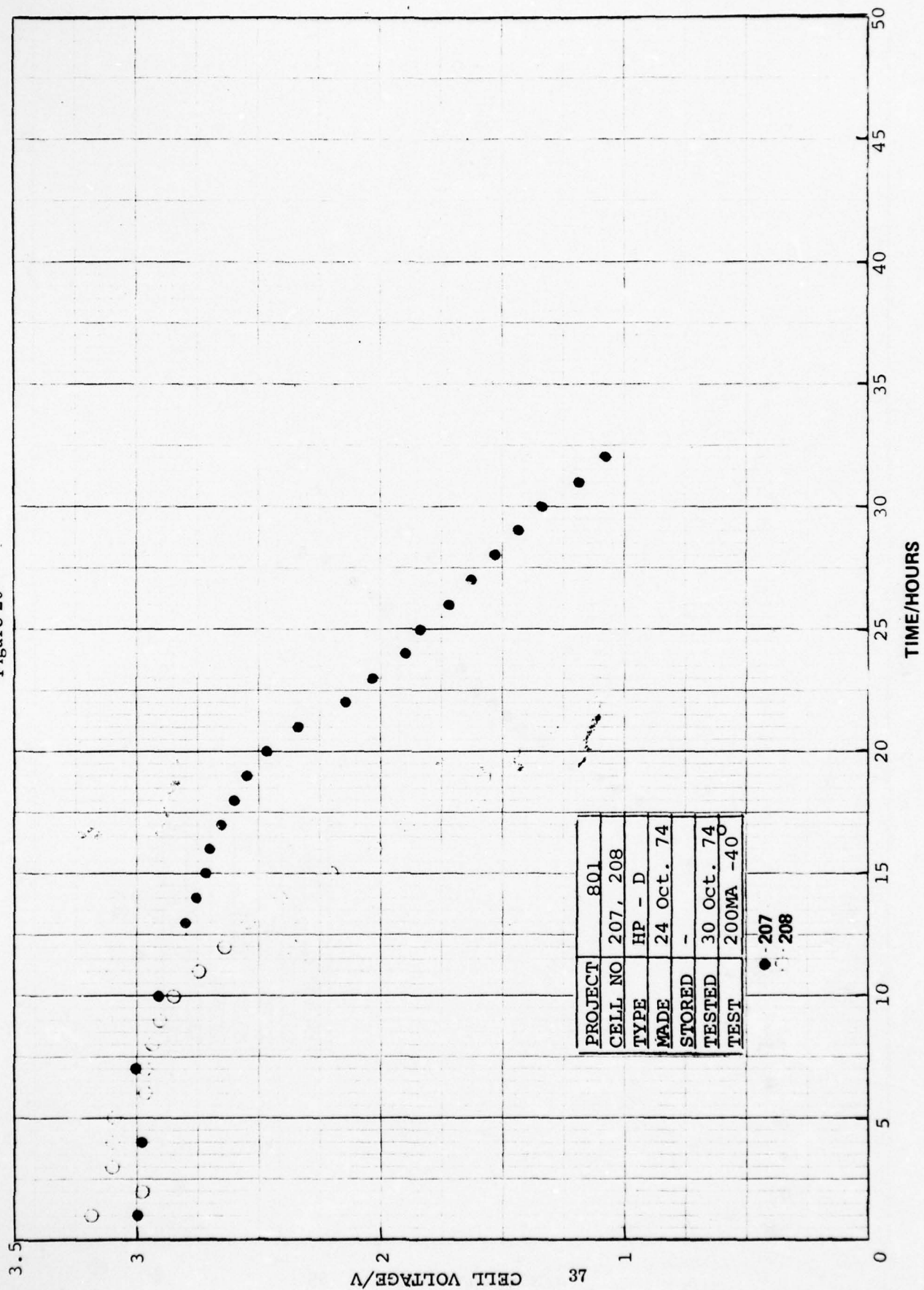


Figure 20



PROJECT	801
CELL NO	207, 208
TYPE	HP - D
MADE	24 Oct. 74
STORED	-
TESTED	30 Oct. 74
TEST	200MA -40

● - 207
○ - 208

Figure 21

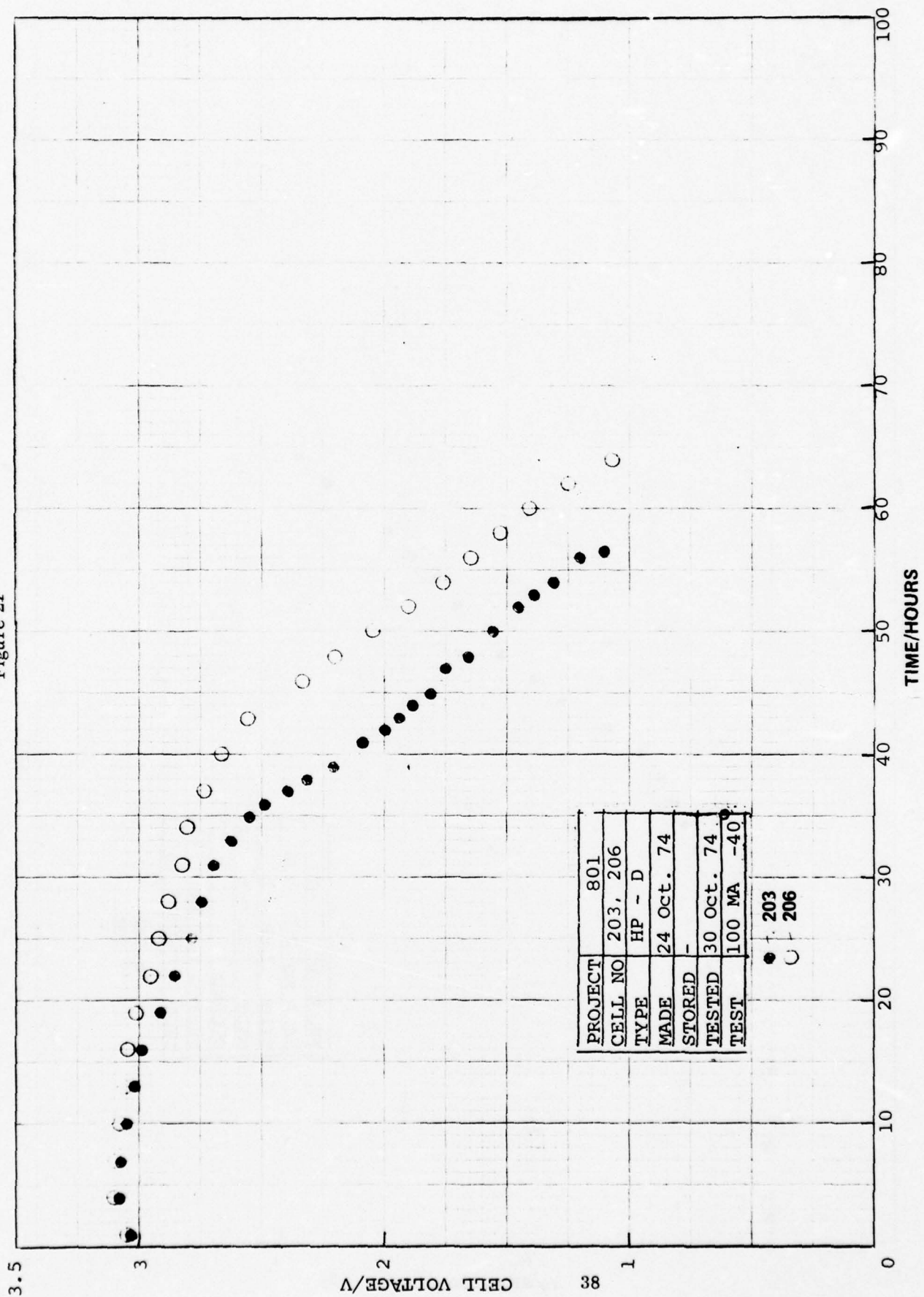


Figure 22

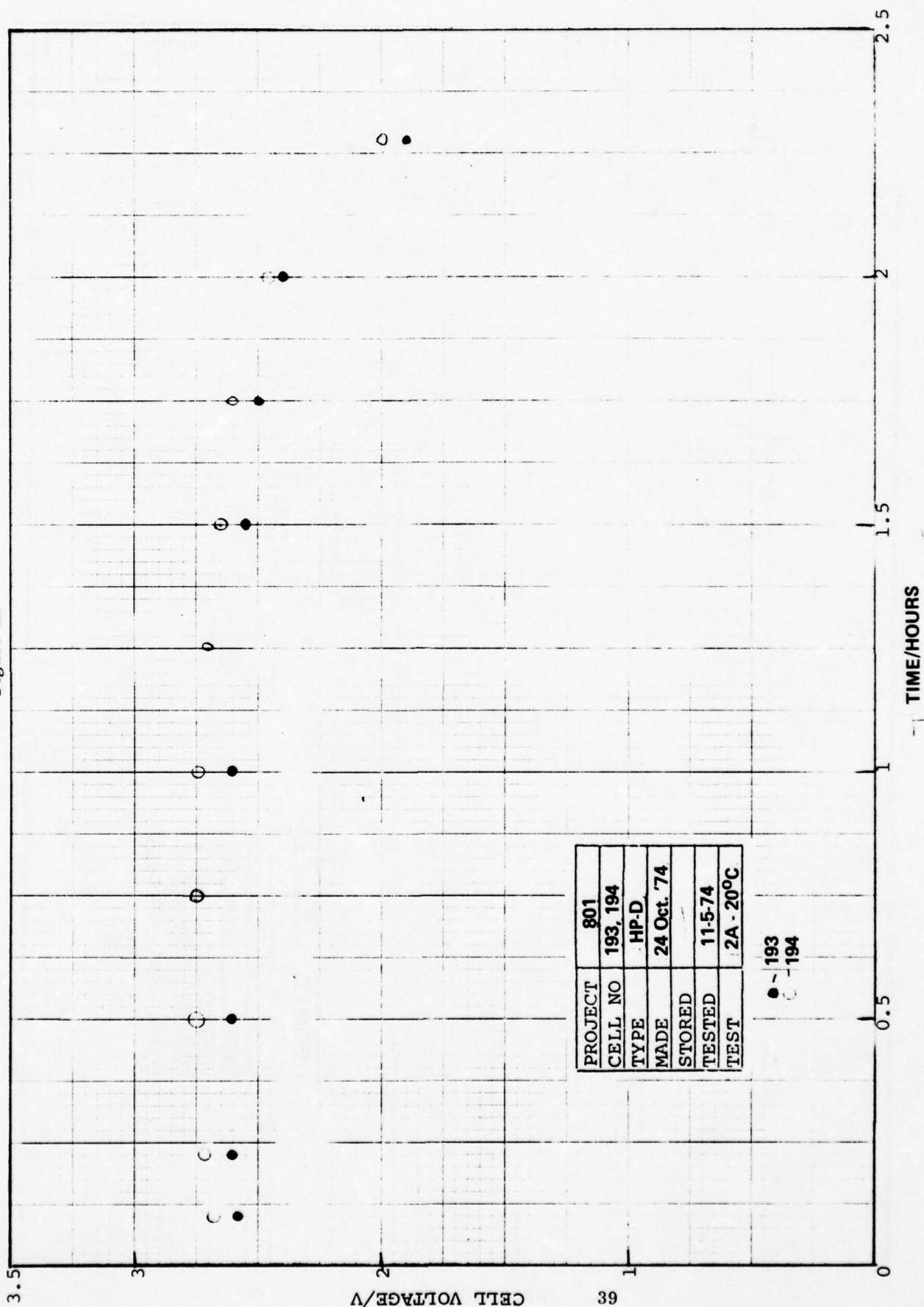


Figure 23

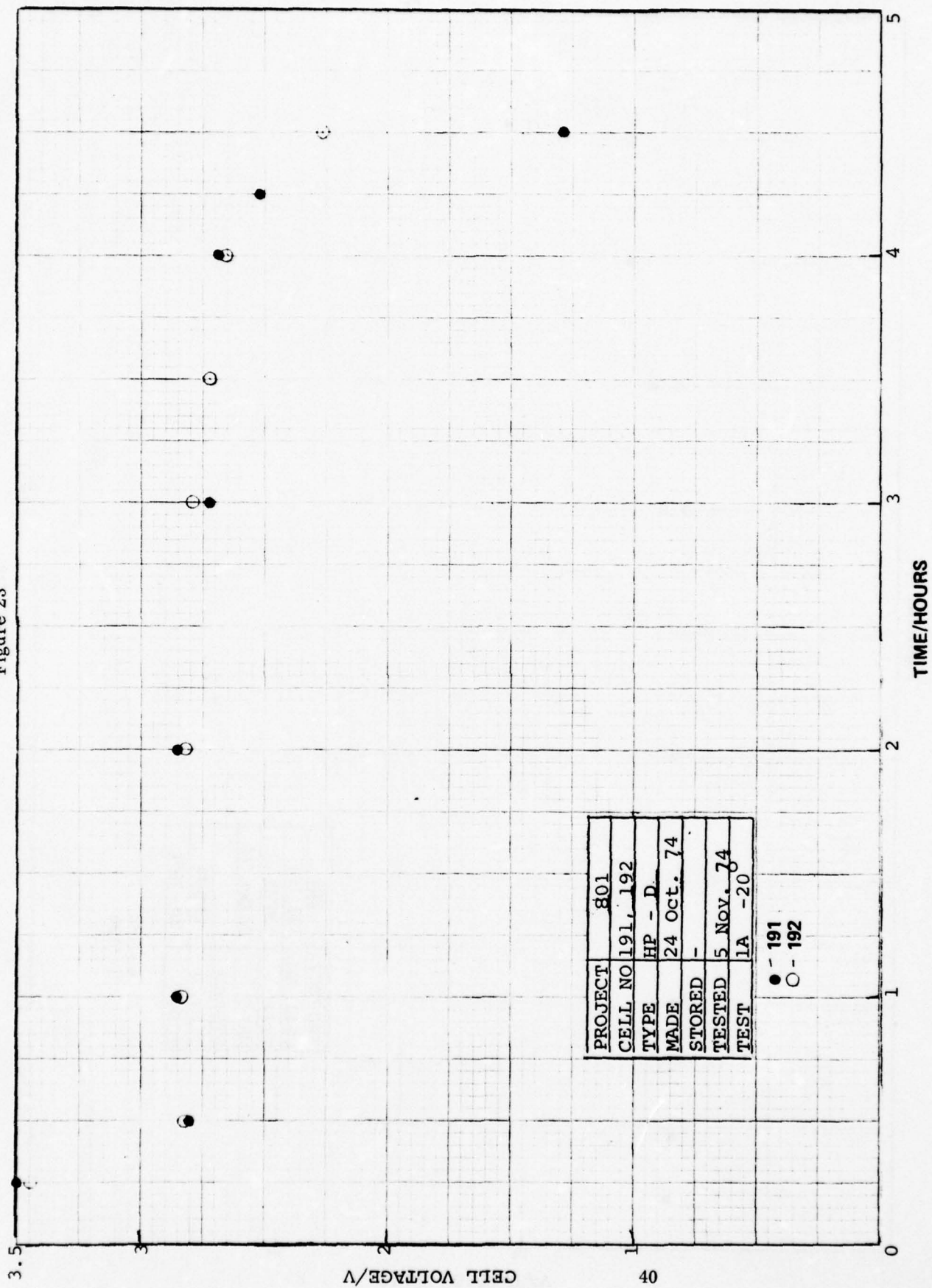


Figure 24

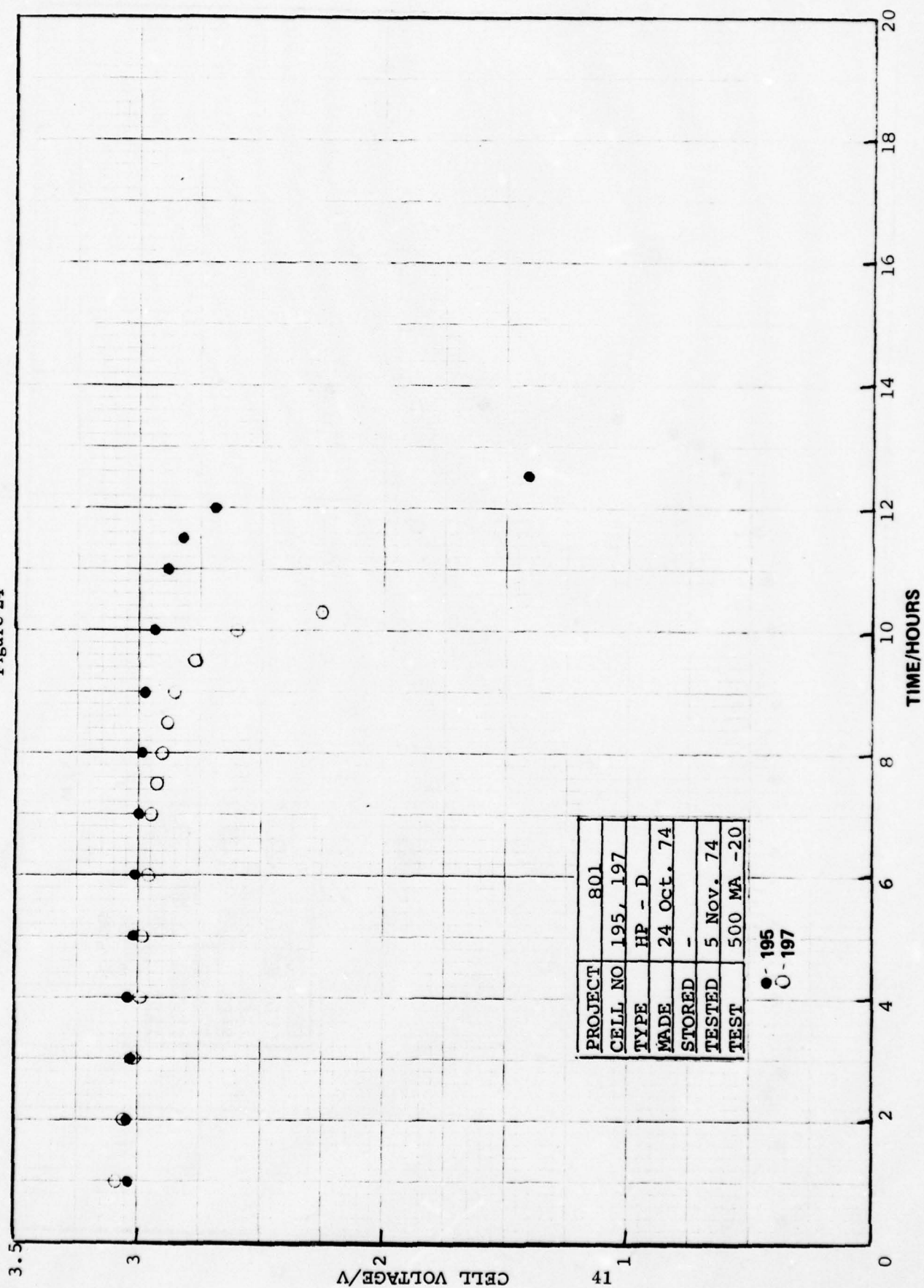
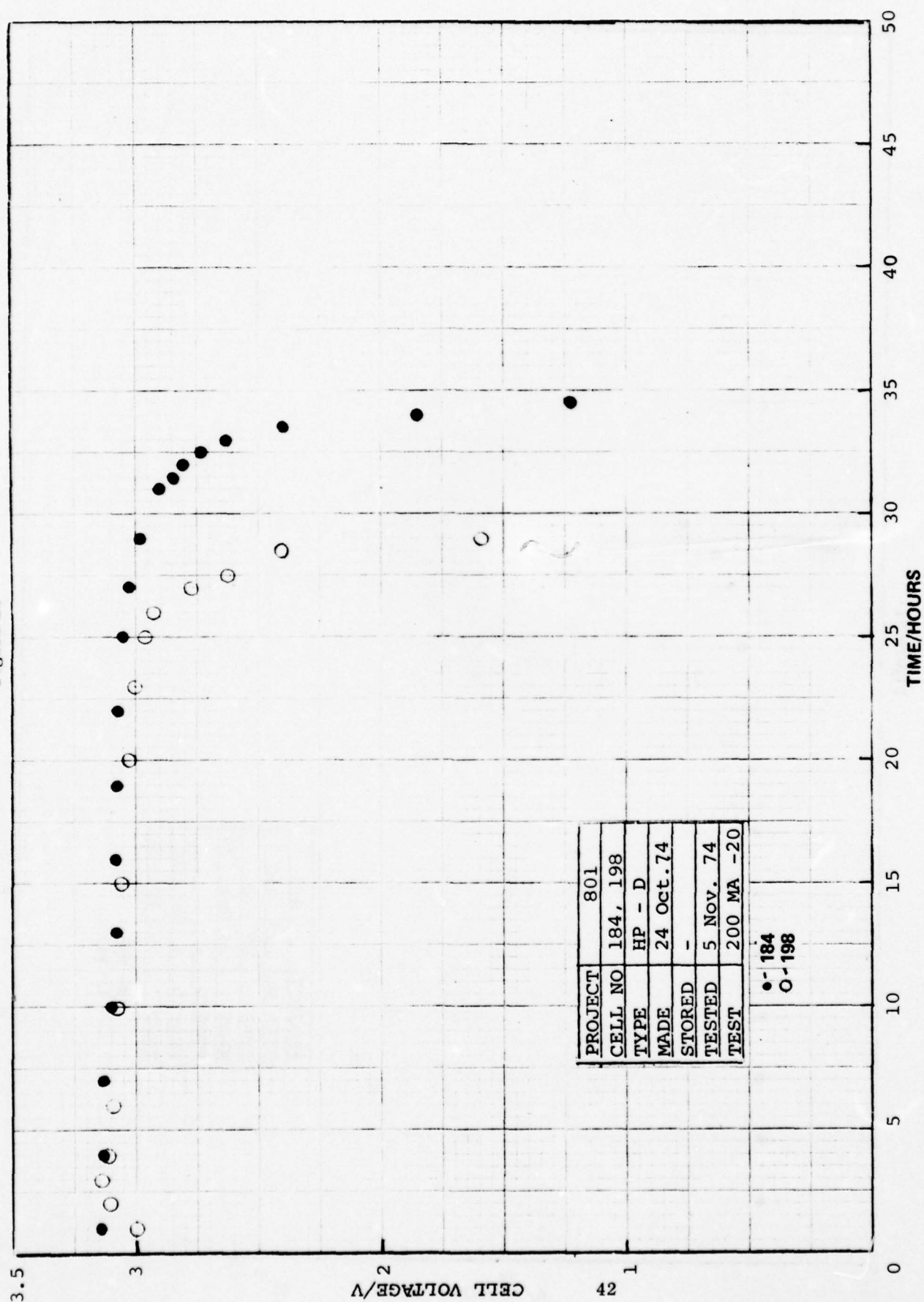
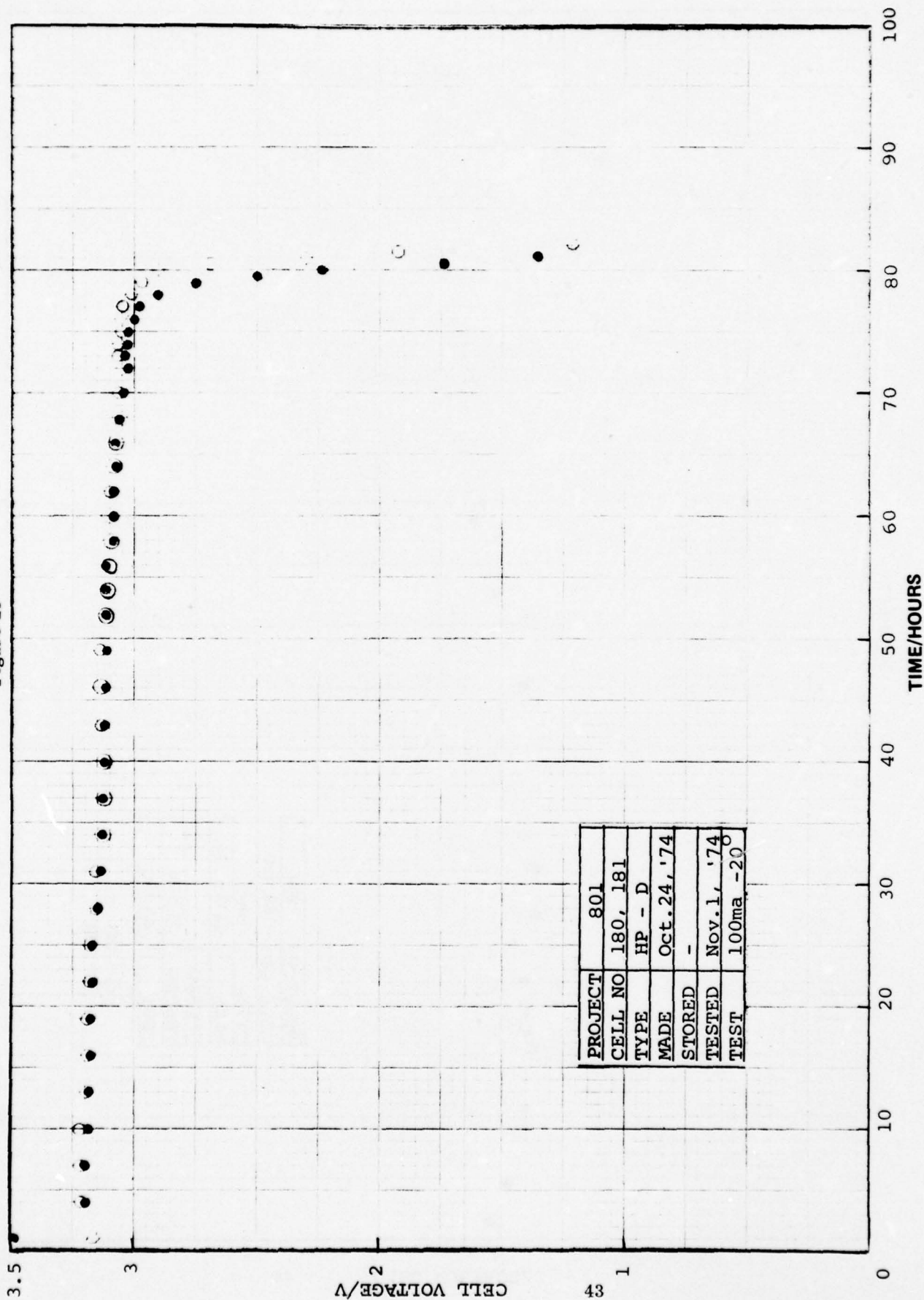


Figure 25



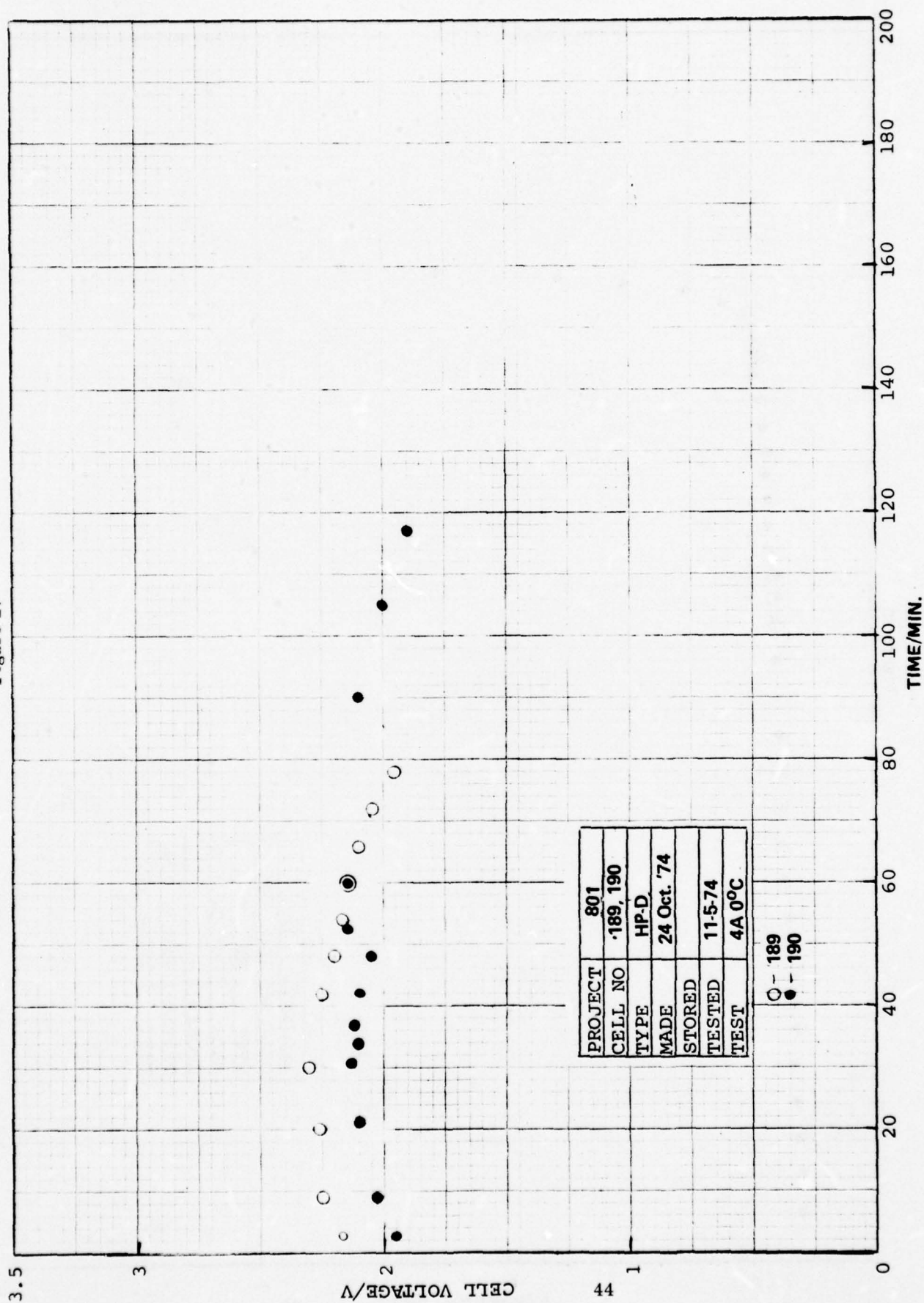
45

Figure 26



PROJECT	801
CELL NO	180, 181
TYPE	HP - D
MADE	Oct. 24, '74
STORED	-
TESTED	Nov. 1, '74
TEST	100ma -20

Figure 27



PROJECT	801
CELL NO	189, 190
TYPE	HP-D
MADE	24 Oct. '74
STORED	
TESTED	11-5-74
TEST	4A 0°C

○ - 189
● - 190

Figure 28

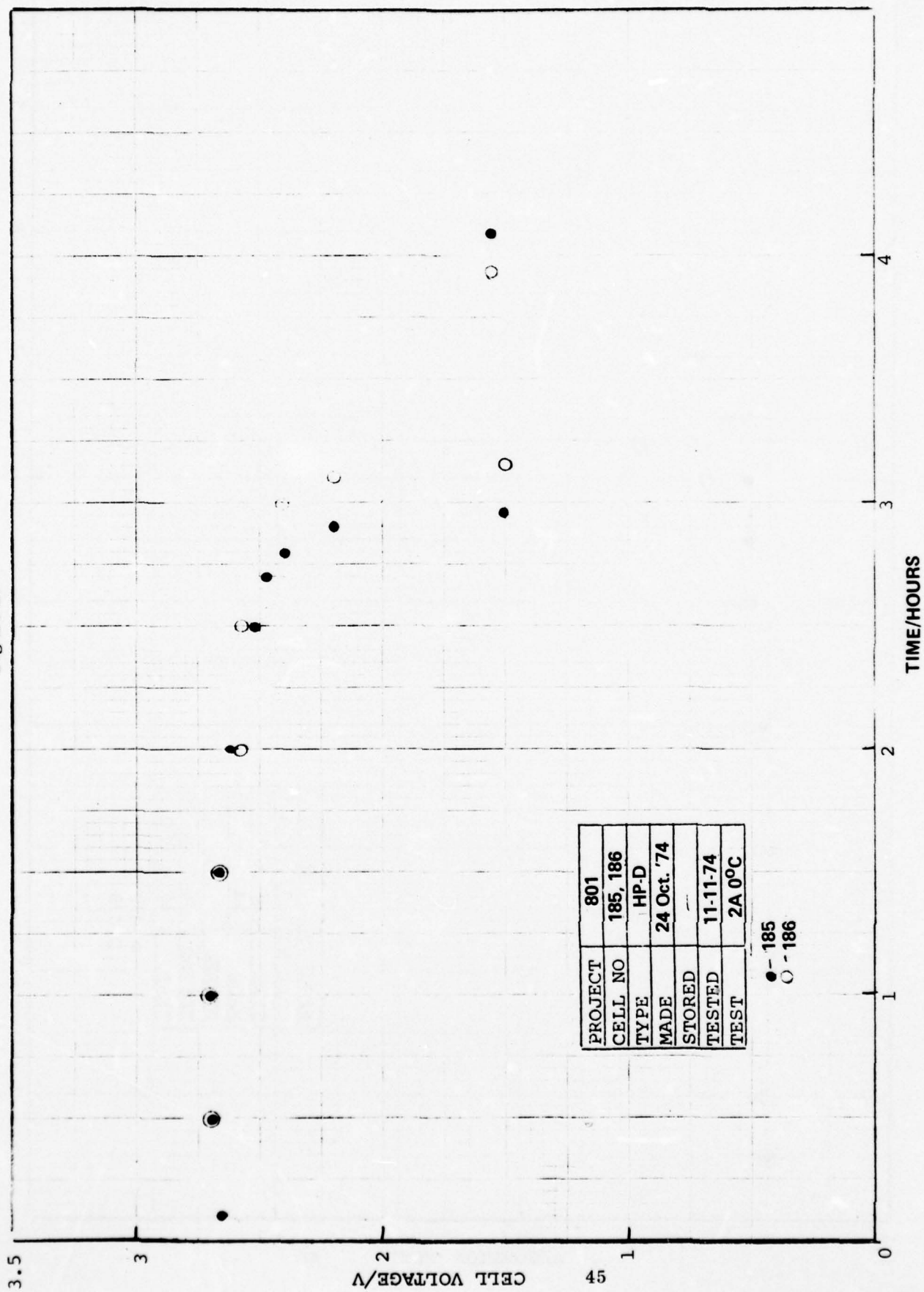
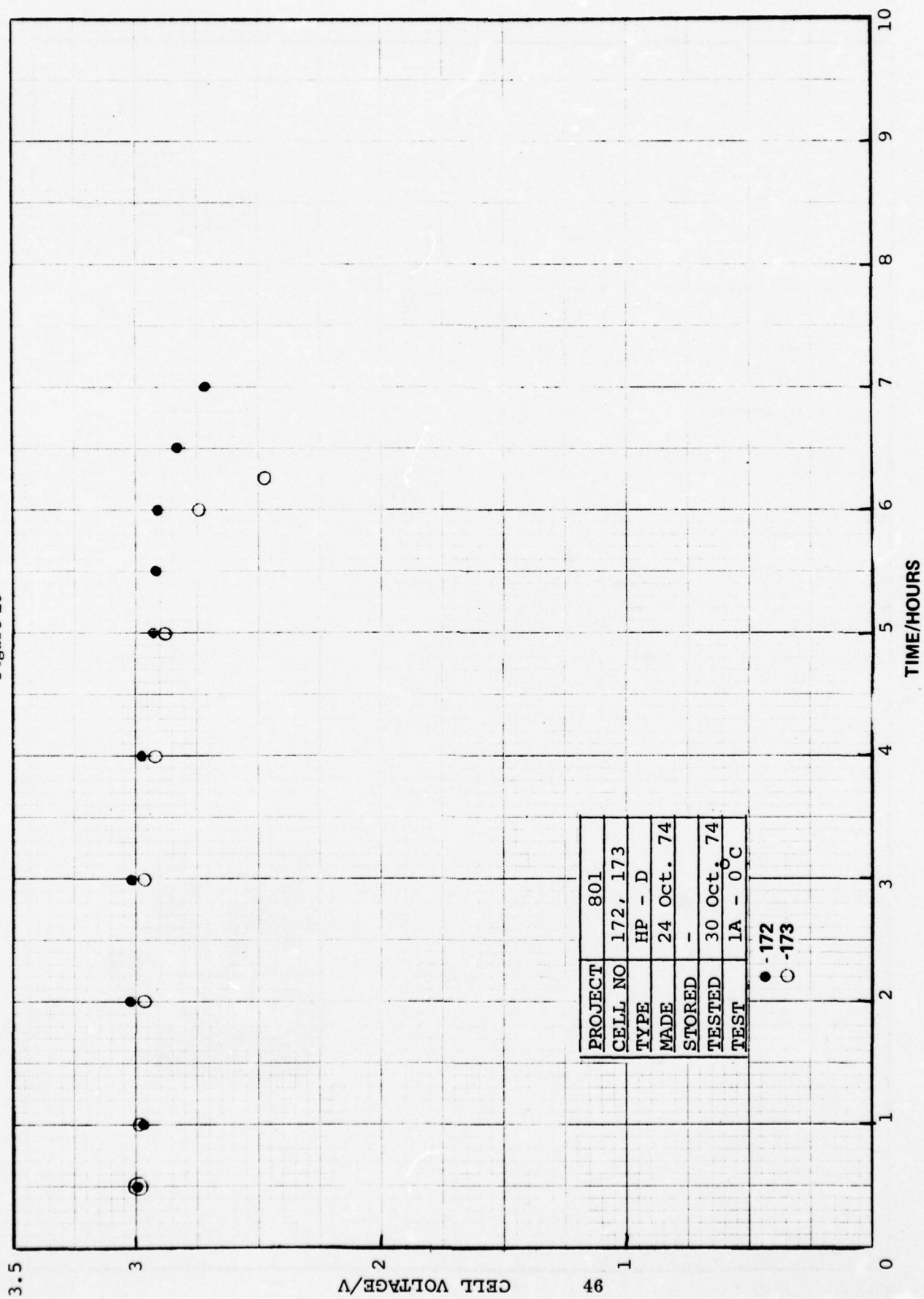


Figure 29



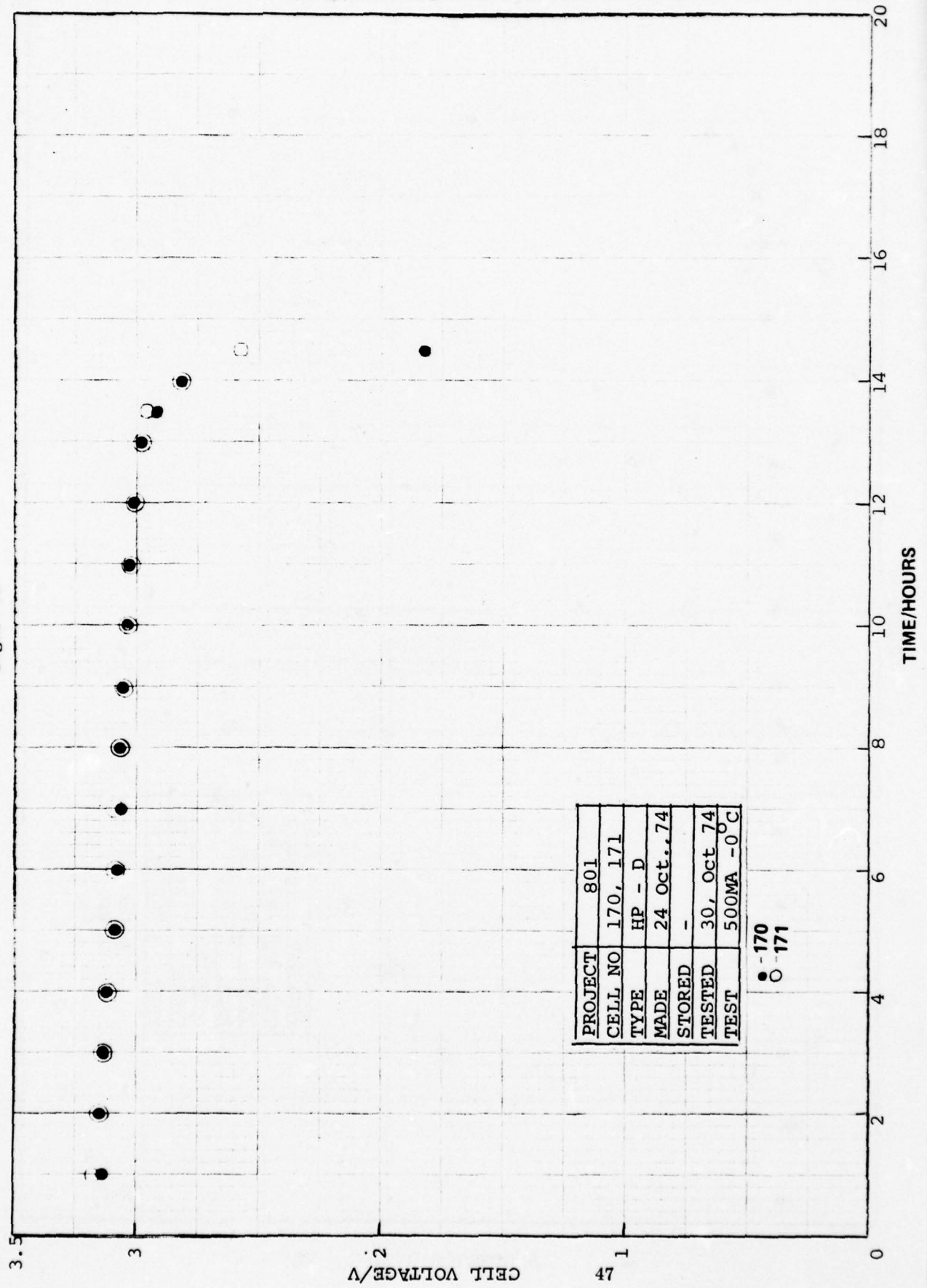
PROJECT	801
CELL NO	172, 173
TYPE	HP - D
MADE	24 Oct. 74
STORED	-
TESTED	30 Oct. 74
TEST	1A - 0°C

● -172
○ -173

1.25 MAX TO THE HIGH
1.25 MIN TO THE LOW

45 (72)

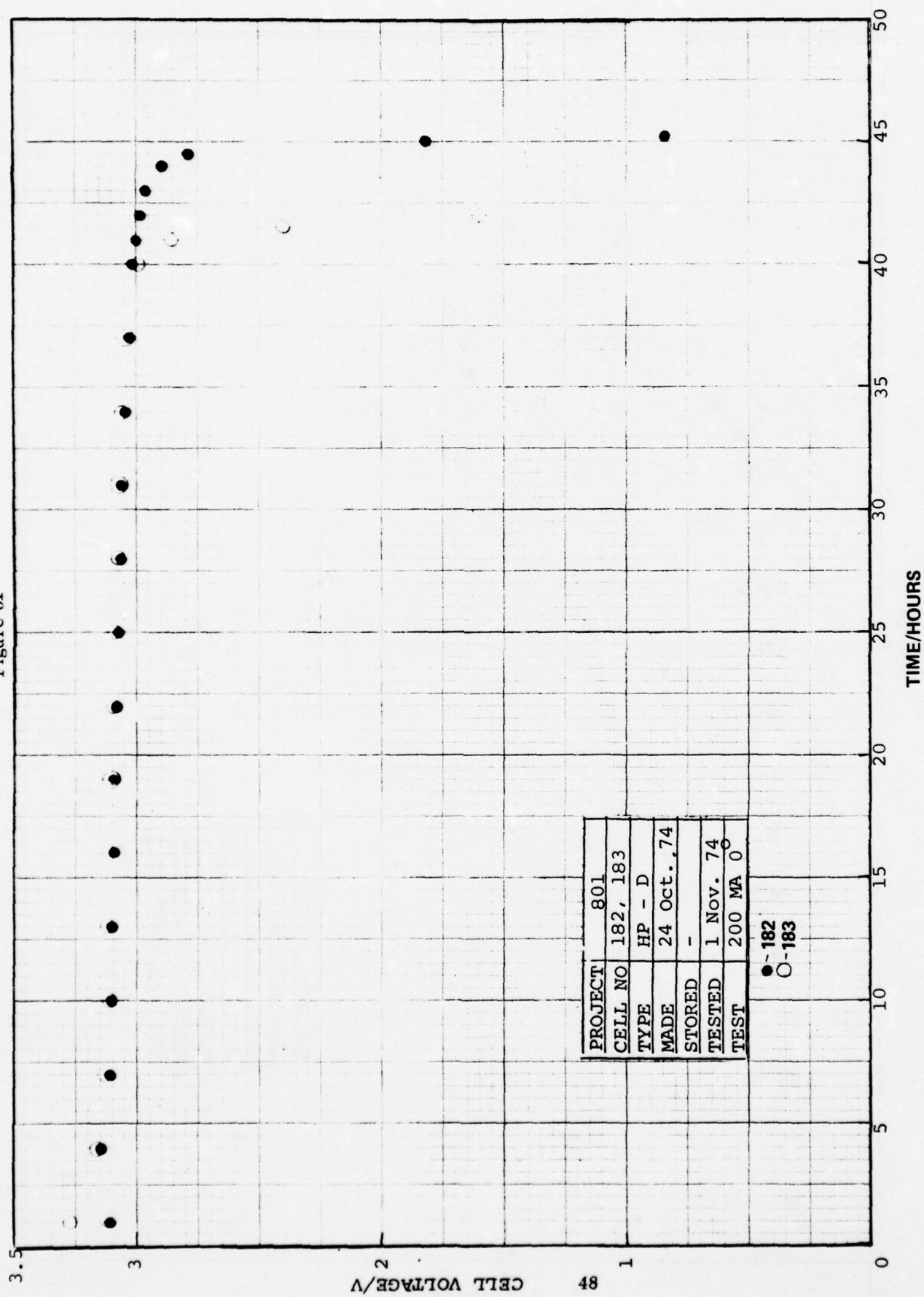
Figure 30



PROJECT	801
CELL NO	170, 171
TYPE	HP - D
MADE	24 Oct., 74
STORED	-
TESTED	30, Oct 74
TEST	500MA -0 C

● - 170
○ - 171

Figure 31



PROJECT	801
CELL NO	182, 183
TYPE	HP - D
MADE	24 Oct., 74
STORED	-
TESTED	1 Nov. 74
TEST	200 MA 0

●-182
○-183

Figure 32

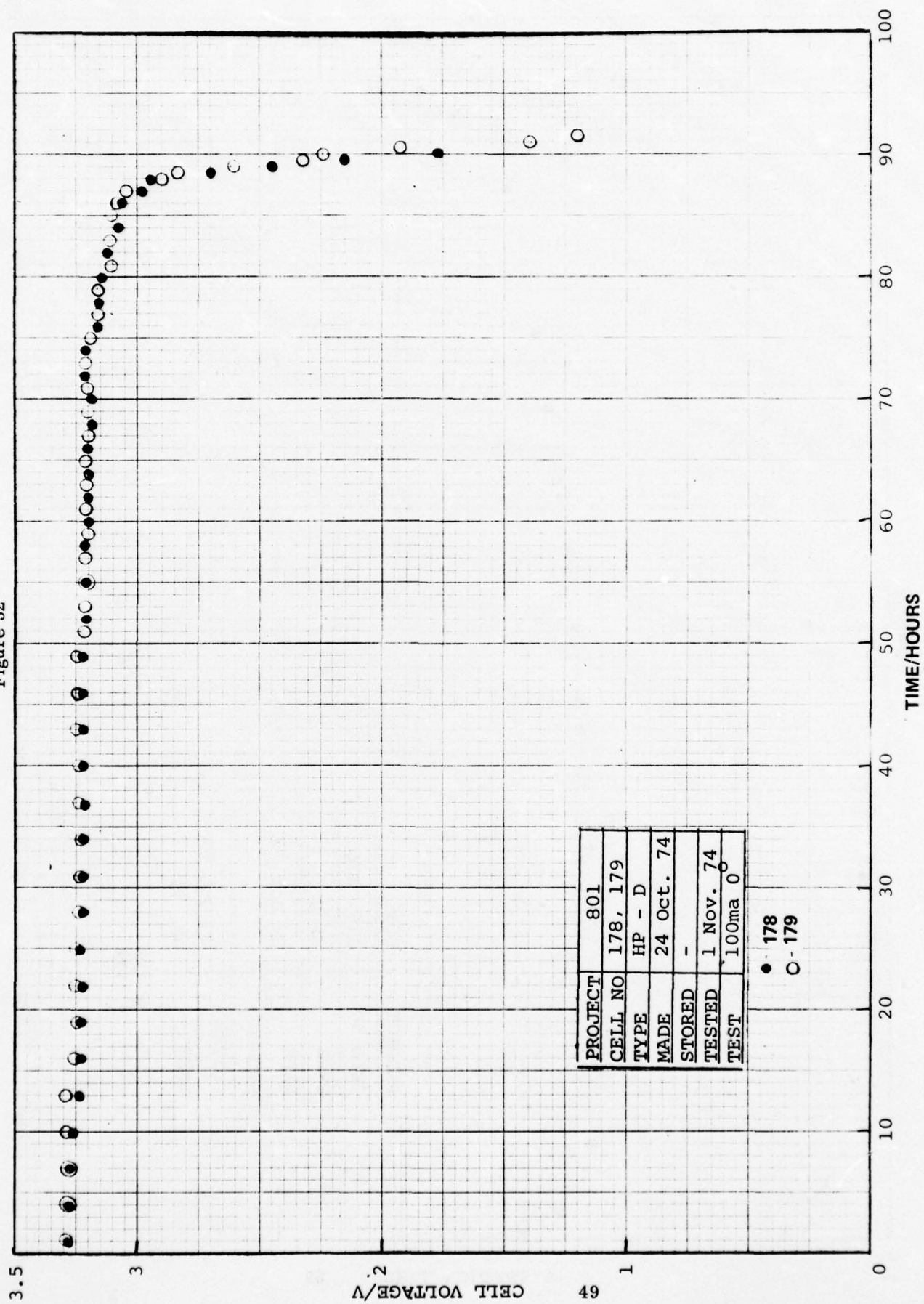


Figure 33

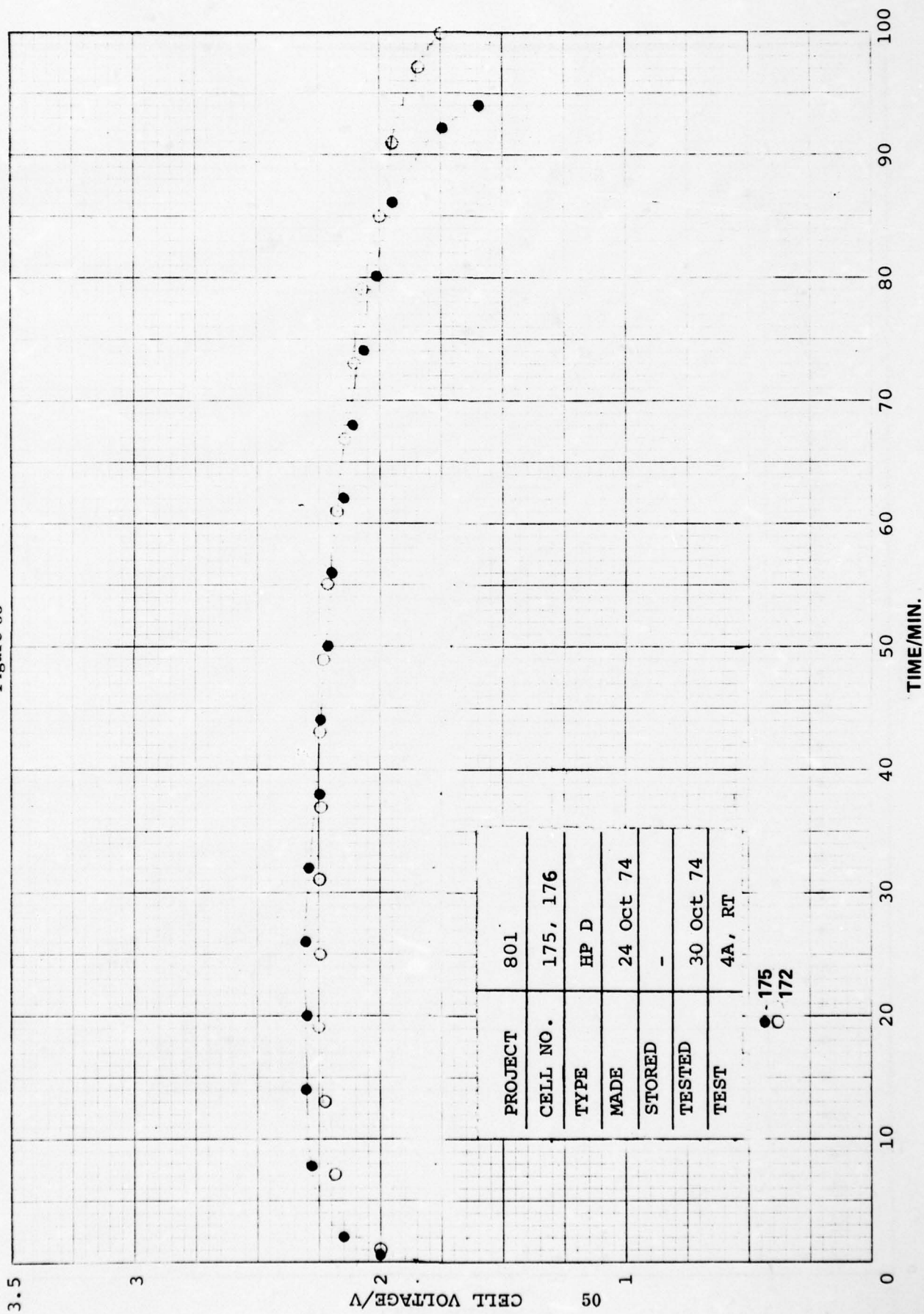


Figure 34

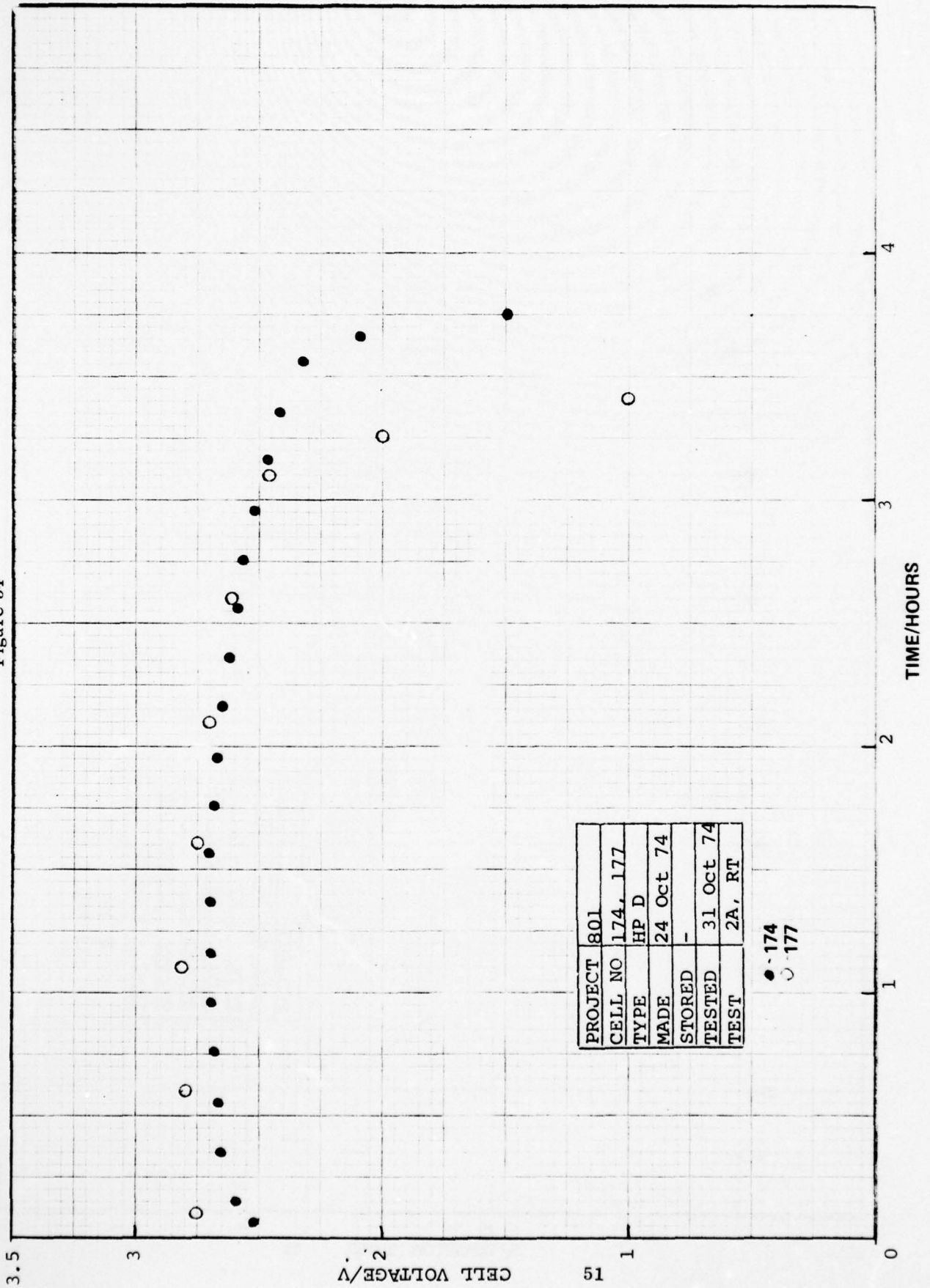
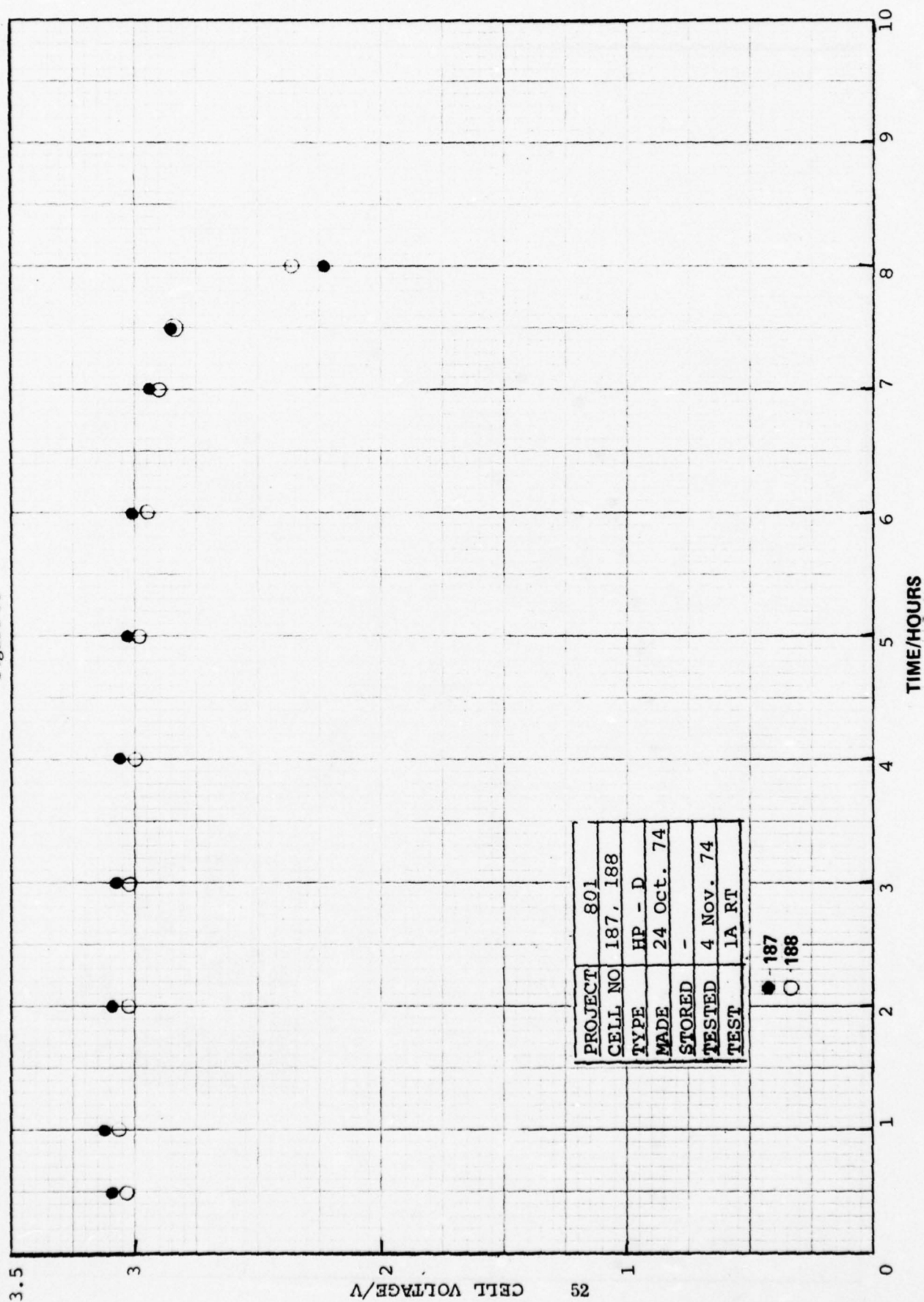


Figure 35



PROJECT	801
CELL NO	187, 188
TYPE	HP - D
MADE	24 Oct. 74
STORED	-
TESTED	4 Nov. 74
TEST	1A RT

● 187
○ 188

Figure 36

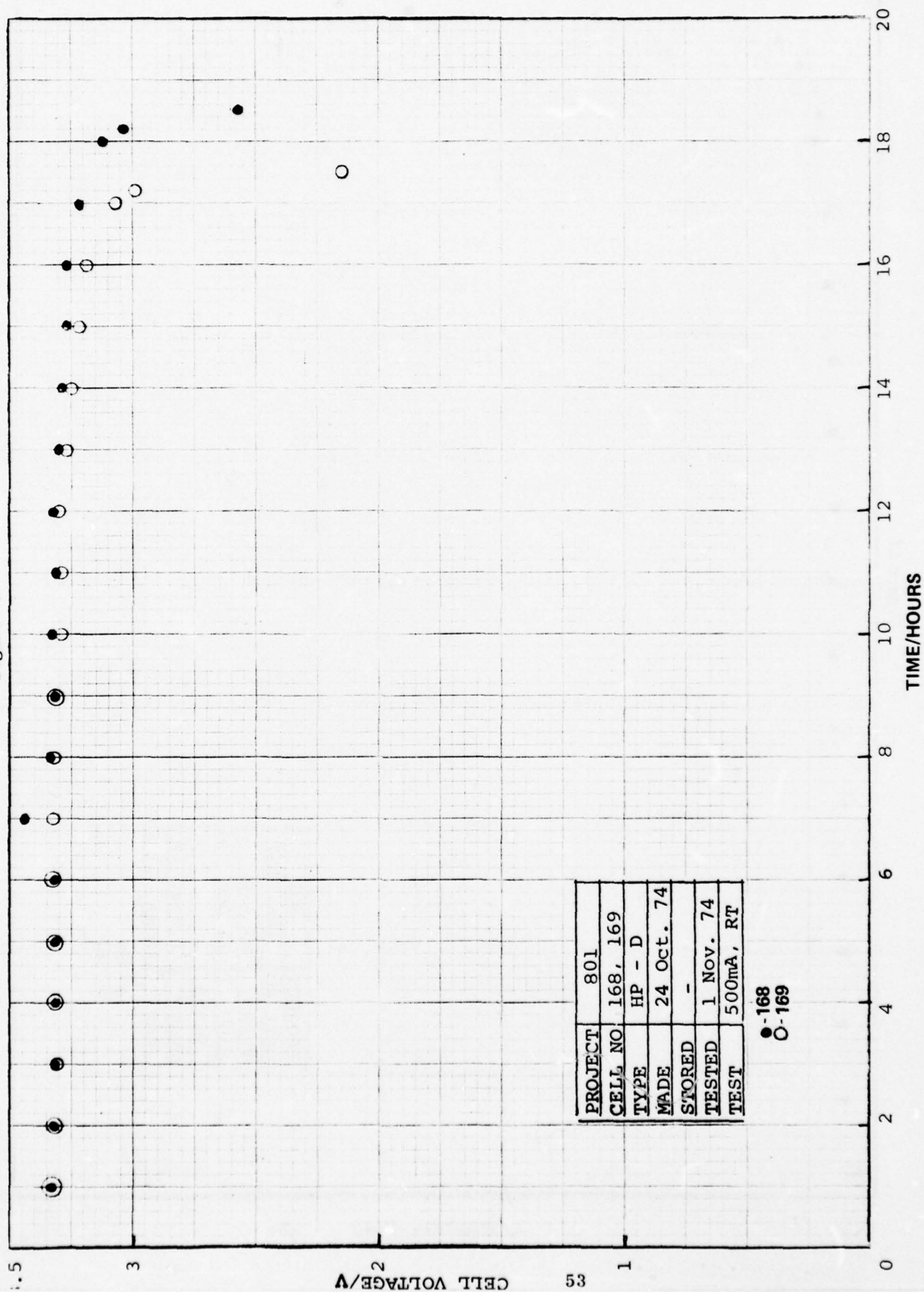


Figure 37

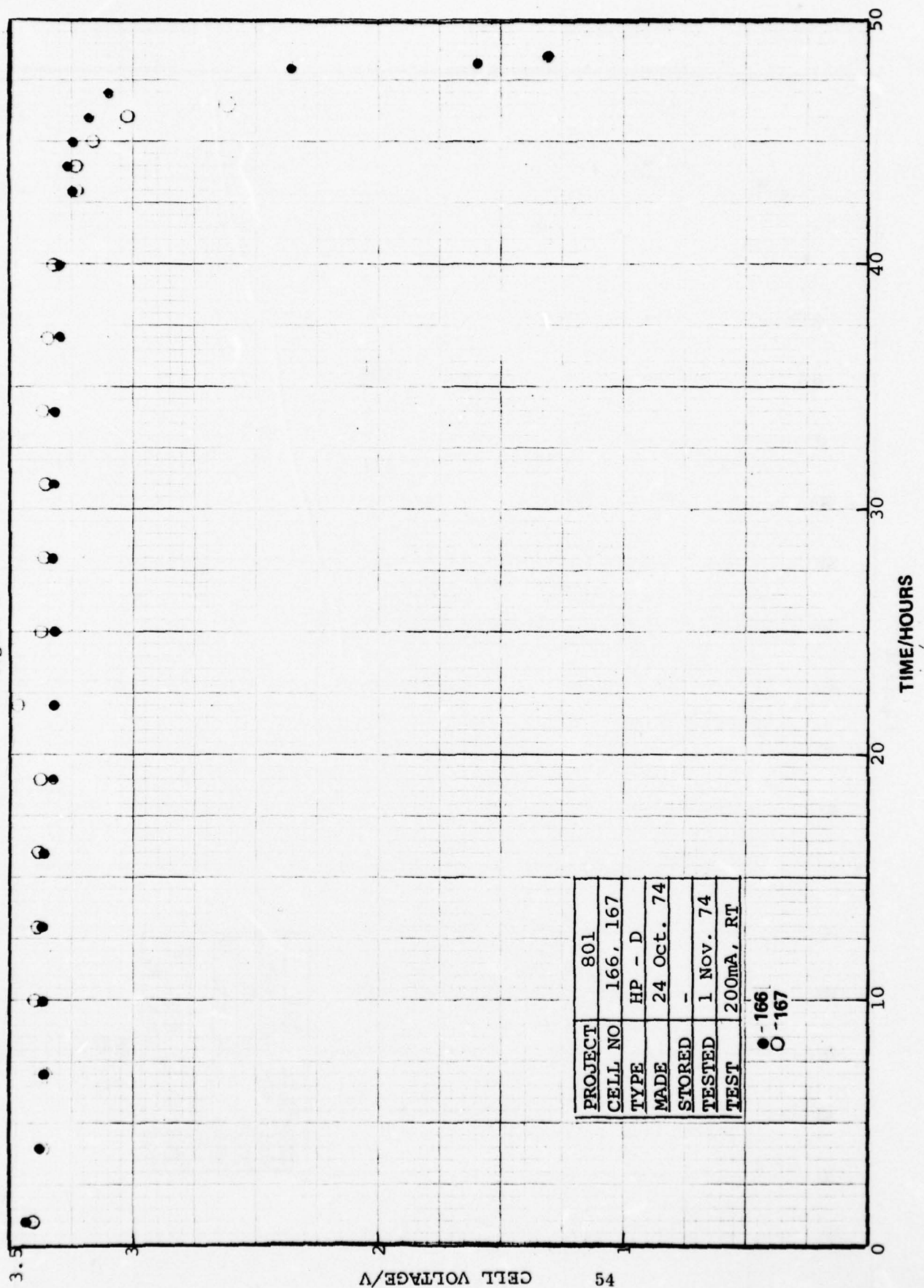


Figure 38

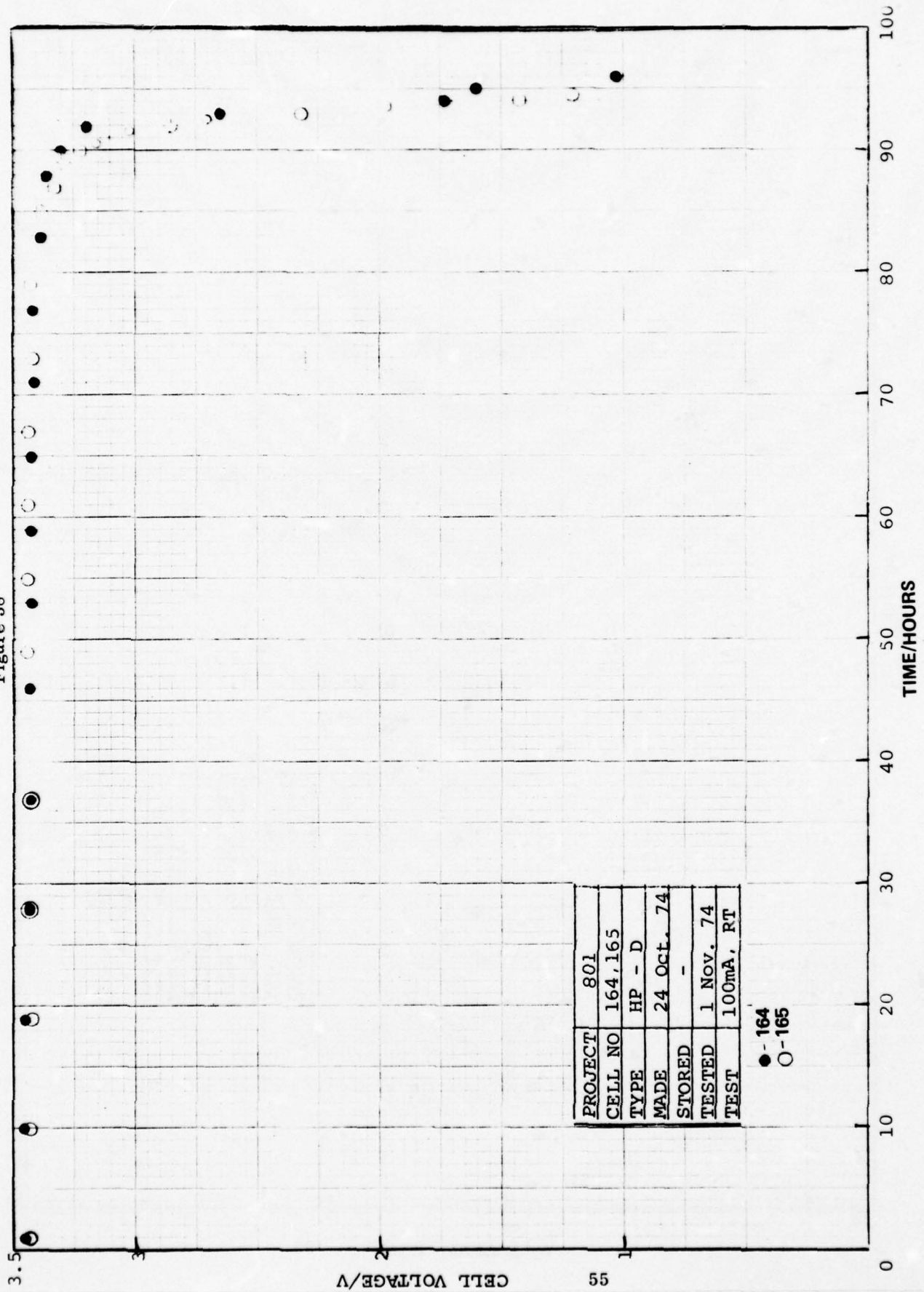


Figure 39

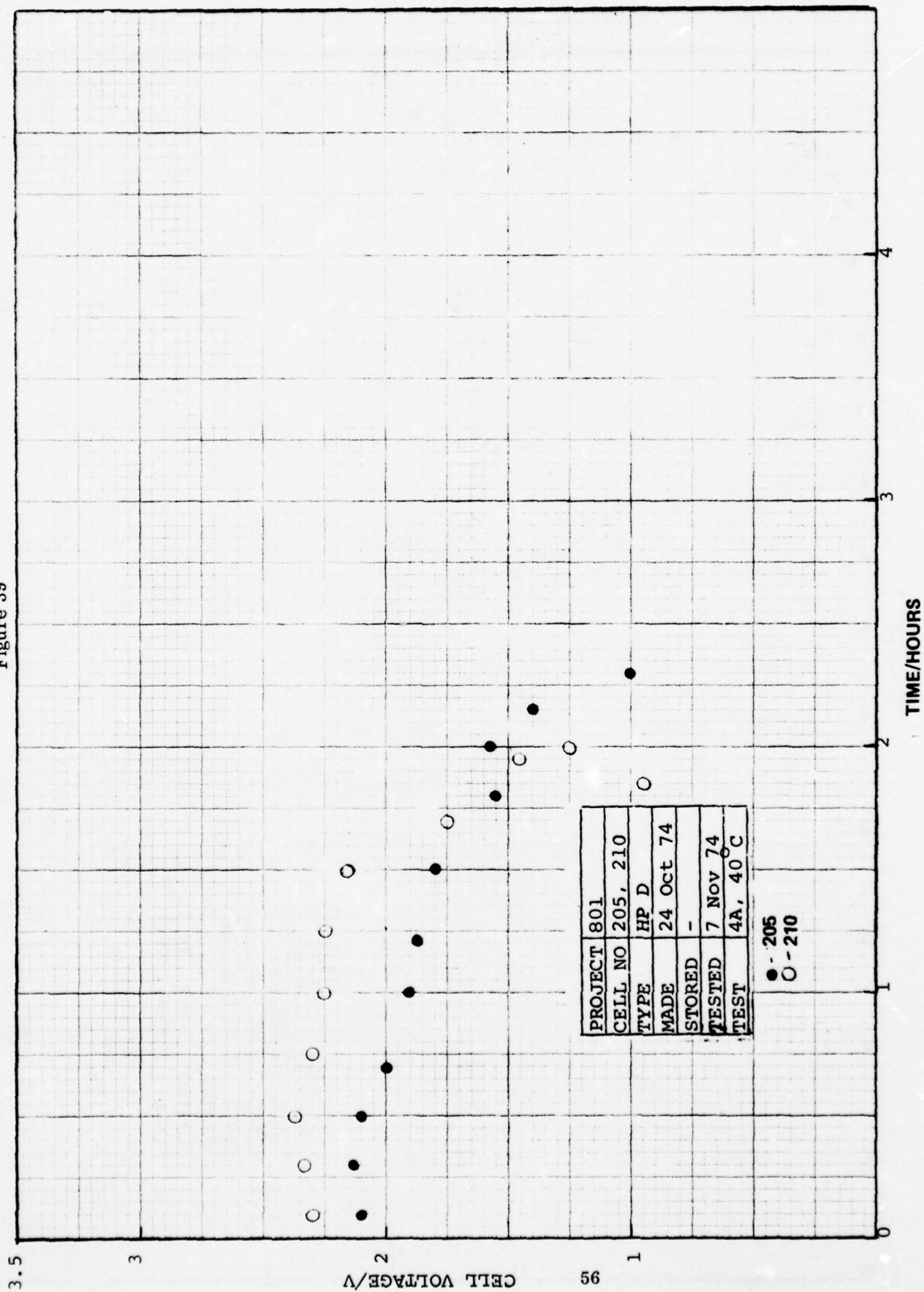


Figure 40

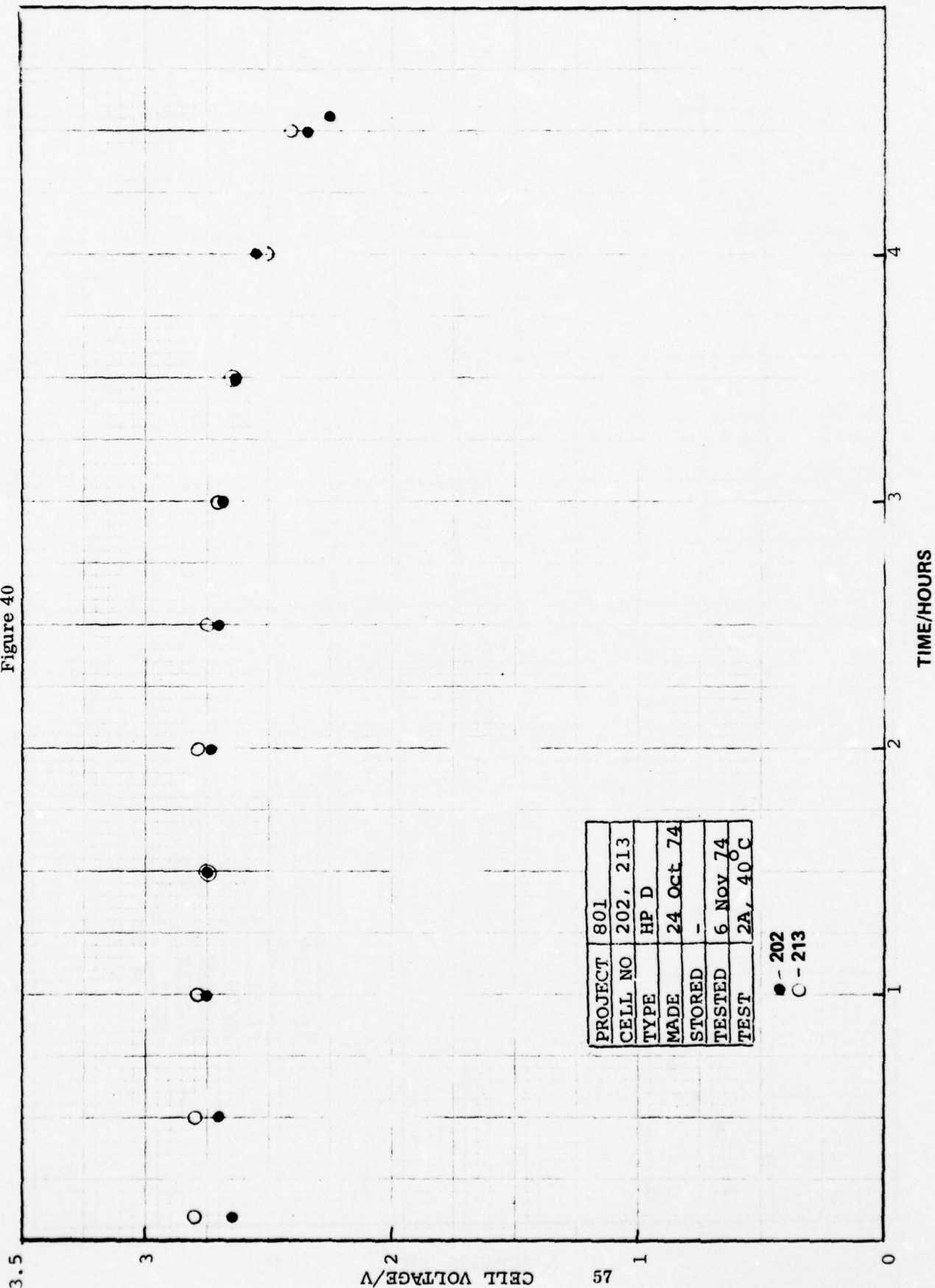
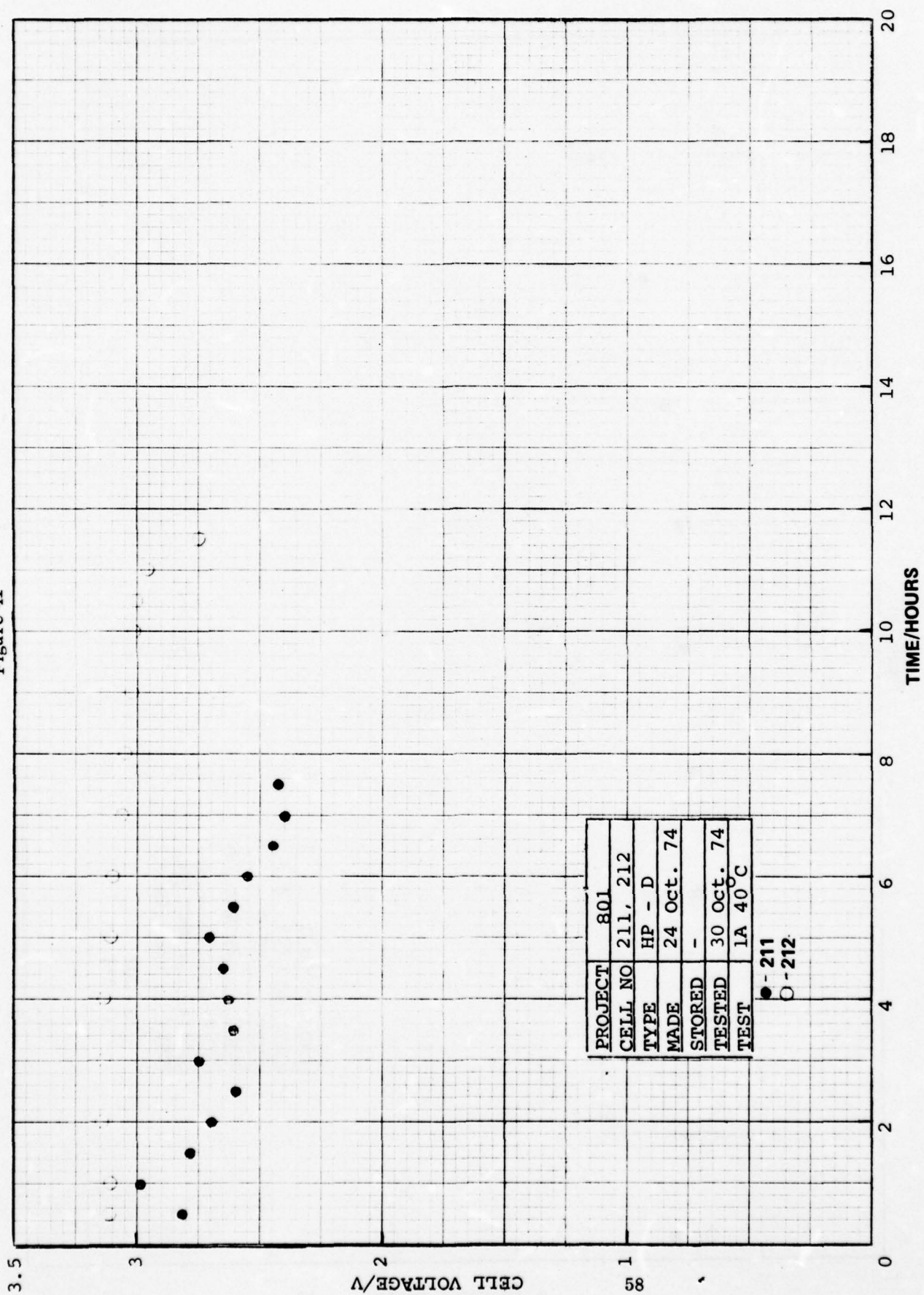


Figure 41

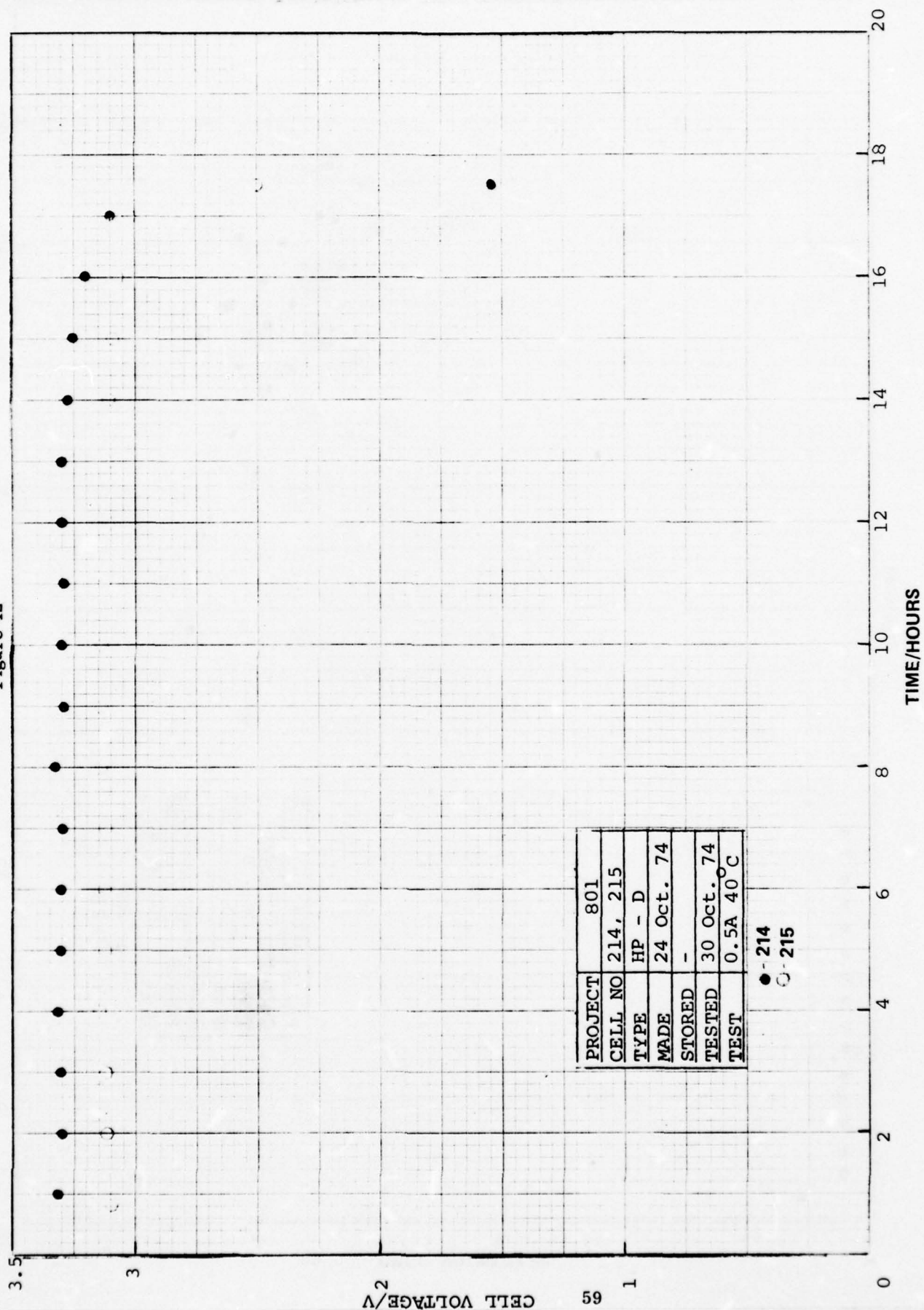


PROJECT	801
CELL NO	211, 212
TYPE	HP - D
MADE	24 Oct. 74
STORED	-
TESTED	30 Oct. 74
TEST	1A 40°C

● - 211

○ - 212

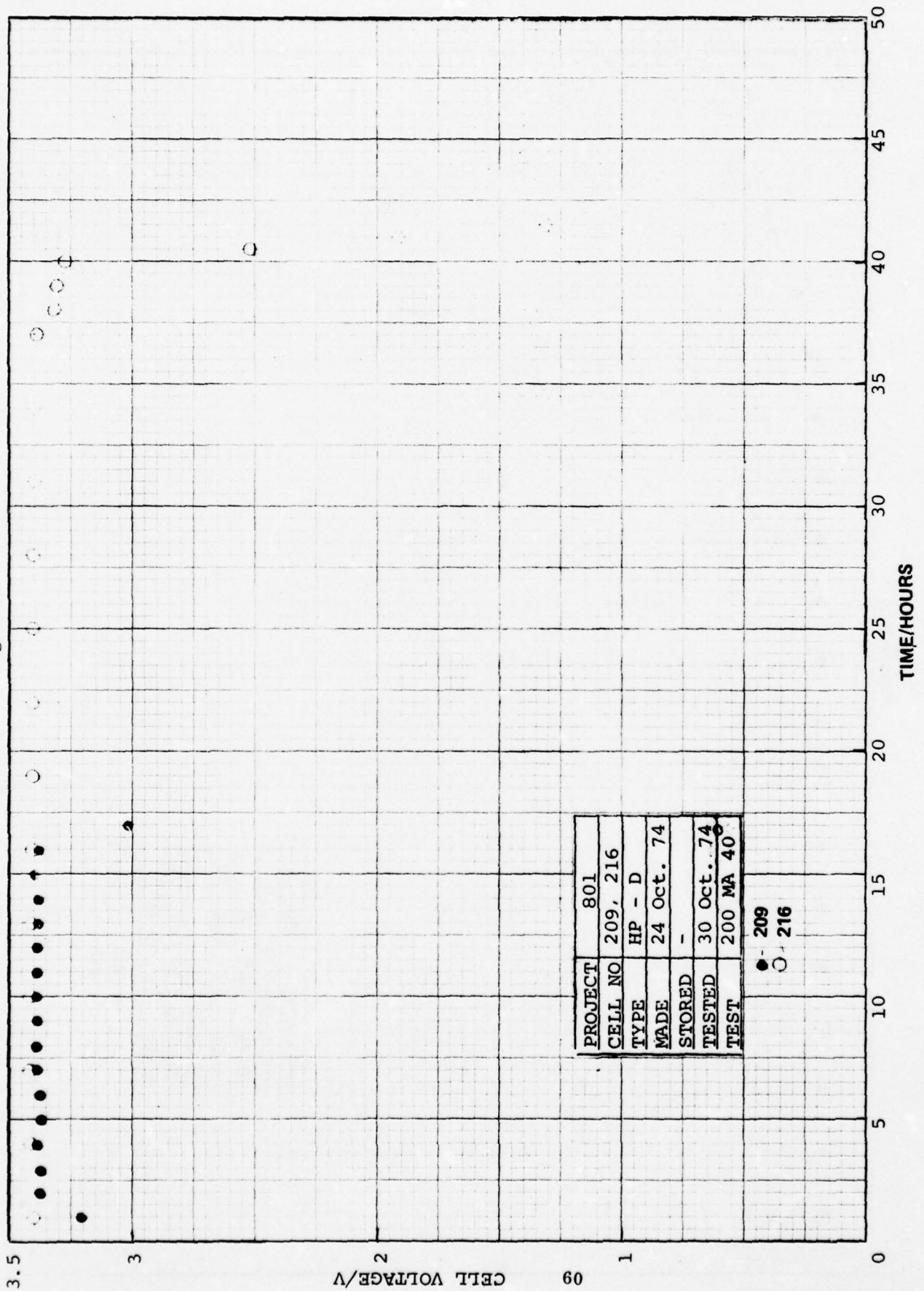
Figure 42



PROJECT	801
CELL NO	214, 215
TYPE	HP - D
MADE	24 Oct. 74
STORED	-
TESTED	30 Oct. 74
TEST	0.5A 40°C

● - 214
○ - 215

Figure 43



PROJECT	801
CELL NO	209, 216
TYPE	HP - D
MADE	24 Oct. 74
STORED	-
TESTED	30 Oct. 74
TEST	200 MA 40

● - 209
○ - 216

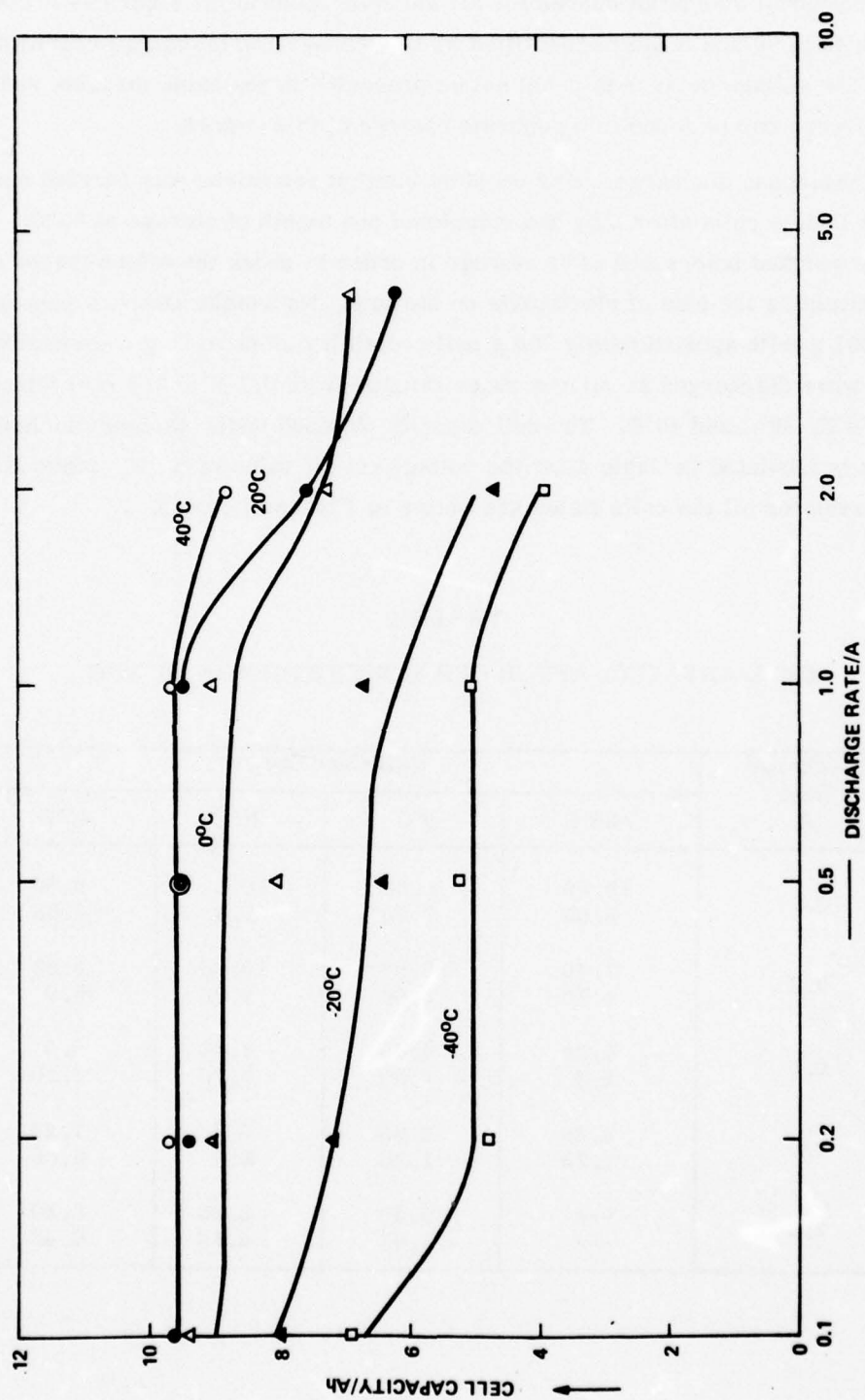


Figure 44. Capacity-Rate Behavior of Lithium/SOCl₂ Cells After One Month at Room Temperature

Individual discharge curves for all the cells included in Figure 44 are shown in Figures 45 to 70 and could be identified by the storage and discharge conditions indicated. The voltage delay data could not be presented in the same diagram and the relevant figures can be found in a separate chapter of this report.

Continuous discharge under constant current conditions was carried out on a number of D-size cells after they had completed one month of storage at 55°C. The cells were weighed before and after storage in order to check the effectiveness of the seal in preventing the loss of electrolyte on storage. No weight loss was measurable within 0.001 g with approximately 100 g cell containing close to 50 g of electrolyte. The cells were discharged at various rates ranging from 0.1 A to 2.0 A at temperatures of -20°C, 0°C, 20°C and 40°C. The cell capacity obtained under various discharge conditions is tabulated in Table 4 for the voltage cut off value of 2.0V. Individual discharge curves for all the cells listed are shown in Figures 71 to 90.

TABLE 4
CELL CAPACITY AFTER ONE MONTH STORAGE AT 55°C

Discharge Rate A	Cell Capacity at			
	-20°C	0°C	20°C	40°C
0.1	10.30	9.30	10.6	9.80
	8.00	7.20	9.6	9.65
0.2	7.40	10.00	10.05	8.80
	4.70	9.50	9.00	8.0
0.5	6.50	4.45	7.40	8.0
	5.4	4.30	5.75	7.10
1.0	4.20	2.00	8.2	7.25
	1.75	1.00	6.6	6.60
2.0	---	2.50	5.40	6.80
	---	1.86	4.70	6.40

Figure 45

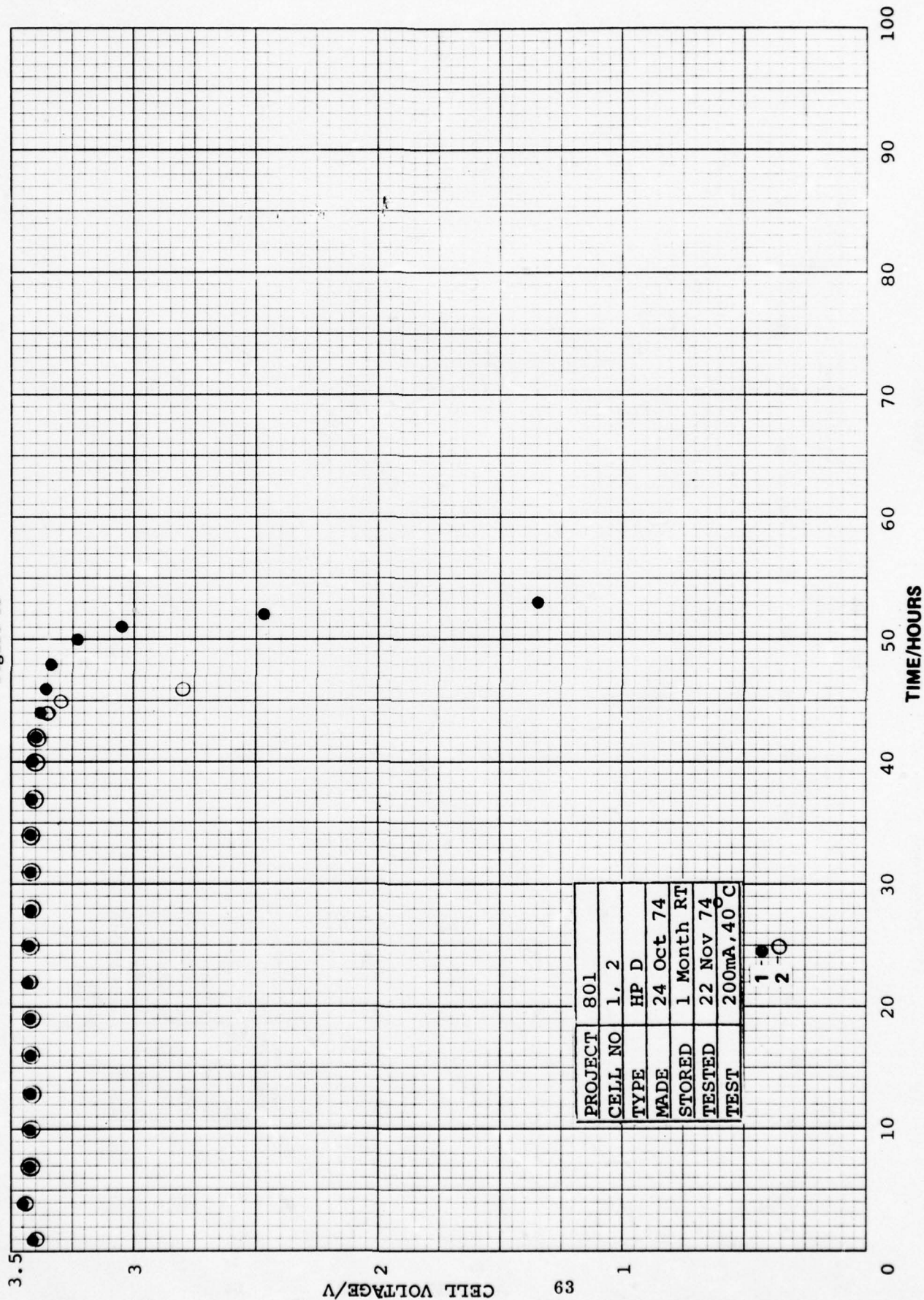
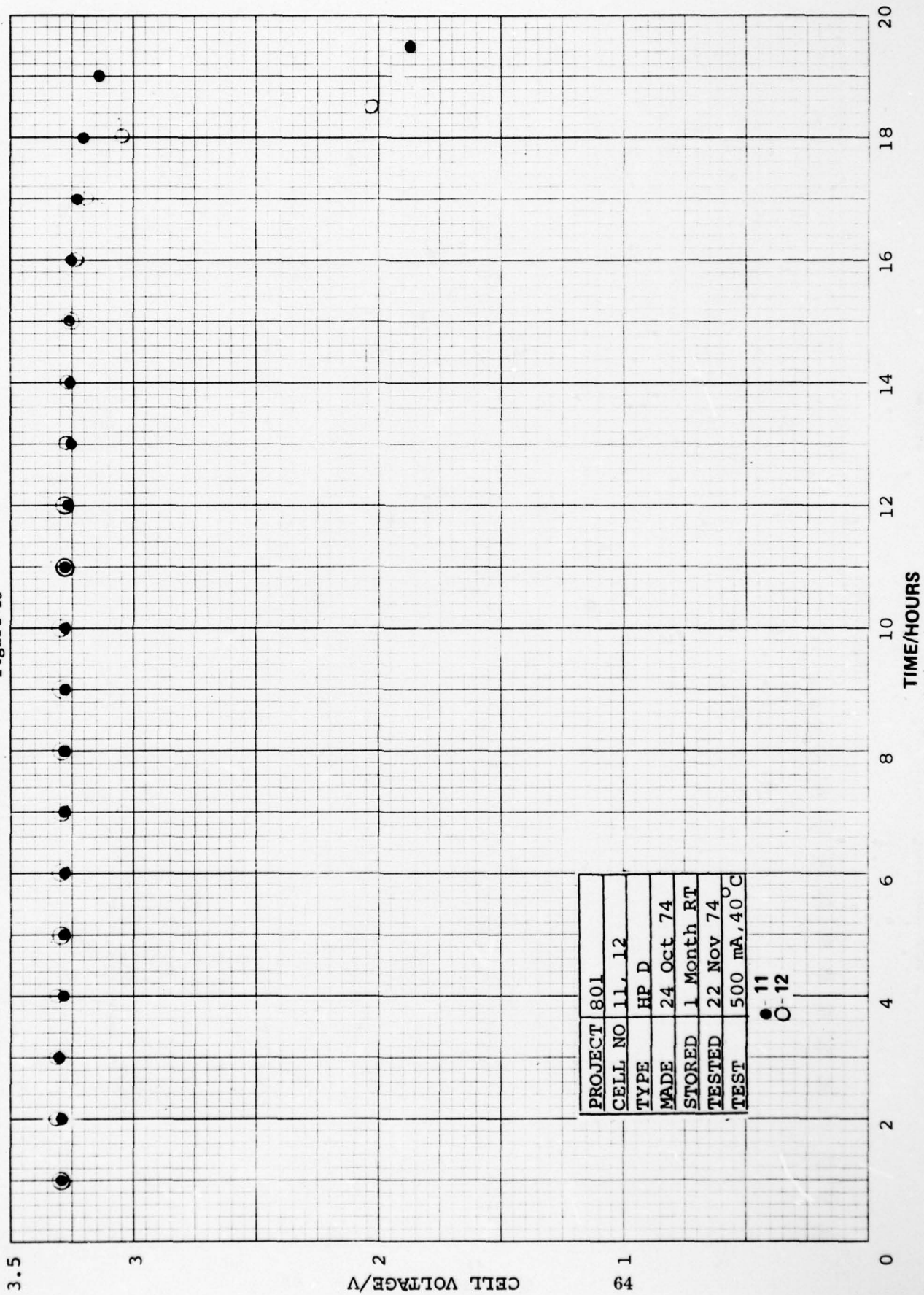


Figure 46



PROJECT	801
CELL NO	11, 12
TYPE	HP D
MADE	24 Oct 74
STORED	1 Month RT
TESTED	22 Nov 74
TEST	500 mA, 40 °C

● 11
○ 12

Figure 47

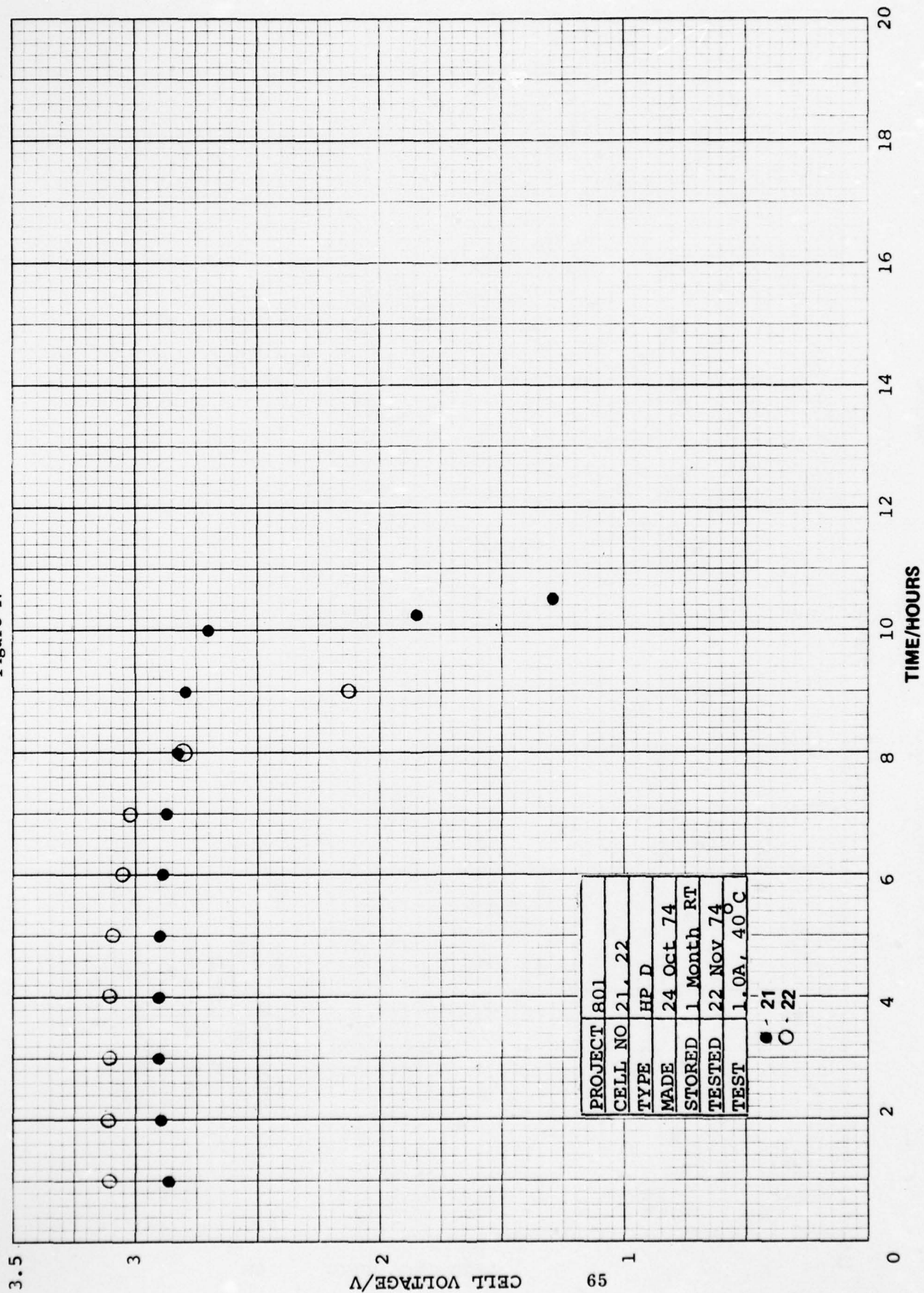


Figure 48

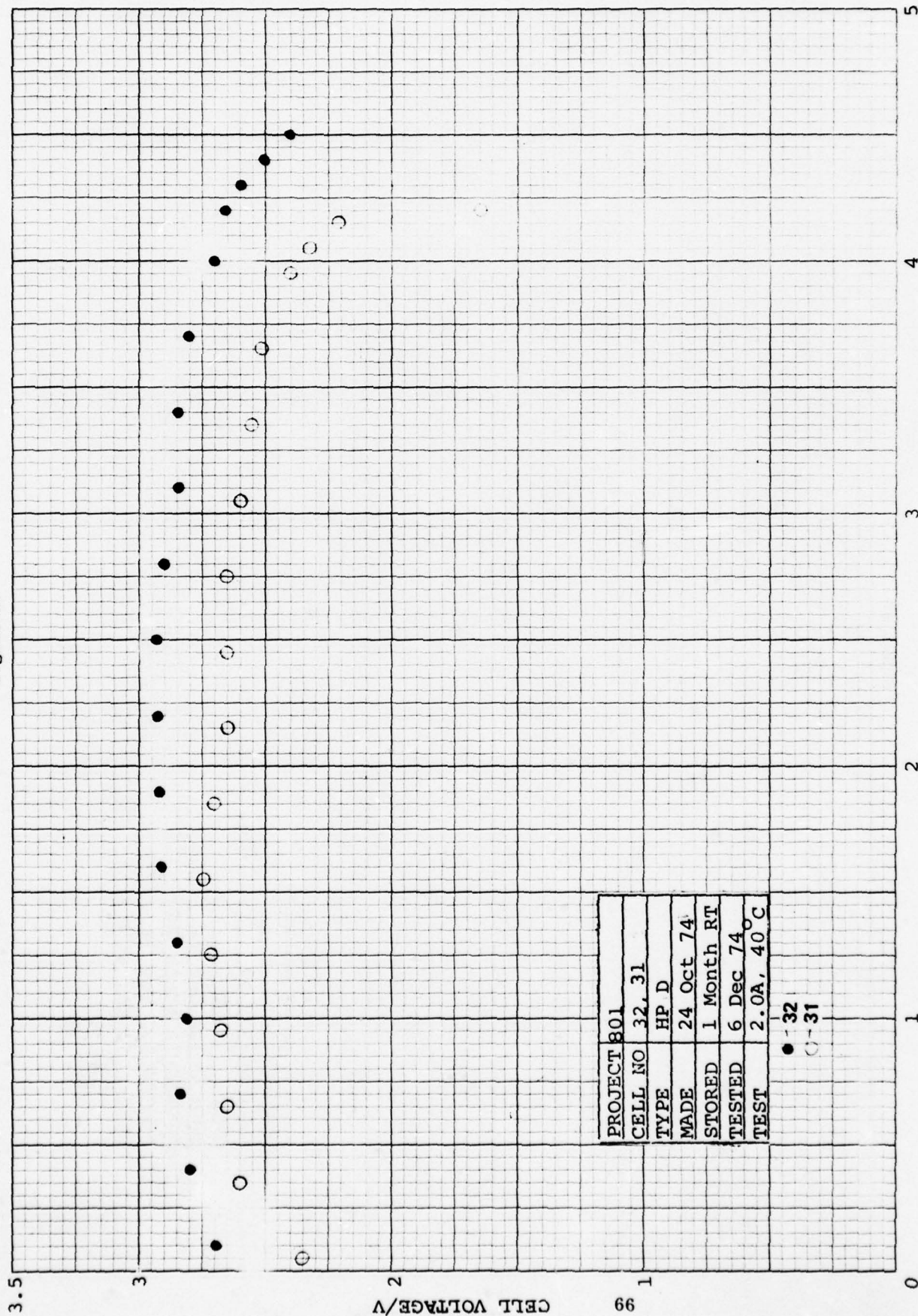


Figure 49

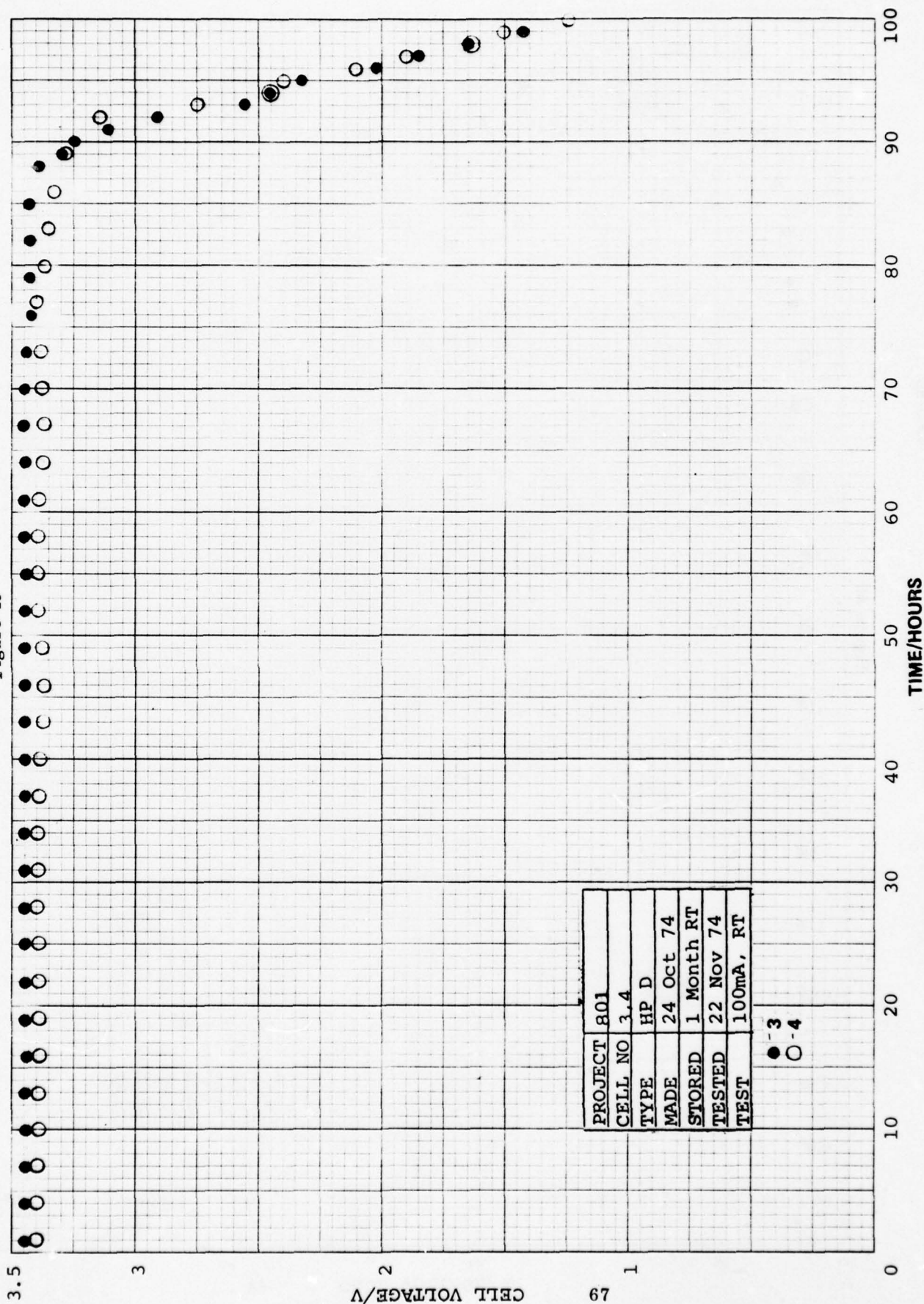
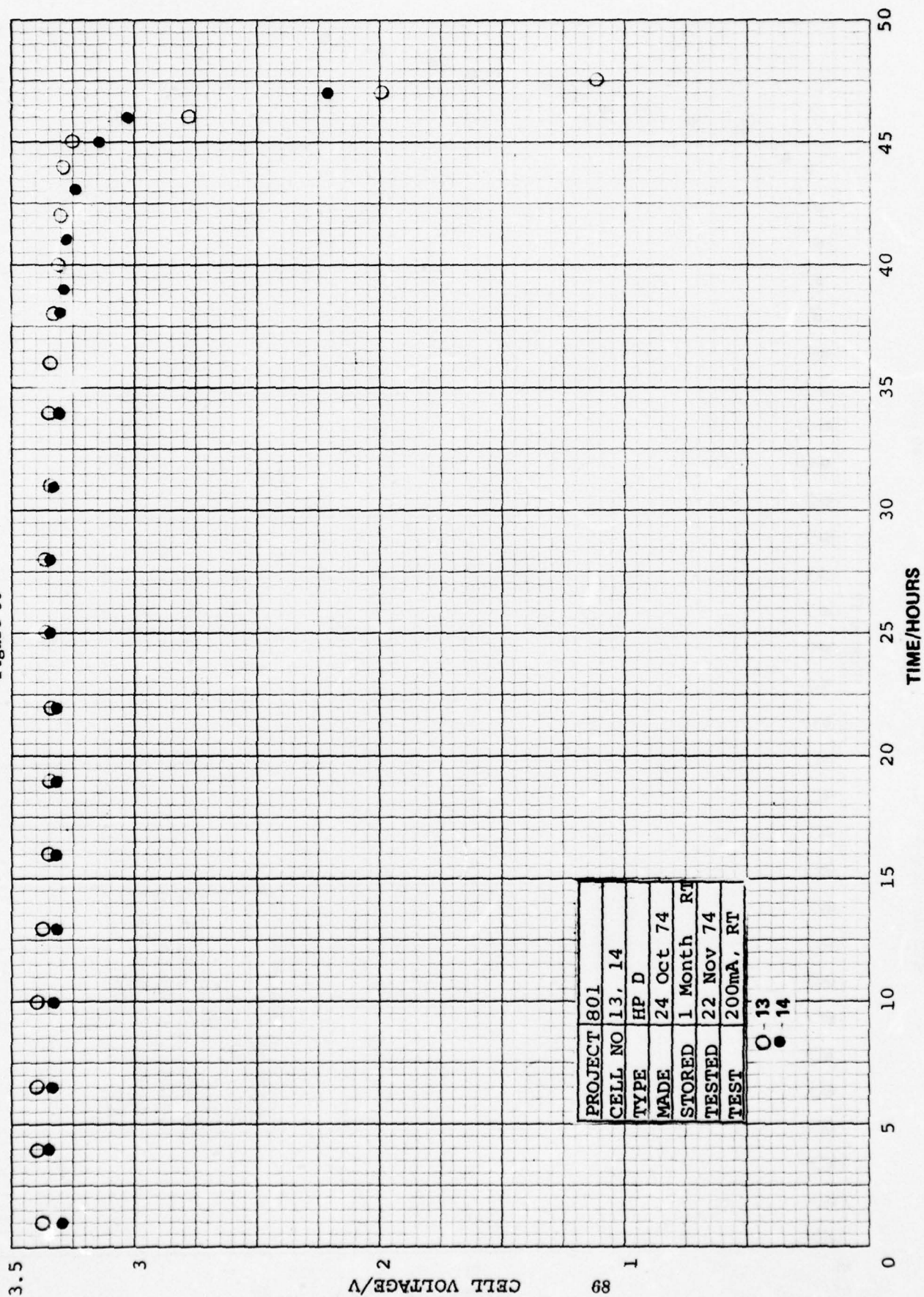


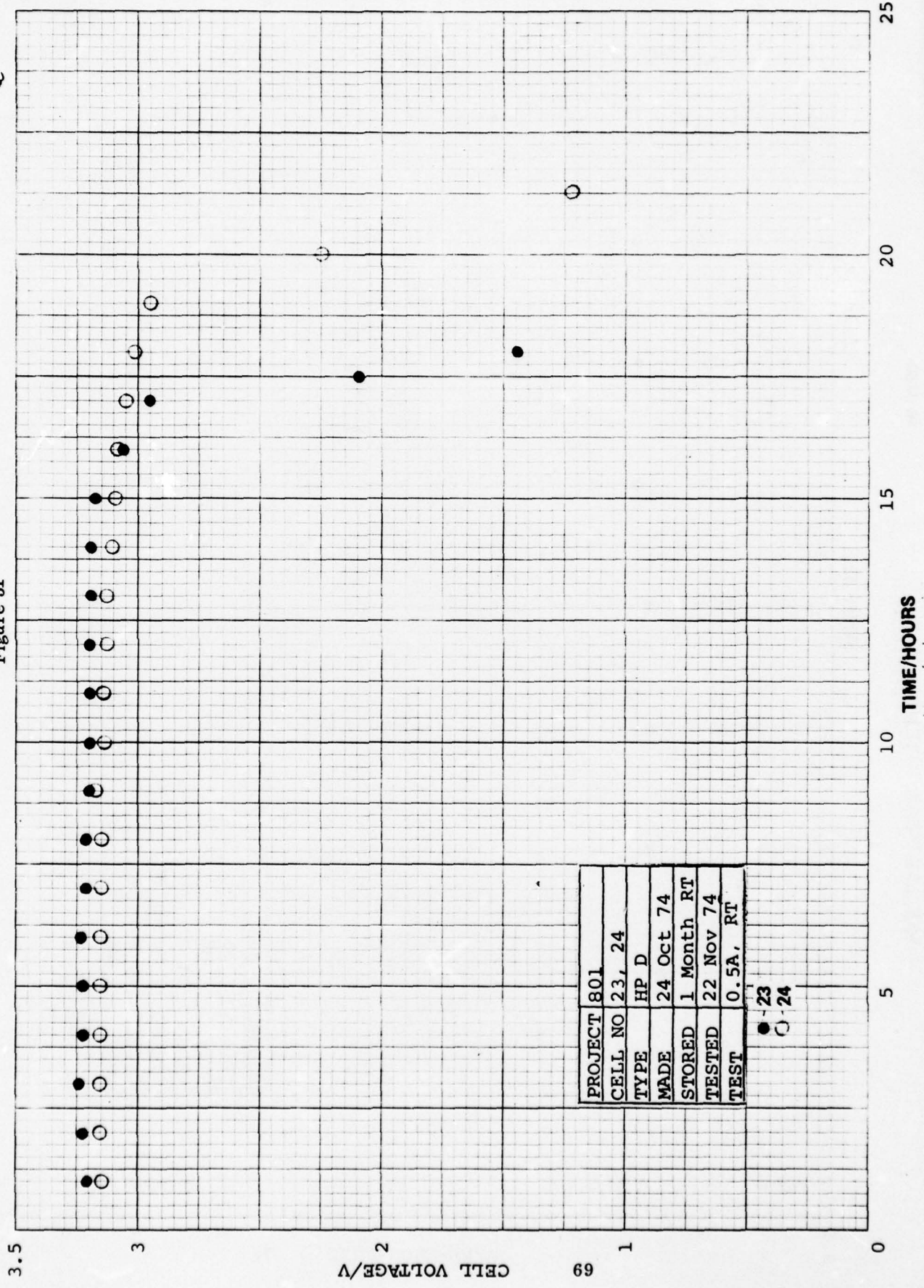
Figure 50



PROJECT	801
CELL NO	13, 14
TYPE	HP D
MADE	24 Oct 74
STORED	1 Month RT
TESTED	22 Nov 74
TEST	200mA, RT

O-13
●-14

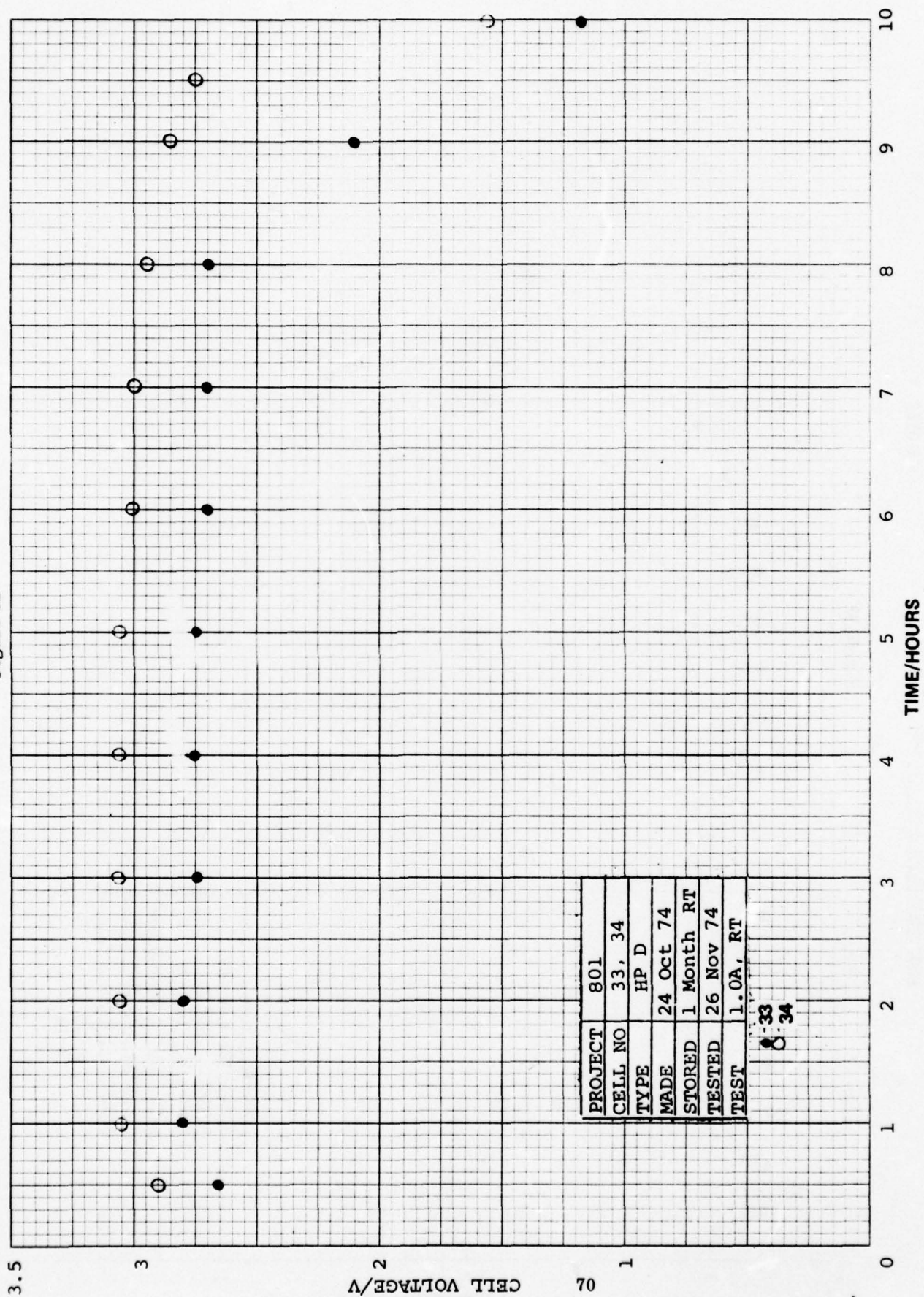
Figure 51



PROJECT	801
CELL NO	23, 24
TYPE	HP D
MADE	24 Oct 74
STORED	1 Month RT
TESTED	22 Nov 74
TEST	0.5A, RT

● - 23
○ - 24

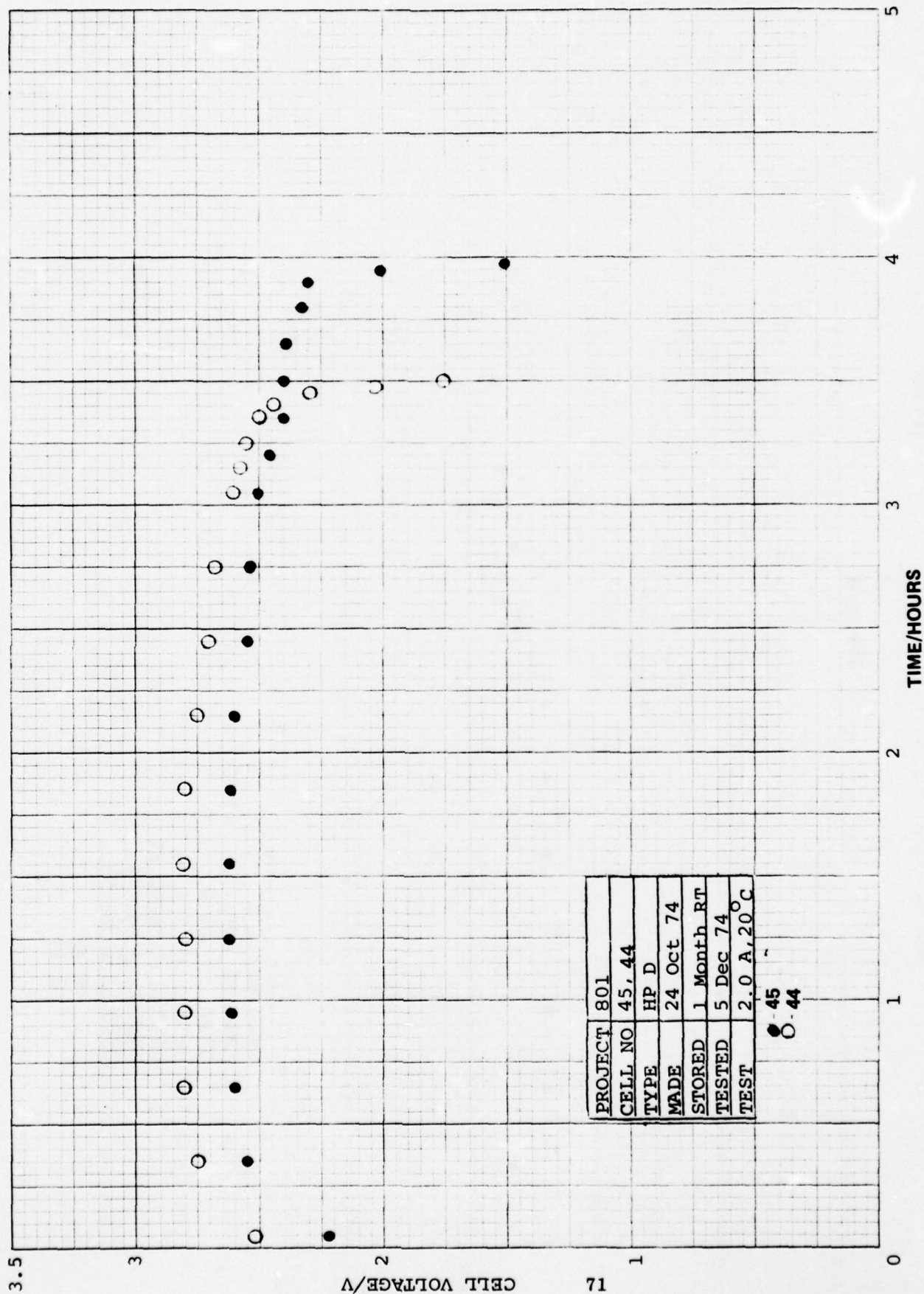
Figure 52



PROJECT	801
CELL NO	33, 34
TYPE	HP D
MADE	24 Oct 74
STORED	1 Month RT
TESTED	26 Nov 74
TEST	1.0A, RT

8:33
8:34

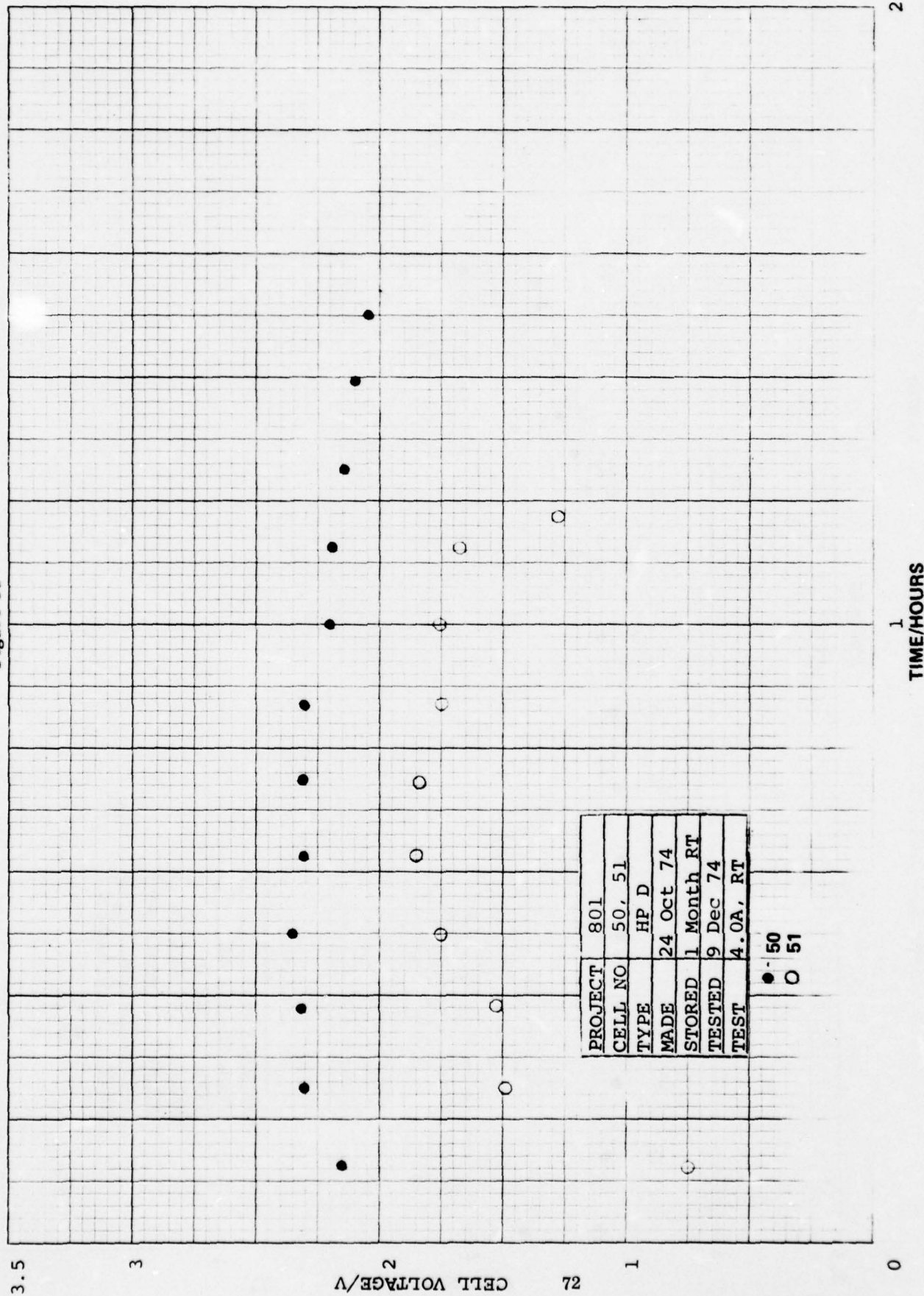
Figure 53



PROJECT	801
CELL NO	45.44
TYPE	HP D
MADE	24 Oct 74
STORED	1 Month RT
TESTED	5 Dec 74
TEST	2.0 A, 20°C

● 45
O 44

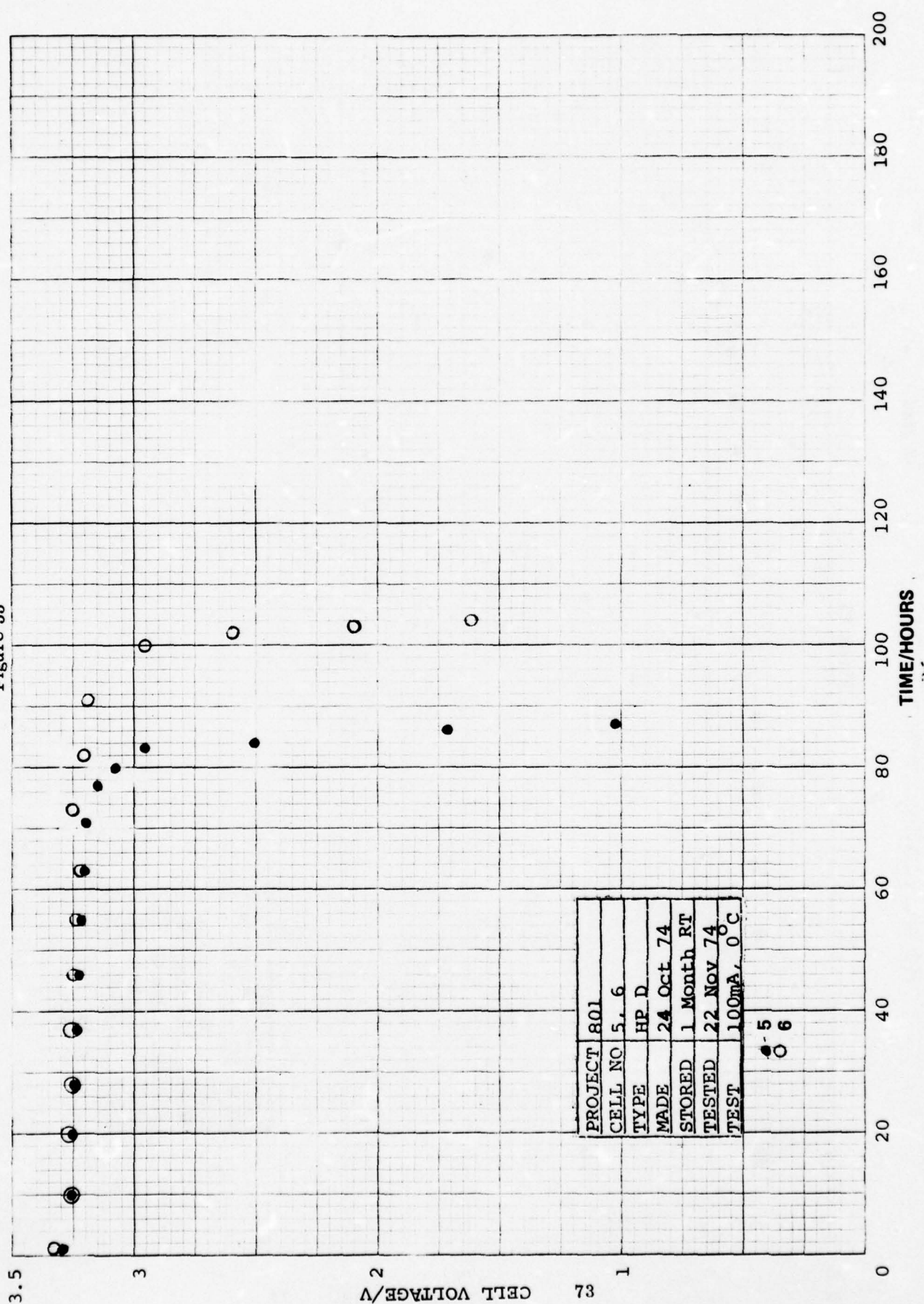
Figure 54



PROJECT	801
CELL NO	50, 51
TYPE	HP D
MADE	24 Oct 74
STORED	1 Month RT
TESTED	9 Dec 74
TEST	4.0A, RT

● 50
○ 51

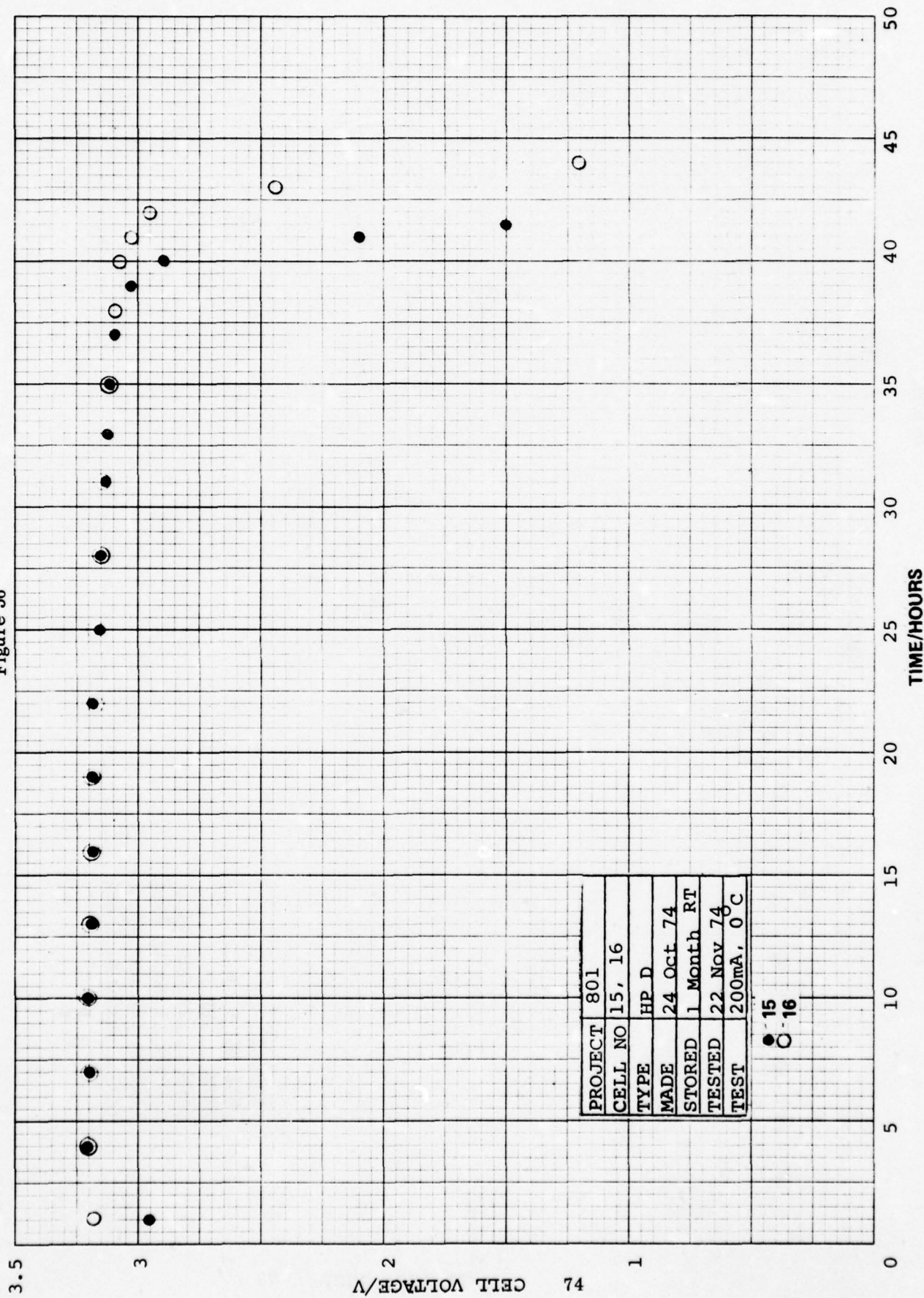
Figure 55



PROJECT	801
CELL NO	5, 6
TYPE	HP D
MADE	24 Oct 74
STORED	1 Month RT
TESTED	22 Nov 74
TEST	100mA, 0°C

4-5
0 6

Figure 56



PROJECT	801
CELL NO	15, 16
TYPE	HP D
MADE	24 Oct 74
STORED	1 Month RT
TESTED	22 Nov 74
TEST	200mA, 0°C

● 15
○ 16

Figure 57

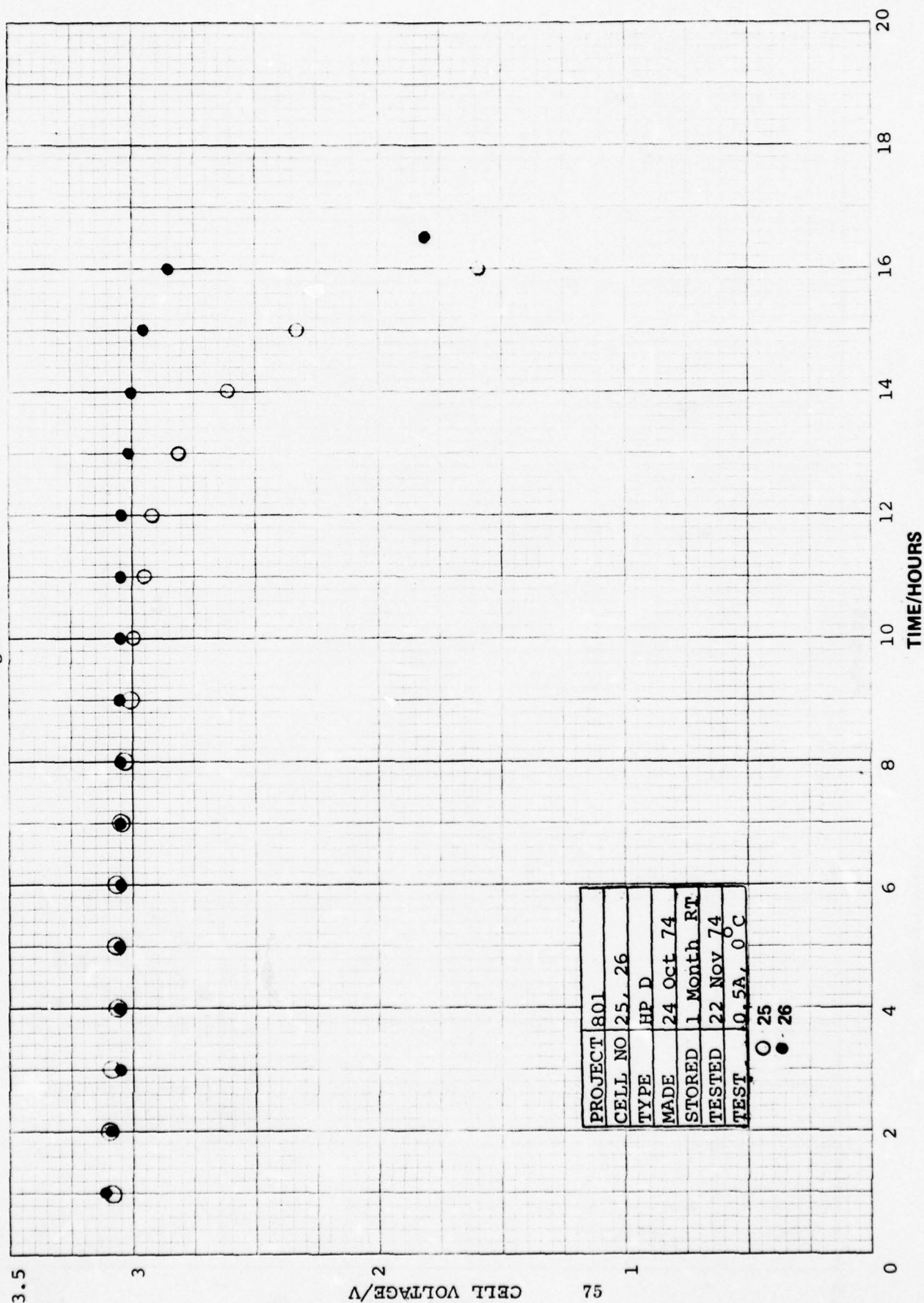
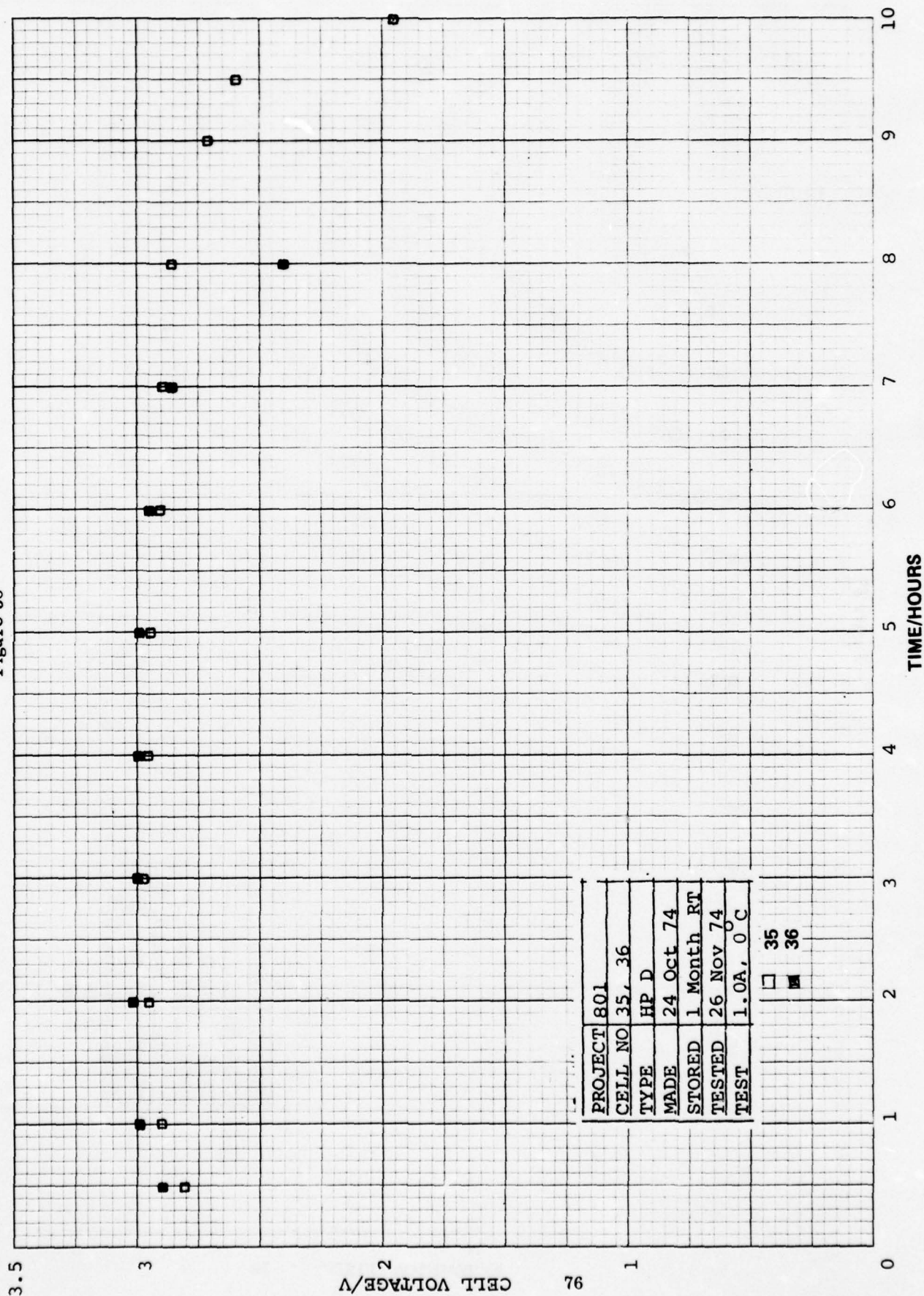


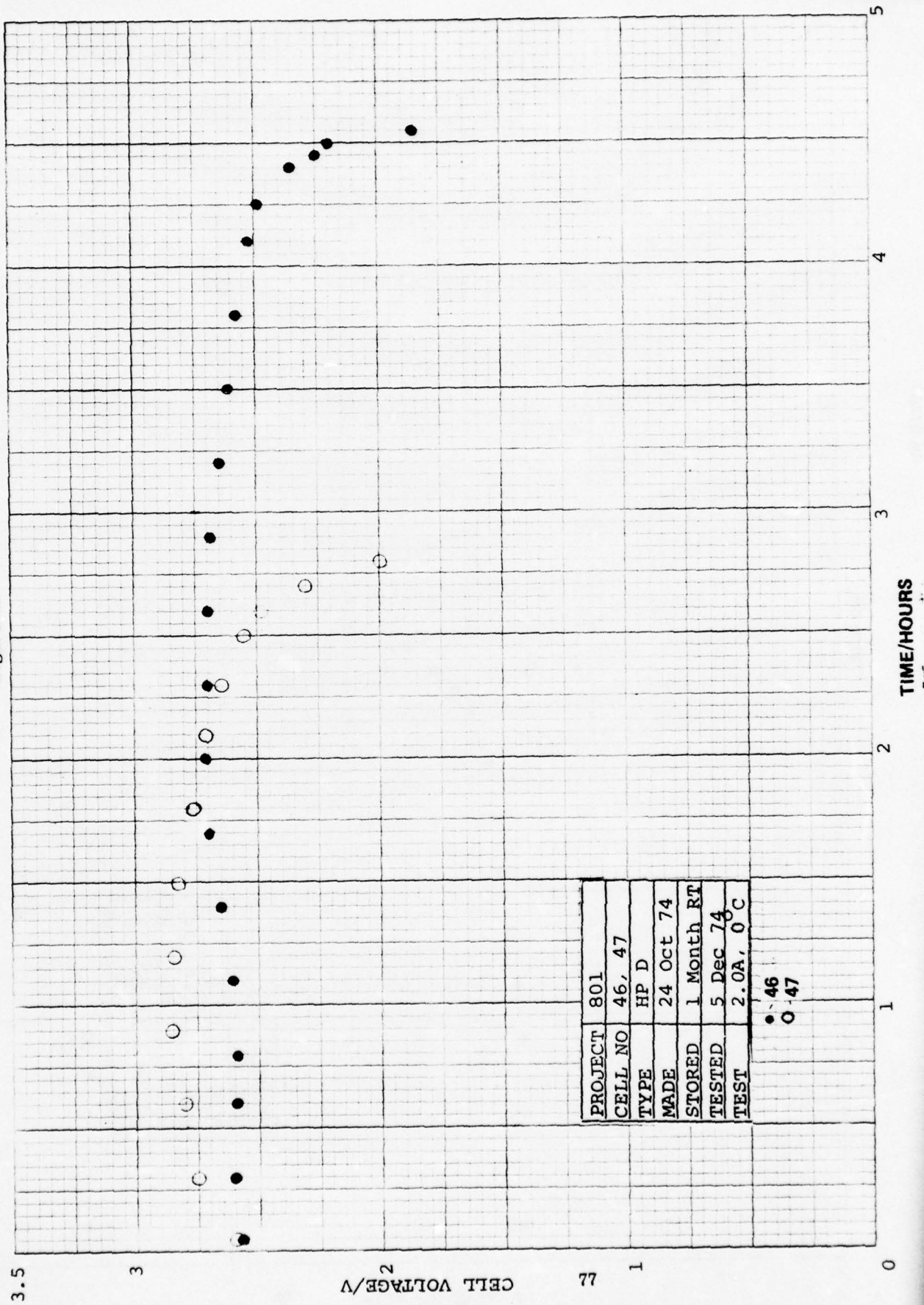
Figure 58



PROJECT	801
CELL NO	35, 36
TYPE	HP D
MADE	24 Oct 74
STORED	1 Month RT
TESTED	26 Nov 74
TEST	1.0A, 0 C

□	35
■	36

Figure 59



PROJECT	801
CELL NO	46, 47
TYPE	HP D
MADE	24 Oct 74
STORED	1 Month RT
TESTED	5 Dec 74
TEST	2.0A, 0°C

• 46
○ 47

Figure 60

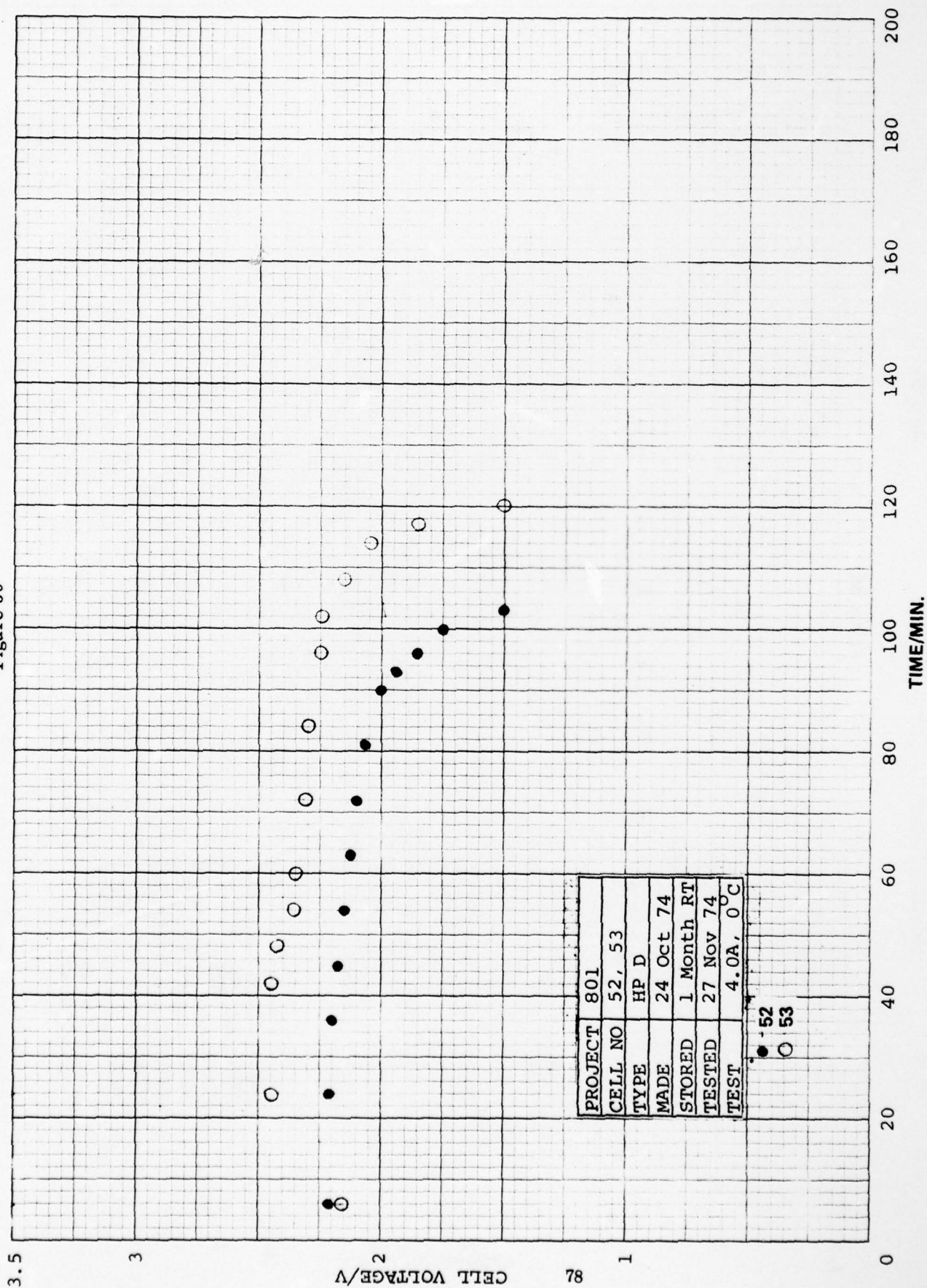


Figure 61

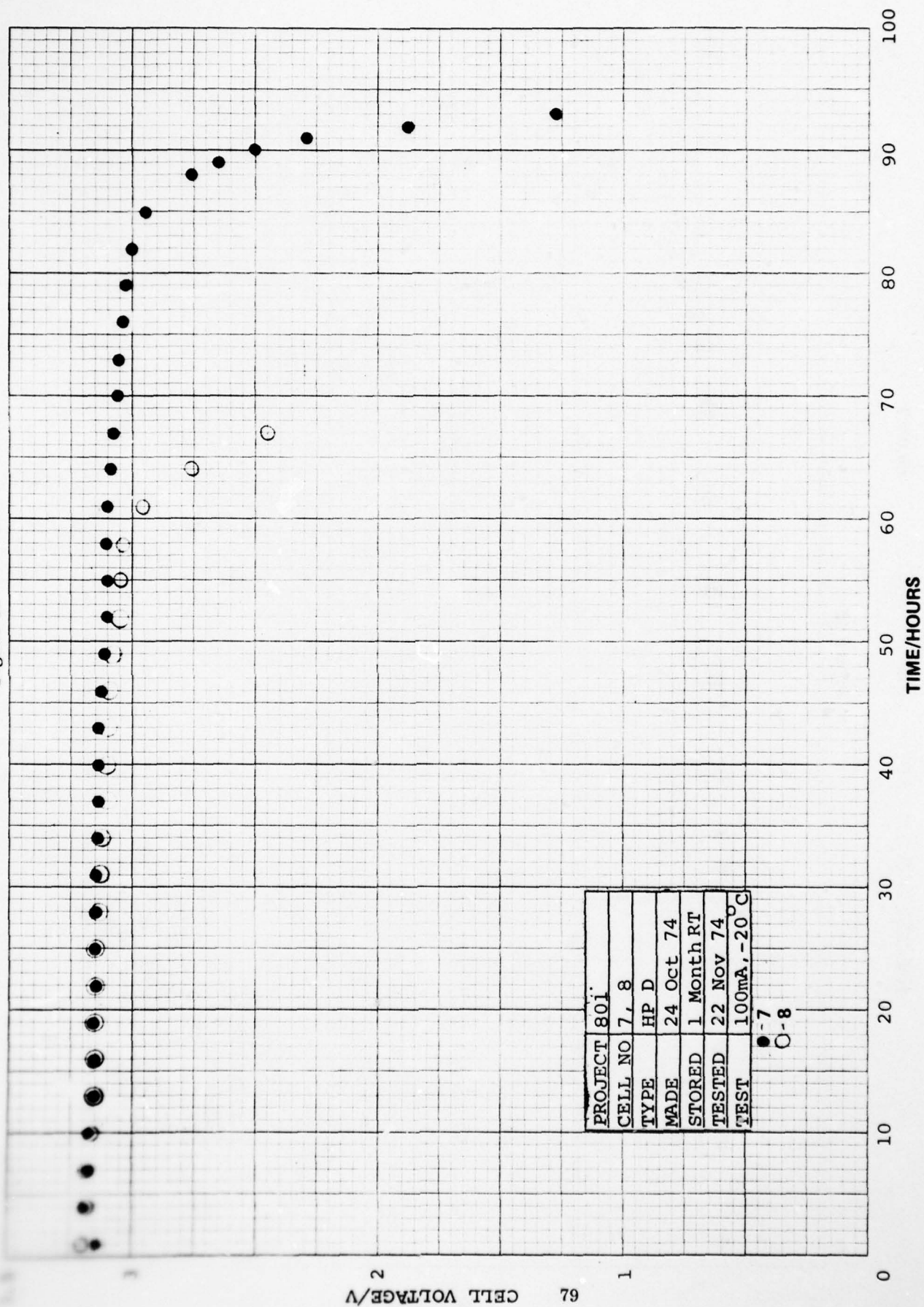


Figure 62

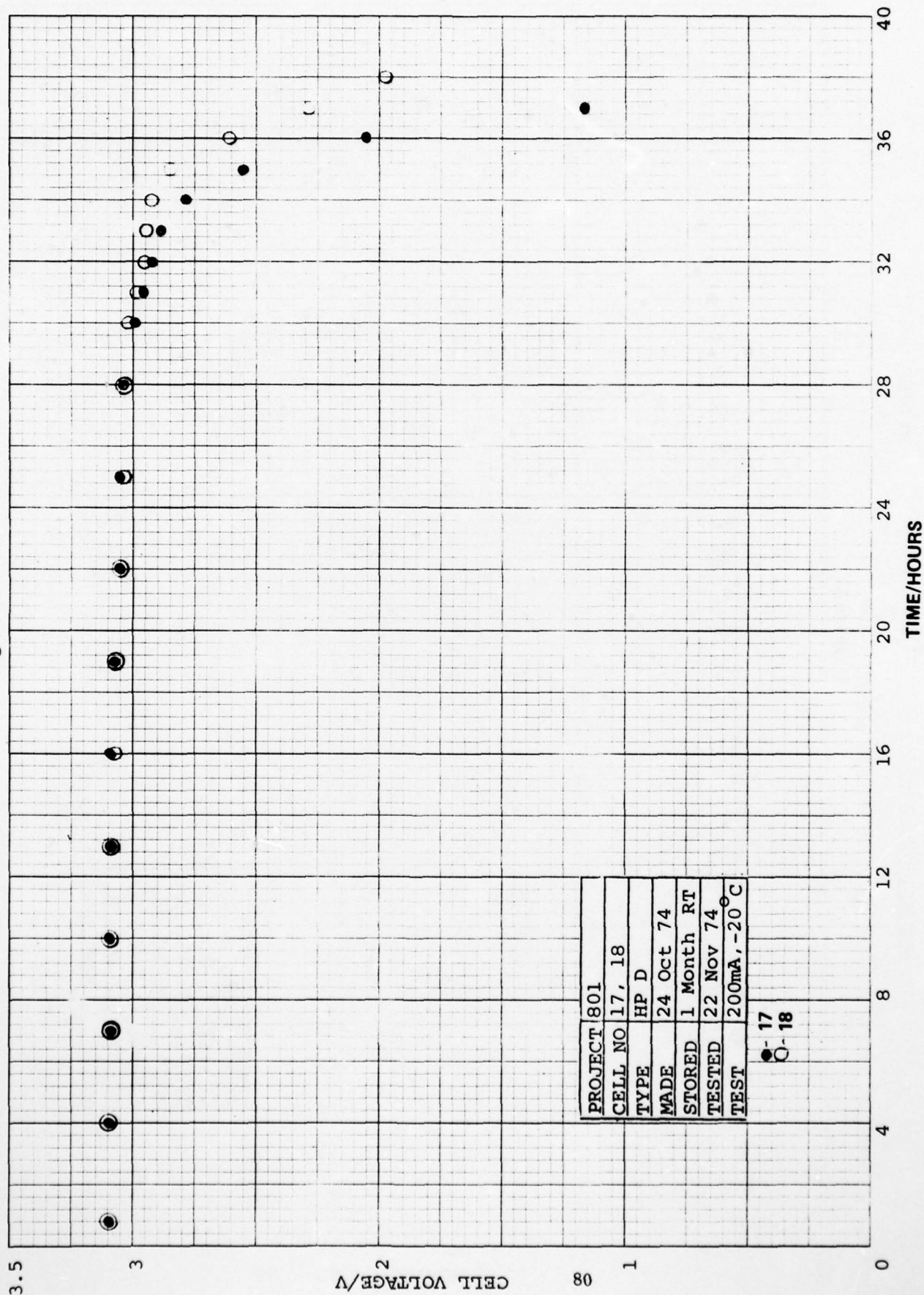
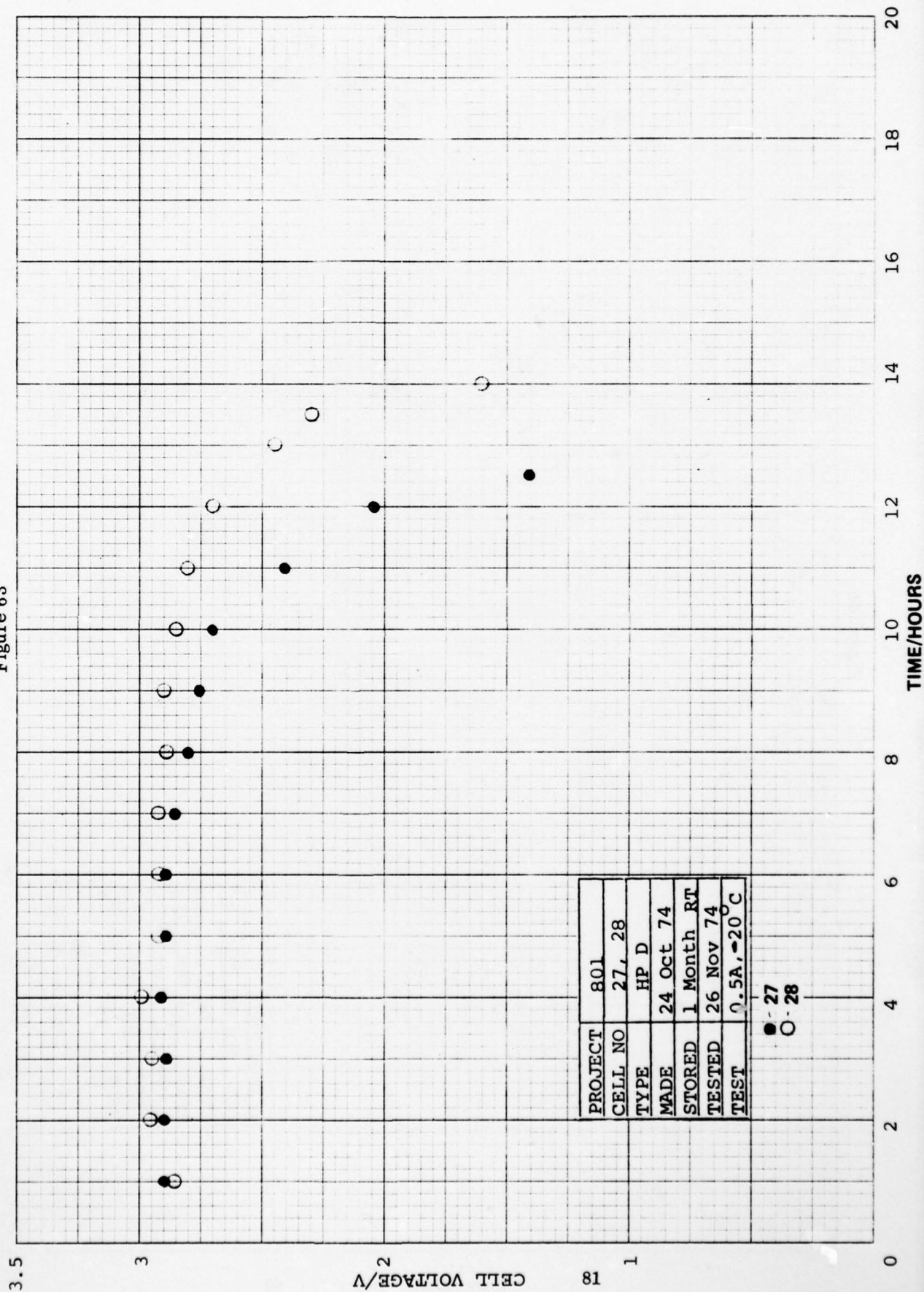


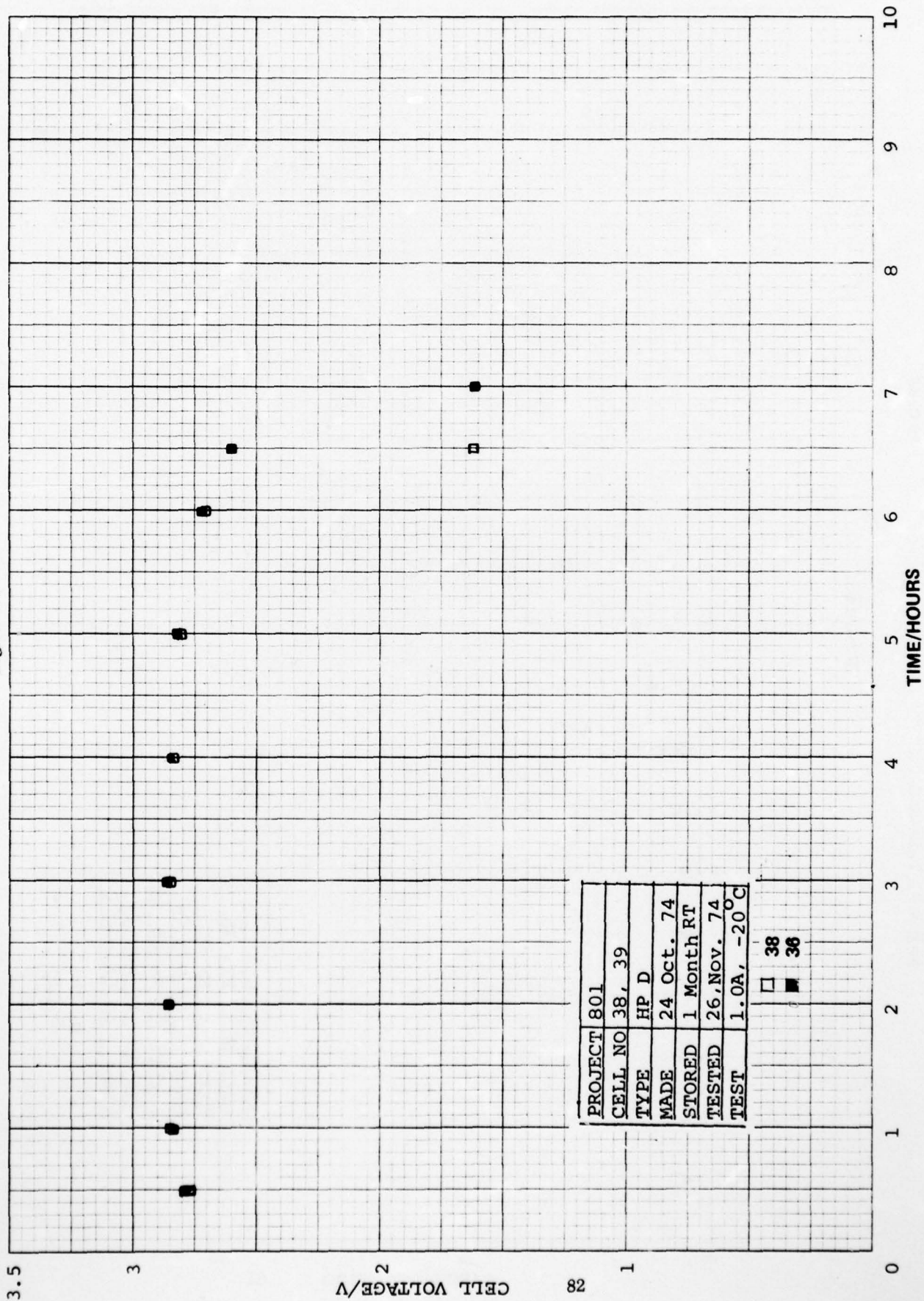
Figure 63



PROJECT	801
CELL NO	27, 28
TYPE	HP D
MADE	24 Oct 74
STORED	1 Month RT
TESTED	26 Nov 74
TEST	0.5A, -20°C

● - 27
○ - 28

Figure 64



PROJECT	801
CELL NO	38, 39
TYPE	HP D
MADE	24 Oct. 74
STORED	1 Month RT
TESTED	26, Nov. 74
TEST	1.0A, -20°C

□ 38
■ 36

Figure 65

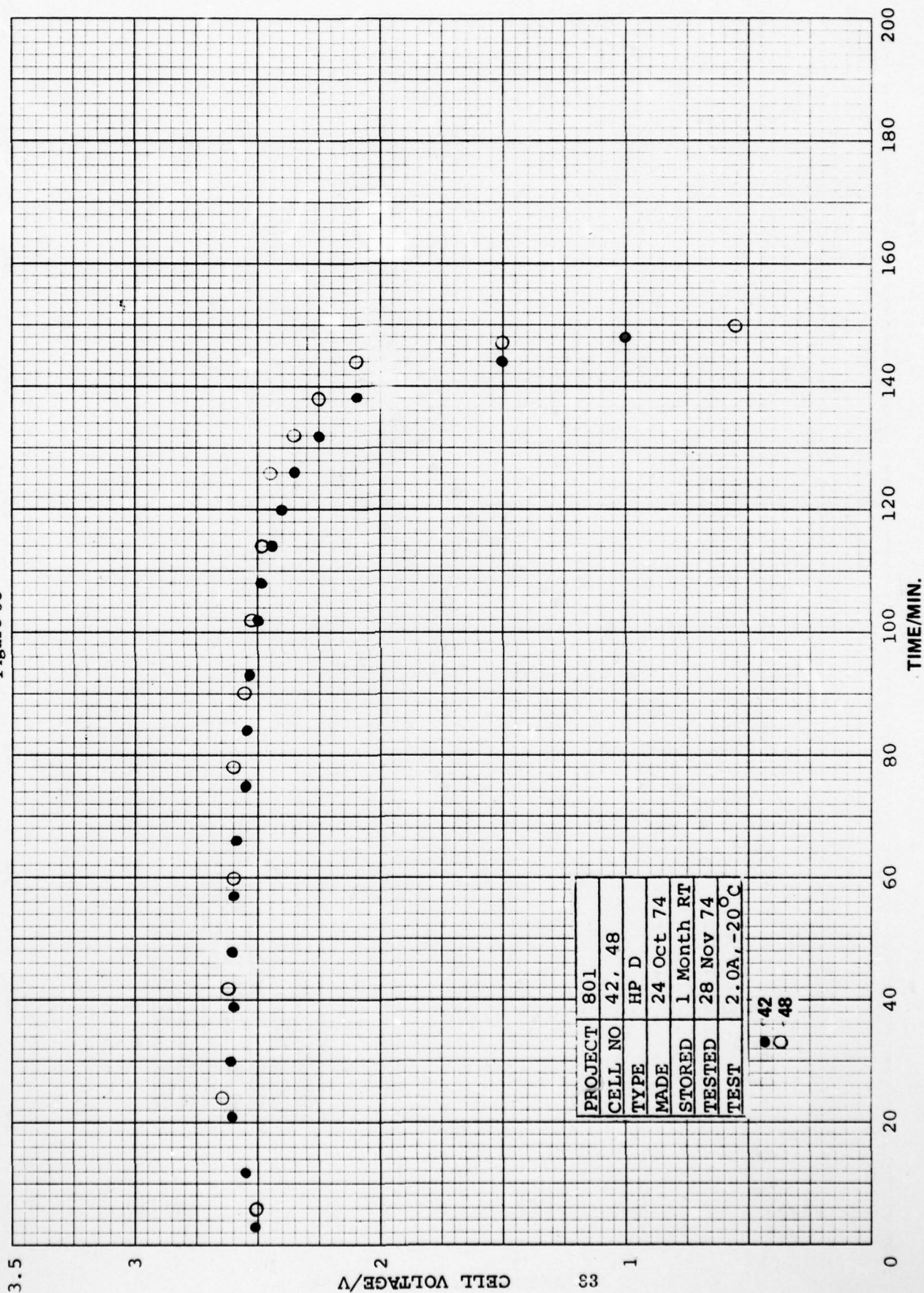
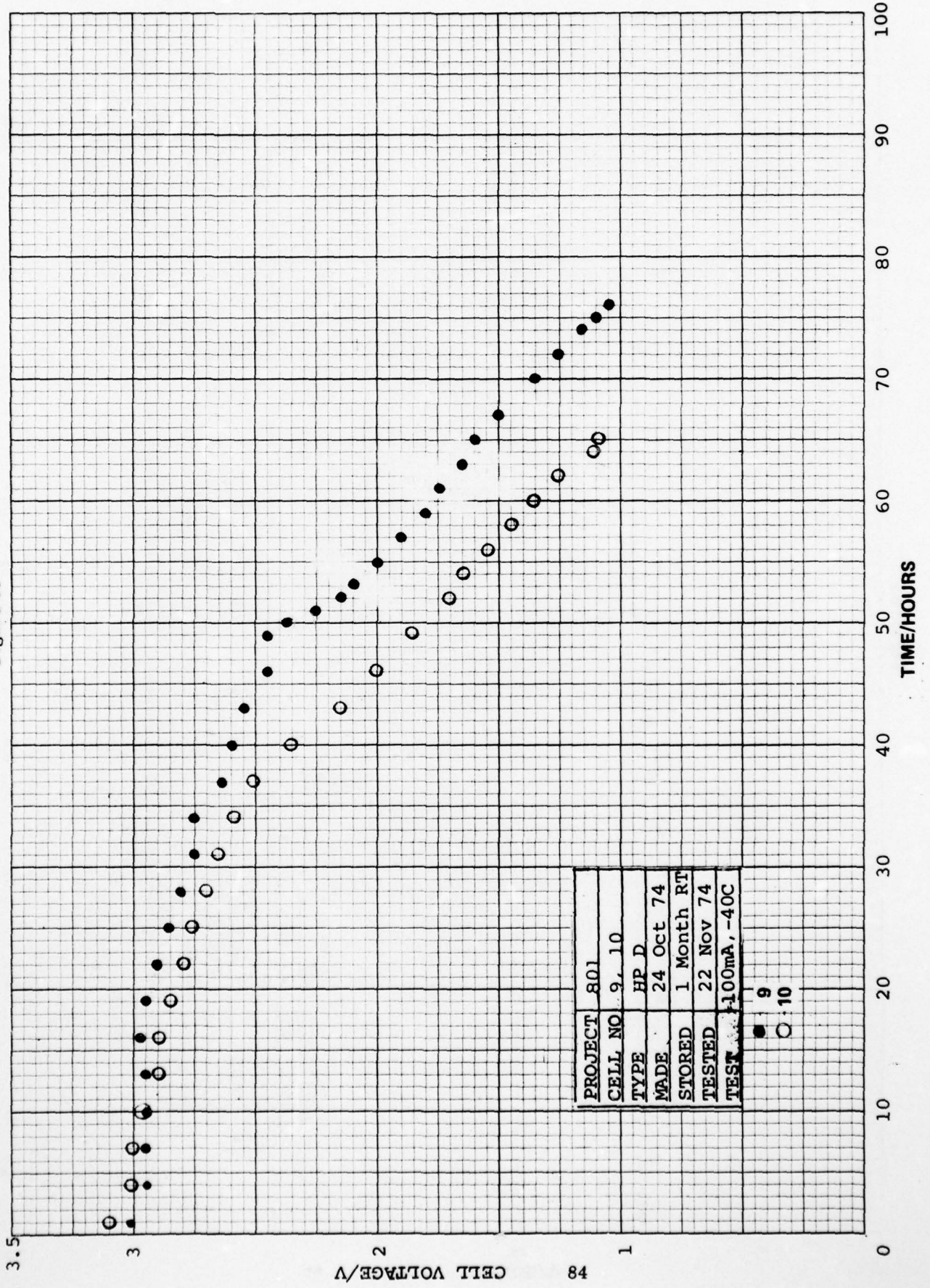


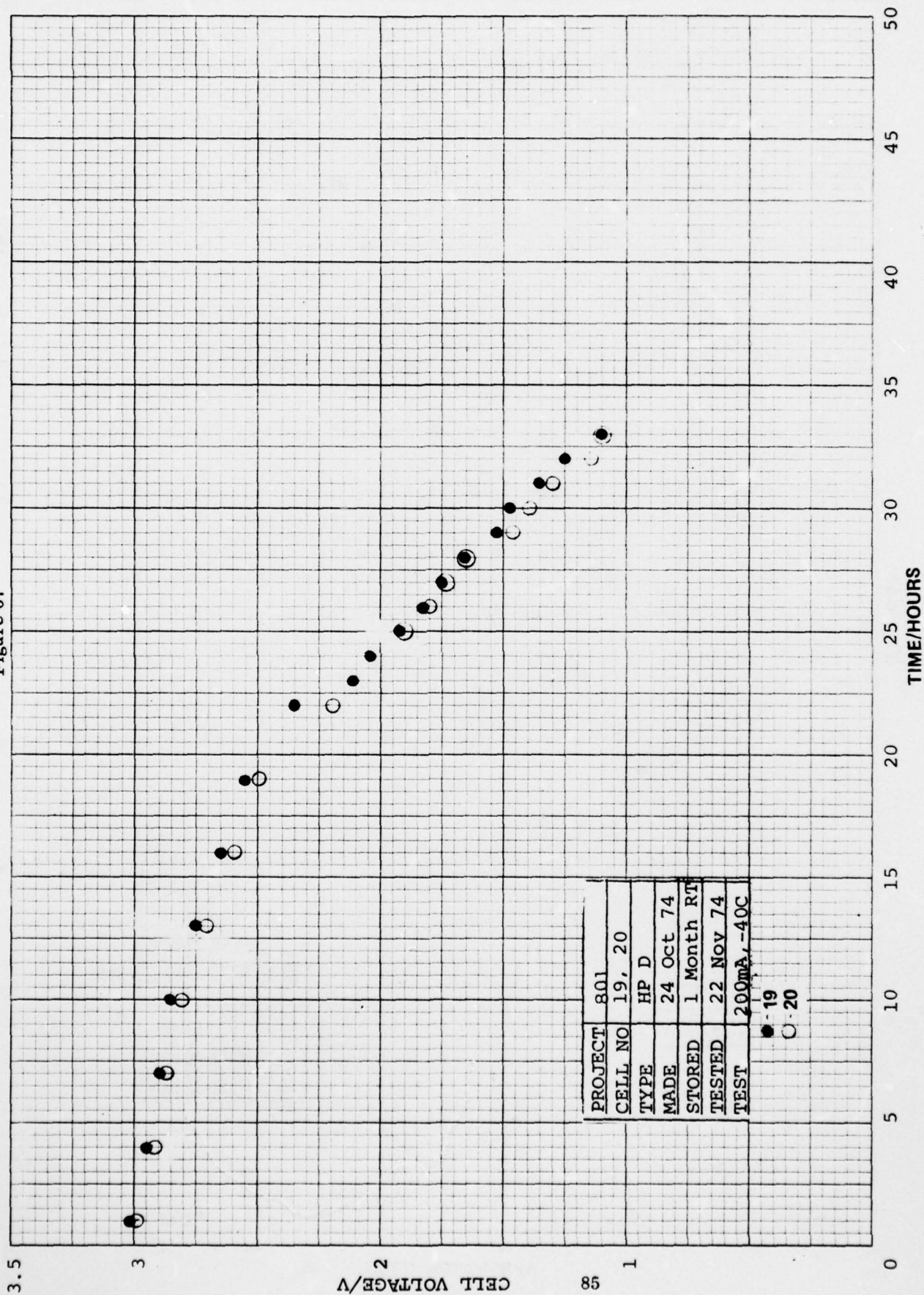
Figure 66



PROJECT	801
CELL NO	9, 10
TYPE	HP D
MADE	24 Oct 74
STORED	1 Month RT
TESTED	22 Nov 74
TEST	100mA, -40C

● 9
○ 10

Figure 67



PROJECT	801
CELL NO	19, 20
TYPE	HP D
MADE	24 Oct 74
STORED	1 Month RT
TESTED	22 Nov 74
TEST	200mA, -40C

Figure 68

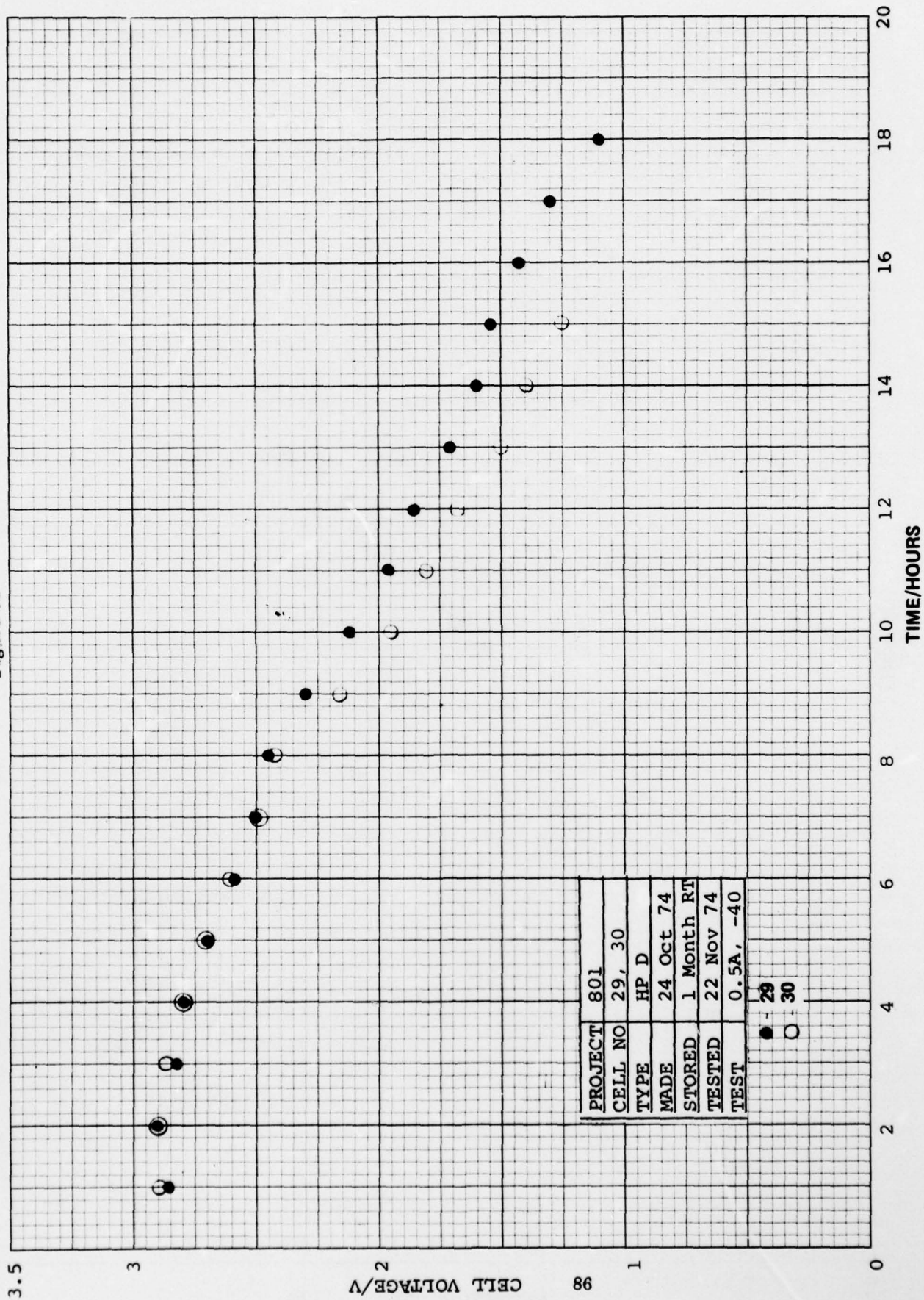


Figure 69

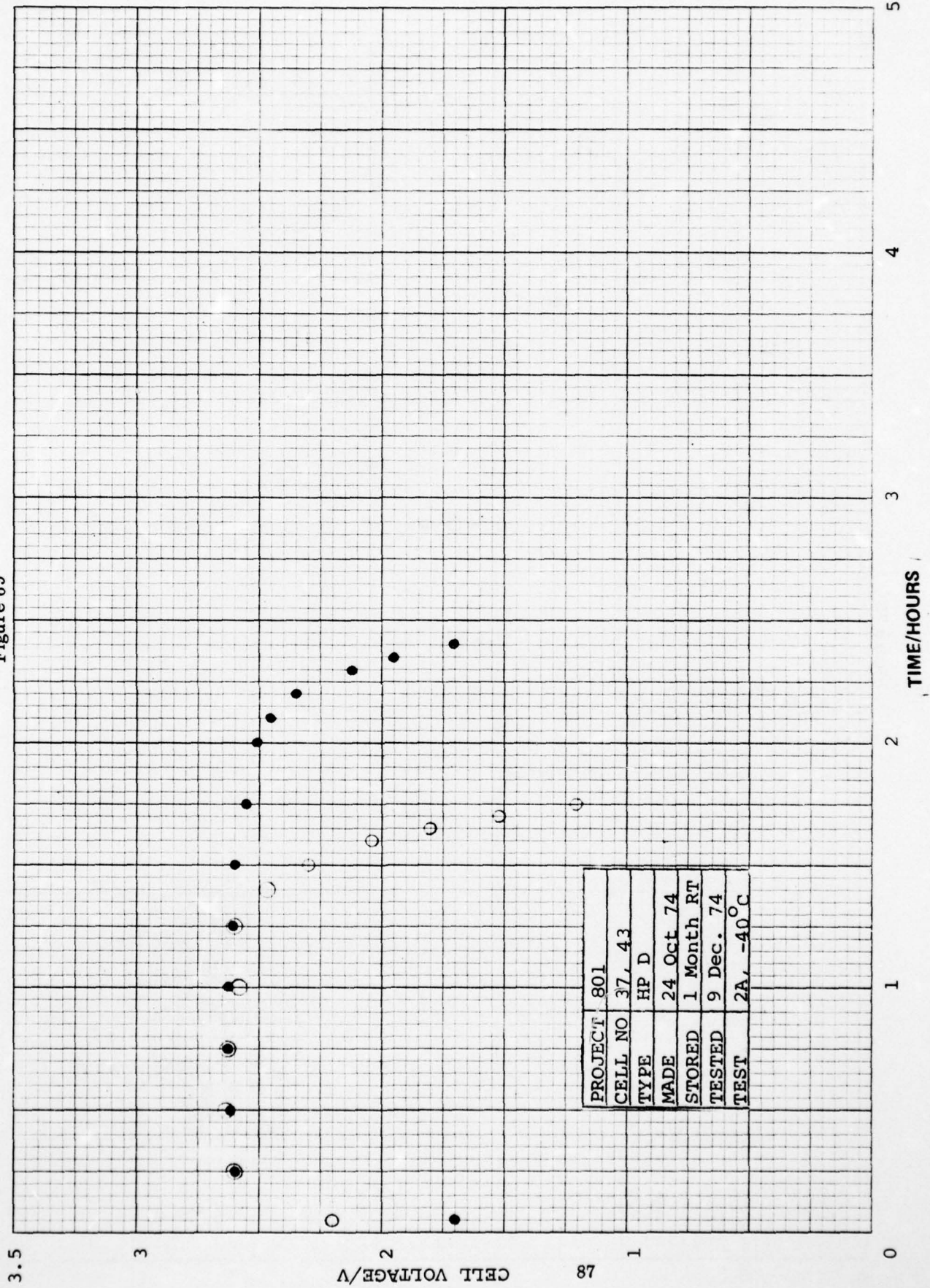


Figure 70

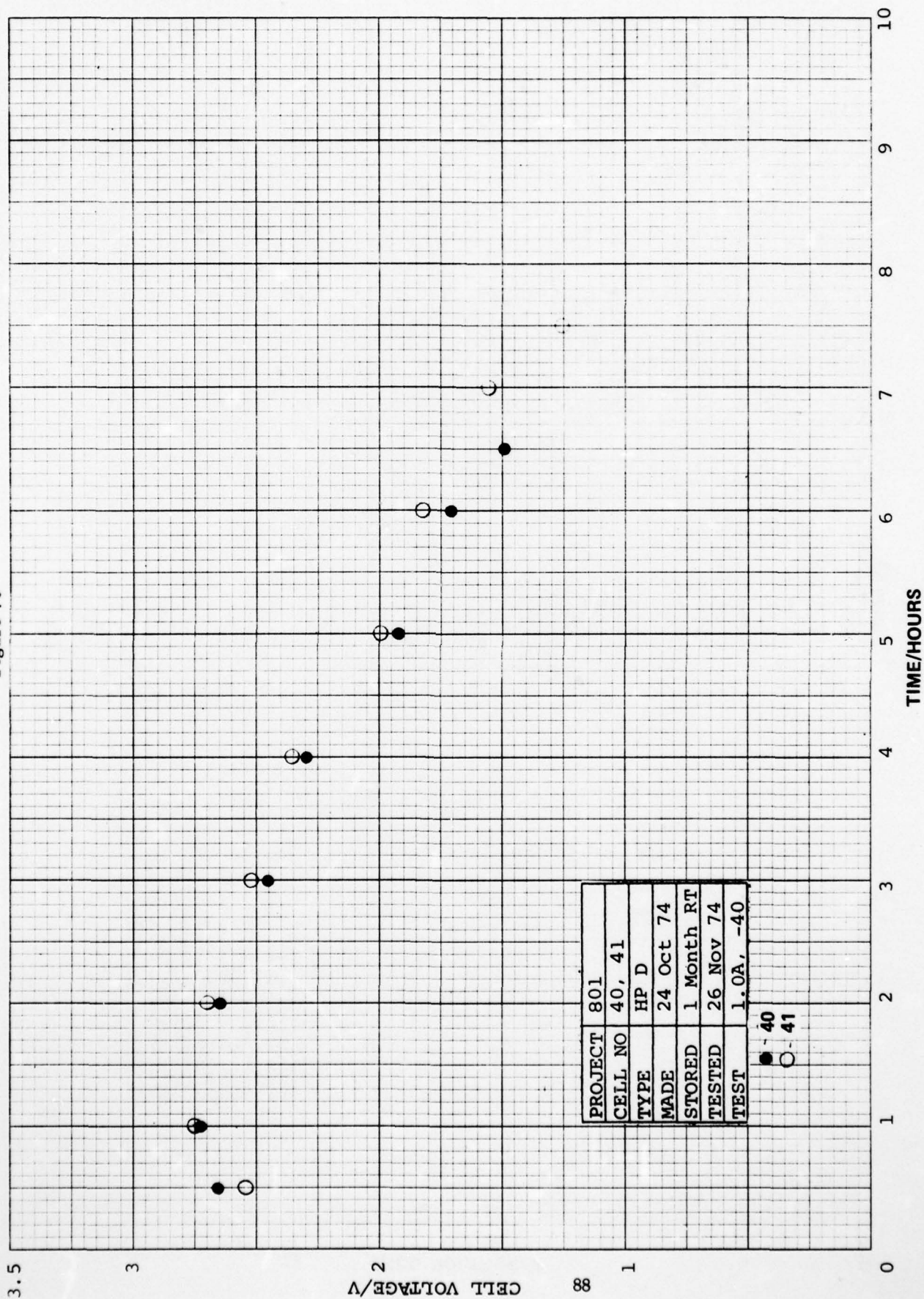


Figure 71

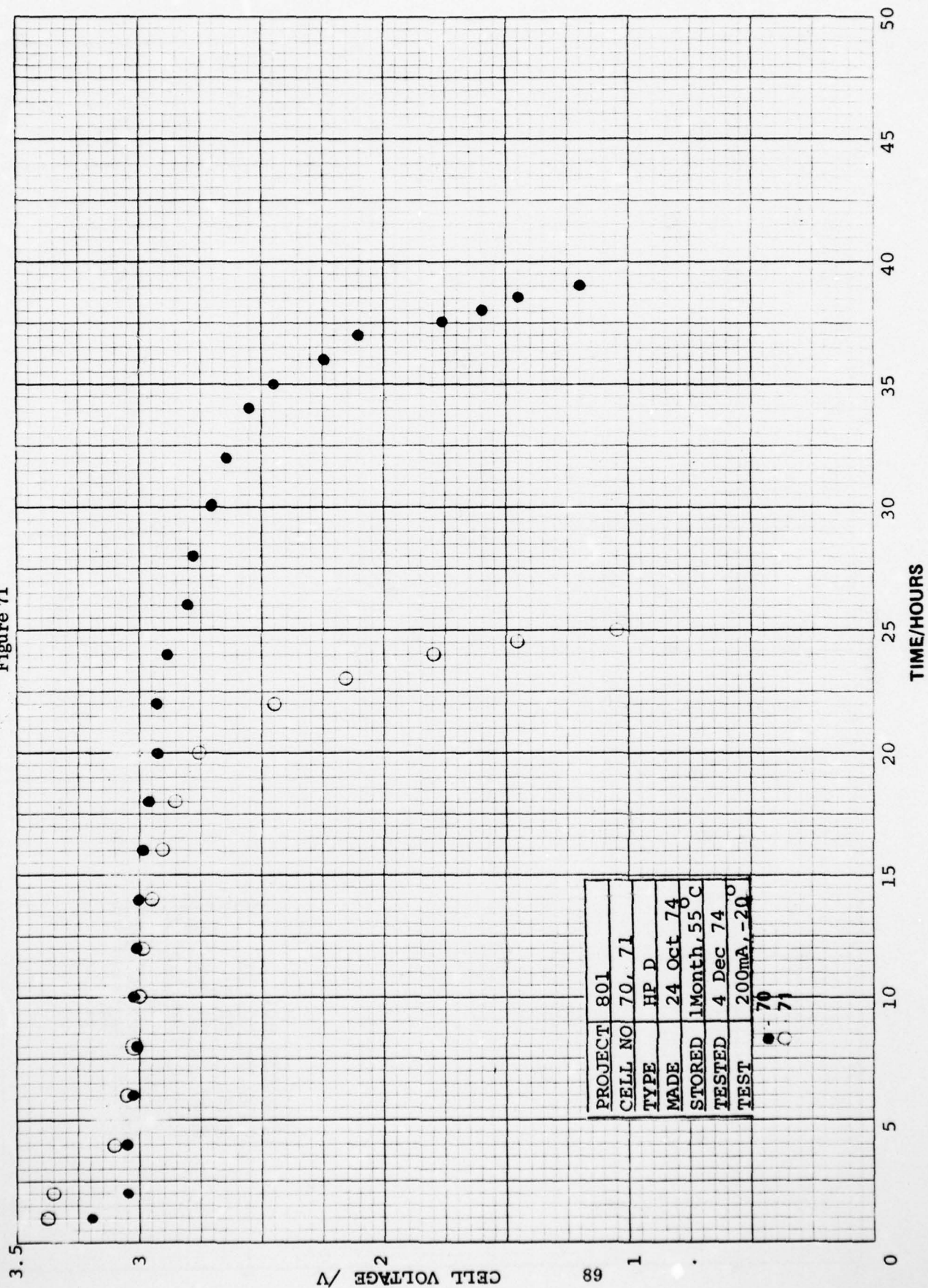


Figure 72

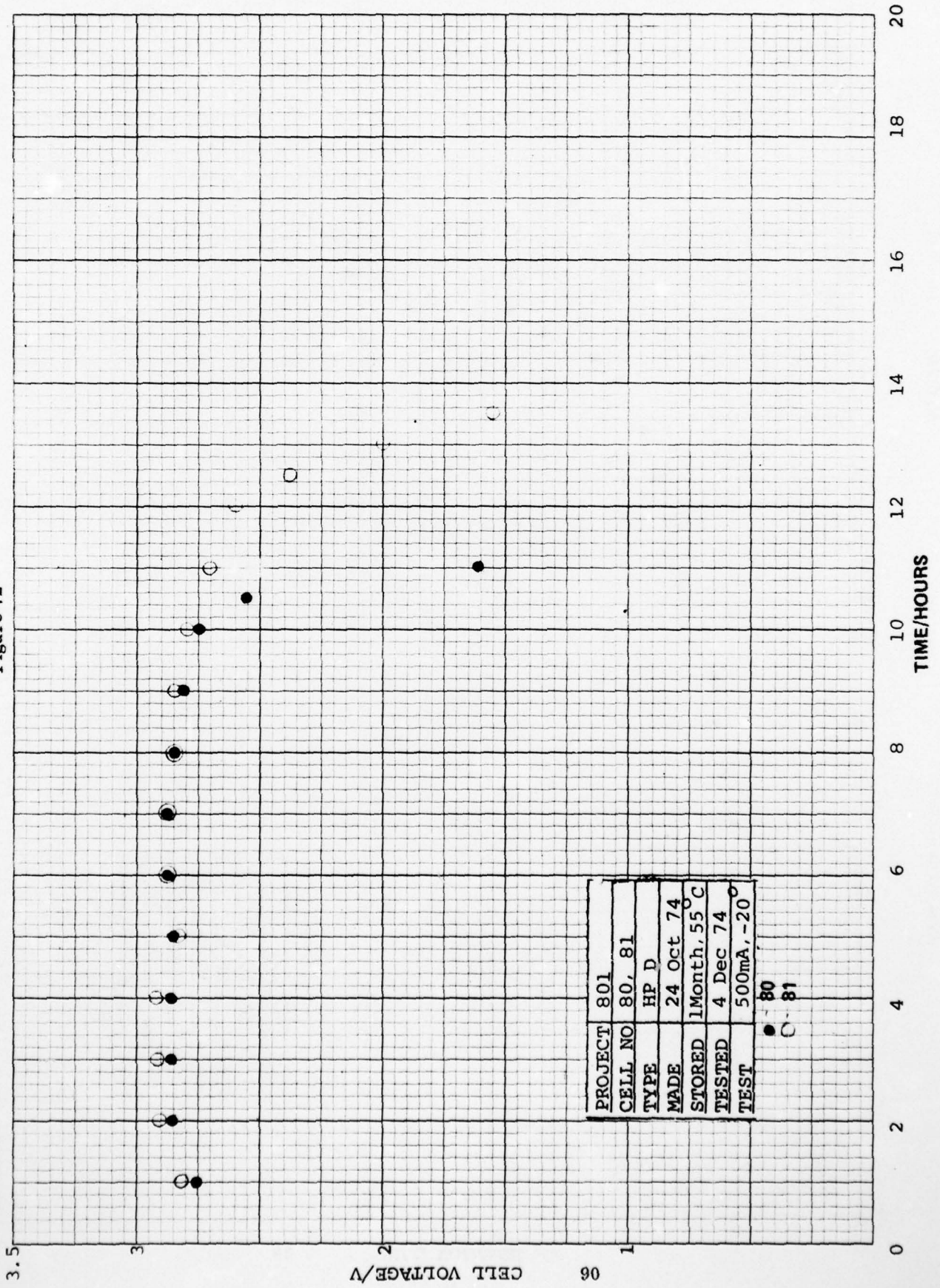


Figure 73

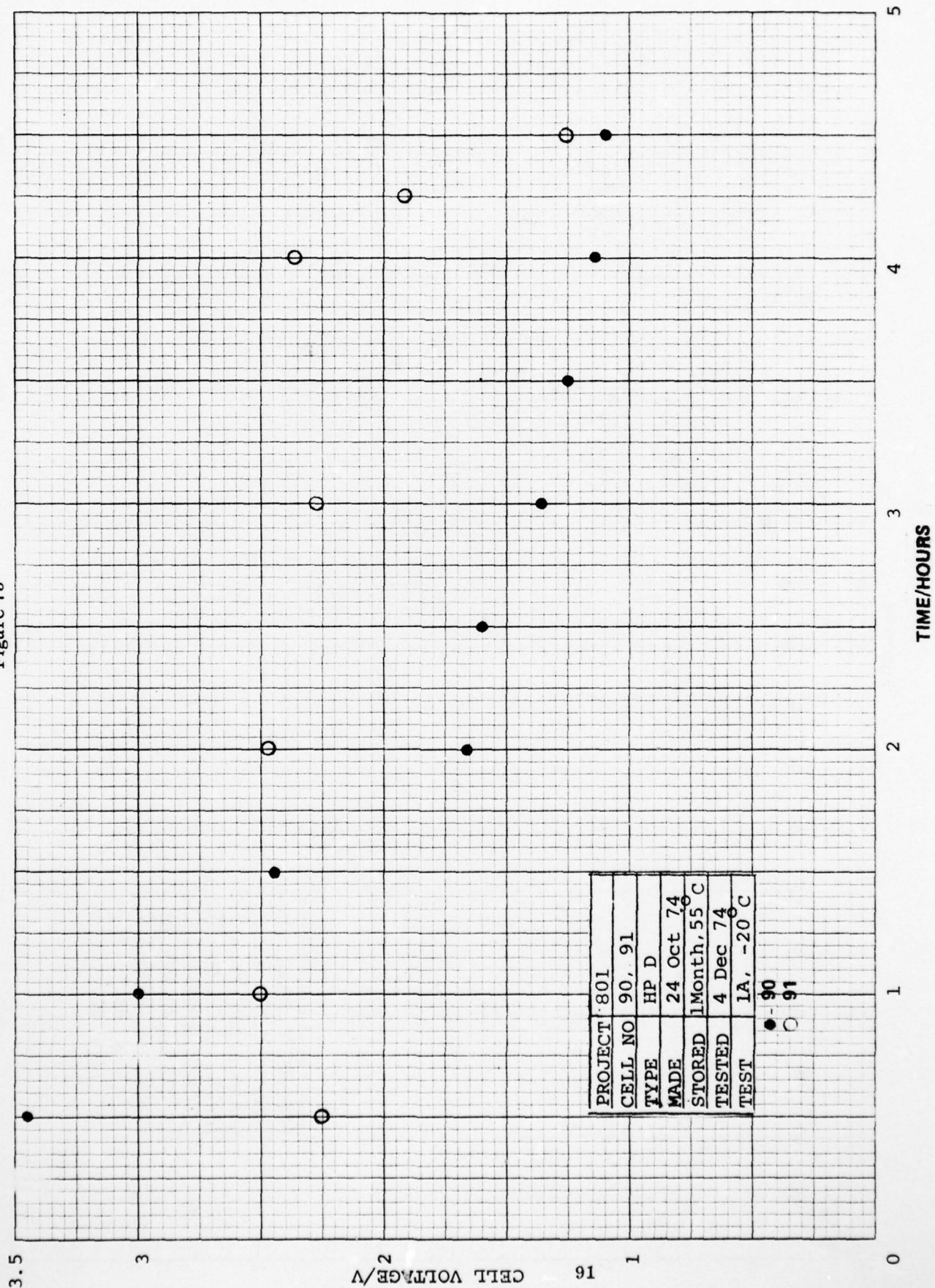
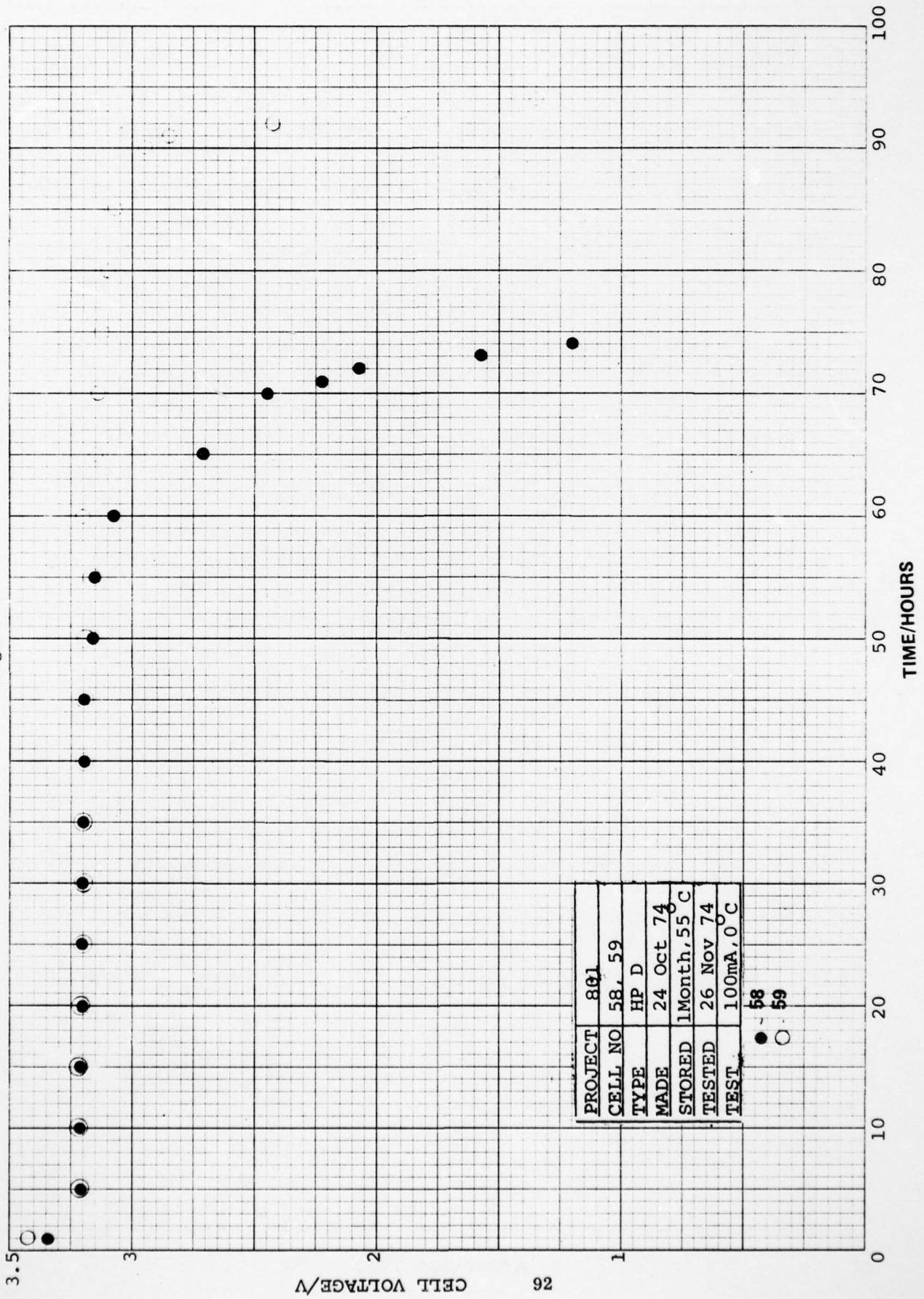


Figure 74



PROJECT	801
CELL NO	58, 59
TYPE	HP D
MADE	24 Oct 74
STORED	1 Month, 55 C
TESTED	26 Nov 74
TEST	100mA, 0 C

● 58
○ 59

AD-A039 336

GTE LABS INC WALTHAM MASS
SEALED LITHIUM INORGANIC ELECTROLYTE CELL.(U)
APR 77 N MARINCIC, A LOMBARDI

F/G 10/3

UNCLASSIFIED

ECOM-74-0108-F

DAAB07-74-C-0108

NL

2 OF 3
ADA
039336



Figure 75

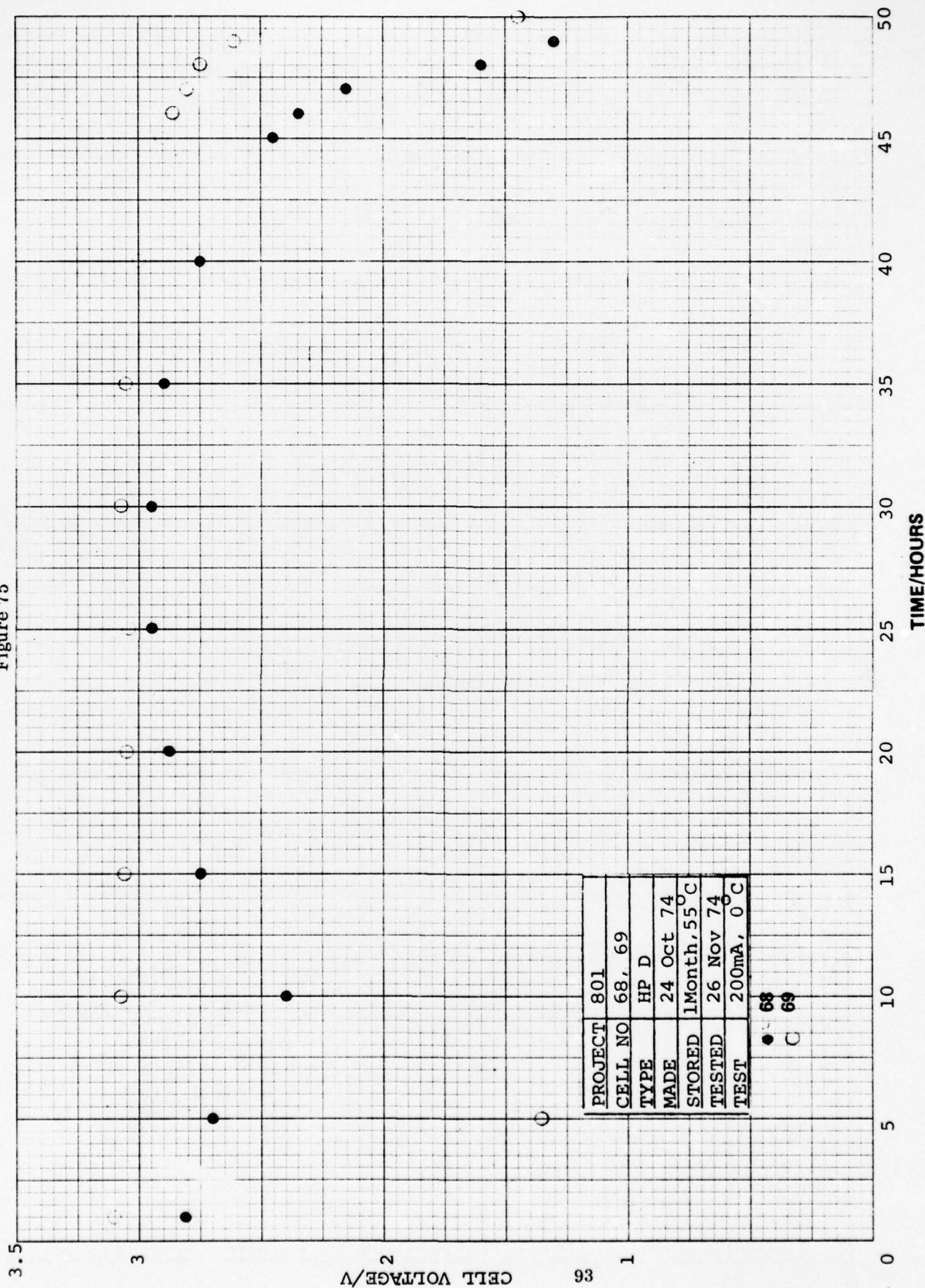
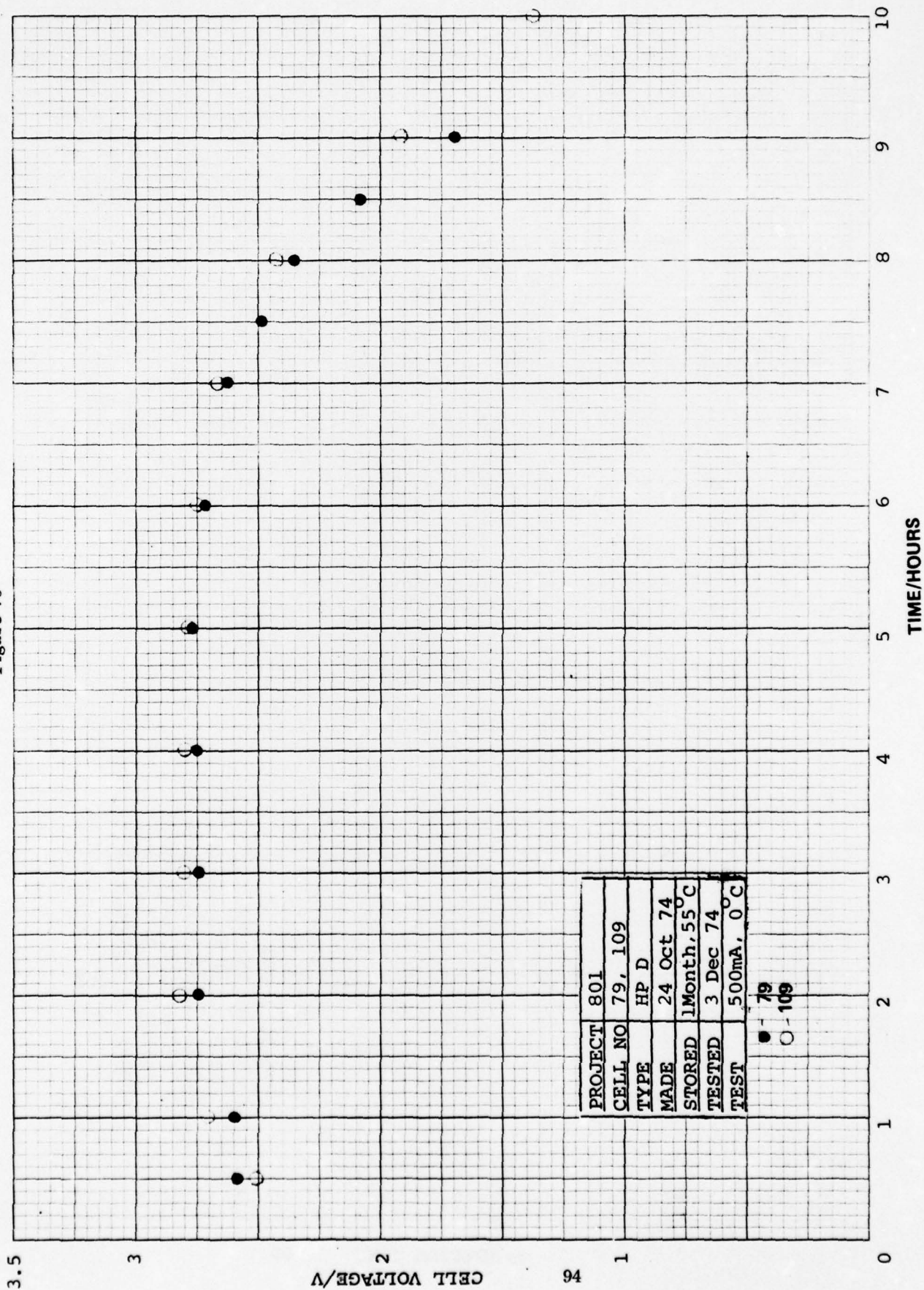


Figure 76



PROJECT	801
CELL NO	79, 109
TYPE	HP D
MADE	24 Oct 74
STORED	1 Month, 55°C
TESTED	3 Dec 74
TEST	500mA, 0°C

● - 79
○ - 109

Figure 77

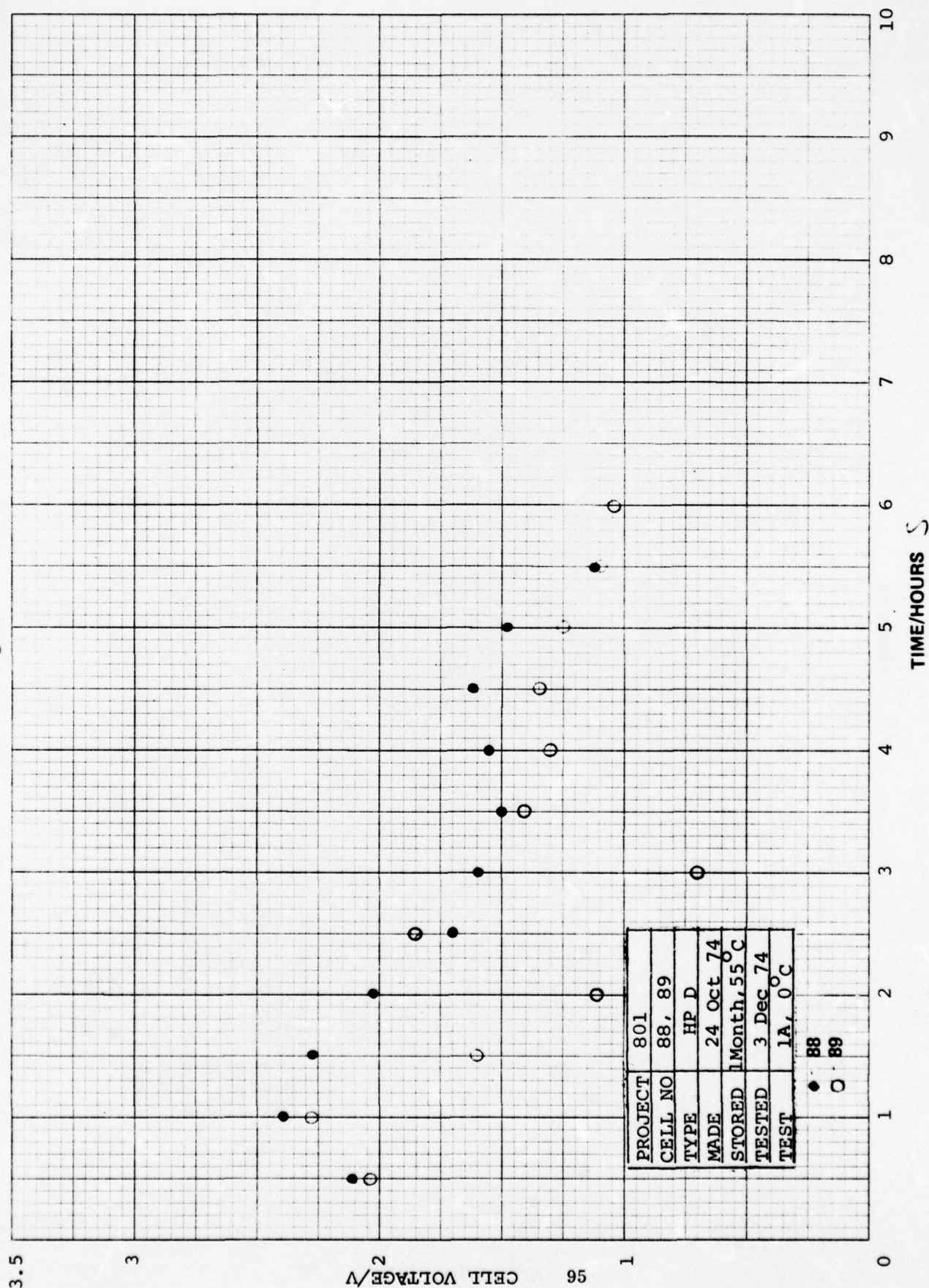
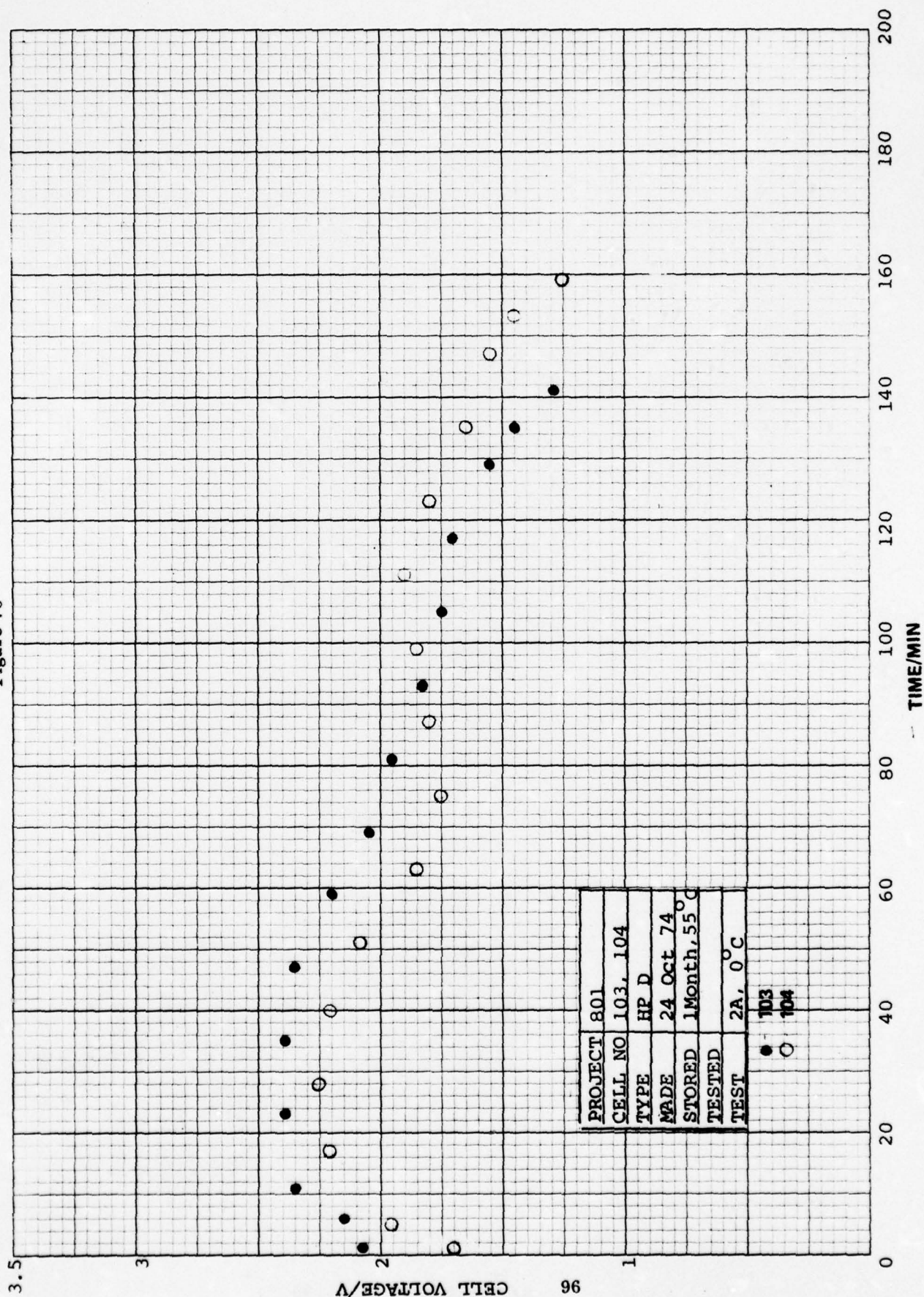


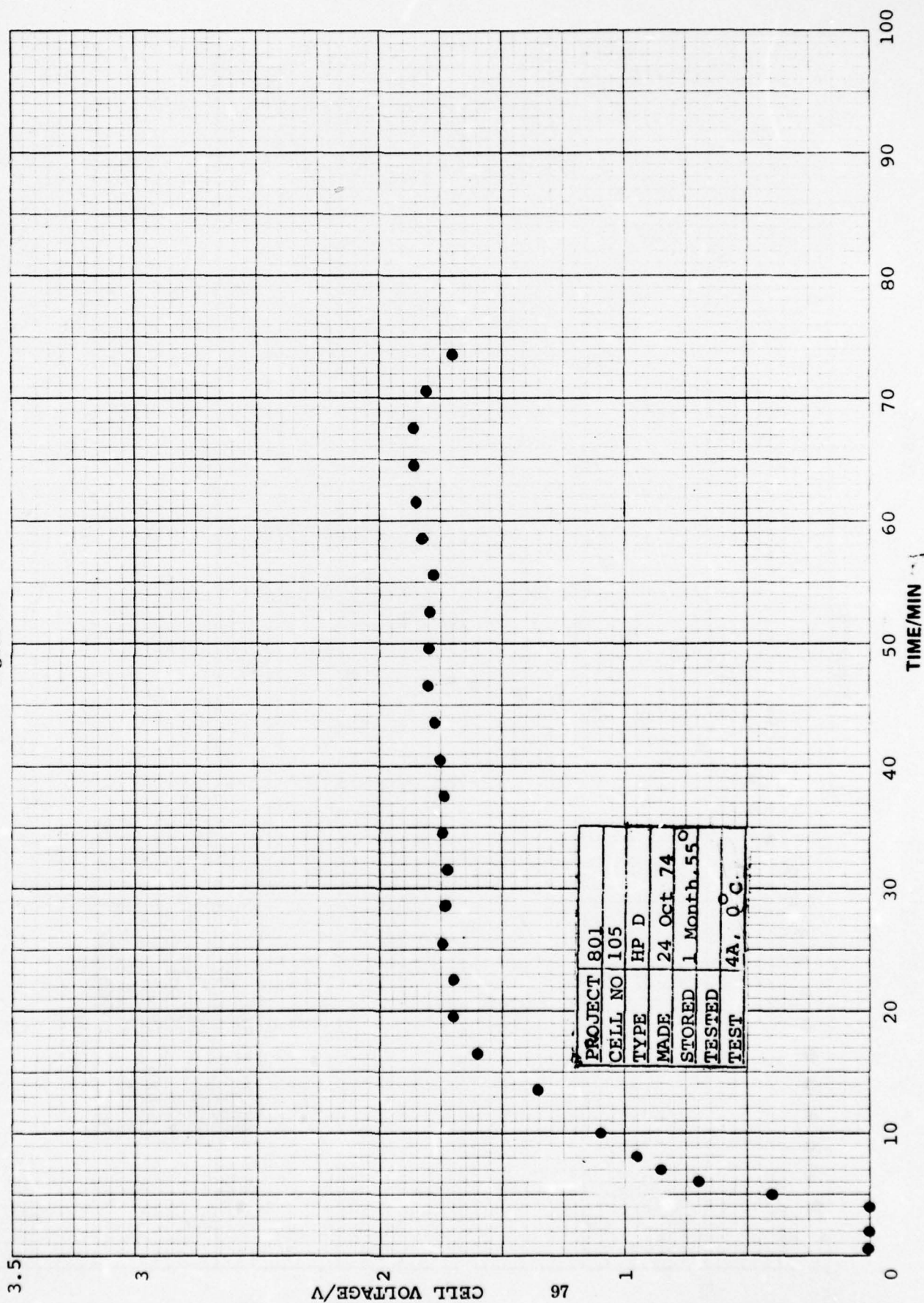
Figure 78



PROJECT	801
CELL NO	103, 104
TYPE	HP D
MADE	24 Oct 74
STORED	1 Month, 55°C
TESTED	
TEST	2A, 0°C

● 103
○ 104

Figure 79



PROJECT	801
CELL NO	105
TYPE	HP D
MADE	24 Oct 74
STORED	1 Month, 55°
TESTED	
TEST	4A, Q.C.

Figure 80

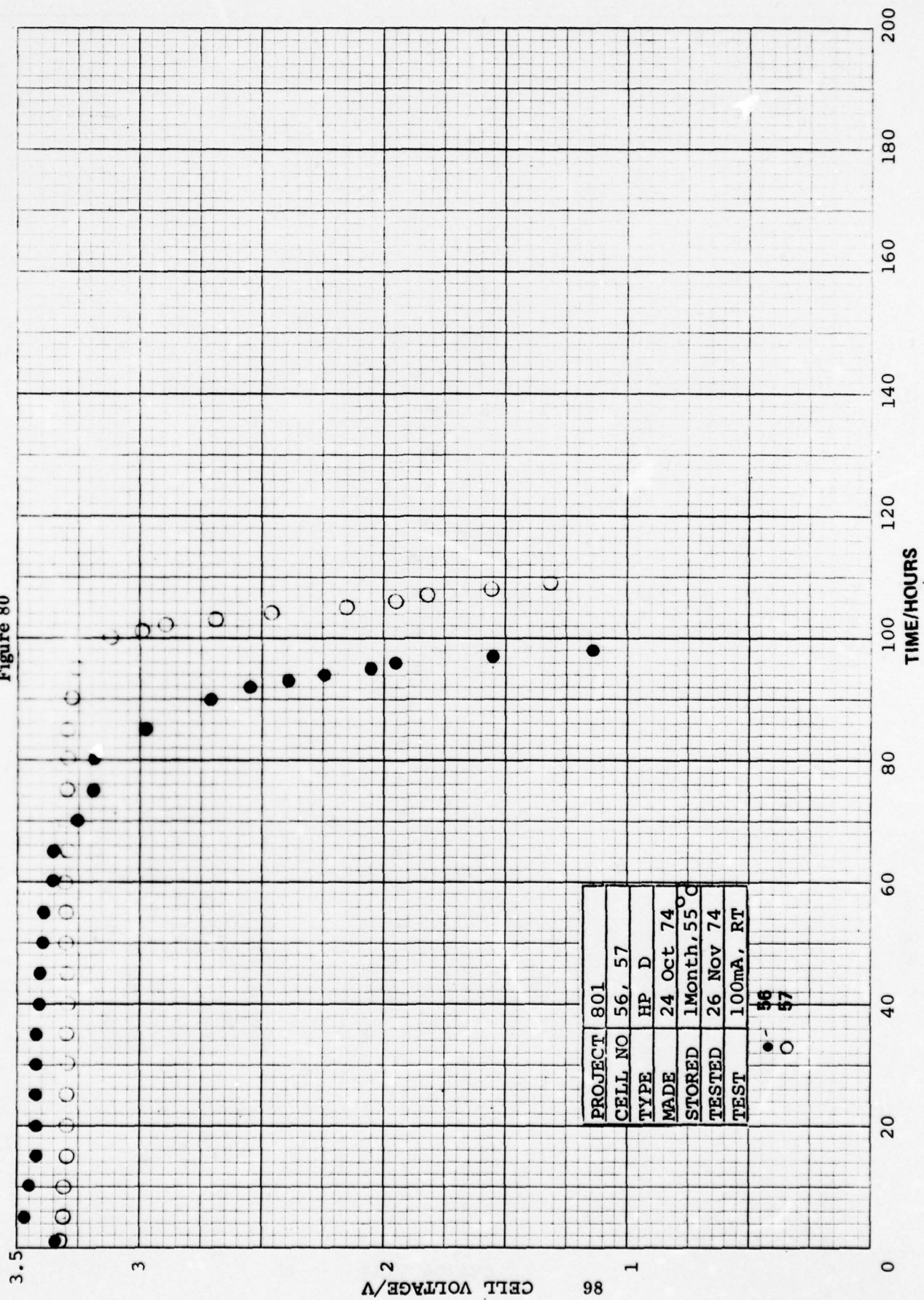
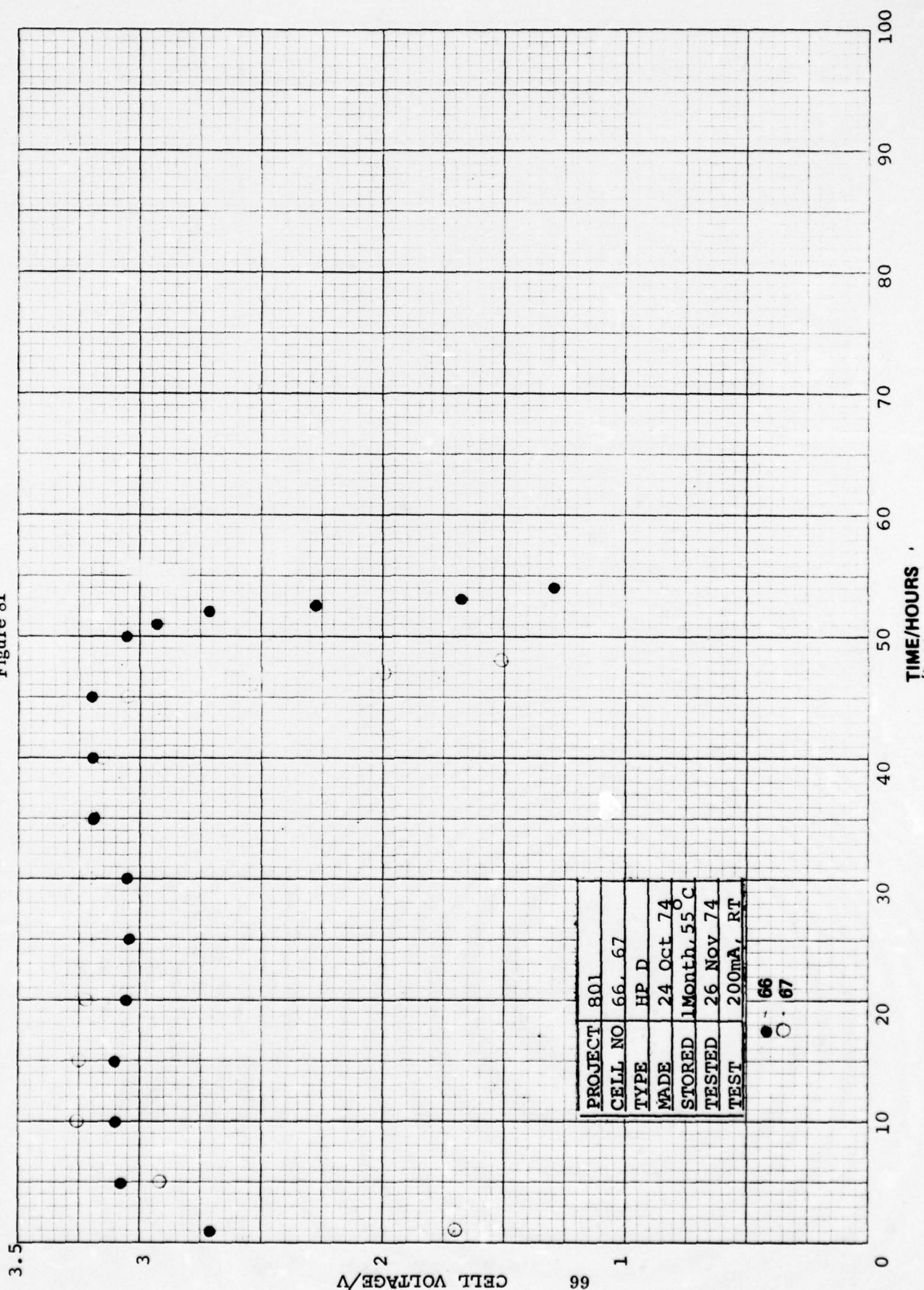


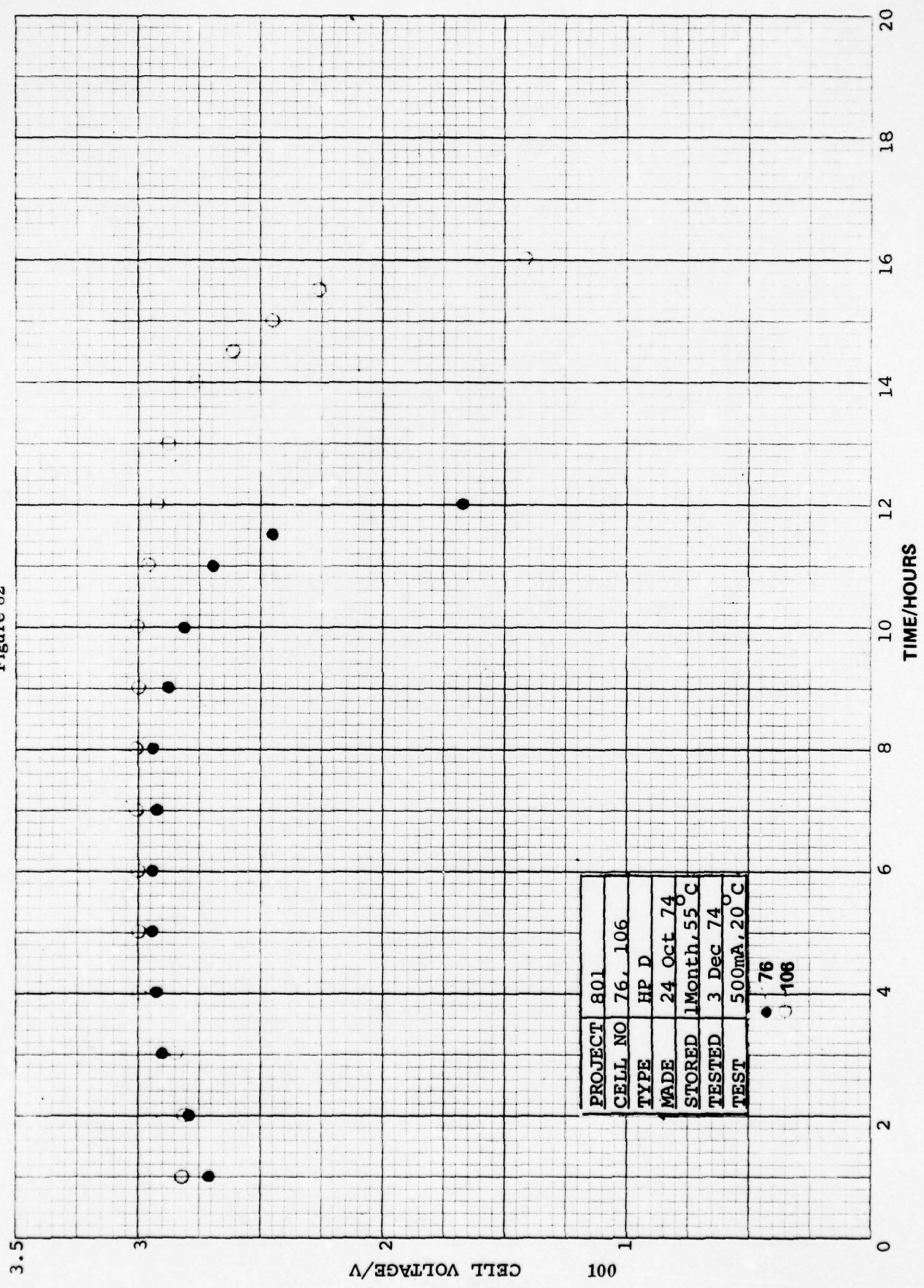
Figure 81



PROJECT	801
CELL NO	66, 67
TYPE	HP D
MADE	24 Oct 74
STORED	1 Month, 55°C
TESTED	26 Nov 74
TEST	200mA, RT

● 66
○ 67

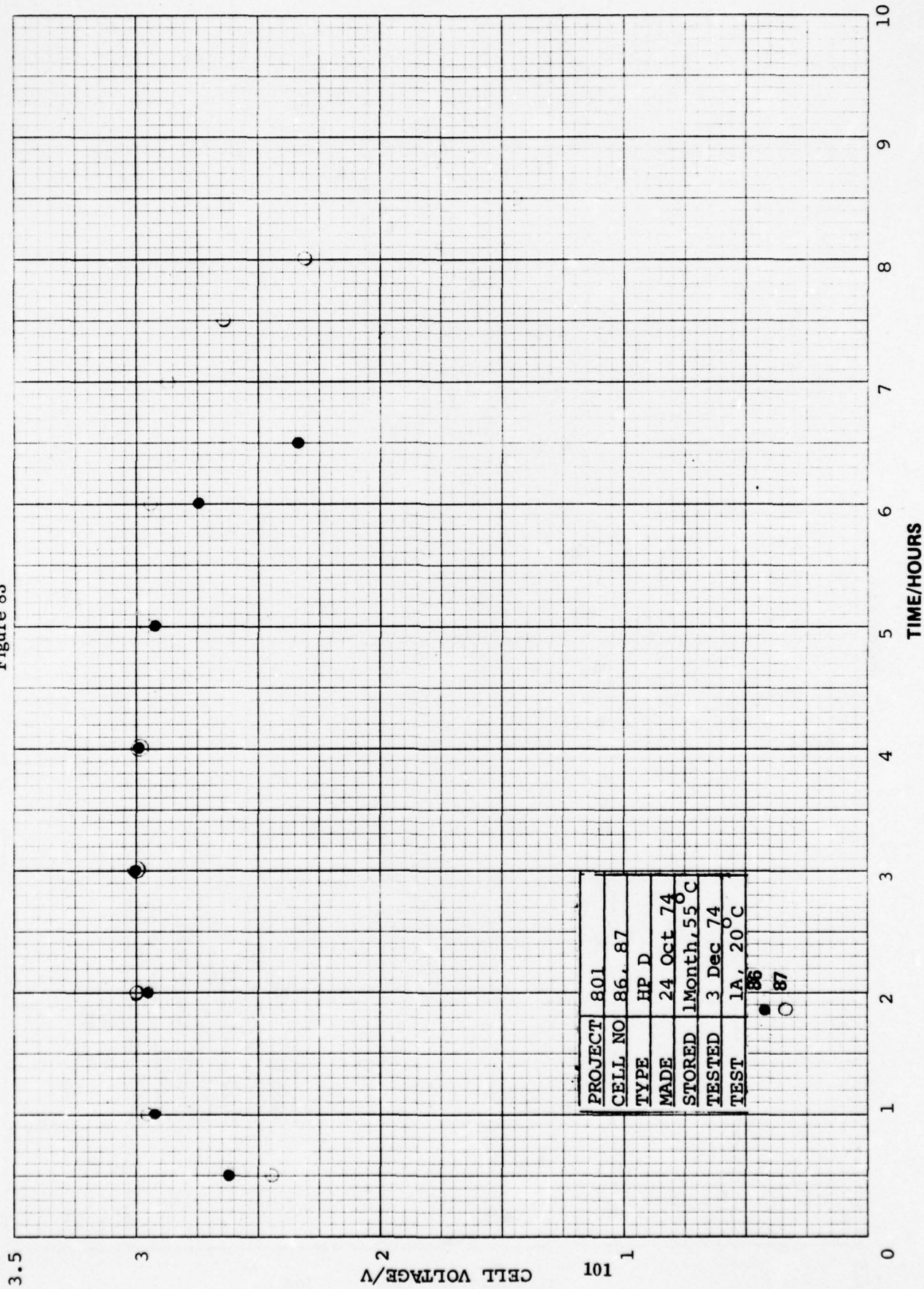
Figure 82



PROJECT	801
CELL NO	76, 106
TYPE	HP D
MADE	24 Oct 74
STORED	1 Month, 55°C
TESTED	3 Dec 74
TEST	500mA, 20°C

● 76
○ 106

Figure 83



PROJECT	801
CELL NO	86, 87
TYPE	HP D
MADE	24 Oct 74
STORED	1Month, 55°C
TESTED	3 Dec 74
TEST	1A, 20°C

Figure 84

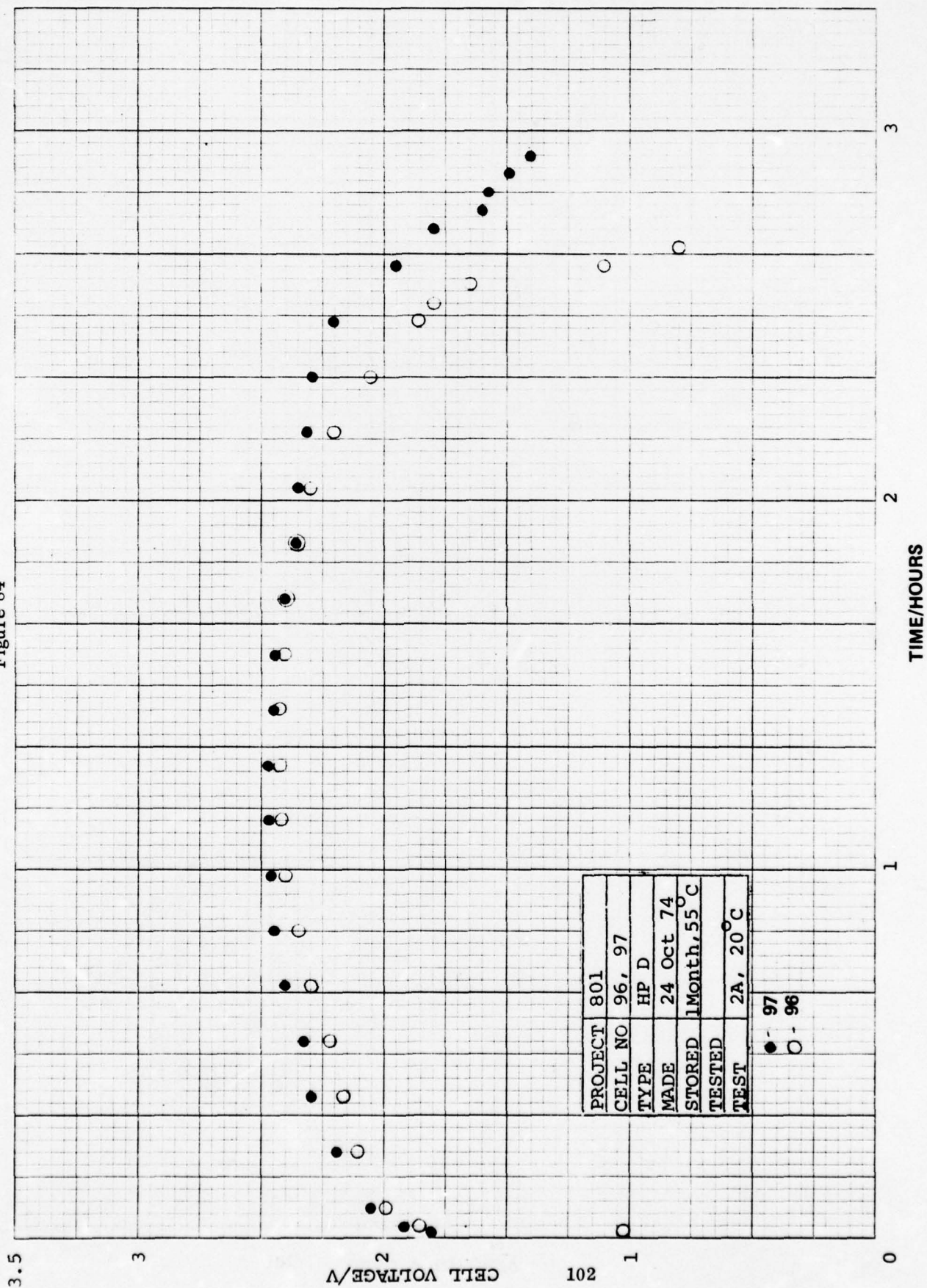


Figure 85

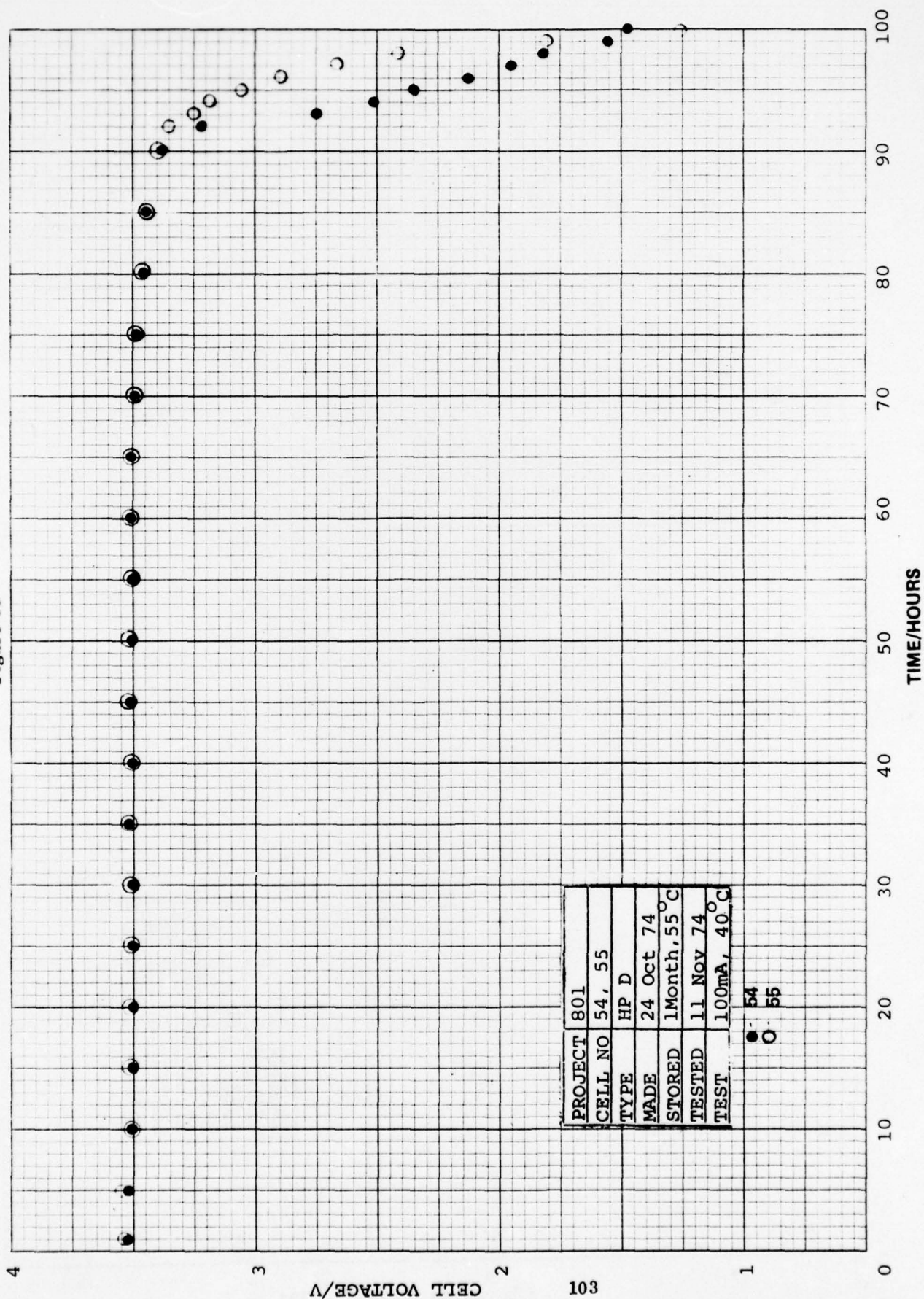
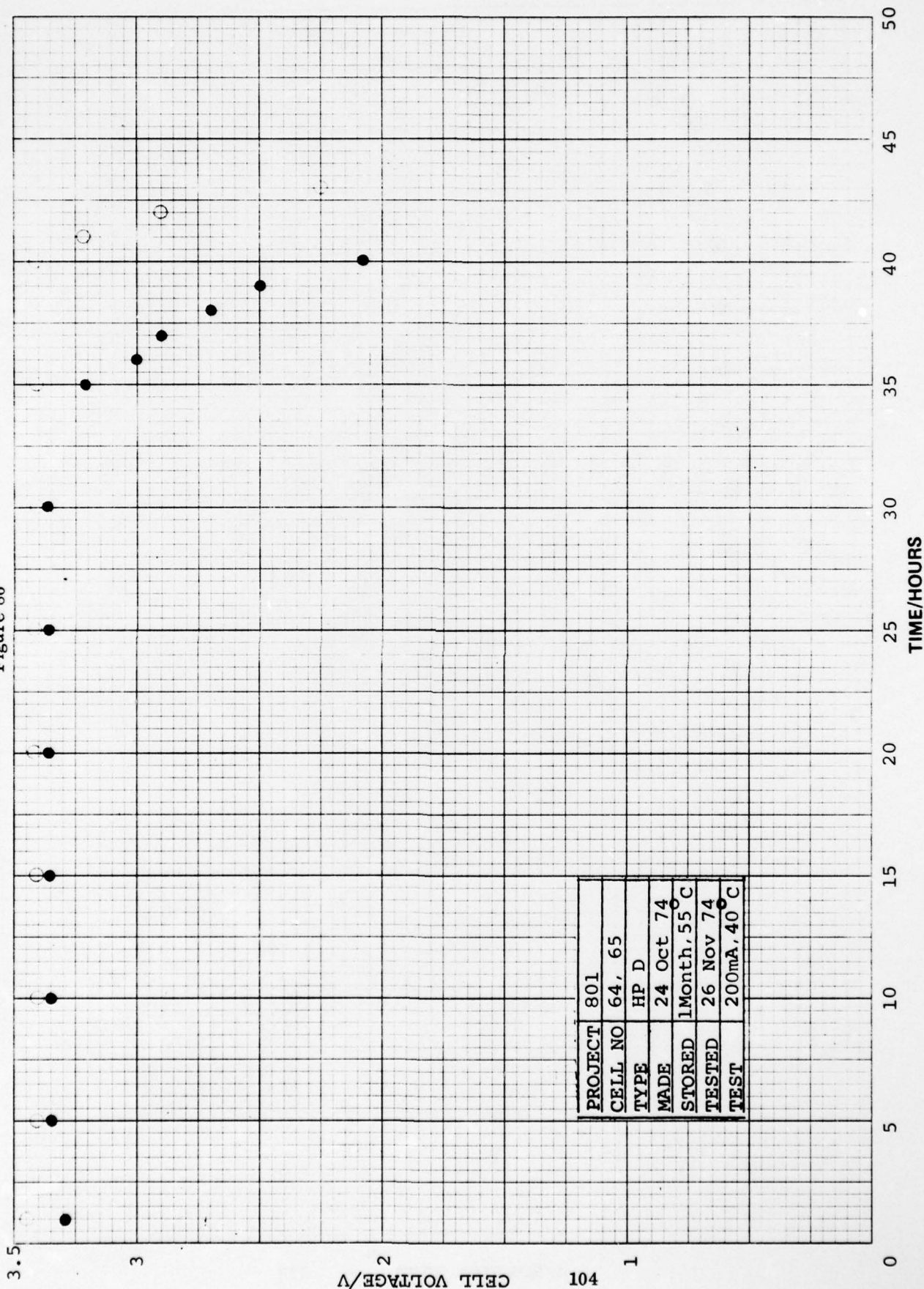


Figure 86



PROJECT	801
CELL NO	64, 65
TYPE	HP D
MADE	24 Oct 74
STORED	1 Month, 55 °C
TESTED	26 Nov 74
TEST	200mA, 40 °C

Figure 87

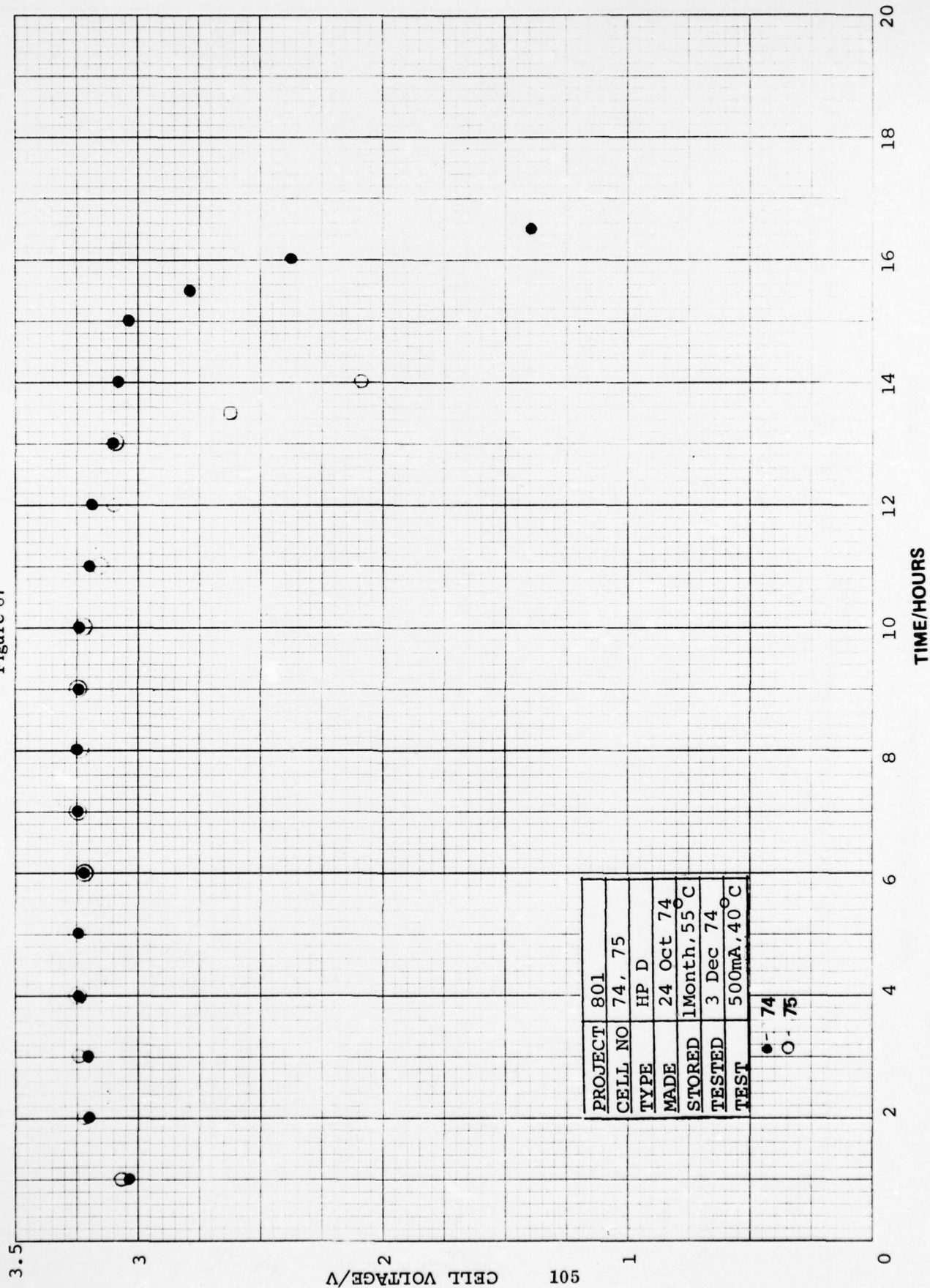
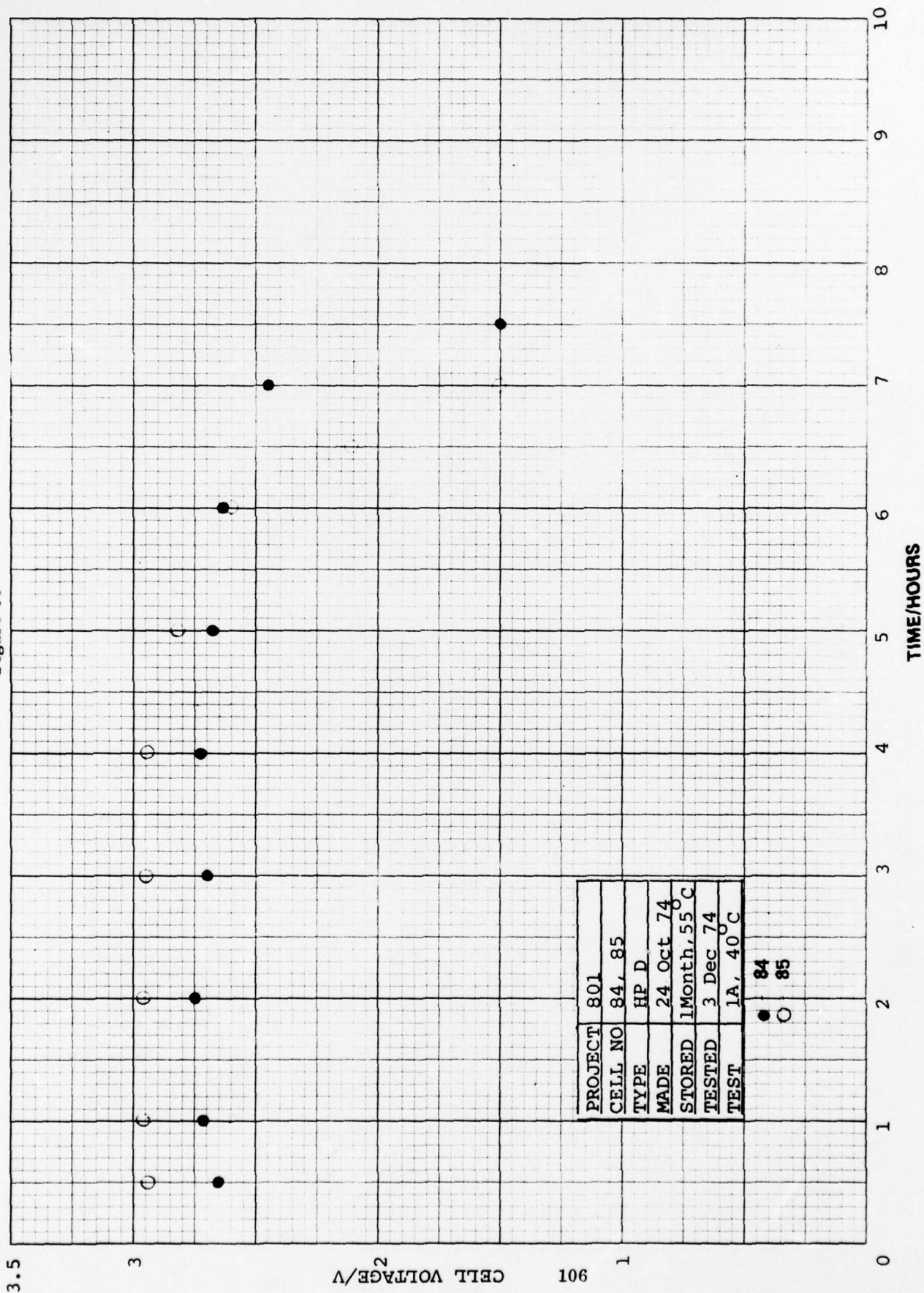


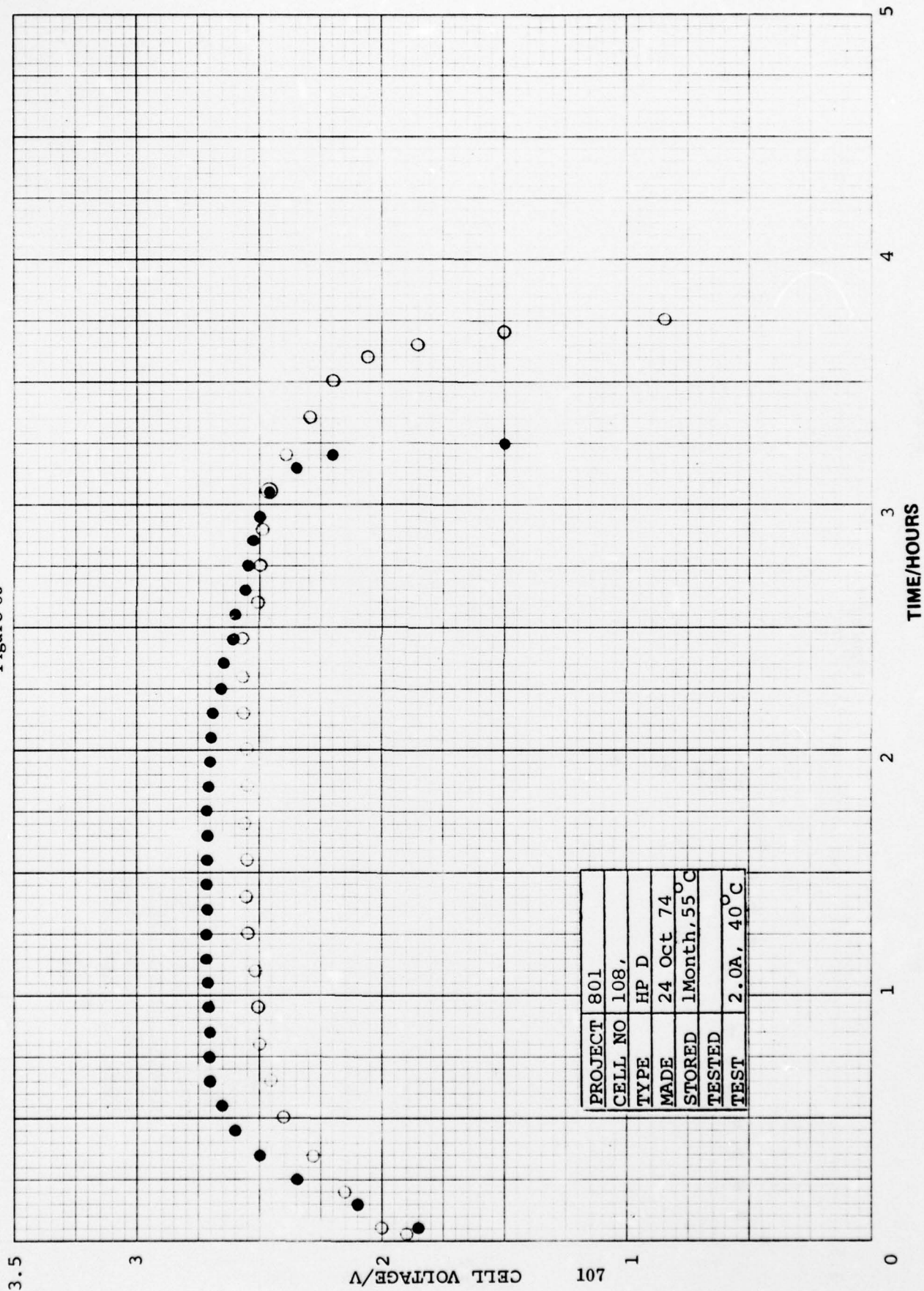
Figure 88



PROJECT	801
CELL NO	84, 85
TYPE	HP D
MADE	24 Oct 74
STORED	1 Month, 55°C
TESTED	3 Dec 74
TEST	1A, 40°C

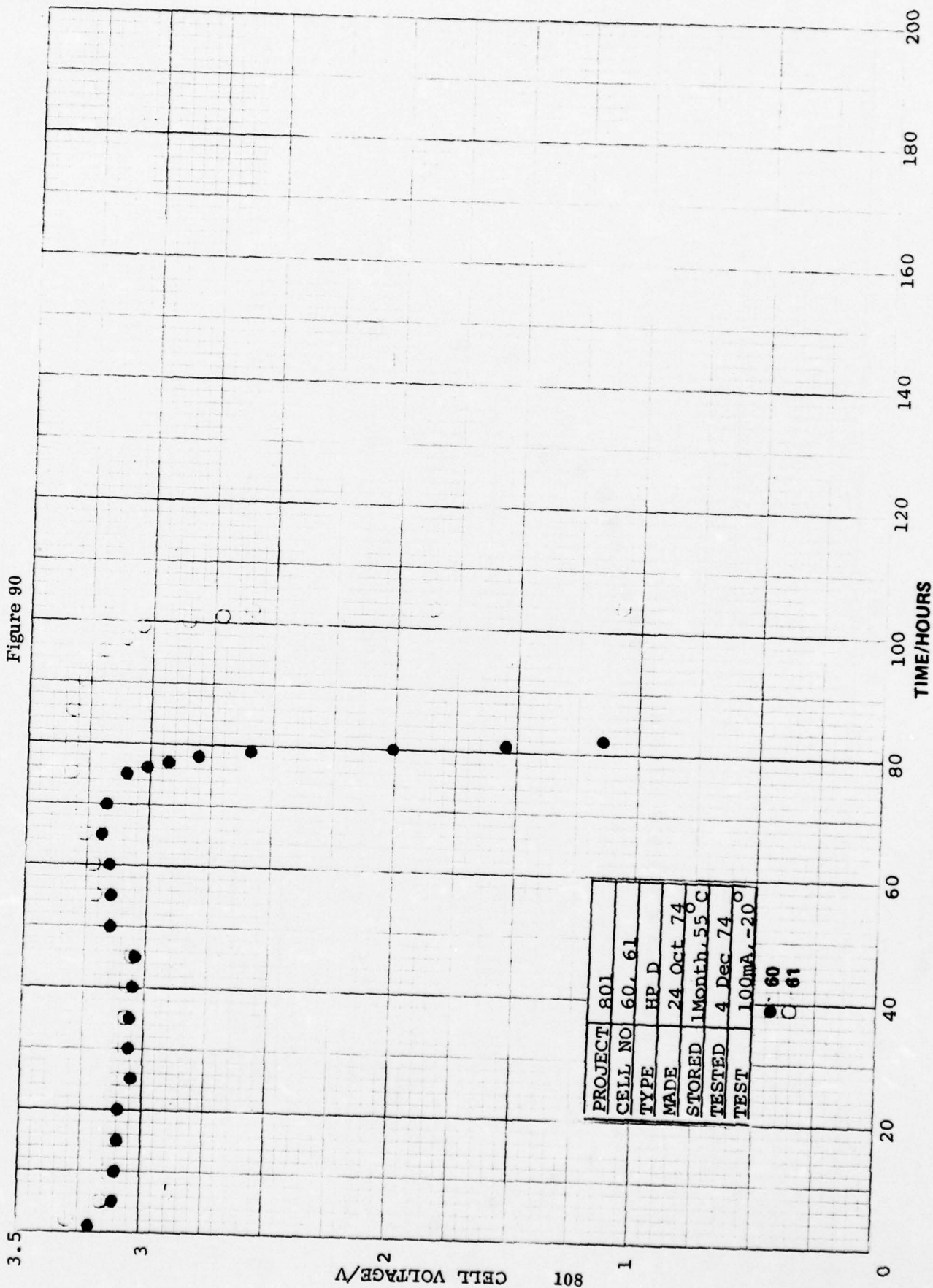
● 84
○ 85

Figure 89



PROJECT	801
CELL NO	108,
TYPE	HP D
MADE	24 Oct 74
STORED	1 Month, 55°C
TESTED	
TEST	2.0A, 40°C

Figure 90



The discharges at low rates (0.1 to 0.2 A) showed the cell capacity essentially unchanged, relative to the results obtained with the fresh cells. A rather erratic behavior is observed in cell capacity vs. discharge rate, as the rate was increased. In most cases it reflects the effect of the increased internal resistance on storage, particularly at lower discharge temperatures. The most significant observation was made when these cells were discharged at elevated temperatures (40°C). The cell performance was quite satisfactory in the entire range of discharge rates. The individual discharge curves showed that the cells delivered most of their energy at fairly high voltage levels, not different from those experienced with the fresh cells. The beginning of the discharge (voltage delay) of these cells was somewhat different and is discussed further below.

Most of the cells stored at 72°C for one month showed an apparent loss in capacity delivered above the selected cutoff voltage of 2.0 V, even at low discharge rates. The exceptions were the cells discharged at 40°C, as the data in Table 5 show. The individual discharge curves for the cells listed are shown in Figures 91 to 103. The legend on each of the discharge curves also shows the time elapsed between the completion of the storage test and the beginning of the discharge test, during which time the cells were kept at room temperature.

TABLE 5
CELL CAPACITY AFTER ONE MONTH STORAGE AT 72°C

Discharge Rate A	Cell Capacity at			
	-20°C	0°C	20°C	40°C
0.05	6.40	5.40	1.75	8.00
	--	--	2.60	4.00
0.1	7.40	6.00	7.40	8.60
	2.30	6.70	8.40	10.50
0.2	4.00	3.20	8.6	9.80
	2.75	4.20	0	10.00
0.5	--	--	--	4.00
	--	--	--	4.00

Figure 91

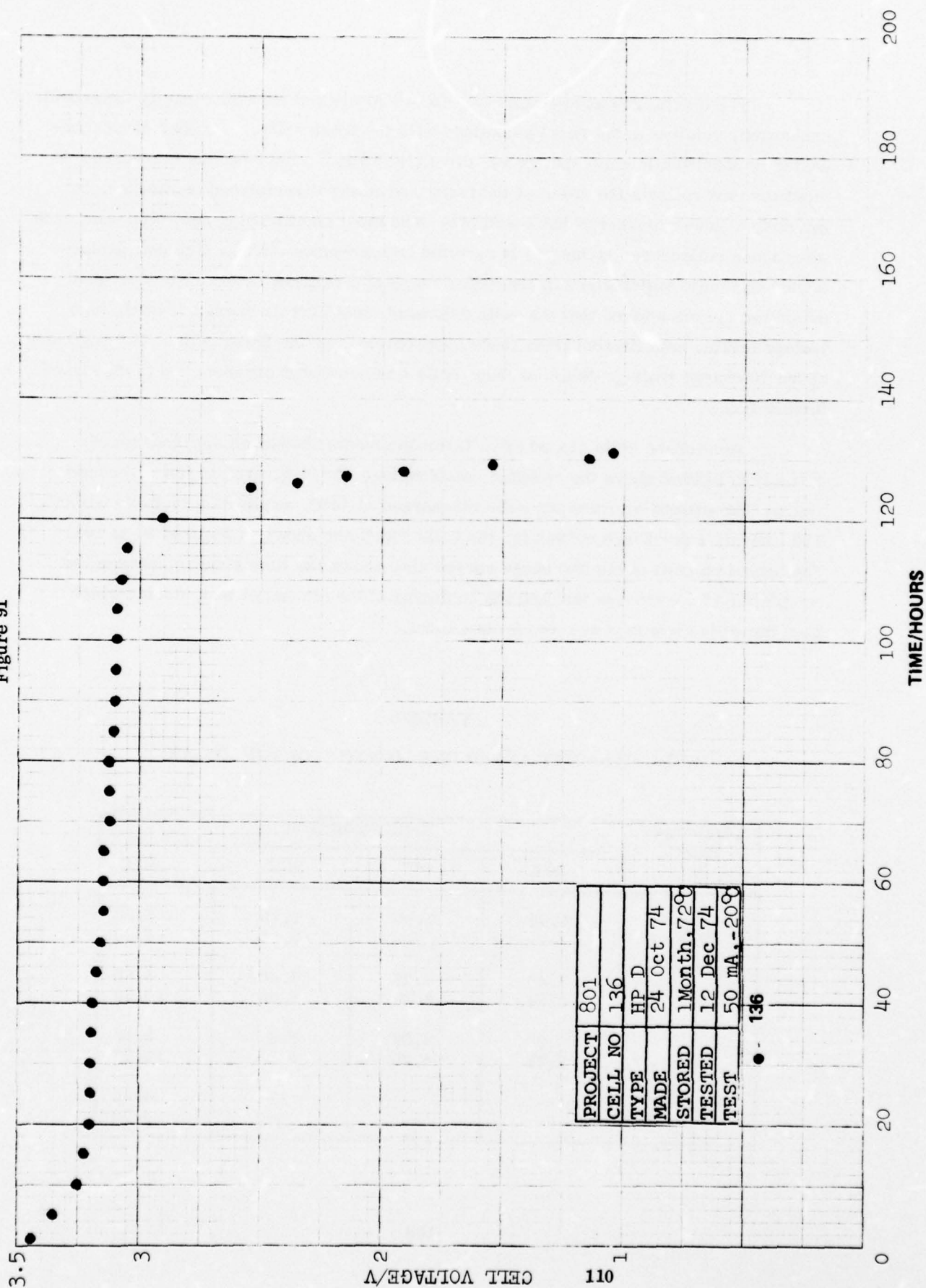
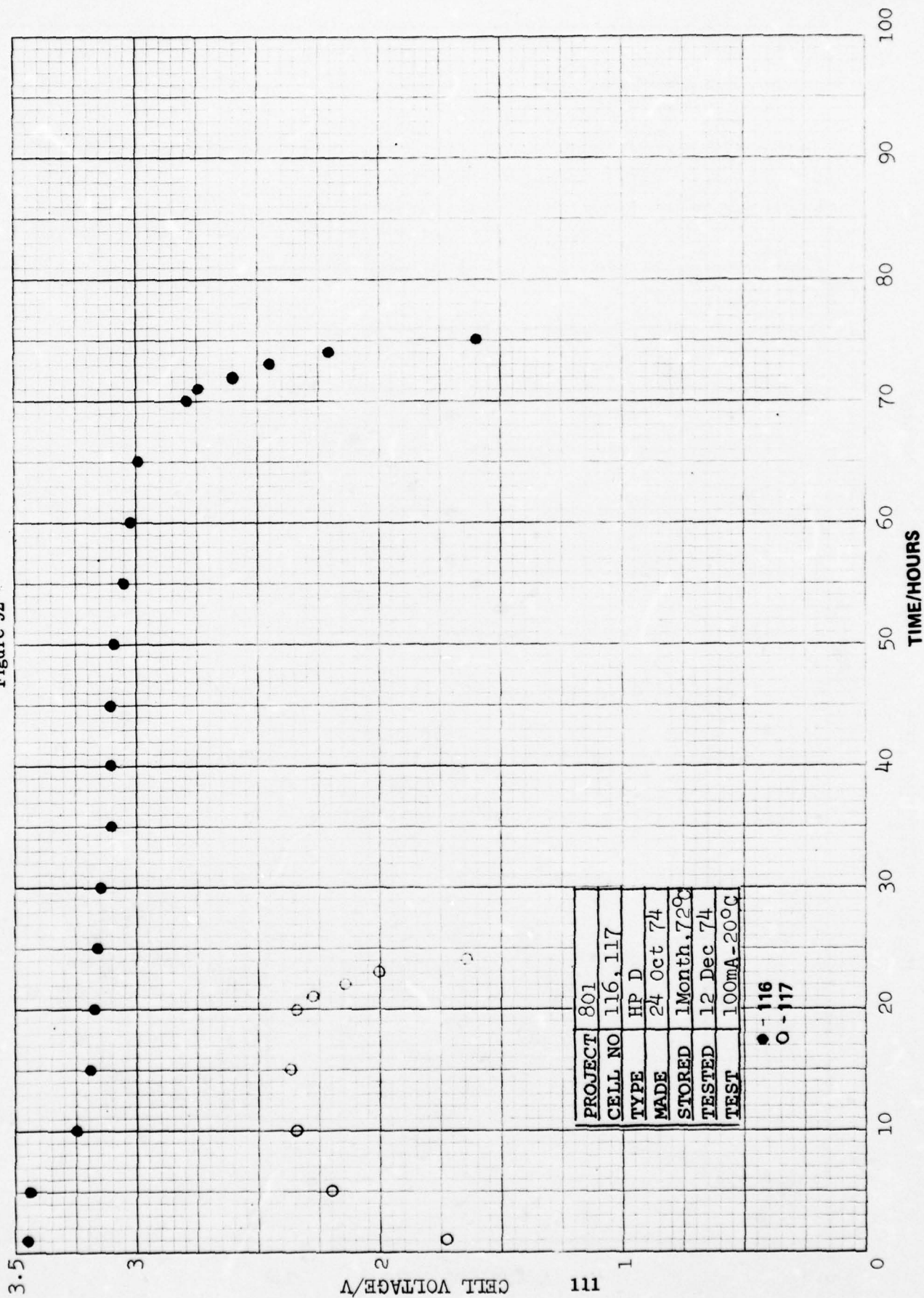


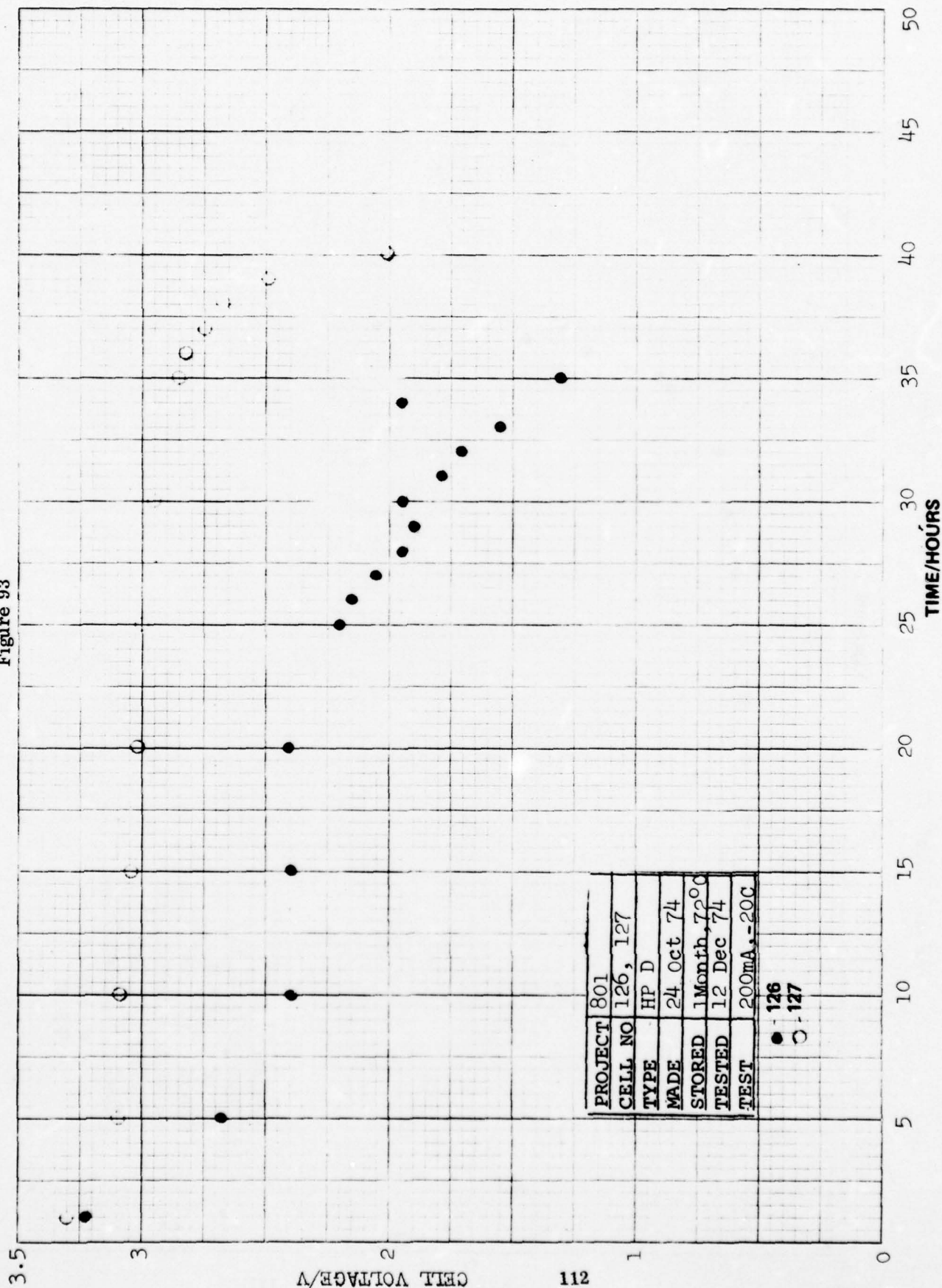
Figure 92



PROJECT	801
CELL NO	116, 117
TYPE	HP D
MADE	24 Oct 74
STORED	1 Month, 72°C
TESTED	12 Dec 74
TEST	100mA - 20°C

● - 116
○ - 117

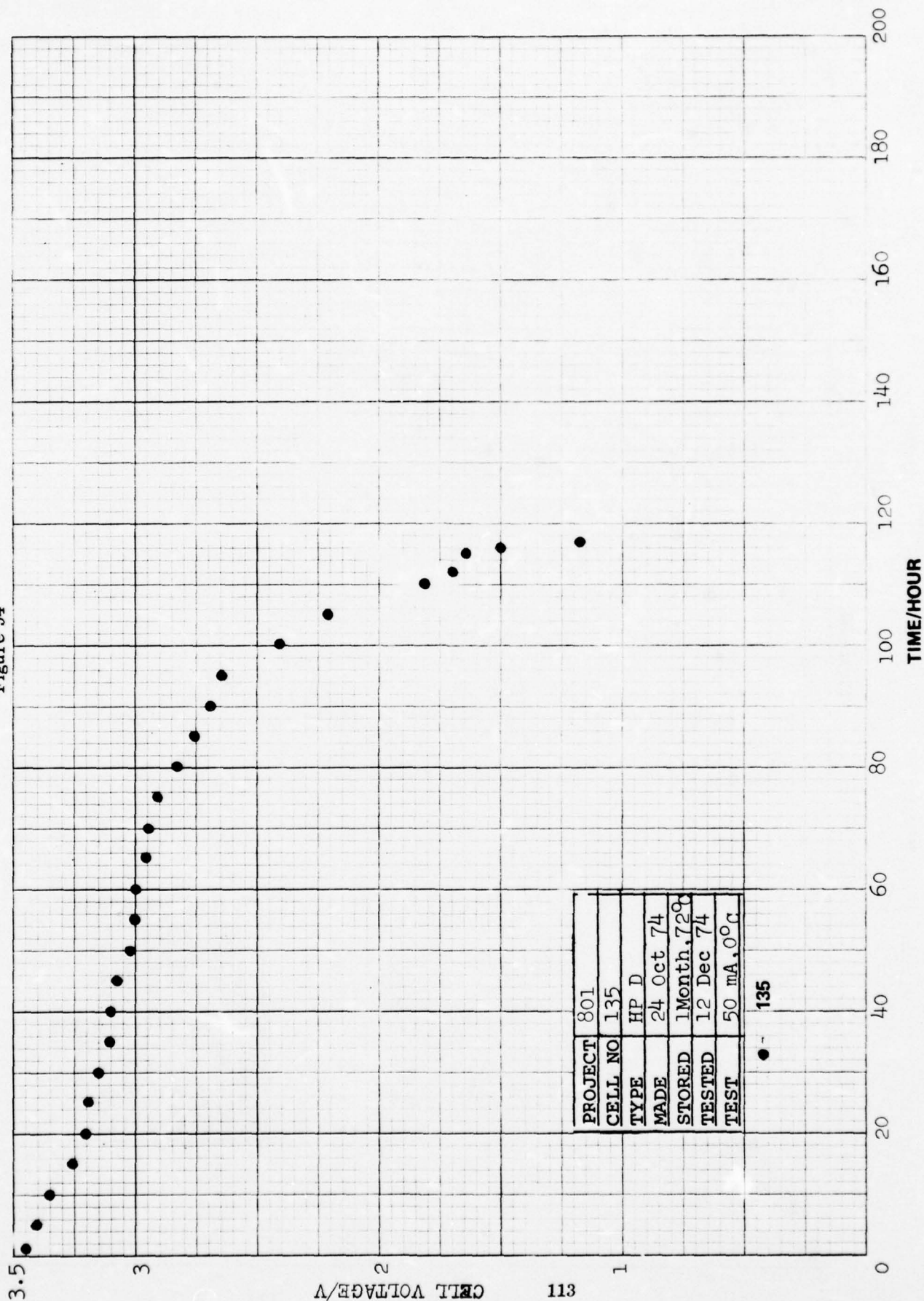
Figure 93



PROJECT	801
CELL NO	126, 127
TYPE	HP D
MADE	24 Oct 74
STORED	1 Month, 72°C
TESTED	12 Dec 74
TEST	200mA, -20C

● 126
○ 127

Figure 94



PROJECT	801
CELL NO	135
TYPE	HP D
MADE	24 Oct 74
STORED	1 Month, 72°C
TESTED	12 Dec 74
TEST	50 mA, 0°C

Figure 95

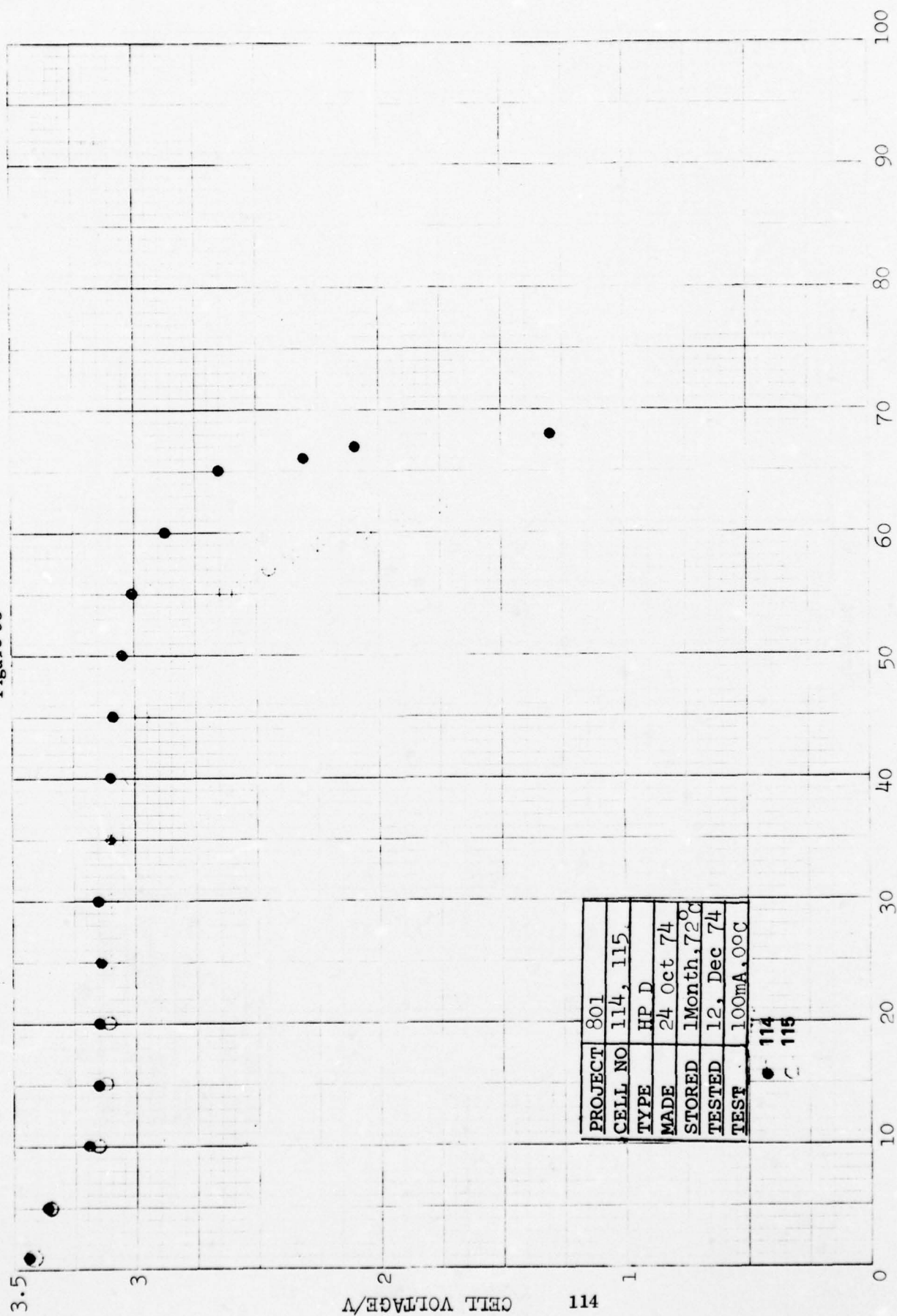
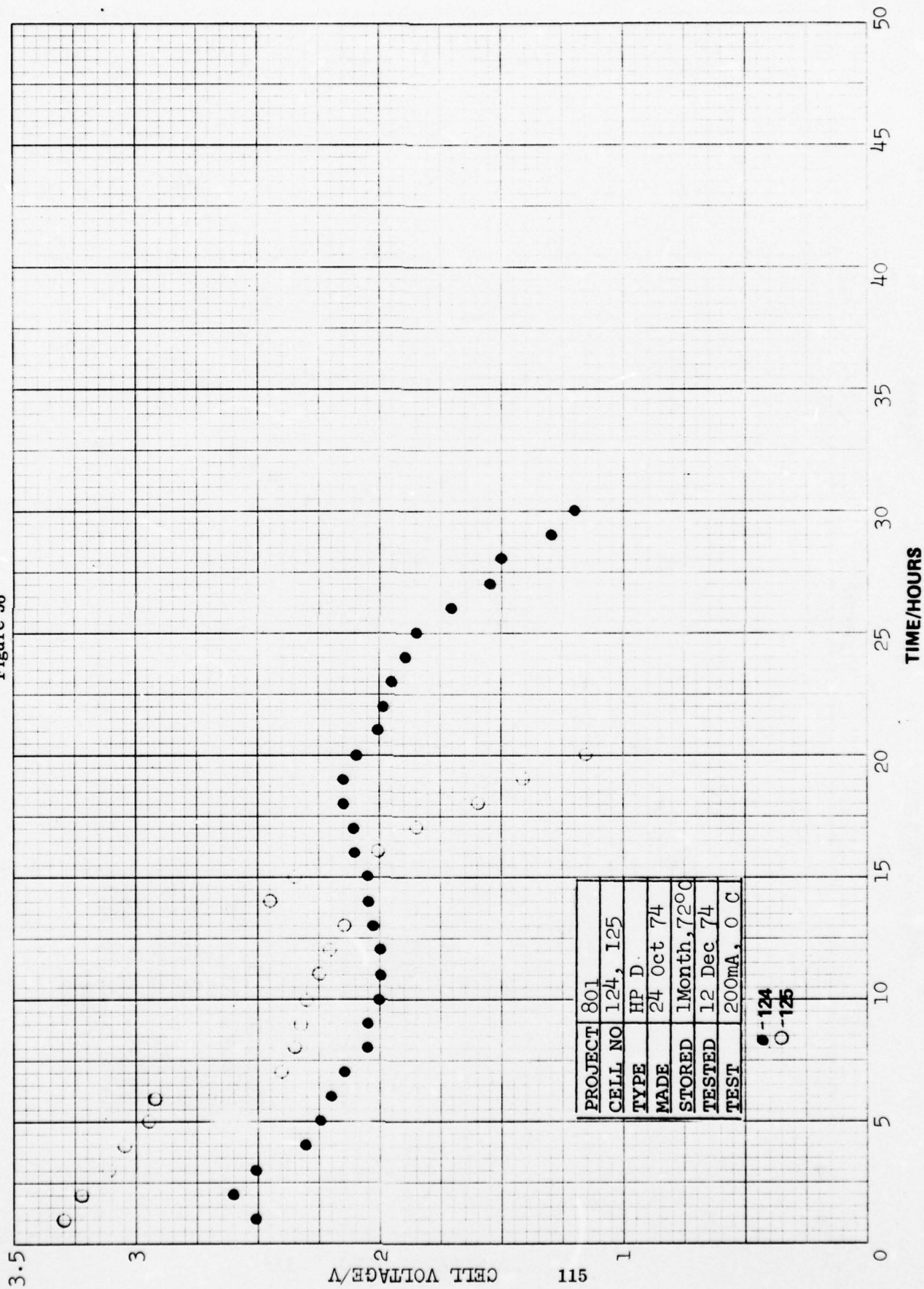


Figure 96



PROJECT	801
CELL NO	124, 125
TYPE	HP D.
MADE	24 Oct 74
STORED	1 Month, 72°C
TESTED	12 Dec 74
TEST	200mA, 0 C

● - 124
○ - 125

Figure 97

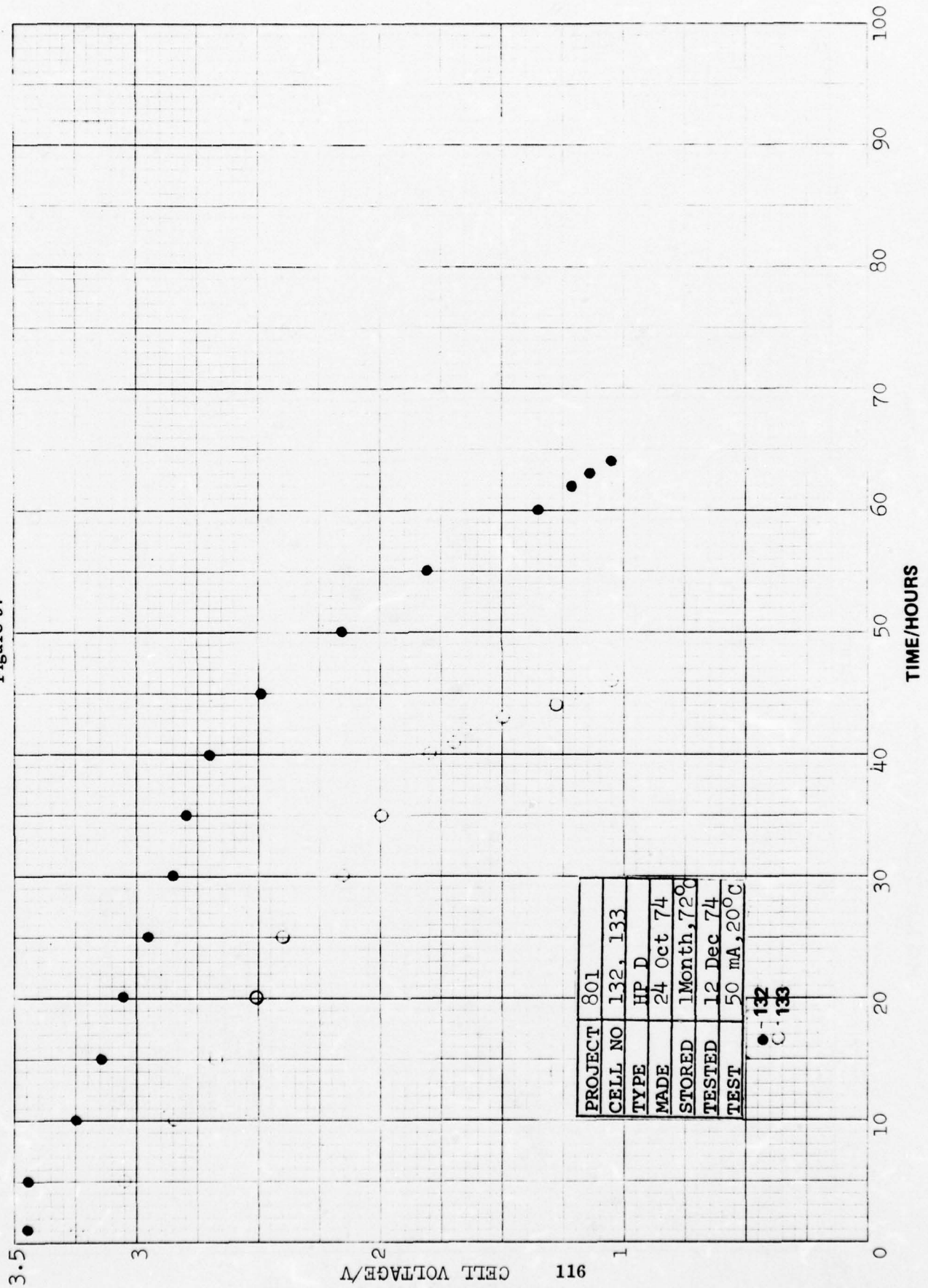
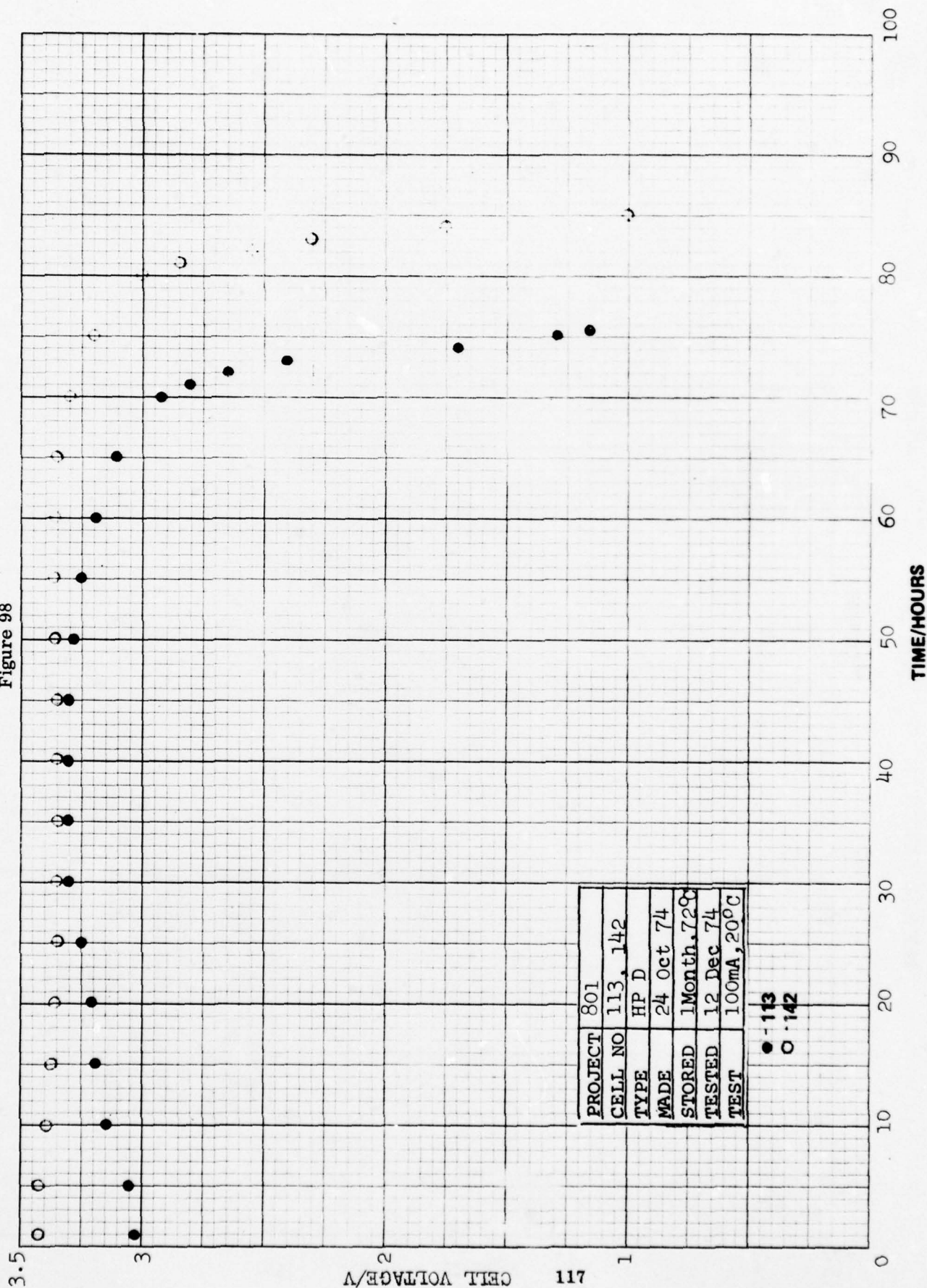


Figure 98



PROJECT	801
CELL NO	113, 142
TYPE	HP D
MADE	24 Oct 74
STORED	1 Month, 72°C
TESTED	12 Dec 74
TEST	100mA, 20°C

● - 113
○ - 142

Figure 99

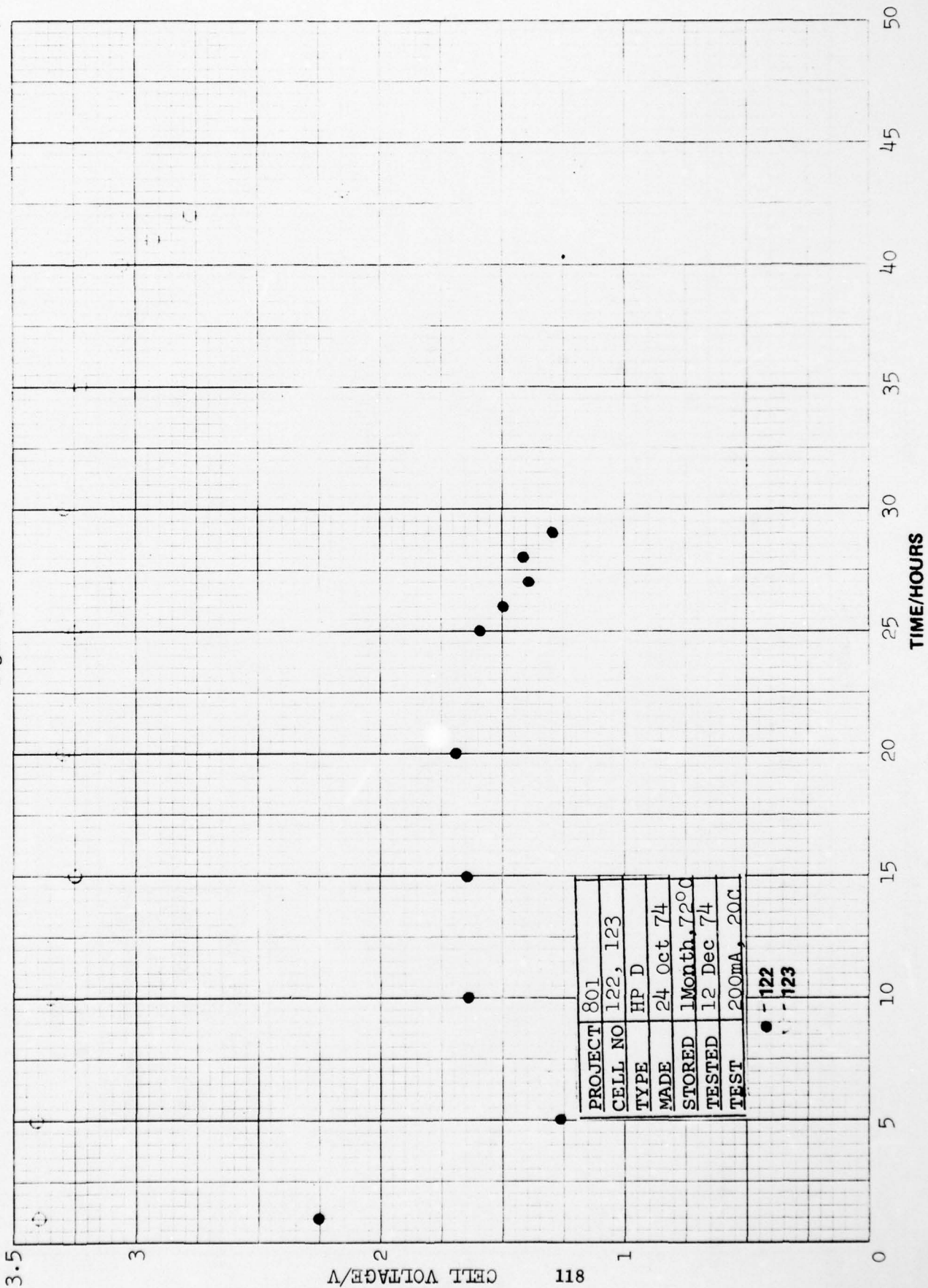
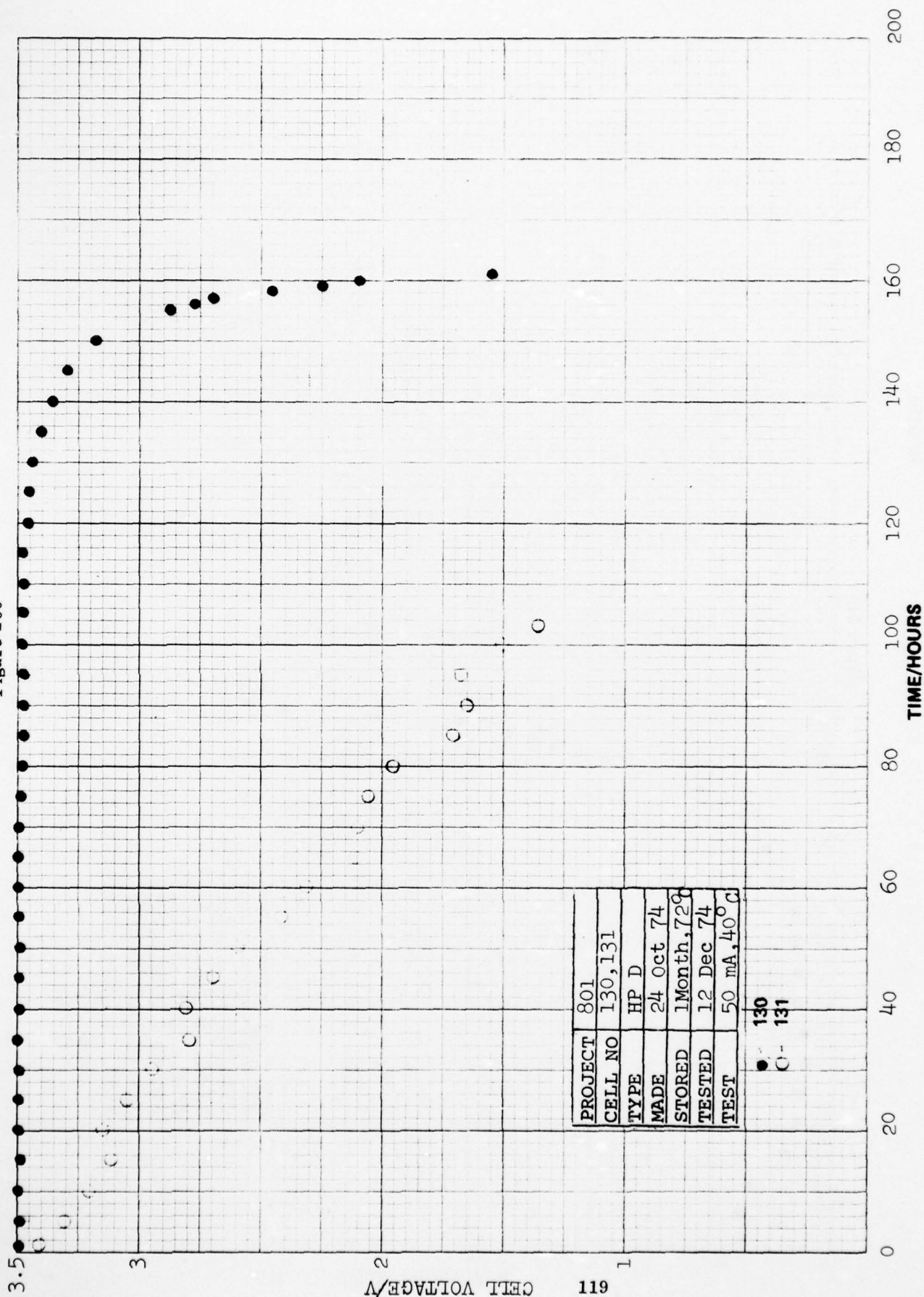


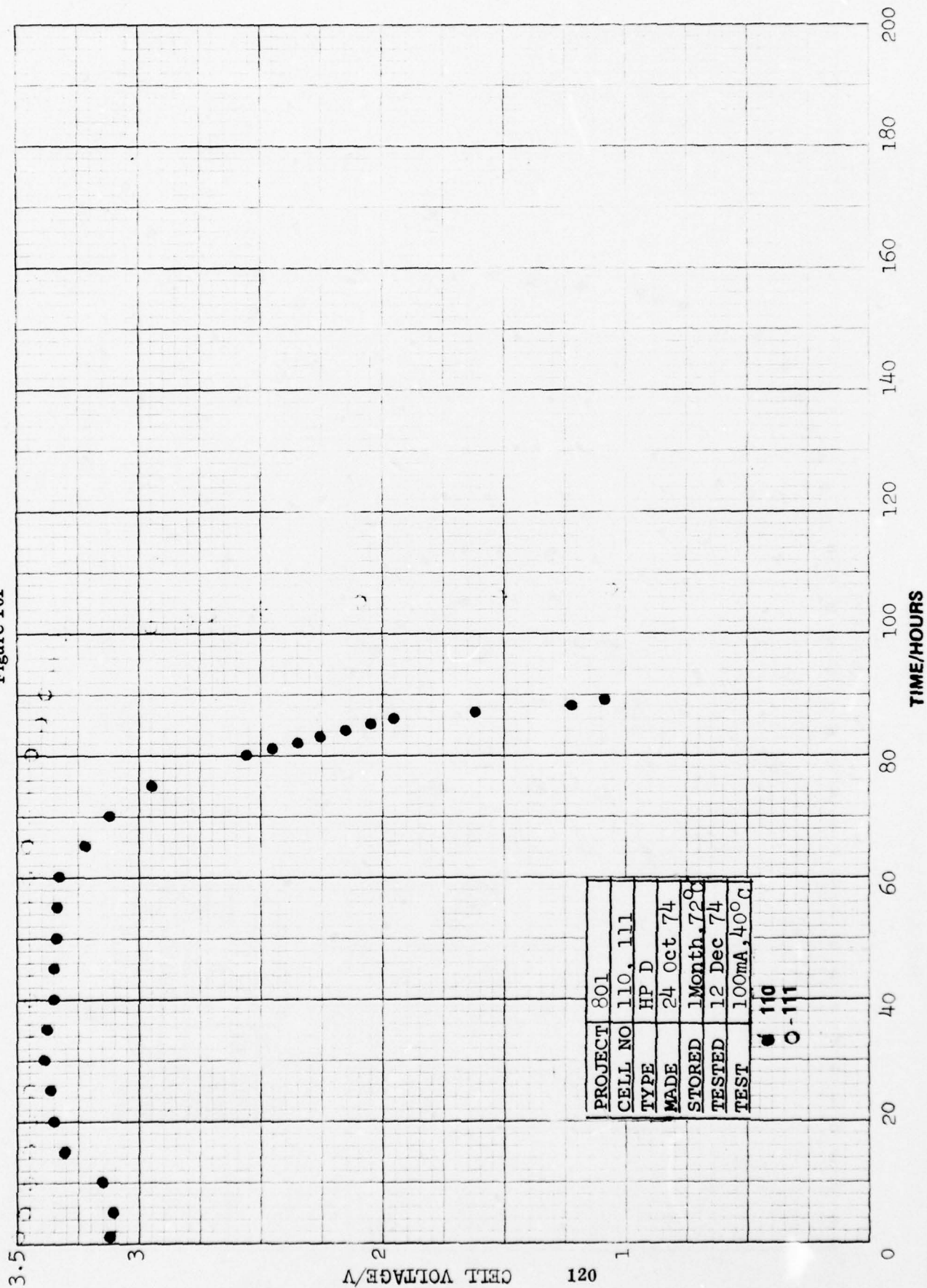
Figure 100



PROJECT	801
CELL NO	130, 131
TYPE	HP D
MADE	24 Oct 74
STORED	1 Month, 72°
TESTED	12 Dec 74
TEST	50 mA, 40° C

● 130
○ 131

Figure 101



PROJECT	801
CELL NO	110, 111
TYPE	HP D
MADE	24 Oct 74
STORED	1 Month. 72°
TESTED	12 Dec 74
TEST	100mA, 40°C

● 110
○ 111

Figure 102

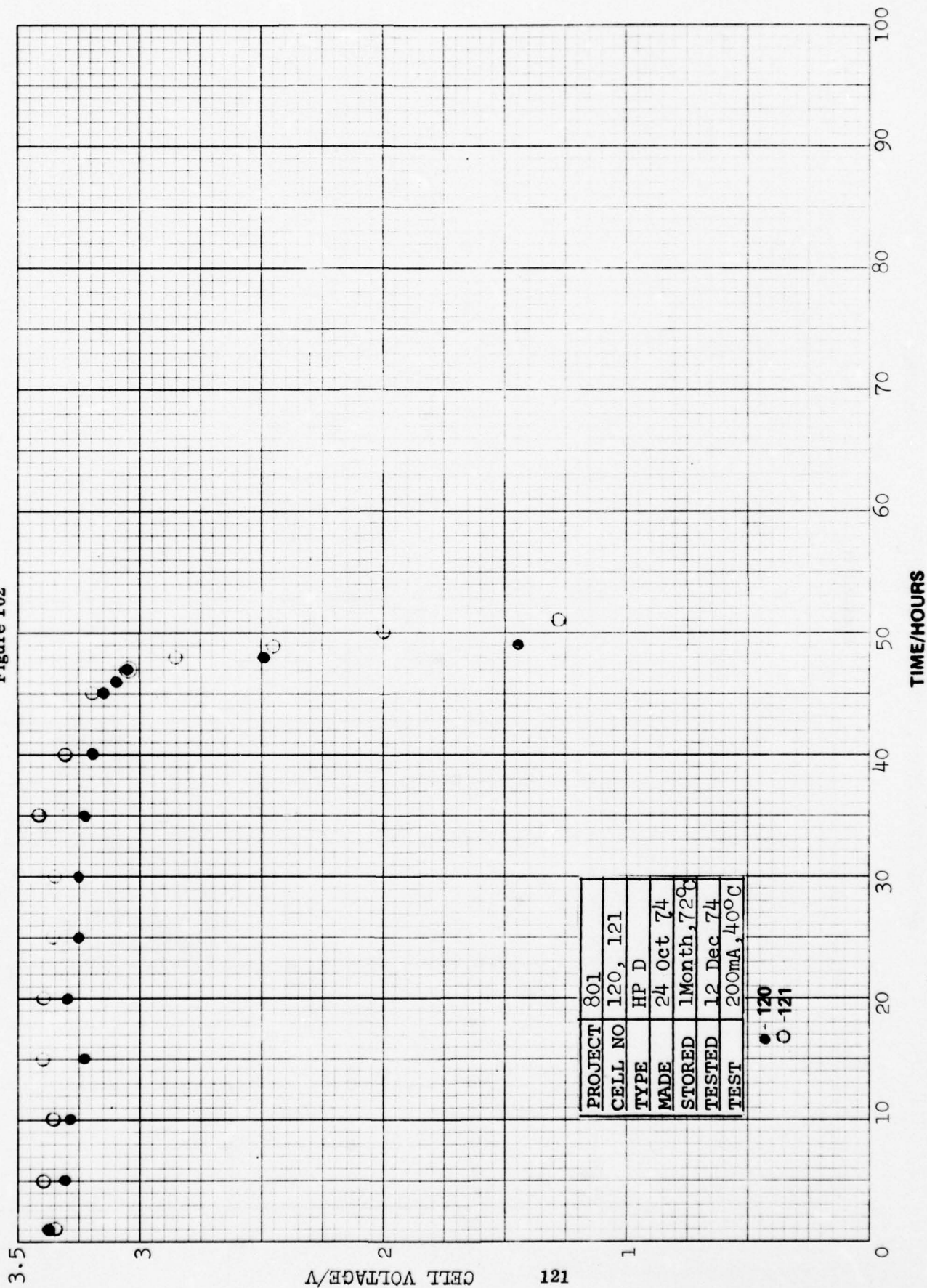
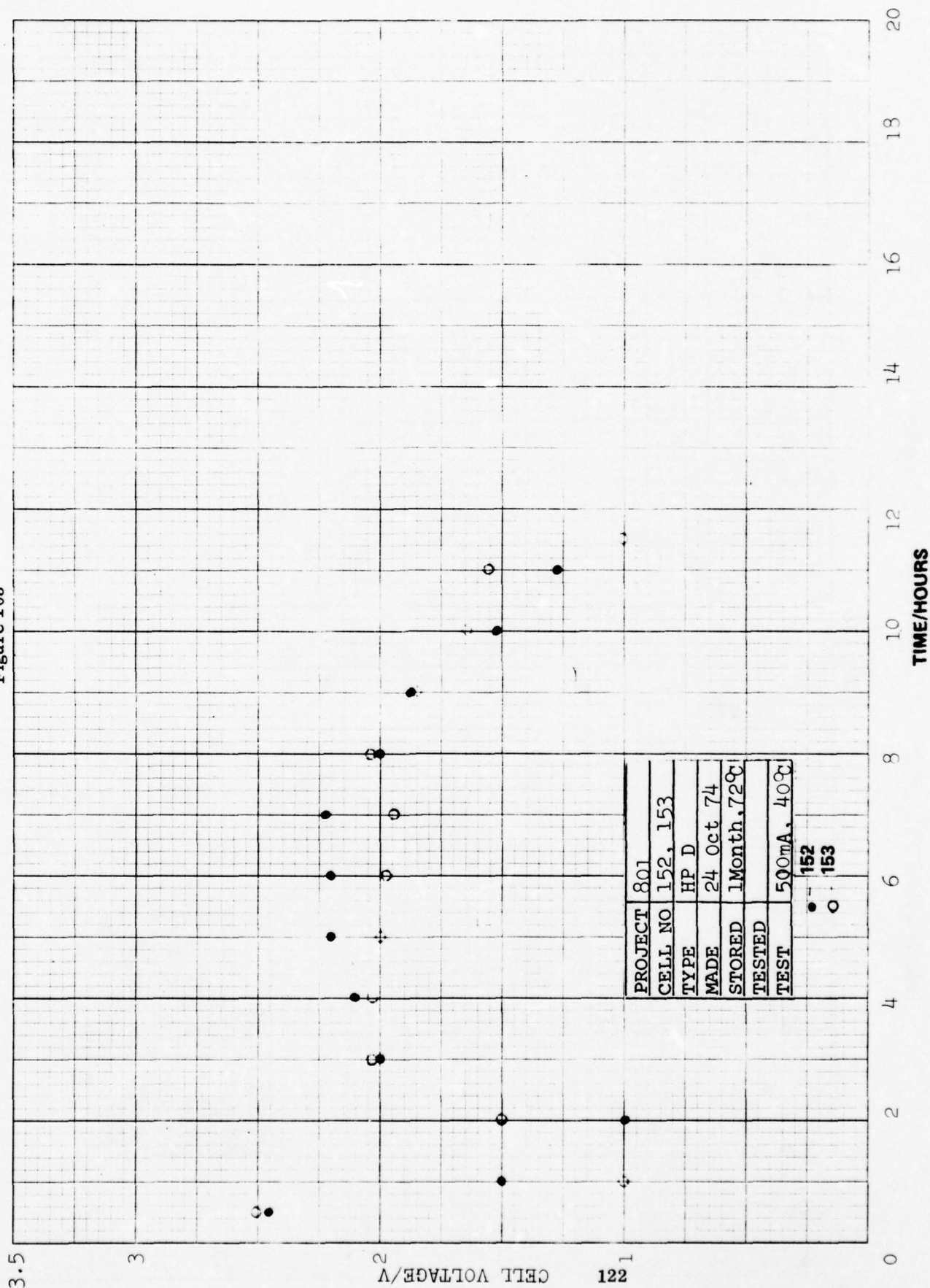


Figure 103



The discharge at 40°C shows that in this storage period no loss of lithium has occurred. The cells delivered their capacity at low rates of discharge equal to that obtained with the fresh cells. Highest discharge rates could not be sustained, even at the elevated temperature, showing a low voltage on discharge at the beginning, continuing the discharge below the 2.0 V cutoff line, or at extreme rates, polarizing the cells even further.

7.4 VOLTAGE DELAY AFTER STORAGE

The operating voltage of the fresh cells was established very fast with no measurable delay. A slight rise of the voltage was observed during discharge only at extreme discharge rates. This is believed to be caused by the internal heating of the cell rather than the removal of any passivating film from the lithium surface.

The extent of the delay observed on the cells after storage of one month at room temperature is shown in Table 6 for various test temperatures and various discharge rates. The delay is presented here as the time required for the cell voltage to recover to 2.0 V, following the start of discharge. This voltage level is selected in order to be able to tabulate all the results together, bearing in mind that, for the lower discharge rates, the time difference between the recovery to 2.0 V and to 2.5 V was very short and can be extracted from the raw data obtained. In general, the delay is longer for lower test temperatures and also for higher discharge rates. The charge passed in the recovery time period at various test conditions does not seem to be related to the extent of the passive film build-up, but only to the rate and temperature of discharge.

The beginning of discharge of these cells was monitored with two recorders in parallel - one slow to follow the cell voltage to the end of discharge, and one faster to register the voltage drop at the beginning of discharge and its recovery to the 2 V cutoff line. The data for the cells stored at 55°C are tabulated in Table 7. At extreme low discharge rates, the voltage drop below 2.0 V was observed only at low discharge temperatures. The behavior becomes very erratic as the discharge rate increases, generally showing a shorter recovery time at higher temperatures. A clear effect of the elevated discharge temperature is demonstrated with the data obtained at 40°C.

After storage at 72°C, the cells could only be discharged at fairly low rates and elevated temperatures, as the data in Table 5 show. Table 8 shows the recovery time to 2.0 V after the beginning of discharge. With a few exceptions, the cells showed

TABLE 6
VOLTAGE DELAY AFTER ONE MONTH STORAGE AT ROOM TEMPERATURE

Discharge Temperature °C	Discharge Rate A	Cell No.	Recovery Time to 2.0 V Second
40	0.2	1	0
		2	0
	0.5	11	0
		12	0
	1.0	21	2.0
		22	6.5
	2.0	32	3.0
		31	9.0
RT	4.0	--	--
		--	--
	0.1	3	0
		4	0
	0.2	13	1.0
		14	1.5
	0.5	23	--
		24	2.8
	1.0	33	5.5
		34	0.5
	2.0	45	30.0
		44	5.0
0	4.0	50	144.0
		51	1260.0
	0.1	5	2.0
		6	0
	0.2	15	14.0
		16	6.0
	0.5	25	9.0
		26	2.5
	1.0	35	21.0
		36	42.0
	2.0	47	28.0
		46	0
	4.0	25	180.0
		53	60.0

TABLE 6 (Cont'd)

Discharge Temperature °C	Discharge Rate A	Cell No.	Recovery Time to 2.0 V Second
-20°C	0.1	7	2.0
		8	0
	0.2	17	1.5
		18	2.0
	0.5	27	5.5
		28	9.5
	1.0	38	97.0
		39	66.0
	2.0	42	46.0
		48	48.0
-40	0.1	9	120.0
		10	4.5
	0.2	19	3.5
		20	4.5
	0.5	29	21.0
		30	96.0
	1.0	40	115.0
		41	106.0
	2.0	43	201.0
		37	251.0

TABLE 7

VOLTAGE RECOVERY ON DISCHARGE AFTER STORAGE OF ONE MONTH AT 55°C

Cell Number	Discharge Rate mA	Discharge Temp. °C	Time to 2 Volts Seconds
54	100	40	0
55	100	40	0
56	100	RT	0
57	100	RT	0
58	100	0	0
59	100	0	0
60	100	-20	0
61	100	-20	208
62	100	-40	280
63	100	-40	22
64	200	40	0
65	200	40	0
66	200	20	71
67	200	20	216
68	200	0	243
69	200	0	414
70	200	-20	27
71	200	-20	0
74	500	40	0
75	500	40	6
76	500	20	0
106	500	20	41
109	500	0	0
79	500	0	63
80	500	-20	90

TABLE 7 (Cont'd)

Cell Number	Discharge Rate mA	Discharge Temp. °C	Time to 2 Volts Seconds
81	500	-20	360
84	1000	40	45
85	1000	40	114
86	1000	20	20
87	1000	20	28 1/2
88	1000	0	Discharge below 2V 54, below 0
89	1000	0	84
90	1000	-20	118
91	1000	-20	103
108	2000	40	816
95	2000	40	270
96	2000	20	321
97	2000	20	324
103	2000	0	174
104	2000	0	408

TABLE 8

VOLTAGE RECOVERY ON DISCHARGE AFTER STORAGE OF ONE MONTH AT 72°C

Cell Number	Discharge Rate mA	Discharge Temp. °C	Time to 2 Volts Seconds
130	50	40	0
131	50	40	0
132	50	20	0
133	50	20	0
135	50	0	0
136	50	-20	0
110	100	40	0
111	100	40	0
142	100	20	0
113	100	20	0
114	100	0	0
115	100	0	0
116	100	-20	0
117	100	-20	7200
120	200	40	0
121	200	40	0
122	200	20	138
123	200	20	0
124	200	0	0
125	200	0	0
126	200	-20	0
127	200	-20	0
152	500	40	135
153	500	40	60

the delay lower than expected on the basis of the tests at 55°C. The scheduling of tests allowed a longer period of time for these cells at room temperature after the storage and before the beginning of discharge. This suggests that changes in the composition of the passivating film may be taking place at room temperature, after the film has been formed during storage at elevated temperatures. The results are, however, quite inconclusive.

The capacity data (Tables 4 and 5) and the recovery data (Tables 6, 7 and 8) strongly suggest that the cells, in fact, do not suffer a loss in capacity on storage, if one discharges them at low rates only. The amount of lithium involved in the build up of the passivating film is, obviously, very small compared with the total amount present in the cell. The removal of the passivating film at the beginning of discharge seems to be the most important step determining the capacity that will be delivered following this step. The conductivity of the film seems to depend on temperature in the same fashion in which the electrolyte's ability to accept the primary discharge product depends on temperature. Since the passivating film is anodically inactive, the stripping must depend on the conductivity of the film and the ability of the electrolyte to leach the products formed underneath the film at the beginning of discharge. The rate of formation of products (rate of discharge) cannot be higher than the rate of mass transport through the film, since in that case the products are precipitated and accumulated on the lithium surface, causing further polarization of the cell. The fact that the cell discharged at 40°C does not show either a capacity loss or a significant voltage delay regardless of the storage history, suggests that a procedure could be devised for activating the cells after a prolonged storage prior to their use.

The cells were opened for inspection of the components at various stages in the course of storage and discharge. The cells are normally built with an excess of both the electrolyte and lithium. The discharge is terminated when all the active carbon sites are blocked by the discharge products. Cathodes on discharge slowly turn from flexible porous structures to rigid dense structures, as the pores are more and more filled with the discharge products.

No visible change in the cell interior has been observed as a result of storage alone, except for a slight yellowing of the separators. The flexibility of the cathode was always in an inverse proportion with the amount of charge obtained from the cell before it was opened. The anode in the discharged cell will show perforation as a result of dissolution, but a sufficient amount of lithium has been left at the end of discharge.

The cells that could not be discharged at high rates after storage at elevated temperatures were inspected in this manner and found apparently intact. Without loss of the electrolyte, without loss of lithium, with still flexible soft cathodes and with all good welded contact one has to blame the passivating film on the lithium surface for the cell failure to discharge at excessive rates.

Our regular type electrolyte, prepared with care, was used in the next series of experiments, whereby the cells were partially discharged before they were put in storage. Fresh cells of this group were all discharged for one hour with 1 A constant current, which amounts to approximately 20% of the total cell capacity available in the lithium anode. After storage of one month, the cells were tested for voltage delay according to the program shown in Table 9.

The voltage delay data obtained with these cells are the best so far. All cells established at stable operating voltage above 2.0 V after 3.5 minutes maximum after one month storage at 72°C, which in all other experiments produced totally passivated cells. This confirms previous experience with thionyl chloride cells, showing a much lower rate of passivating film build up with cells that were briefly used in various devices and then turned off and left alone. One could speculate as to the origin of this phenomenon, but at least two factors appear certain. The first is the increase of the roughness factor of lithium surface by anodic etching at the beginning of discharge. Extruded lithium foil, and particularly a rolled one, come from the manufacturer in a very shiny form while a partially discharged foil acquires a dull appearance even in the ultrapure electrolytes. The second factor is the formation of a supersaturated solution in the vicinity of the lithium surface in the course of discharge. It is quite possible that some of the impurities may be removed from the solution either in the course of discharge or when the supersaturated solution of lithium species finally breaks up and LiCl precipitates within the cathode pores.

These results deserve more attention. It would be of interest to establish the minimum fraction of prior discharge that would still show this effect and also the most favorable conditions under which the prior discharge is conducted. It might be possible to come up with a procedure that would be practical in reducing the voltage delay. The discharge, at 200 mA following the voltage delay measurements, yielded the expected cell capacities for each of the storage temperatures above the cutoff voltage of 2.0 V. There was no indication of any unexpected capacity deterioration on storage following the partial discharge.

TABLE 9
VOLTAGE DELAY AFTER STORAGE OF PARTIALLY DISCHARGED CELLS
TIME OF RECOVERY TO 2.0V STORAGE TIME 30 DAYS

Cell No.	Storage Temp °C	Current Density mA/cm ²	Voltage Delay
121 122	25	2.8	0 0
123 124		5.6	12 sec. 6 sec.
125 126		11.2	12 sec. 12 sec.
127 128		2.8	2 min. 1 min. 18 sec.
129 130		5.6	2.5 min. 1 min. 15 sec.
131 132		11.2	4 min. 25 sec. 4 min.
133 134	72	2.8	2 min. 30 sec. 2 min. 48 sec.
135 136		5.6	2 min. 3 min.
137 138		11.2	3 min. 30 sec. 3 min.

7.5 PRESSURE BUILD UP IN SEALED CELLS

There are many difficulties in measuring the pressure generated inside a sealed cell. The main one is associated with the void space available for the gas expansion in the cell alone and in the measuring device at various stages of the pressure build-up. The void space must be left inside the sealed cells to allow for the expansion of cell electrolyte at elevated temperature. It must be entered into the design of the cell components and then maintained by observing the cell assembling procedures.

Attaching a pressure sensing device to the sealed cell usually changes the total void space, so that the pressure readings have to be corrected to arrive at the actual pressures that would have been generated inside the cell alone.

Steady-state pressure measurements are somewhat simpler, since one could allow enough time for achieving equilibria with respect to both the temperature and the concentration of soluble gases in liquid and gas phases of the system. However, the dynamic measurement of the pressure (at various states of discharge) yields much more information about the behavior of the system. This method can be made very accurate and it uncovered transients that would have escaped recording in the steady-state measurements.

The High Power Type AA cell was used as a test vehicle in these pressure build-up measurements. All standard cell parts were used except the cell cover; this was substituted with one carrying an adapter for connecting the cell to the manometer. The experimental arrangement used is shown schematically in Figure 104.

A mercury filled capillary manometer was attached to the cell top immediately after the cell was closed, with as little as possible of the empty space in the manometer tube. The cell was left on open circuit voltage for at least 15 minutes to equilibrate its temperature with that of its surroundings, before the experiments were started. The cell discharge was carried out with a constant current of a selected value all the way to zero voltage. The cell voltage was recorded throughout discharge, while the pressure reading was made periodically (more often at higher discharge rates). The pressure reading was continued beyond the end of discharge until a stable value was reached.

The tightness of the connections was checked in two ways. In the first few experiments, the entire cell was immersed in vacuum oil, together with the manometer coupling. No gas bubbles were observed at any of the joints. The second way of checking the tightness was by leaving the arrangement overnight at the end of the discharge test at the finally established pressure, and observing the pressure change after this period of time elapsed. No pressure drop was observed.

The void space in the cell was estimated and recorded to be used in pressure correction calculations. The change in the total gas volume, due to the displacement of mercury in the manometer, was calculated as a function of pressure reading. Slight temperature differences were expected between the interior of the cell and the surroundings at extreme discharge rates, but these were not recorded.

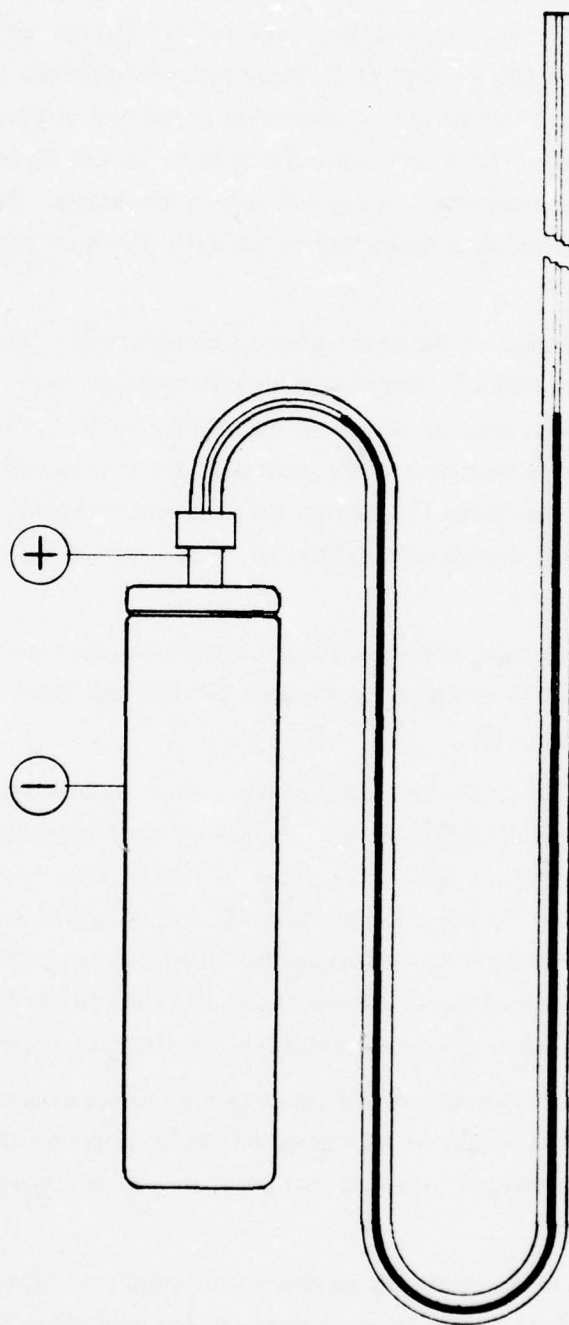


Figure 104. Experimental Arrangements used in Measurements of Cell Pressure During Discharge

The cell voltage is shown as a function of the discharge time, together with the pressure change, in the course of discharge for each of the several selected discharge rates in Figures 105 through 110. Many repetitions of the test shown in Figure 105 demonstrated that no gas is generated in the cell on discharge at 100 mA or below. The starting positive cell pressure of 10 to 12 mm Hg was established during the temperature equilization of the cell before discharge. This value varied from one experiment to another depending on the daily fluctuation of temperature in the laboratory.

The measurements at the next higher discharge rate of 150 mA are shown in Figure 106. A slow increase in pressure was observed here throughout the entire discharge period, almost leveling off by the end of discharge. A sudden increase in pressure was observed here first, as the voltage of the cell approached zero value. Discontinuing the cell discharge terminated the pressure increase, and the pressure inside the discharge cell decreased slightly before it assumed the stable level that was maintained for many hours.

The above pattern of pressure change with discharge was more pronounced at higher current densities as shown in Figures 107 through 110 for rates of 200, 300, 400 and 800 mA, respectively.

It was suspected at the beginning of these experiments that the sudden increase in pressure at the end of discharge may be caused by the heat generated at an increasing rate as the polarization of the cells is increased. Although the heat contribution to the pressure could be easily calculated, the shape of cooling curves and the pressure stability after discharge suggests other possible mechanisms. The most likely of them seems to be the generation of a gaseous product that was redissolved in the electrolyte residue, or re-adsorbed on the cathode soon after the completion of discharge.

Whatever the explanation of the phenomenon, an important lesson follows: The discharge of cells in series at high rates has to be stopped before the weakest of them is completely discharged, since it will generate gas at a very high rate at low voltage or if reversed.

A correction of the pressure readings was attempted here, based on the initial void space, V_0 , of 0.5 cm^3 , and on an increase in the void space with increased pressure at the rate of $0.38 \text{ cm}^3/\text{atmosphere}$ (for the manometer capillary cross-section of 1 mm^2).

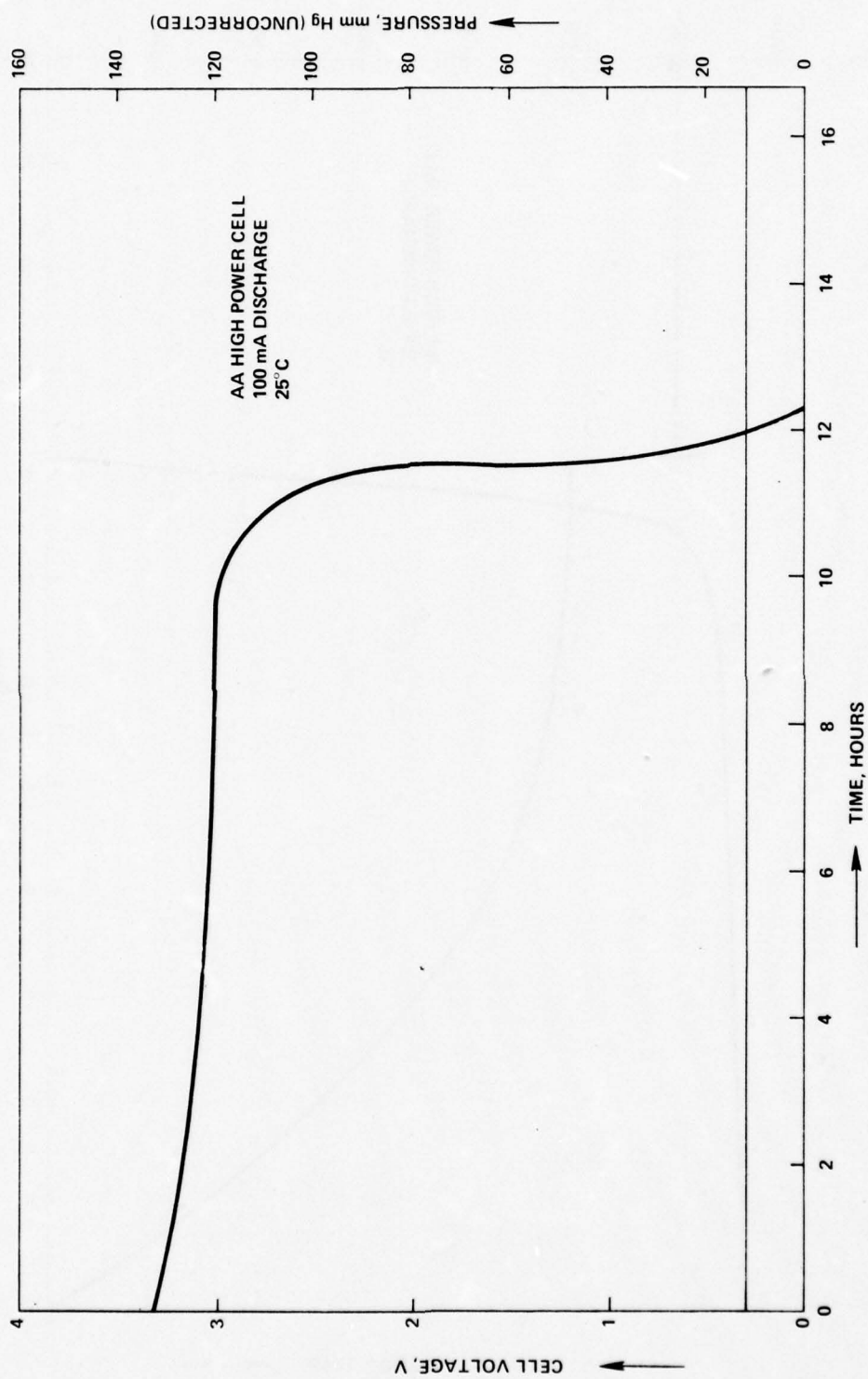


Figure 105. Cell Pressure (Uncorrected) During Discharge with 100 mA

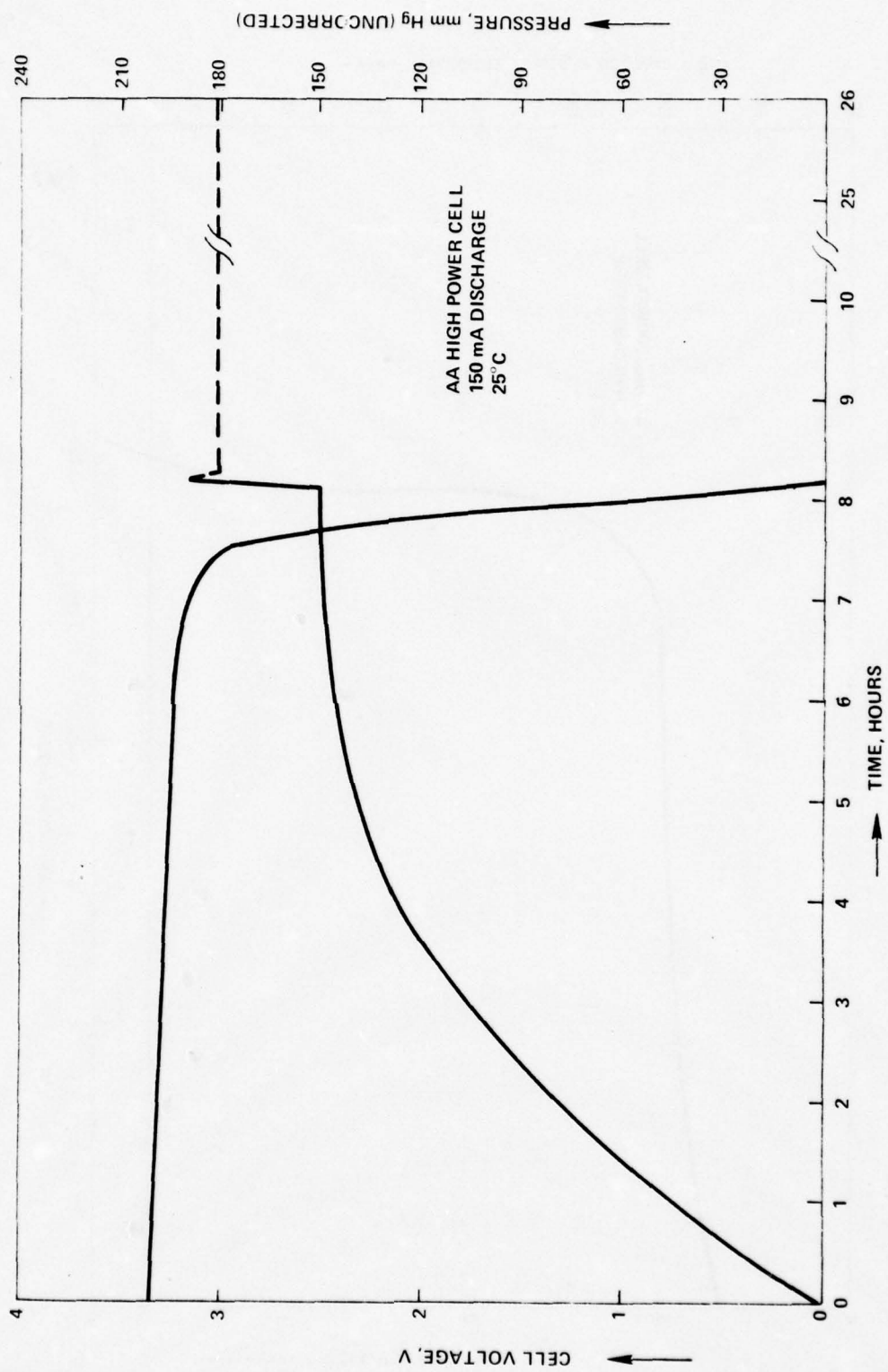


Figure 106. Cell Pressure (Uncorrected) During Discharge with 150 mA

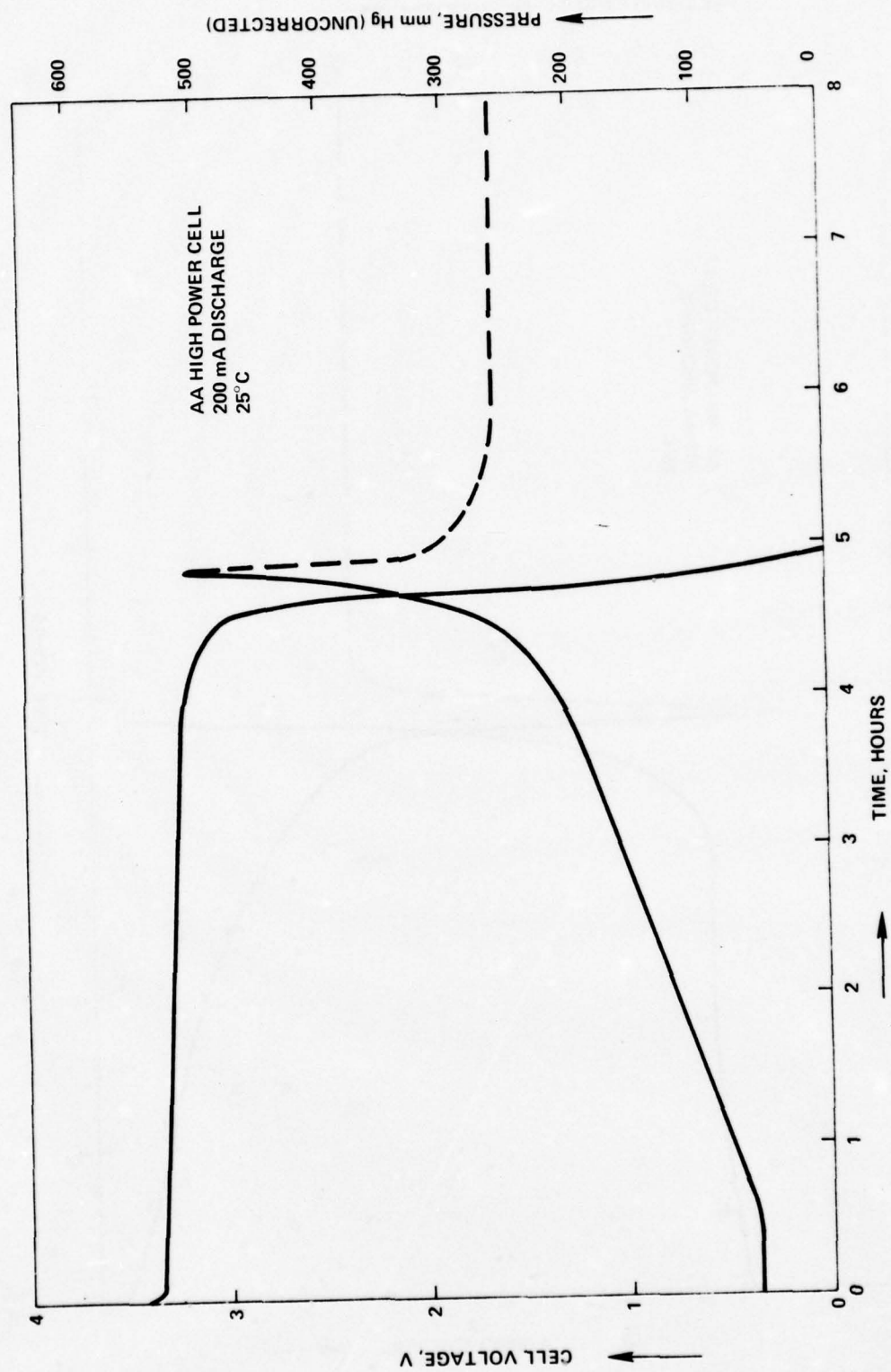


Figure 107. Cell Pressure (Uncorrected) During Discharge with 200 mA

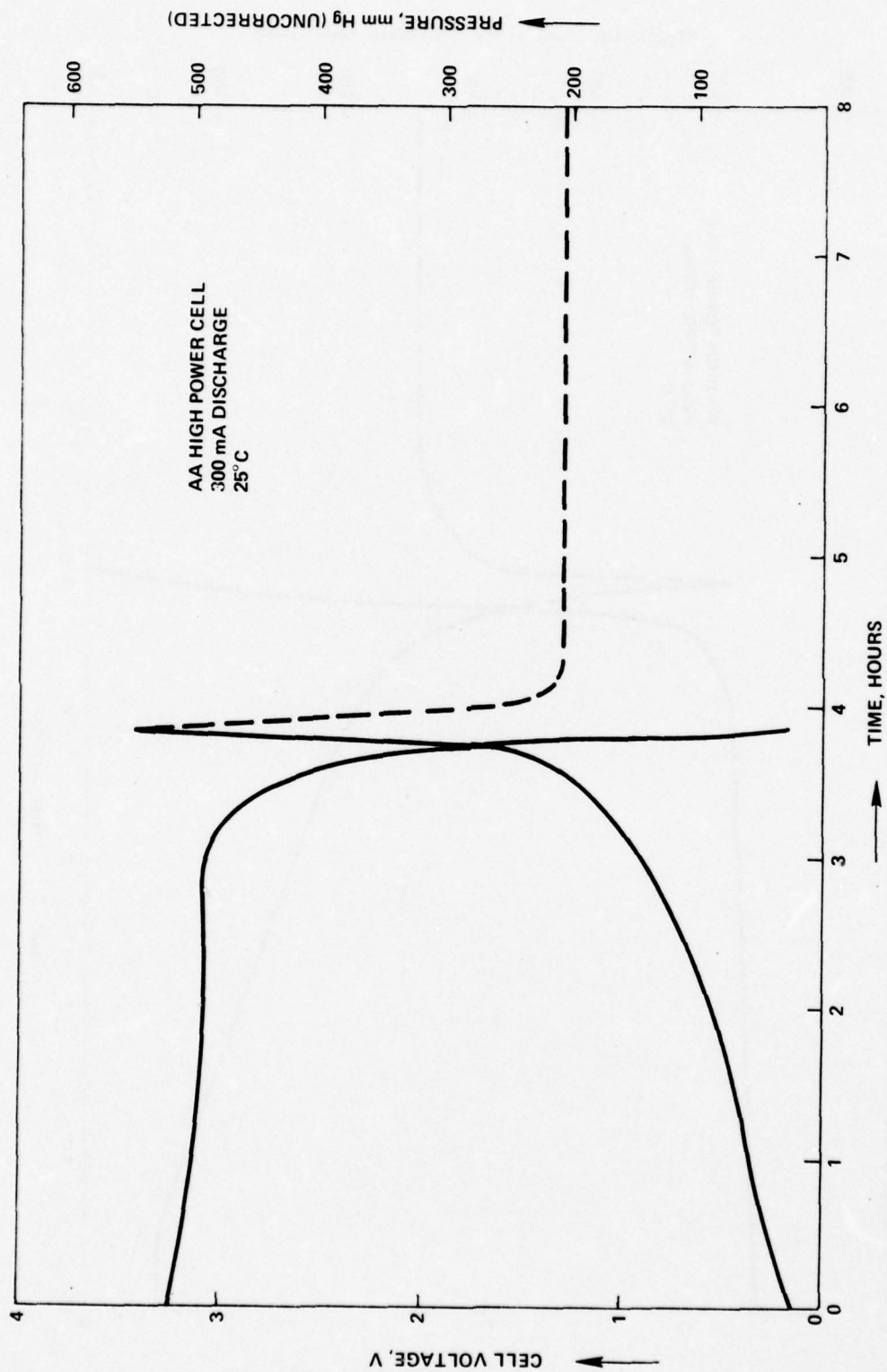


Figure 108. Cell Pressure (Uncorrected) During Discharge with 300 mA

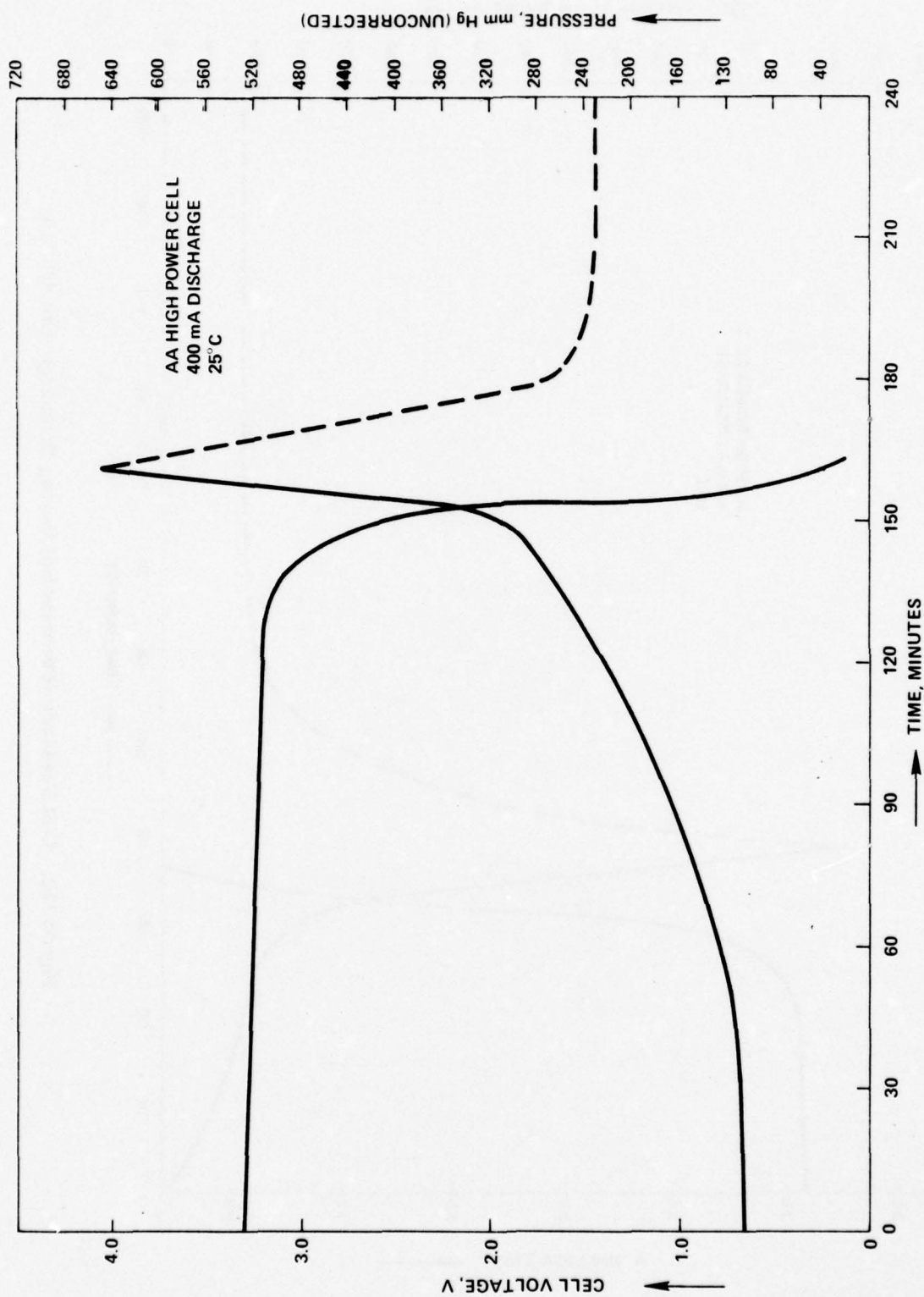


Figure 109. Cell Pressure (Uncorrected) During Discharge with 400 mA

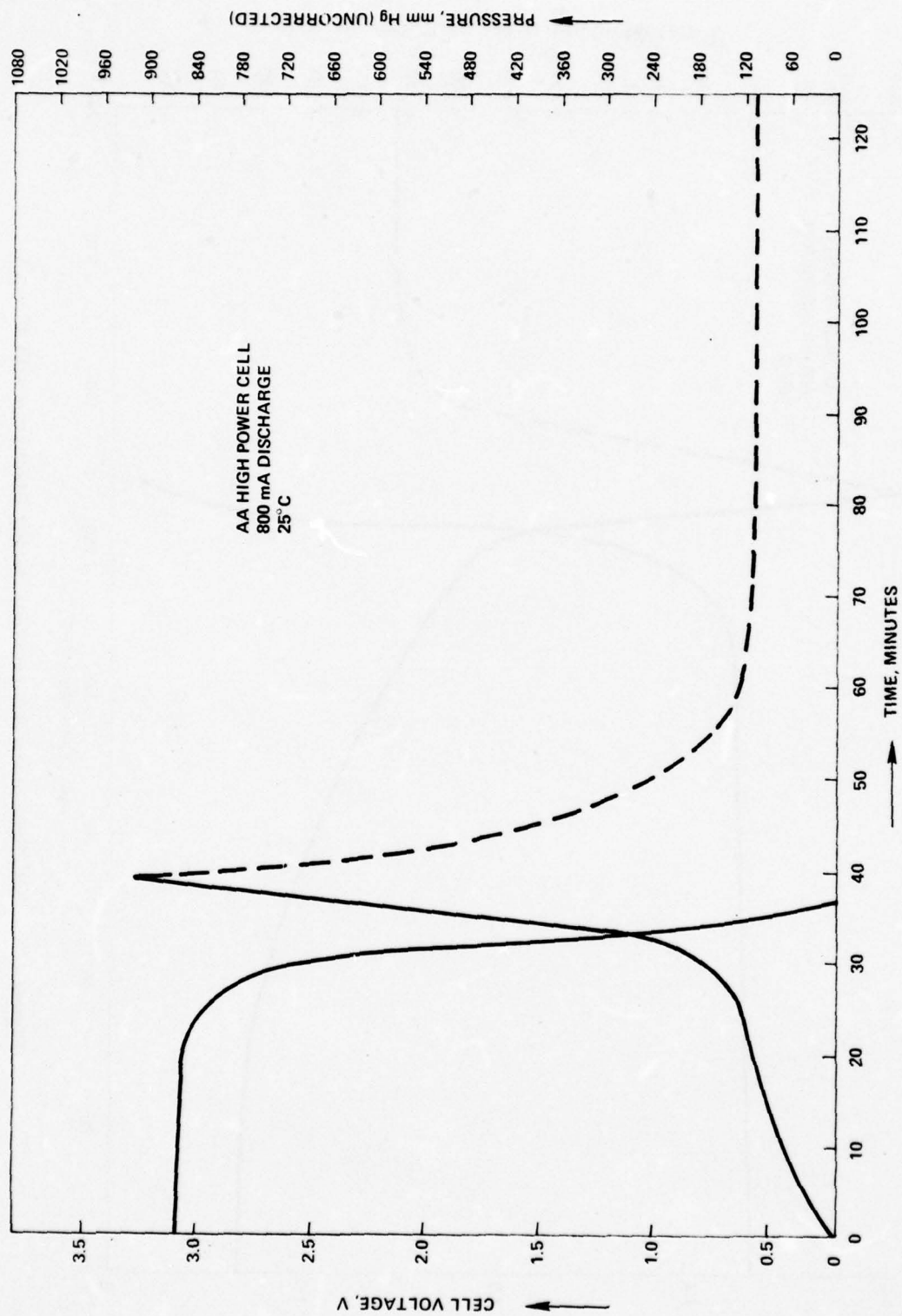


Figure 110. Cell Pressure (Uncorrected) During Discharge with 800 mA

Assuming the ideal gas behavior and constant temperature, one can calculate the corrected pressure P using the V_o value for the initial void space for each value of the pressure reading, P_r :

$$PV_o = P_r [V_o + 0.38 (P_r - 1)]$$

or

$$P = P_r \left[1 + 0.38 \left(\frac{P_r - 1}{V_o} \right) \right]$$

The actual volume of gas generated under pressure ($P_o = 1$ atm) during the discharge at each rate is calculated as follows:

$$P V_o = P_o (V + V_o)$$

or

$$V = V_o \left(\frac{P}{P_o} - 1 \right)$$

The values of corrected pressure and the volume of gas generated during discharge are tabulated in Table 10 for each discharge rate applied. The last column in the table represents a specific volume of gas generated for each Ah of the cell capacity realized.

Since the major goal of this program is engineering and development of usable cells, no further interpretation of these results will be attempted here. However, several interesting conclusions seem straightforward:

1. Internal cell pressures, generated during discharge of these cells in a wide range of discharge rates, represents no obstacle to the cell design provided that a proper void space is secured in the assemblage of cells.
2. At low rates, the cell discharge mechanism does not generate any gas pressure.

3. There is a radical change in the cell discharge mechanism as the discharge rate is increased. This mechanism involves a formation of gas in very small quantities, with a negligible amount of charge associated with its formation, relative to the total mass of reactants involved in the discharge.
4. The amount of gas generated is proportional to the discharge capacity obtained, irrespective of rate, in a wide range of discharge rates.

TABLE 10
GAS GENERATION DURING DISCHARGE

Discharge Rate mA	Over Pressure, Atm.		Gas Volume cm ³	Specific Gas cm ³ /Ah
	Reading	Corrected		
100	0	0	0	0
150	1.237	0.460	0.230	0.188
200	1.343	0.690	0.345	0.352
300	1.274	0.540	0.270	0.233
400	1.303	0.610	0.305	0.281
800	1.153	0.286	0.143	0.294

8. ELECTROLYTE ADDITIVES

Standard size hardware has been used in the construction of test cells with various electrolytes. The electrode structure has been modified, however, to limit the surface area and the maximum available capacity of lithium anodes. The size of the anode was $2.0 \times 4.5 \times 0.03$ cm weighing 1.45 g, with the total surface area of 180 cm^2 . The theoretical anode capacity was 5.6 Ah. The cathode and separators and the volume of electrolyte were kept unchanged. The cell closing was done by crimping, with an additional potting seal to keep water vapors away from the seal area. The storage was done in constant temperature chambers for a predetermined period of time prior to the measurements of the cell voltage delay on discharge. Three various discharge currents were applied to the cell, 0.5, 1 and 2 A, corresponding to three various anode current densities of 2.8, 5.6 and 11.2 mA/cm^2 . A total of 144 cells were built and tested fresh, after one month storage at room temperature, 55° and 72°C .

8.1 ULTRAPURE ELECTROLYTES

The electrolyte was prepared using the purest chemicals available. Triple distilled thionyl chloride was from Eastman Kodak. Lithium Chloride was from J. T. Baker Chemical Co. with 99.3% LiCl, 10 ppm of heavy metals as Pb, and 5 ppm of Fe. Aluminum Chloride was from Fluka A.G., purissimum grade, free of water and iron. Twenty-four cells were built and tested for voltage delay according to the test program shown in Table 11. The table also shows the voltage delay data obtained with these cells after one month's storage. The fresh cells and the cells stored at room temperature performed satisfactorily at these high discharge rates. However, the high temperature storage showed very long delays, and, in the extreme case at 72°C , the cells just could not be brought above the operating voltage of 2 V at these discharge rates. The fresh cells and the cells stored at room temperature yielded the same capacity, when discharged at 200 mA, following the voltage delay measurements. The average capacity obtained at this rate was 4.4 Ah above the 2.0 V cutoff line, which is about 20% below the figures corresponding to the amount of lithium present. The cells stored at elevated temperatures were opened for inspection after the voltage delay measurements. The anodes were found intact, with no change in thickness or appearance. The passivating film on the lithium surfaces was, obviously, too dense and too resistive to be removed after discharge at this high rate.

TABLE 11
VOLTAGE DELAY WITH ULTRAPURE ELECTROLYTES,
TIME FOR RECOVERY TO 2.0V

Storage Days	Cell No.	Storage Temp. °C	Current Density mA/cm ²	Voltage Delay
0	139		2.8	0
	140			
	141		5.6	0
	142			
	143		11.2	0
	144			
	145	25	2.8	0
	146			
	147		5.6	5 sec.
	148			
	149		11.2	3 sec.
	150			
30	151	55	2.8	15 min.
	152			
	153		5.6	30 min.
	154			
	155		11.2	30 min.
	156			
	157	72	2.8	No Recovery
	158			
	159		5.6	No Recovery
	160			
	161		11.2	No Recovery
	162			

8.2 ELECTROLYTE WITH EXCESS CHLORINE

Gaseous chlorine was bubbled through our regular type electrolyte at a slow rate at room temperature overnight, with a tap water condenser mounted on the flask to minimize the loss of thionyl chloride carried by the gas stream. No change in volume was observed as a result of the saturation of the electrolyte with chlorine, suggesting a limited solubility. No analysis of the electrolyte was made to establish the exact solubility figure. The electrolyte was used to build 24 cells under identical conditions as in the preceding test. Fresh cells, as well as those stored at various temperatures for one month, were tested for voltage delay at the same three rates. The results are shown in Table 12.

The fresh cells were placed on discharge within 24 hours following their construction and the voltage delay measurements. A uniform discharge behavior at the rate of 200 mA was observed, but the capacity obtained was significantly lower than expected on the basis of the amount of lithium present. An average of 3.5 Ah showed a loss of over 1 Ah within a few days. The storage at room temperature for one month resulted in a further reduction in the cell capacity. The discharge at 200 mA, yielded an average value of the cell capacity of 3.2 Ah following the voltage delay tests. The voltage delay values are comparable to those obtained with regular electrolytes. The storage at 55°C resulted in a complete deterioration of the cell capacity yielding less than 1 Ah at the 200 mA rate with four cells after only 17 days. Two cells, assigned to the voltage delay tests at 2 A, did not even show the proper open circuit voltage at the end of the storage period. Storage at 72°C was also discontinued after 17 days. All cells were found inoperable. The post mortem showed intact cathodes and spent anodes.

It was generally concluded that the excess of chlorine in the electrolyte is highly detrimental to the stability of lithium anodes in thionyl chloride electrolytes. Although the exact concentrations were not known, it seems that the lithium corrosion is continued beyond the stoichiometric relations of the chlorine and the lithium involved as suggested by the results at 72°C where the entire amount of lithium dissolved.

8.3 ELECTROLYTE WITH EXCESS AlCl_3

The idea that slightly more acidic electrolyte might be able to keep the lithium surface free from excessive passivation was tested in the next series of experiments. An electrolyte was prepared with a 10% excess of AlCl_3 over the amount required to

TABLE 12
VOLTAGE DELAY WITH EXCESS Cl_2 IN ELECTROLYTE
TIME FOR RECOVERY TO 2.0V

Storage Days	Cell No.	Storage Temp. °C	Current Density mA/cm ²	Voltage Delay
0	73		2.8	0
	74			0
	75		5.6	0
	76			0
30	77	25	11.2	0
	78			0
	79		2.8	12 sec.
	80			6 sec.
17	81	55	5.6	0
	82			1 sec.
	83		11.2	30 sec.
	84			26 sec.
17	85	55	2.8	2 min.
	86			
	87		5.6	50 sec.
	88			35 min.
17	89	72	11.2	Failed
	90			Failed
	91		2.8	Discontinued
	92			
17	93	72	5.6	Discontinued
	94			
	95		11.2	Discontinued
	96			

match the concentration of LiCl. Although it was known that the large excess of AlCl_3 would show a direct attack on lithium, a moderate excess was hoped to show an acceptable corrosion rate, keeping the anode surface free from the excessive passivation. Twenty-four cells were built using the above type electrolyte and tested according to the program shown in Table 13, together with the voltage delay data obtained.

It is obvious from Table 13 that the excess AlCl_3 causes a rapid corrosion of the lithium anodes. The cells either showed no delay or they were heavily passivated, depending on the time period and the temperature of storage. Fresh cells were discharged at 200 mA following the voltage delay tests and yielded an average capacity well below that obtained from the cells with the regular electrolyte. An average of 3.6 Ah, in fact, is very close to the value obtained with the excess chlorine electrolyte under the same conditions. The results after storage at room temperature for one month are also similar to those obtained with the excess chlorine electrolyte. An average of 3.0 Ah was obtained. The storage at both 55° and 72°C resulted in a total deterioration of cell capacity, either for lack of lithium or for inability of the remainder of the anode to deliver the capacity at the operating voltage above 2 V with these high discharge rates.

It is quite clear that the excess of AlCl_3 in the electrolyte cannot be tolerated. All of it has to be neutralized with LiCl, shifting this Lewis acid-base equilibrium as far as possible in the alkaline direction. In fact, an excess of LiCl in suspension seems like a good idea to avoid the use of acid electrolyte.

8.4 ELECTROLYTE WITH SO_2

Lithium forms a passivating film of $\text{Li}_2\text{S}_2\text{O}_4$ in contact with SO_2 in organic electrolyte cells. Sulfur dioxide is found in aged thionyl chloride and also in sulfuryl chloride as a product of a slow decomposition of these compounds. It seemed of interest in the voltage delay studies to establish if an excess of SO_2 over the concentration found in thionyl chloride would have any effect on the rate of formation or on the conductive characteristics of the passivating film in lithium cells with thionyl chloride electrolyte. SO_2 gas was bubbled overnight through a batch of regular thionyl chloride electrolyte until saturated under similar conditions as in the previously described preparation of the electrolyte with excess chlorine. The exact concentration of SO_2 reached has not been analyzed in this test, but the concentration at room temperature could have been

TABLE 13
VOLTAGE DELAY WITH 10% EXCESS OF AlCl_3 IN ELECTROLYTE
TIME FOR RECOVERY TO 2.0 V

Storage Days	Cell No.	Storage Temp. C°	Current Density mA/cm ²	Voltage Delay
0	49		2.8	0
	50			0
	51		5.6	0
	52			0
	53		11.2	0
	54			0
30	55	25	2.8	14
	56			11
	57		5.6	29
	58			14
	59		11.2	No Recovery
	60			
	61	55	2.8	No Recovery
	62			
	63		5.6	
	64			
	65		11.2	
	66			
	67	72	2.8	No Recovery
	68			
	69		5.6	
	70			
	71		11.2	
	72			

as high as 0.76 moles/l. Cells were built using the SO₂ saturated thionyl chloride electrolyte and tested according to the program shown in Table 14 along with the voltage delay data obtained.

Fresh cells and those stored at room temperature for one month did not show any voltage delay at these high rates of discharge. The cell behavior is similar to that observed with ultrapure electrolytes as well as with our regular electrolytes prepared with care. The elevated temperature storage does not seem to have been affected significantly by the presence of SO₂. One could actually see no difference in the voltage delay characteristics between these and the cells made with pure electrolytes.

The discharge at 200 mA following the voltage delay tests showed that SO₂ has no effect on the capacity obtained after storage either. Fresh cells, those stored at room temperature and those stored at 55°C for one month, all delivered an average capacity that is the same as the value obtained with regular fresh cells. A slight improvement was observed at the extreme storage temperature 72°C. Of the six cells involved, three was found with poor internal contacts and the remaining three delivered an average of 4.14 Ah. The voltage delay data are tabulated in Table 14.

8.5 IRON IMPURITIES

Iron is always found in commercial grade AlCl₃ in concentrations that could reach 70 ppm. Cell hardware may contribute to the contamination of the electrolyte with iron by corrosion, or it could be introduced by the solvent itself. A batch of electrolyte was prepared with 200 ppm of iron added in the form of FeCl₃. Cells were made and tested according to the program shown in Table 15 along with the voltage delay data obtained.

As the data in Table 15 shows, iron species in the thionyl chloride electrolyte produced the strongest negative effect so far on the passivation of lithium anodes. The fresh cells, placed on discharge within 24 hours after assemblage, already showed in some cases an excessive passivation. The discharge at 200 mA showed that more than half of the cell capacity was unavailable at this rate at operating voltages higher than 2.0 V. The post mortem showed a heavy dark brown layer on intact lithium anodes. It is obvious that iron must have deposited on the lithium surface and formed a passivating layer with poor conductive characteristics. The concentration of iron used in these experiments was, obviously, very high. The results suggest, however, that

iron species present even in low concentrations could produce the same effect over a longer period of time and with a high ratio of electrolyte volume to the total lithium surface area available.

TABLE 14
VOLTAGE DELAY WITH EXCESS SO₂ IN ELECTROLYTE
TIME FOR RECOVERY TO 2.0 V

Storage Days	Cell No.	Storage Temp. °C	Current Density mA/cm ²	Voltage Delay
0	25		2.8	0
	26			0
	27		5.6	0
	28			0
	29		11.2	0
	30			0
30	31	25	2.8	0
	32			0
	33		5.6	0
	34			0
	35		11.2	0
	36			0
	37	55	2.8	3 min.
	38			5 min.
	39		5.6	9 min.
	40			6 min.
	41		11.2	No Recovery
	42			
	43	72	2.8	No Recovery
	44			
	45		5.6	
	46			
	47		11.2	
	48			

TABLE 15
VOLTAGE DELAY WITH 200 ppm OF Fe IN SOLUTION
TIME FOR RECOVERY TO 2.0V

Storage Days	Cell No.	Storage Temp. °C	Current Density mA/cm ²	Voltage Delay
0	97		2.8	0
	98			0
	99		5.6	No Recovery
	100			36 sec.
	101		11.2	No
	102			Recovery
30	103	25	2.8	No Recovery
	104			1 min.
	105		5.6	No Recovery
	106			
	107		11.2	No Recovery
	108			
	109	55	2.8	No Recovery
	110			
	111		5.6	No Recovery
	112			
	113		11.2	No Recovery
	114			
	115	72	2.8	No Recovery
	116			
	117		5.6	No Recovery
	118			
	119		11.2	No Recovery
	120			

9. CORROSION OF CELL HARDWARE

9.1 LABORATORY TESTS

It has been the contention of the authors of this report that there would be no hardware corrosion in cold rolled steel cans, due to cathodic protection of the can by the lithium. Recent data⁶ showed that thionyl chloride is reduced very slowly on the surface of nickel and stainless steel, when these materials were in contact with a lithium anode in thionyl chloride electrolyte. This study also showed that a passivating film was formed on these materials. It was assumed that similar films would be formed on the surface of cold rolled steel protecting it from corrosion in storage. It was also assumed that the galvanic corrosion of the anode would not result in a significant loss of lithium before the bare surface of the cold rolled steel was completely passivated and the reduction of the thionyl chloride discontinued.

The following experiment was done to confirm the fact that the cold rolled steel, when held potentiostatically at the lithium potential, does not corrode. This experiment was done concurrently with an in situ test reported in the next section.

A glass cell was constructed as shown in Figure 111. A fine frit divided the two chambers. A second joint was built into one of the chambers to accommodate a lithium reference electrode. The tube holding the reference electrode was separated from the bulk of the solution by a fine frit and a slight positive pressure was maintained by overfilling the reference tube. The entire cell was immersed in an oil bath at 72°C and brought to equilibrium. The working electrode was a round disk of cold rolled steel 11.28 cm² (one side). The Li reference electrode was placed directly above the back side of the working electrode in very close proximity. Each chamber contained 200 cm² of electrolyte. The working electrode was kept at the potential of the lithium reference electrode, while the current was monitored between the working and the lithium counter electrodes.

Upon initiation of the test, there was a strong cathodic current indicating the reduction of thionyl chloride on the surface of the working electrode (cold rolled steel). The current was 260 mA, or 23 mA/cm² of electrode area. As shown in Figure 112 the current decayed in a few hours to 6 mA, after 25 hours to 4 mA, leveled off at 1.3 mA at 45 hours and remained there until completion of the experiment. This decay is attributed to the forming of a passivating film of reduction products deposited on the surface of the working electrode.

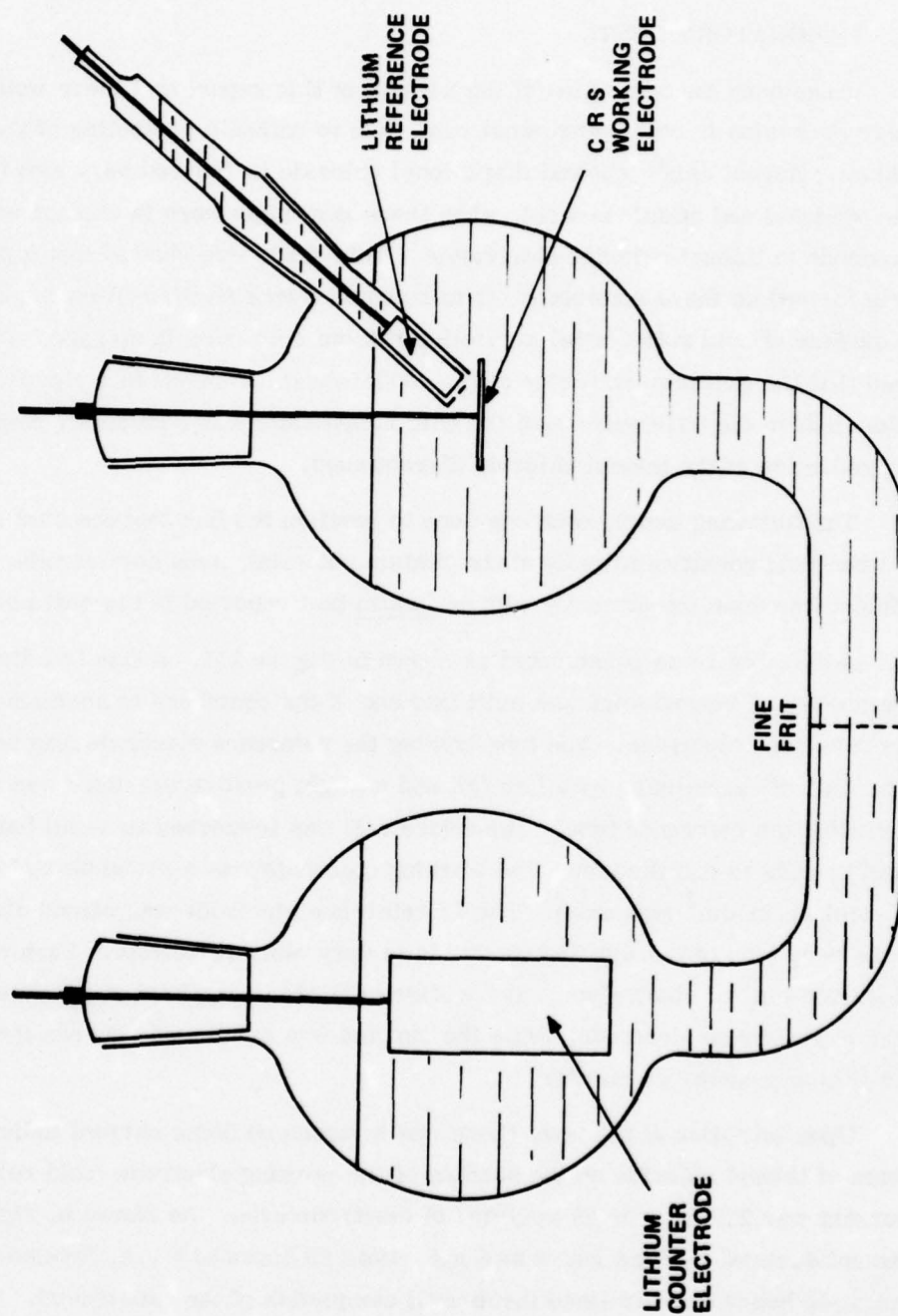


Figure 111. Glass Cell Arrangement for Corrosion Studies

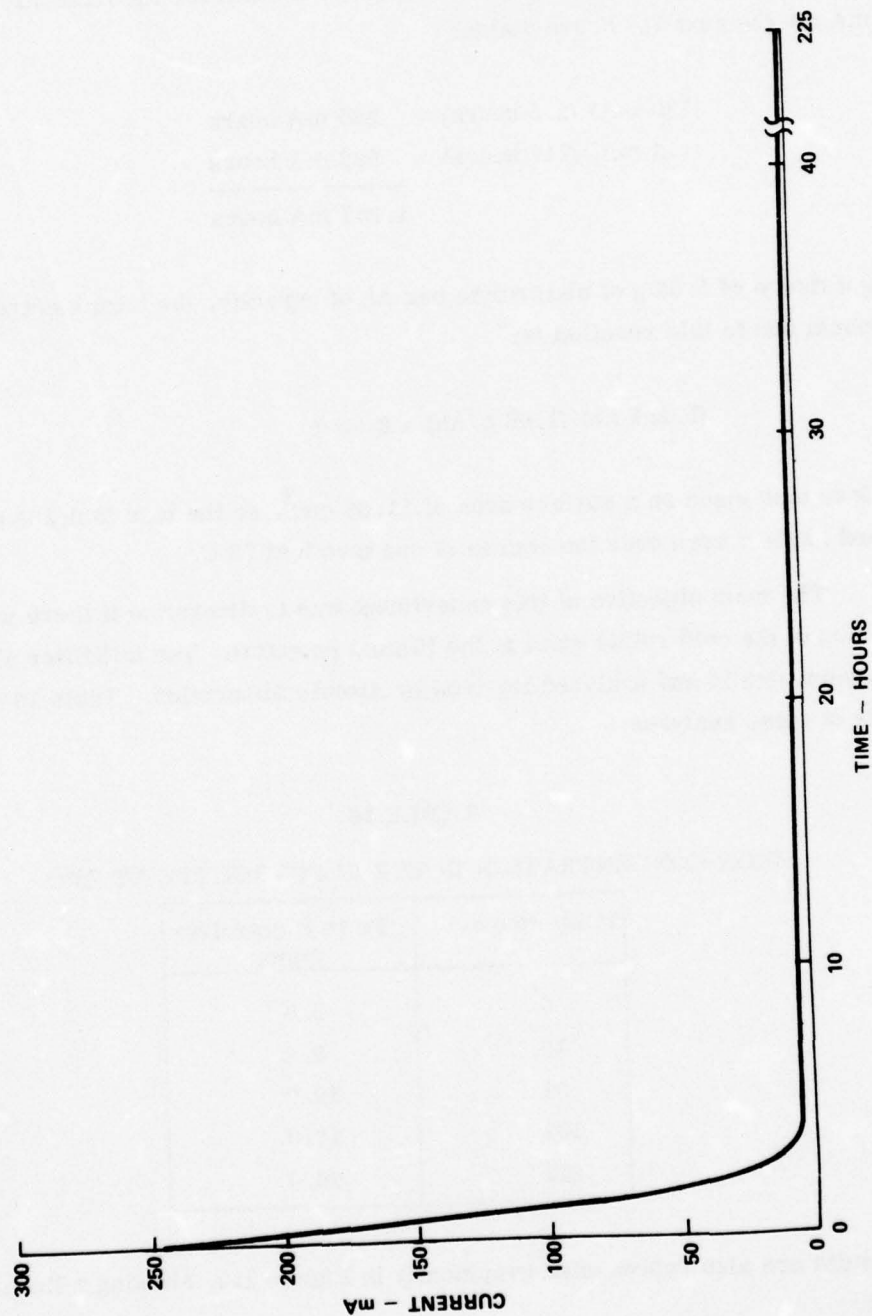


Figure 112. Self Discharge on Cold Rolled Steel

Calculating the amount of electrolyte lost to reduction over the course of one month on this surface area, using an average of 130 mA for the first 2 1/2 hours and 1.3 mA for the next 717 hours yields:

$$\begin{array}{rcl} (130 \text{ mA}) (2.5 \text{ hours}) & = & 325 \text{ mA hours} \\ (1.3 \text{ mA}) (717 \text{ hours}) & = & 932 \text{ mA hours} \\ \hline & & 1.257 \text{ mA hours} \end{array}$$

Using a figure of 1.66 g of electrolyte per Ah of capacity, the total electrolyte lost in one month due to this reaction is:

$$(1.257 \text{ Ah}) (1.66 \text{ g/Ah}) = 2.09 \text{ g}$$

This loss took place on a surface area of 11.28 cm^2 , so the loss is 0.185 g/cm^2 of exposed surface area over the course of one month at 72°C .

The main objective of this experiment was to determine if there was any corrosion of the cold rolled steel at the lithium potential. Ten milliliter aliquots were drawn periodically and analyzed for iron by Atomic Absorption. Table 16 shows the results of these analyses:

TABLE 16
IRON CONCENTRATION IN THE ELECTROLYTE AT 72°C

Time Hours	Fe in Electrolyte (ppm)
0	9.0
19	9.8
91	13.0
163	17.0
225	20.0

The results are also represented graphically in Figure 113, showing a linear dependence on time.

The loss of SOCl_2 by reduction on the surface of cold rolled steel is accompanied by an equivalent loss of lithium, amounting to 0.325 g.

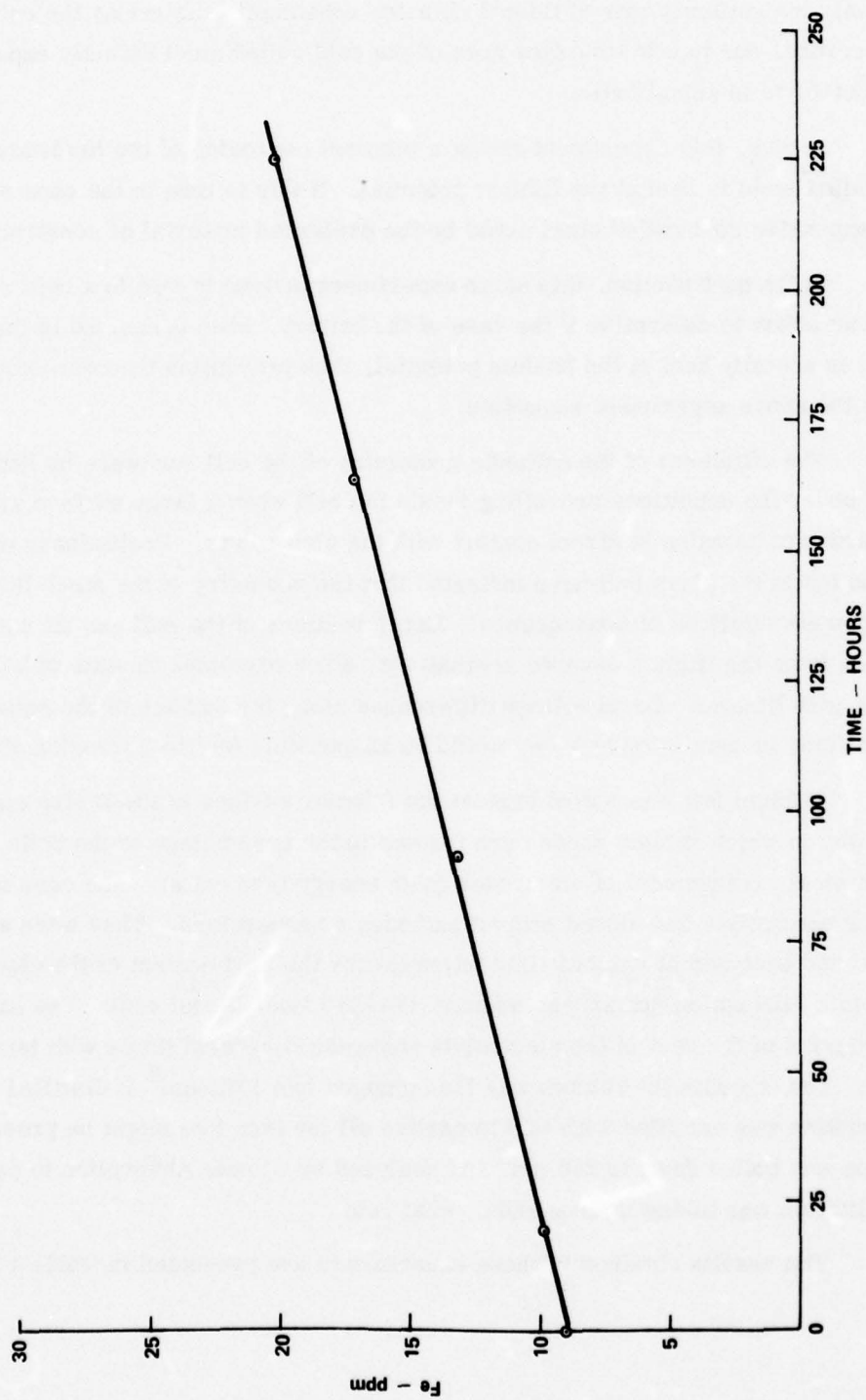


Figure 113. Iron Corrosion at Lithium Potential

One of the first conclusions to be drawn from this experiment would be a relatively insignificant rate of thionyl chloride consumption as far as the cell capacity is concerned, due to a low surface area of the cold rolled steel directly exposed to the electrolyte in actual cells.

Second, this experiment shows a minimal corrosion of the hardware when the cold rolled steel is held at the lithium potential. If this is true in the case of a battery, the inexpensive cold rolled steel would be the preferred material of construction.

In the next section, this same experiment is done in situ in a cold rolled steel can in an effort to determine if the case of the battery, when connected to the lithium anode, is actually held at the lithium potential, thus preventing the corrosion of the can as the above experiment suggested.

The efficiency of the cathodic protection of the cell hardware by lithium was tested under the conditions prevailing inside the cell when a large surface area of the cell hardware remains in direct contact with the electrolyte. Preliminary experiments carried out in the glass cell have indicated that the geometry of the steel-lithium arrangement might be of consequence. Large sections of the cell can (at some distance from the lithium covered section) may show corrosion in spite of being in contact with lithium. Local voltage differences along the surface of the same piece of steel may be generated and they would be responsible for the corrosion observed.

Lithium foil was rolled against the interior surface of the D size cans in the same way in which lithium anodes are formed in the assemblage of the cells with the concentric arrangement of electrodes (high energy type cells). The cans were filled with the electrolyte and closed without cathodes or separators. They were all stored at 72°C and analyzed at various time intervals for the iron content of the electrolyte by Atomic Absorption Spectrophotometry (Perkin Elmer Model 460). The can was then emptied of the rest of the electrolyte and washed several times with tetrahydrofuran (THF). The can with the lithium was then plunged into 1600 cm³ of distilled water. The solution was acidified with HCl to oxidize all the iron that might be present. This solution was boiled down to 250 cm³ and analyzed by Atomic Absorption to determine if the lithium was taking up iron and at what rate.

The results obtained in these experiments are presented in Table 17.

TABLE 17
IRON FOUND IN ELECTROLYTE AND IN THE ANODE AFTER STORAGE AT 72°C

CELL NO.	DAYS STORED	Fe ELECTROLYTE (ppm)	Fe ON LITHIUM (ppm)	TOTAL mg
1	5	6	27	0.249
2	10	146	8	5.410
3	13	256	15	9.450
4	19	252	4	9.328
5	26	180	16	6.676
6	31	39	35	1.478

The table shows a gradual increase of the iron concentration in the electrolyte with the time of storage for approximately the first two weeks, followed by a gradual decrease over the next two weeks. The iron content of the lithium anode was found to be extremely erratic, suggesting, among other things, that the analytical procedure used may not have been appropriate. The total amount of iron formed by corrosion is shown in the last column of the table. Obviously, it showed inadequacies either in the analytical procedures or in the experimental arrangements, since the iron corroded must be found either in the electrolyte or on the anode.

The results of this experiment were inconclusive. It was theorized that initially, if there is any corrosion, it should be quite rapid because the can surface is clean and active. As reduction products build up on the surface of the steel, the corrosion should decline to a very small rate. It was further assumed that the concentration of iron in the electrolyte should increase to a maximum and then decrease to some unknown value due to a plating out on lithium.

Figure 114 graphically depicts the data from Table 17. The graph correlates to the theory as previously explained. There is a gradual rise in Fe concentration, a leveling out and then a slow decline, all as predicted. The confusion arises when the lithium is analyzed as described above. There is no significant rise in the Fe

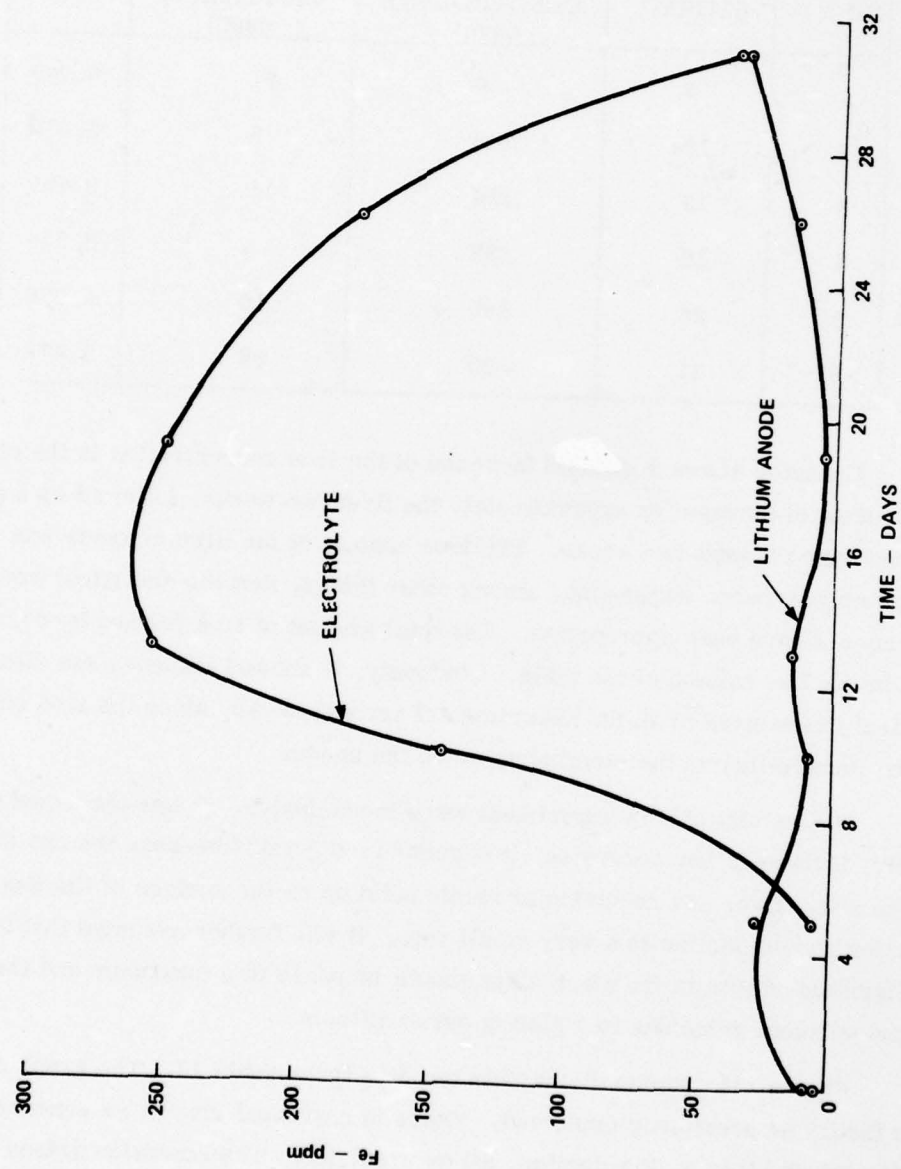


Figure 114. Distribution of Iron Generated by Corrosion in Standard Size D Cells

concentration on lithium. A blank of lithium will yield an iron concentration of approximately 5 to 10 ppm. As the electrolyte iron concentration was decreasing it was assumed lithium was picking it up, but the lithium analysis did not prove that. One possible explanation may be in the washing technique. After the electrolyte was taken out of the can, it was gently sprayed with THF to wash out any extraneous electrolyte, since it would, in contact with water, attack the can and form more iron in the solution. The iron which plates out on lithium may not be adhering very well and the spraying with the THF may be washing it off.

The experiments conducted in a glass cell showed that the cathodic protection of cell hardware in contact with the anode may be affected by the geometry of the cell interior. We have found that a large cold rolled steel anode, with a piece of lithium attached at one end, will show visible signs of corrosion at its other end, when kept in an SOCl_2 electrolyte 72°C . A series of experiments with D size cans was conducted for the purpose of demonstrating whether the relative magnitude of the can interior that is not covered by lithium would affect the amount of iron in the electrolyte generated by corrosion. The experiments included the three different arrangements one could have, with the can attached to the cathode, to the anode or unattached (floating can). It was assumed that the can interior could be effectively covered with the solid lithium foil, so it was necessary to investigate various ratios of covered and bare surfaces. With cathodes, however, one had to assume the exposure of the total can interior to the electrolyte, due to the high porosity of cathode materials.

Sections of various sizes of the can interior were covered with lithium using 0.5 in., 1 in. and 1.5 in. wide foils, by rolling the foil against the can wall. The effectiveness of coverage by lithium was tested by attempting to peel off the lithium layer. A good bonding of lithium to the clean surface of a stainless steel can was achieved, since one could only remove lithium from the rolled composite by cutting it in small sections and removing the sections one at a time. The can bottom and walls uncovered by lithium were exposed to the electrolyte during the tests. Following were the relative surface areas involved:

Coverage By Lithium (Height, inches)	Exposed Can Area cm^2
0	58.65
0.5	45.98
1.0	33.31
1.5	20.64

The cans with various coverage by lithium of the interior were filled with the electrolyte to a height of 2 in. The electrolyte volume was 38.0 cm² maximum, and only slightly lower for the cans with more lithium, since a thin foil (0.010 in.) was used in the rolling operation. The cans were stored at 72°C and the electrolyte was analyzed for iron after 1 week, 2 weeks and 4 weeks of storage. Lithium was allowed to react with water and the resultant solution was acidified with HCl before it was also analyzed for iron by Atomic Absorption (Perkin Elmer Model 460). A control analysis was run on a blank made of lithium (3.5 × 1.5 × 0.010 in.) rolled into a can, allowed to react with water immediately thereafter and subjected to the same analytical procedure. A total of 0.023 mg of iron was found in the solution. The data obtained are shown in Table 18.

TABLE 18
IRON CONTENT OF THE ANODE AND THE ELECTROLYTE

Storage Weeks	Lithium Height (inches)	Iron in the Electrolyte (mg)	Iron on Lithium (mg)	Total Iron (mg)
1	0	3.121	-	3.121
	0.5	1.360	0.002	1.362
	1	1.850	0.007	1.857
	1.5	1.490	0.032	1.523
2	0	3.872	-	3.872
	0.5	1.793	0.004	1.797
	1	1.812	0.009	1.821
	1.5	2.575	0.022	2.597
4	0	4.462	-	4.462
	0.5	2.450	0.002	2.452
	1	1.903	0.004	1.906
	1.5	2.050	0.004	2.054

The experiments involving the cathode attached to the can were carried out in an arrangement similar to that used with lithium. A single layer of porous cathode, 0.034 in. thick, was placed against the interior of the cell can with the cathode current collector welded to the can wall. Three different cathode sizes were used, 0.5, 1.0 and 1.5 in. wide in the can filled with the same amount of electrolyte as in the preceding tests. All cans were stored at 72°C and the electrolyte was analyzed for iron after 1 week, 2 weeks and 4 weeks of storage. The results obtained are summarized in Table 19.

TABLE 19
IRON CONTENT OF THE ELECTROLYTE AFTER STORAGE
WITH CANS IN CONTACT WITH CATHODES

Storage (weeks)	Cathode Height (Inches)	Iron Content (mg)
1	0	3.121
	0.5	4.005
	1.0	3.046
	1.5	4.151
2	0	3.872
	0.5	4.783
	1	4.717
	1.5	5.409
4	0	4.462
	0.5	4.462
	1	3.971
	1.5	3.872

The data for cans without electrolyte are shown in Table 19 as well for an easy comparison with the other results obtained.

It is evident from the results in Table 18 that the anode in contact with the can reduces the amount of iron generated by corrosion by approximately a factor of 2 relative to the amount found in the experiments involving cans alone. It is also evident that most of the iron generated by corrosion remains in the electrolyte even after the longest period of storage of 4 weeks. With the exception of the 4 week group, the iron content of lithium is proportional to the surface area of the lithium foil used. Small differences between the results for various periods of storage suggest a rapid reduction of the corrosion rate with time within the first week of storage and a relatively insignificant increase in the iron content beyond the one week period.

Table 18 also shows two unpredictable results. First is the fact that the iron content found on lithium does not increase beyond the first week of exposure for any of the tests conducted. It almost suggests some sort of self inhibition by iron of the exchange reaction between the metallic lithium and iron species in the solution. A rough estimate of the amount of iron distributed over this lithium surface could be made by considering the total amount of iron detected and the total surface area of lithium involved. The result was of the order of magnitude of $3.77 \cdot 10^{-7}$ g of iron per cm^2 of lithium surface, or the thickness of iron film on lithium of 48.3 nm, assuming no alloying effects between lithium and iron. Since the presence of lithium chloride on the passivated lithium surface has been established, one must assume that iron does not form a uniform film on lithium but, rather, must be scattered around and incorporated into voids of the lithium chloride film. The combined effects of these two substances was a total passivation of lithium surface, demonstrated in D size cells with iron added to their electrolyte.

The second fact indicated in Table 18 is an apparent independence of the total iron generated on storage upon the bare surface area of the can. Although the surface areas investigated varied only for a little over a factor of 2, one should expect more iron formed on a larger surface area exposed. There is no explanation for this phenomenon at the moment and the matter, obviously, should be explored in more detail.

The tests with cathodes, Table 19, showed approximately twice the amount of iron generated by corrosion relative to the results obtained in the tests with anodes. In fact, the amount of iron generated in contact with cathodes is the same as that found

in tests with cans alone, suggesting that the contact with the cathode has no effect on the rate of corrosion of stainless steel hardware.

Tests were carried out with Kovar as a possible hardware material. Kovar was tested in three different situations, relative to the active electrode materials:

- with a piece of lithium attached
- with a piece of carbon electrode attached
- with no attachments of electrode materials

The sample was weighed before and after the test to see if a loss of weight during the test could be detected directly. The tests consisted of a continuous boiling (refluxing) of the sample analysis of the electrolyte for Ni, Co and Fe. The electrolyte analysis was done at the beginning of the experiments as well, in order to establish starting contents, if any, of the three major constituents of Kovar. The volume of the electrolyte used in each of the tests was 300 ml. The results obtained are shown in Table 20.

TABLE 20
RESULTS OF CORROSION TESTS WITH KOVAR

Test Type	Sample Weight (g)		Electrolyte Content (ppm)		
	Before	After	Ni	Co	Fe
Kovar Alone	3.5607	3.5602	6	5	9
Kovar and Lithium	3.2697	3.2699	5	0.7	2.9
Kovar and Anode	3.5666	3.5661	6	5	9
Electrolyte before test			7	5	9

Lithium foil used in the tests was analyzed separately by a method described earlier and was found to contain only a fraction of ppm of each of the three elements. This, combined with the fact that the amount of lithium involved was several times smaller than the amount of Kovar, makes this portion of the content of the three elements negligible.

The experiments clearly suggest the use of Kovar as a possible alternative to stainless steel as a hardware materials for the can when it is connected to either the cathode or the anode end of the cell.

An additional group of cells was made and tested incorporating the hardware tested and described above.

Eighteen wound "D" cells were made in pure nickel cans with Kovar tops. The electrode dimensions were as follows:

Anode: 15.4 in. long
20 mil thick
1.75 in. wide
Cathode: 14.0 in. long
33 mil thick
1.875 in. wide

Nine of the cells had the carbon cathode attached to the nickel can and the other nine had the lithium attached to the can as usual.

Each cell was vacuum filled with 30 cc of electrolyte and hermetically sealed.

The two groups of cells were divided into 3 sub-groups and stored 1 month at room temperature, 55° and 72°C.

The cells were taken off the storage after one month and allowed to cool down to room temperature for one-half day.

A 500 mA constant current was drawn out of each cell for the delay test. The recovery time to 2.0 V is shown in Table 21. Cells number 1A, 5A, 10A and 4C had their fuses burned out when taken off of storage, this was undoubtedly due to poor construction or mishandling sometime during processing.

TABLE 21

RECOVERY TIME TO 2.0 V FOR WOUND D CELLS IN NICKEL
CANS STORED ONE MONTH AT INDICATED TEMPERATURE

TEMP	CELL NO. /VOLTAGE DELAY (SECONDS)					
	ANODE ON CAN			CATHODE ON CAN		
ROOM TEMP.	Test 1A Discontinued	2 2A	4 3A	Test 4C Discontinued	3 5C	5 6C
55°C	90 4A	Test 5A Discontinued	78 8A	42 7C	24 8C	39 9C
72°C	14 9A	Test 10A Discontinued	57 11A	24 10C	24 11C	24 12C

After testing for delay the cells were discharged at 100 mA and the capacity recorded to a 2.0 V cutoff voltage. The capacities are listed in Table 22.

TABLE 22

CAPACITIES TO 2.0 V FOR WOUND D CELLS IN NICKEL CANS
STORED ONE MONTH AT INDICATED TEMPERATURE

TEMP.	CELL NO. /CAPACITY (Ah)					
	ANODE ON CAN			CATHODE ON CAN		
ROOM TEMP.	Test 1A Discontinued	11.9 2A	11.6 3A	Test 4C Discontinued	11.7 5C	12.5 6C
55°C	11.2 4A	Test 5A Discontinued	11.7 8A	11.8 7C	11.7 8C	11.9 9C
72°C	11.7 9A	Test 10A Discontinued	11.2 11A	11.2 10C	11.3 11C	11.8 12C

Unlike the cells made in nickel cans, the cells made in stainless steel cans and stored at 72°C showed a loss of capacity as indicated in Table 23:

TABLE 23
CAPACITIES TO 2.0 V FOR WOUND D CELLS IN STAINLESS STEEL CANS
STORED ONE MONTH AT INDICATED TEMPERATURE

TEMPERATURE	CAPACITIES/AMP-HR	
ROOM TEMP.	13.4	13.2
55°C	12.8	12.8
72°C	9.5	9.6

This loss of capacity with stainless steel cans has been attributed to self discharge against the can. In the case of nickel cans with the anode on the can the self discharge at 72°C appears to be less of a problem.

The following four cells were taken apart after discharge and the amount of remaining lithium was determined. Each cell was constructed with 18.2 Ah of Li. The cells were discharged and the amount of Li used, calculated from the capacity, was subtracted from the original amount of lithium present in the cell. The figure obtained from this subtraction is the amount of lithium that should be remaining in the cell.

The results of the analysis on the remaining lithium in each of the previously mentioned cells are shown in Table 24.

TABLE 24
LITHIUM LOSS ON STORAGE

CELL NUMBER	STORAGE TEMP. °C	ELECTRODE ON CAN	LITHIUM UNACCOUNTED FOR
2A	Room Temp.	Anode	2.0%
11A	72	Anode	12.2%
5C	Room Temp.	Cathode	6.0%
11C	72	Cathode	19.7%

From Table 24 two conclusions can be drawn. The first is that room temperature storage is much less severe on lithium loss, and secondly it appears to make no difference whether the lithium is attached to the can or center pin. This conflicts with an earlier prediction that reversing cell polarity would better preserve the lithium. The loss of lithium at 72°C when attached to the center pin is probably by a direct chemical reaction of lithium with thionyl chloride. There is not enough surface area on the Kovar pin to which the lithium is attached to serve for the reduction of thionyl chloride with a parallel loss of lithium.

A simple analytical procedure was used in generating the data in Table 24. The bottom of the discharged cell was punctured and the cell was evacuated until it showed no voltage. The battery can was then cut open, the electrodes with separator paper were removed, unraveled and evacuated for another hour. The remaining lithium is separated from the roll and washed free of salts with several washings of thionyl chloride. The washed lithium electrode was then allowed to air dry and react with the atmosphere forming LiOH , Li_2CO_3 , Li_3N , and LiHCO_3 . These products were then placed in a beaker with 1000 cm^3 of water and boiled to convert all lithium salts to lithium hydroxide.

Excess HCl was then added to the solution to neutralize the base and the excess HCl was then back-titrated with standardized base solution.

10. VOLTAGE DELAY WITH VARIOUS HARDWARE MATERIALS

An attempt was made to correlate the results of the corrosion studies obtained in the glass cell with the effects of hardware materials on the performance of finished cells. Two sets of cells were built for the purpose, one with stainless steel and one with cold rolled steel hardware, and stored at room temperature, 55° and 72°C. The voltage delay after storage was expected to show a direct influence of the iron present in the solution and also of the rate at which lithium was dissolved in the galvanic corrosion involving the reduction of SOCl_2 on the surface of cell hardware. A high rate of the galvanic corrosion involving lithium dissolution should have resulted in a lower value of the voltage delay, since that would have kept the surface of the lithium free of the passivating film. Another consequence of that would have been significant loss in the cell capacity due to the loss lithium. A high rate of hardware corrosion would have a negative effect on the voltage delay due to the effects of iron plated out on the lithium surface. Another consequence of that would have been a better preservation of the cell capacity (lower lithium losses on storage), at least at low discharge rates. A combined effect of both factors should have been seen in the discharge of the cells after storage.

Twelve cells were constructed for this part of the project; six in cold rolled steel cans and six in stainless steel cans. The wound electrode structure was constructed with computer aided calculations to maximize the cell capacity for a particular thickness of cathodes used (see the next chapter).

The component dimensions were as follows:

	LENGTH-in.	THICKNESS-in.	WIDTH-in.
Cathode	14.0	0.033	1.875
Anode	15.4	0.020	1.75
Separator	35.0	0.005	2.00

All cells were hermetically sealed and filled with electrolyte by pre-evacuation.

As previously mentioned, six cold rolled steel cans were stored, two each at the three different temperatures, along with six stainless steel cans. After one month they were taken out of storage and allowed to equilibrate at room temperature

for one half day. The delays were measured using a current of 340 mA or approximately 1 mA/cm^2 (both sides of cathode). Delays were measured using a Varian Aerograph Model A-5 high speed strip chart recorder and are listed in Table 25. The delay was defined, again as any time the voltage of the cell stays below 2.0 volts during the initial phase of discharge. After the delay tests the cells were completely discharged at a constant current of 100 mA to a 2.0 volt cutoff. The voltage delay data are list in Table 25. The capacities obtained are listed in Table 26. The actual discharge curves are shown in Figures 115 through 124.

TABLE 25
VOLTAGE DELAY AFTER STORAGE FOR ONE MONTH

STORAGE TEMP.	COLD ROLLED STEEL CANS		STAINLESS STEEL CANS	
ROOM TEMP	NO DELAY	NO DELAY	NO DELAY	NO DELAY
55°C	NO RECOVERY AFTER 6 MIN.	15 SEC to 1 V LEVELS OFF AT 1.85 V	3.5 MIN	3 SEC
72°C	NO RECOVERY	NO RECOVERY	NO DELAY	NO DELAY

TABLE 26
DISCHARGE CAPACITY AFTER STORAGE FOR ONE MONTH

CELL NO.	CAN TYPE	STORAGE TEMP.	CAPACITIES — Ahr.
1 2	COLD ROLLED STEEL	ROOM TEMP.	13.2 12.8
3 4		55°C	12.2 11.9
5 6		72°C	INOPERATIVE
7 8	STAINLESS STEEL	ROOM TEMP.	13.4 13.2
9 10		55°C	12.8 12.8
11 12		72°C	9.5 9.6

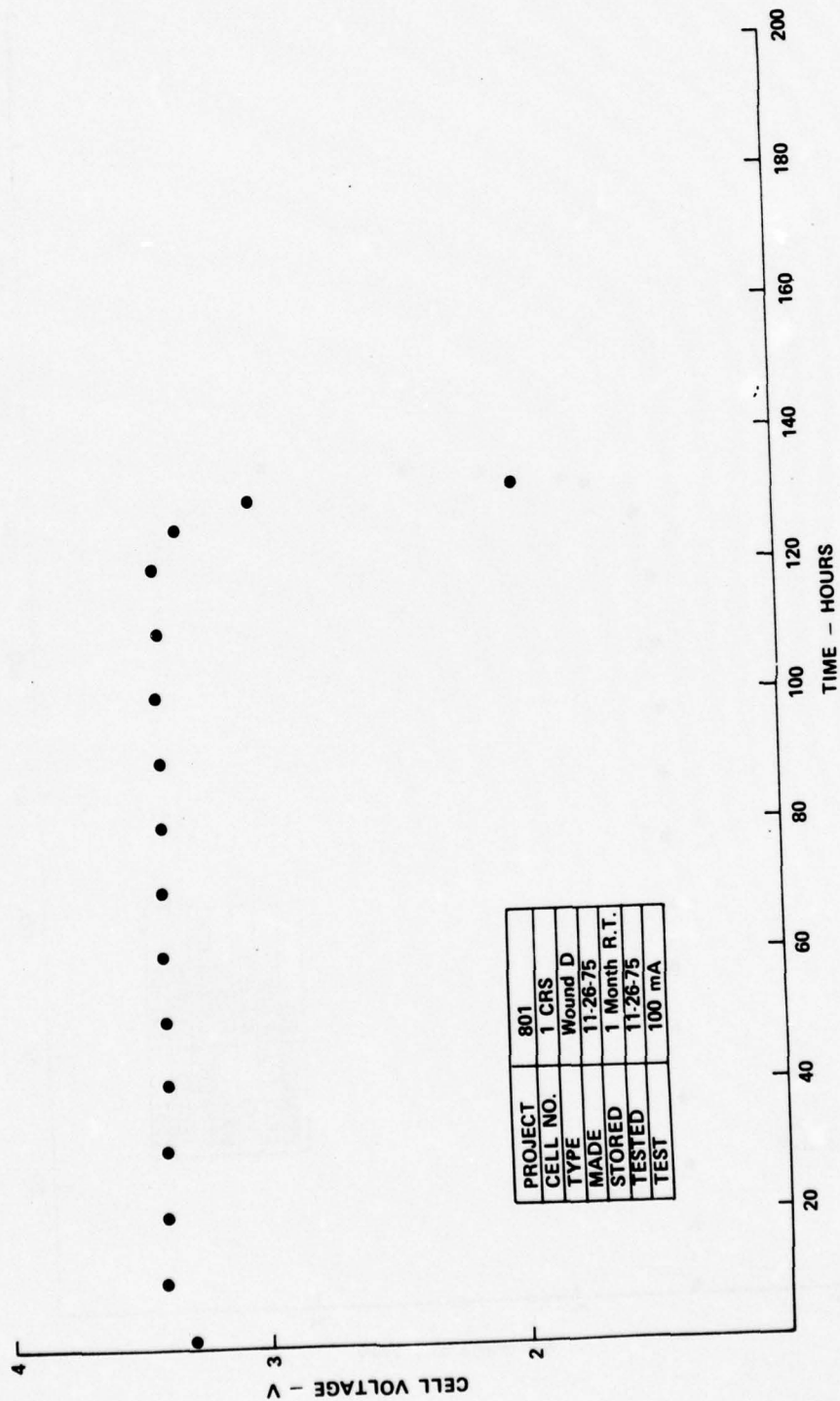


Figure 115. Discharge Curves for Standard Size D Cells after 1 Month Storage at Various Temperatures

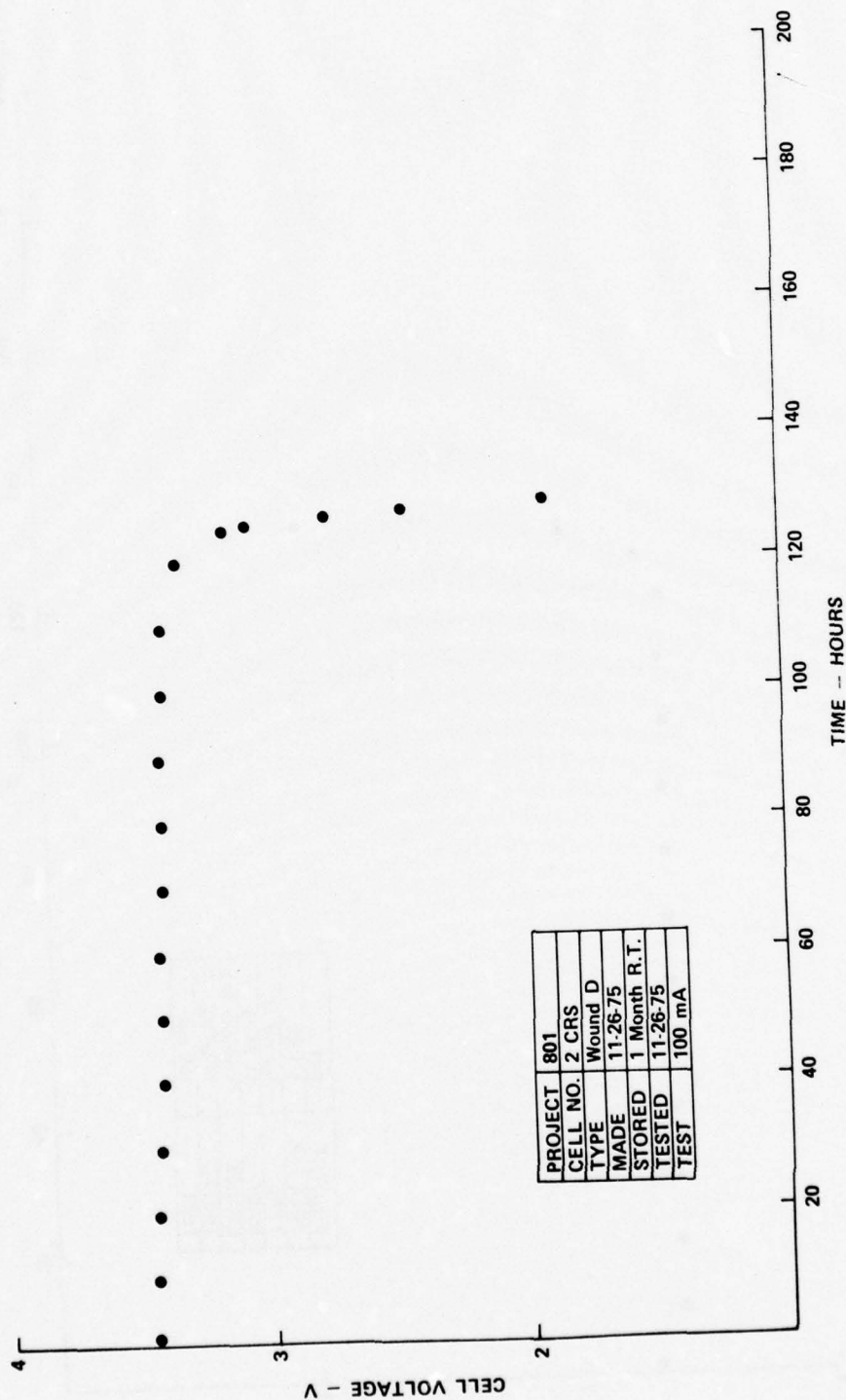


Figure 116. Discharge Curves for Standard Size D Cells after 1 Month Storage at Various Temperatures

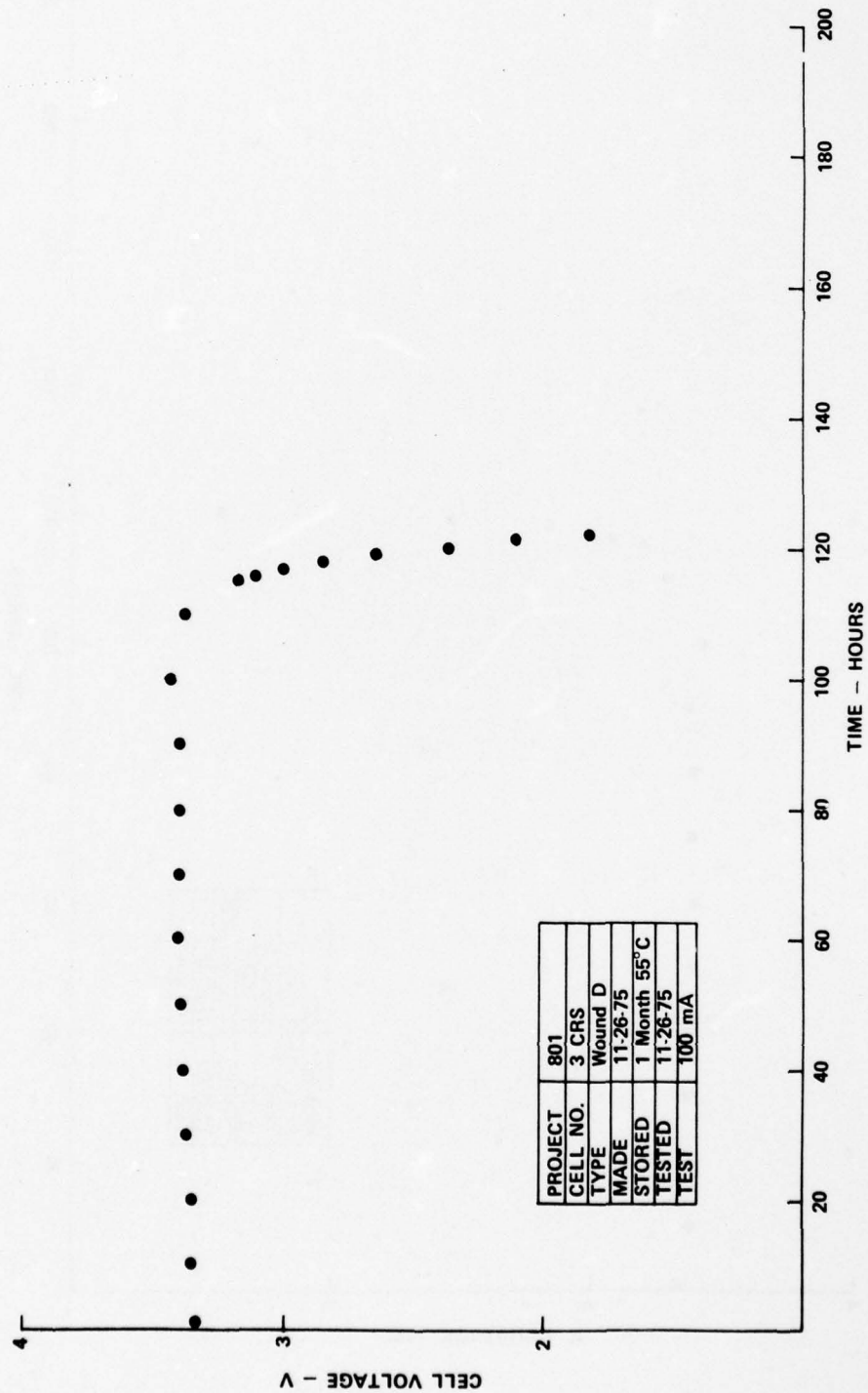


Figure 117. Discharge Curves for Standard Size D Cells after 1 Month Storage at Various Temperatures

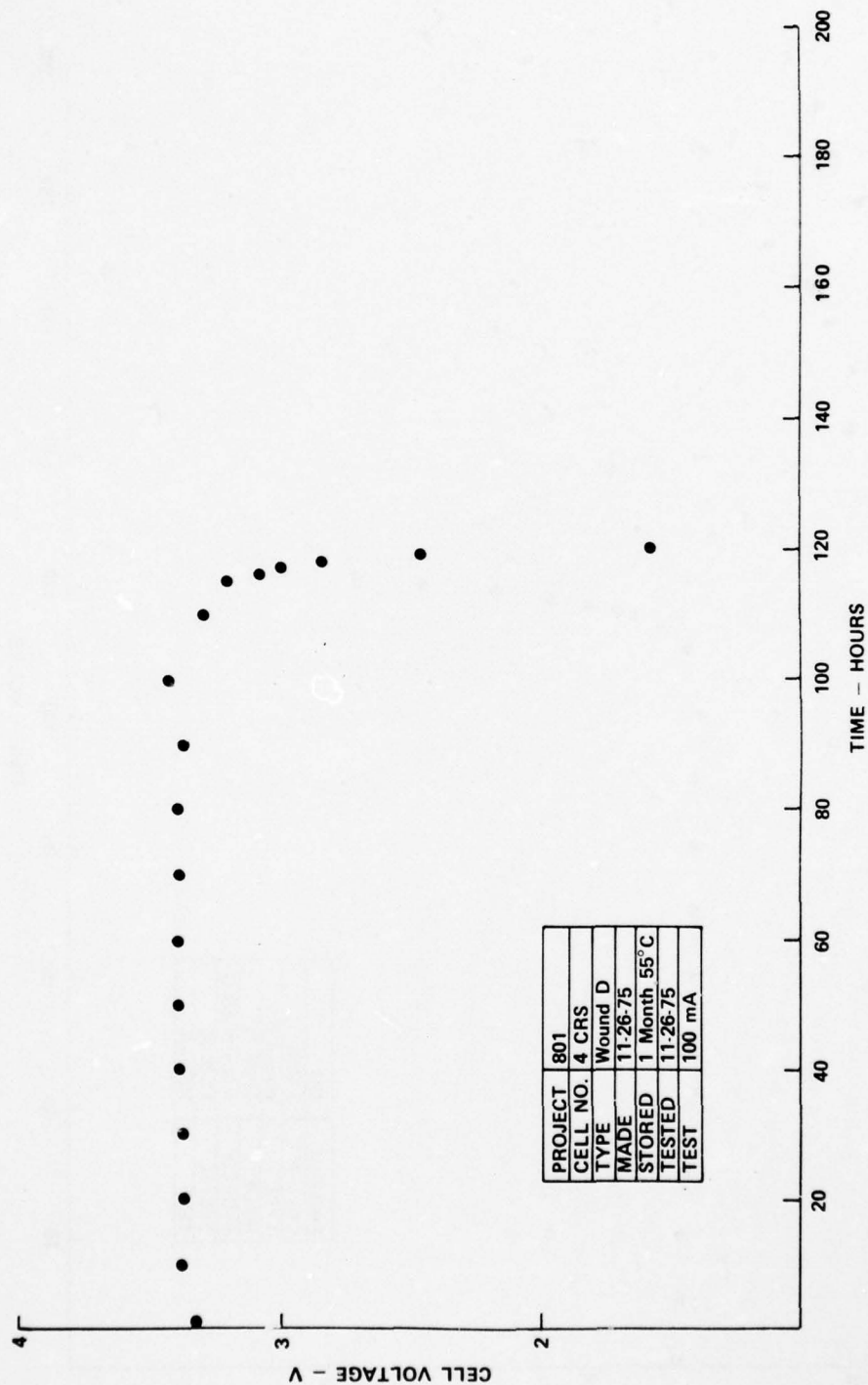


Figure 118. Discharge Curves for Standard Size D Cells after 1 Month Storage at Various Temperatures

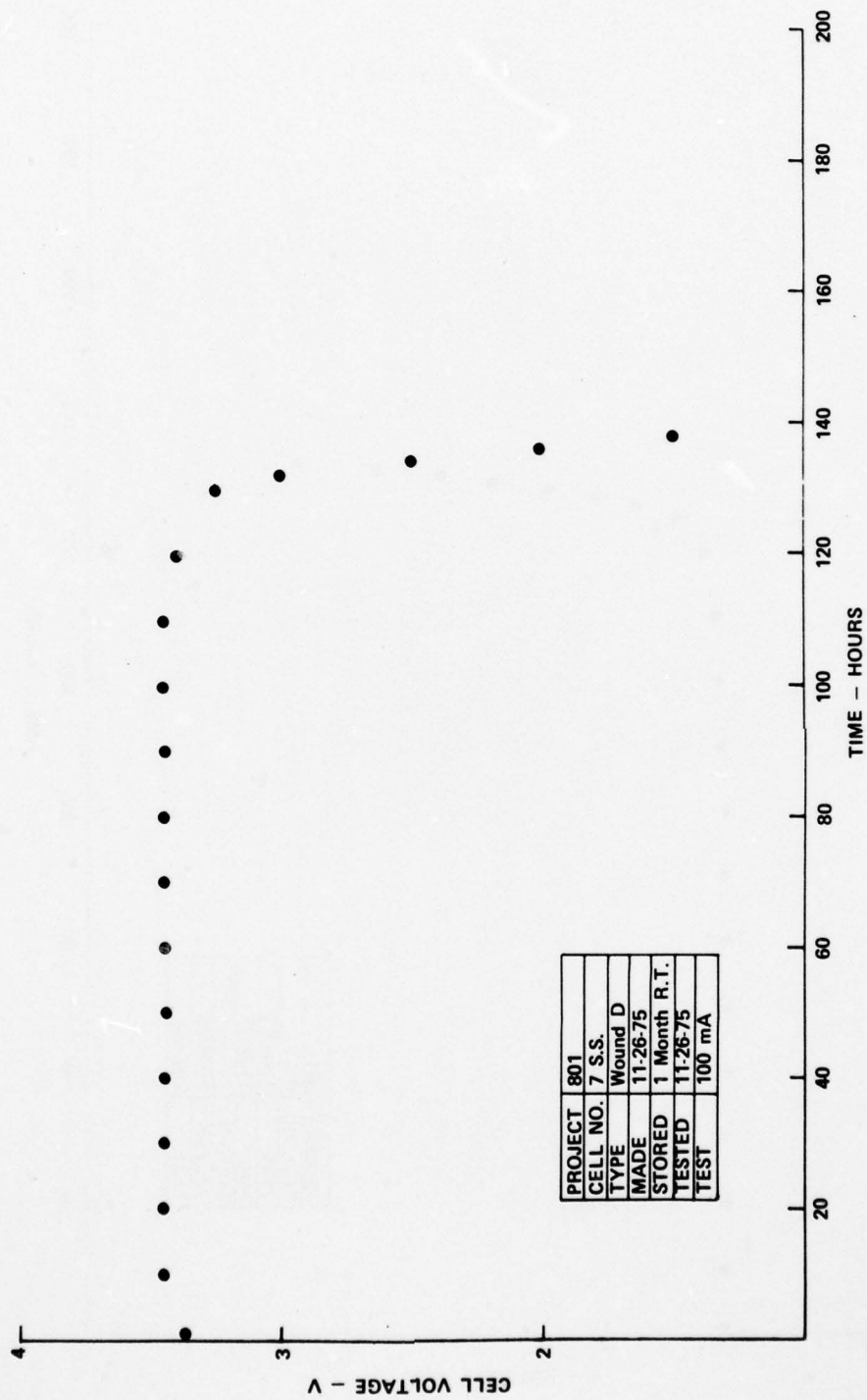


Figure 119. Discharge Curves for Standard Size D Cells after 1 Month Storage at Various Temperatures

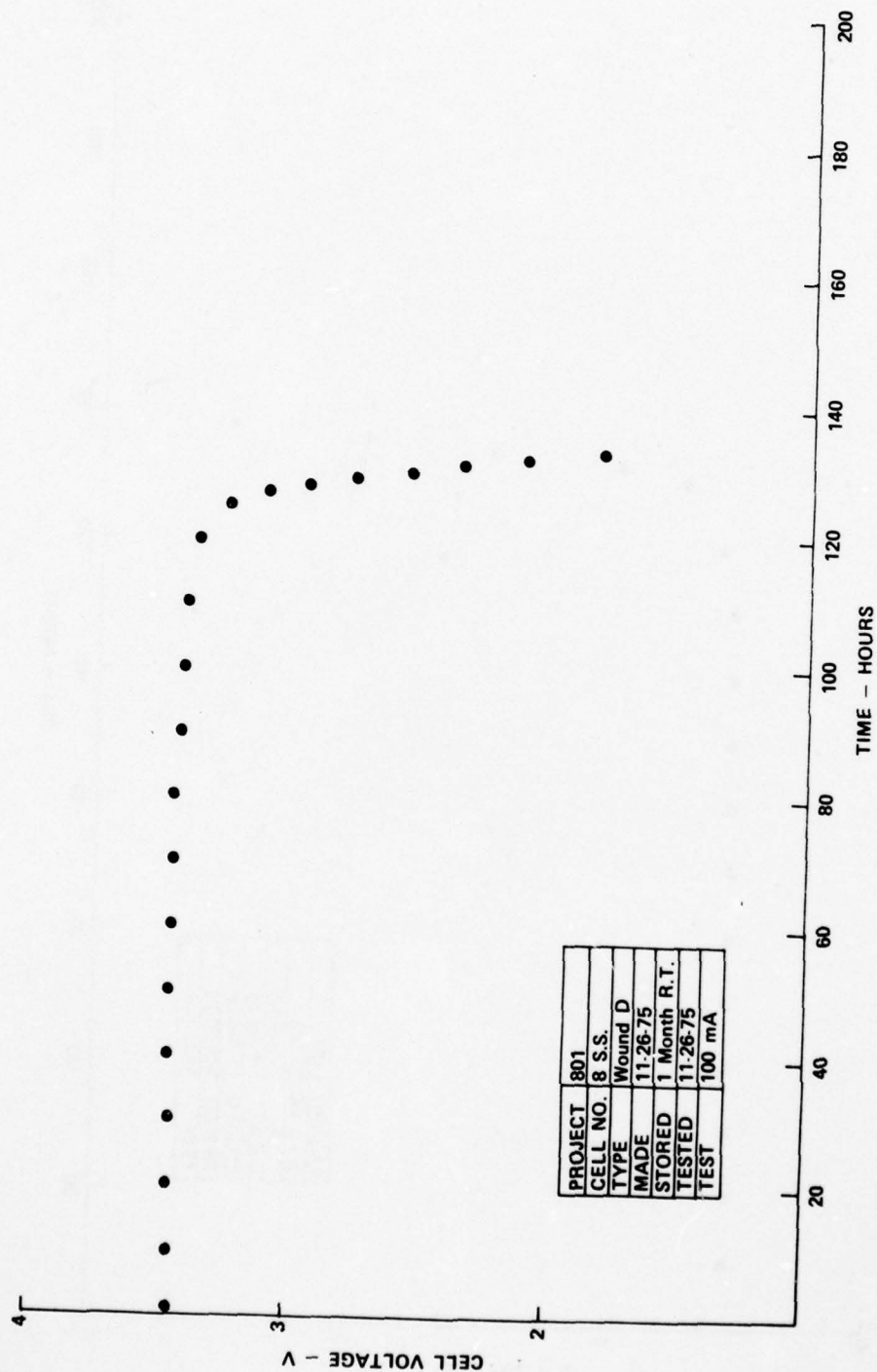


Figure 120. Discharge Curves for Standard Size D Cells after 1 Month Storage at Various Temperatures

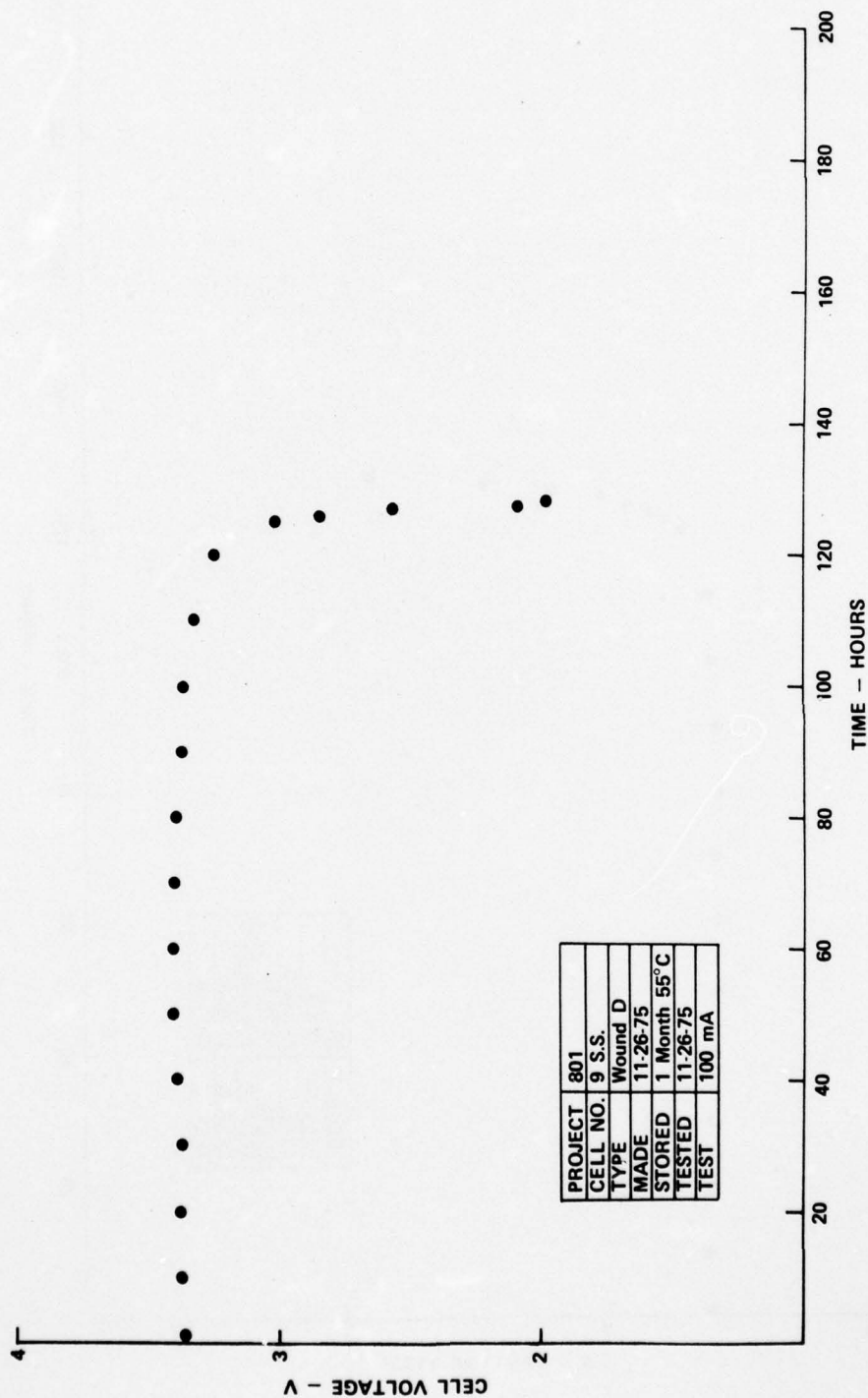


Figure 121. Discharge Curves for Standard Size D Cells after 1 Month Storage at Various Temperatures

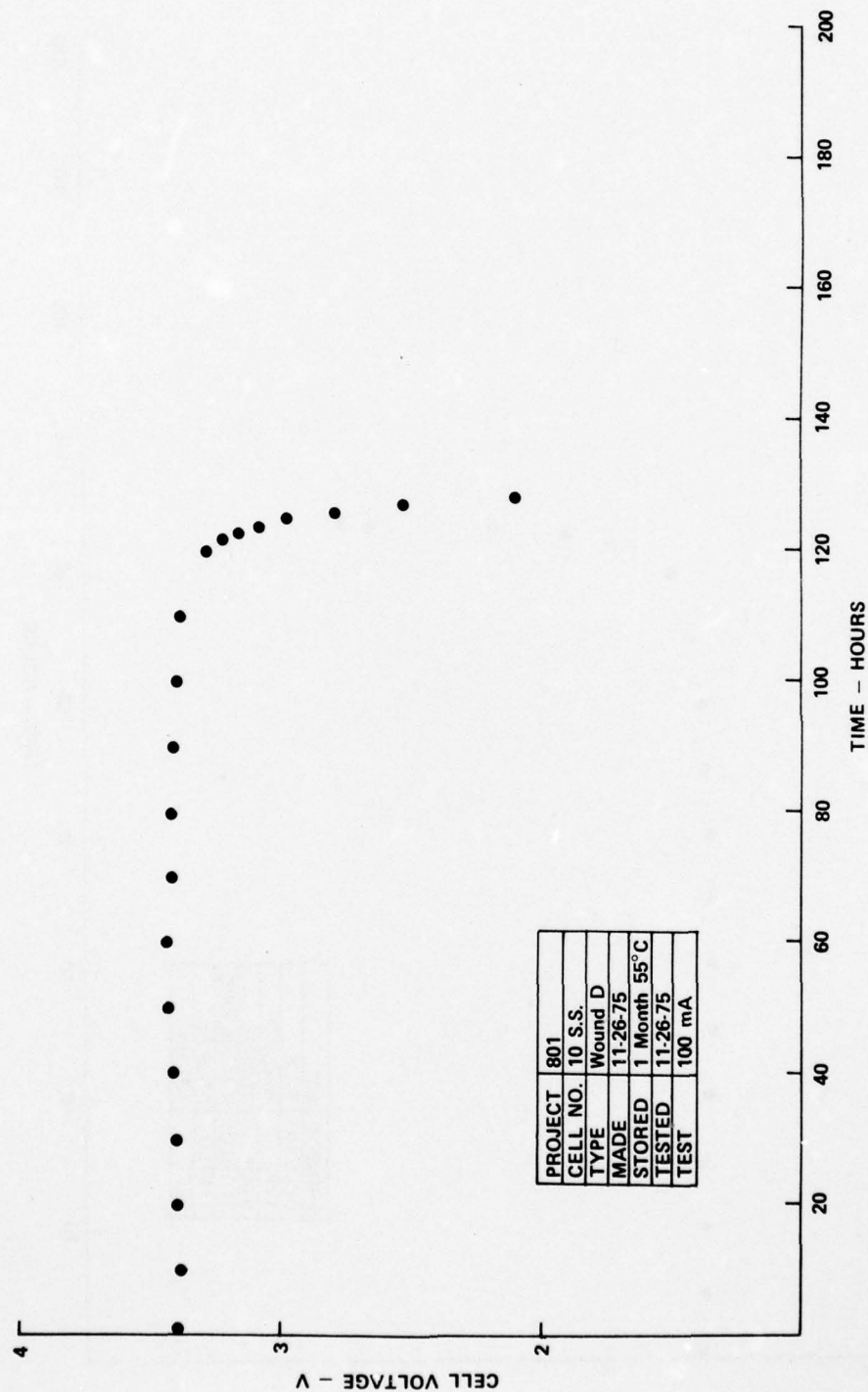


Figure 122. Discharge Curves for Standard Size D Cells After 1 Month Storage at Various Temperatures

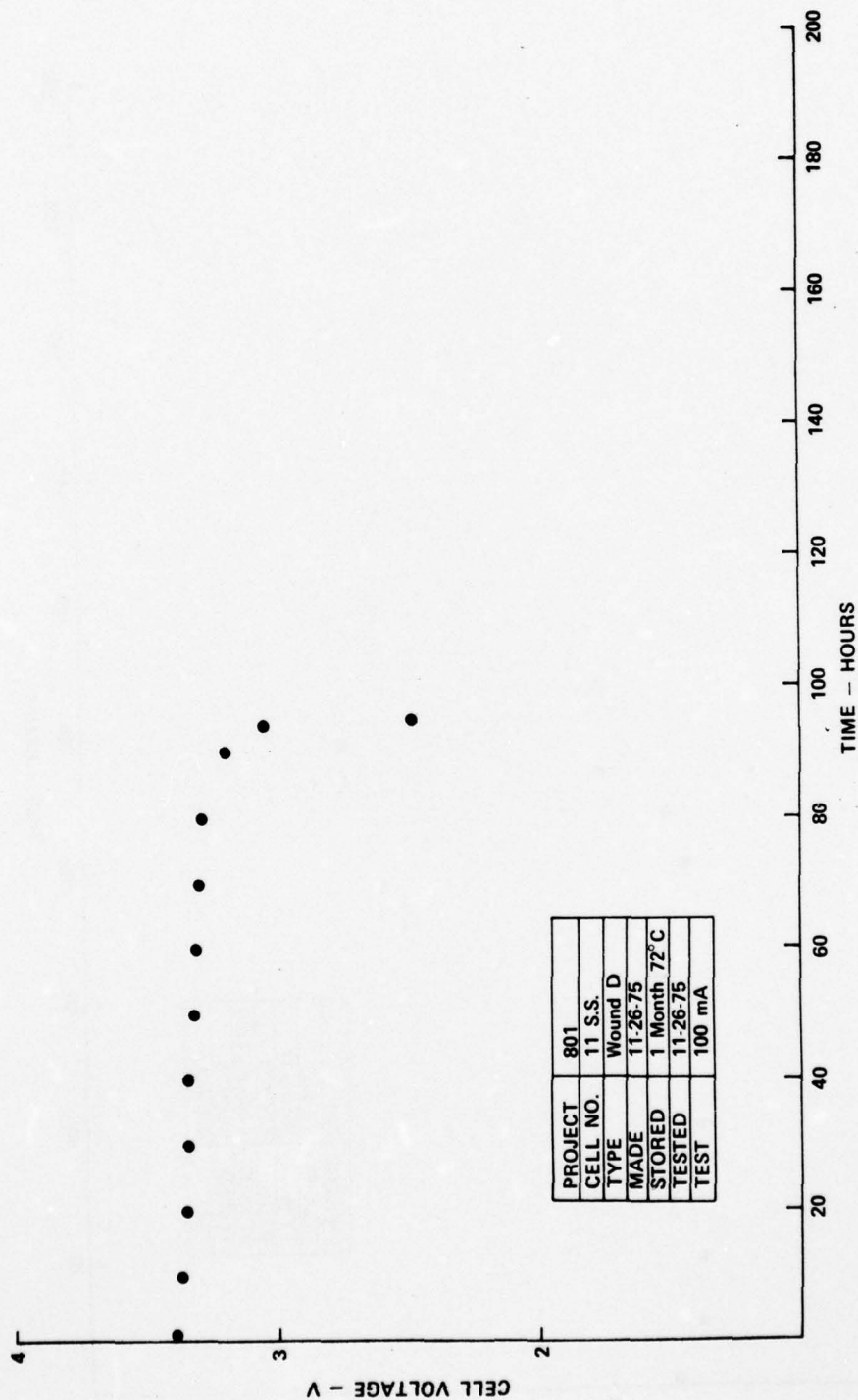


Figure 123. Discharge Curves for Standard Size D Cells after 1 Month Storage at Various Temperatures

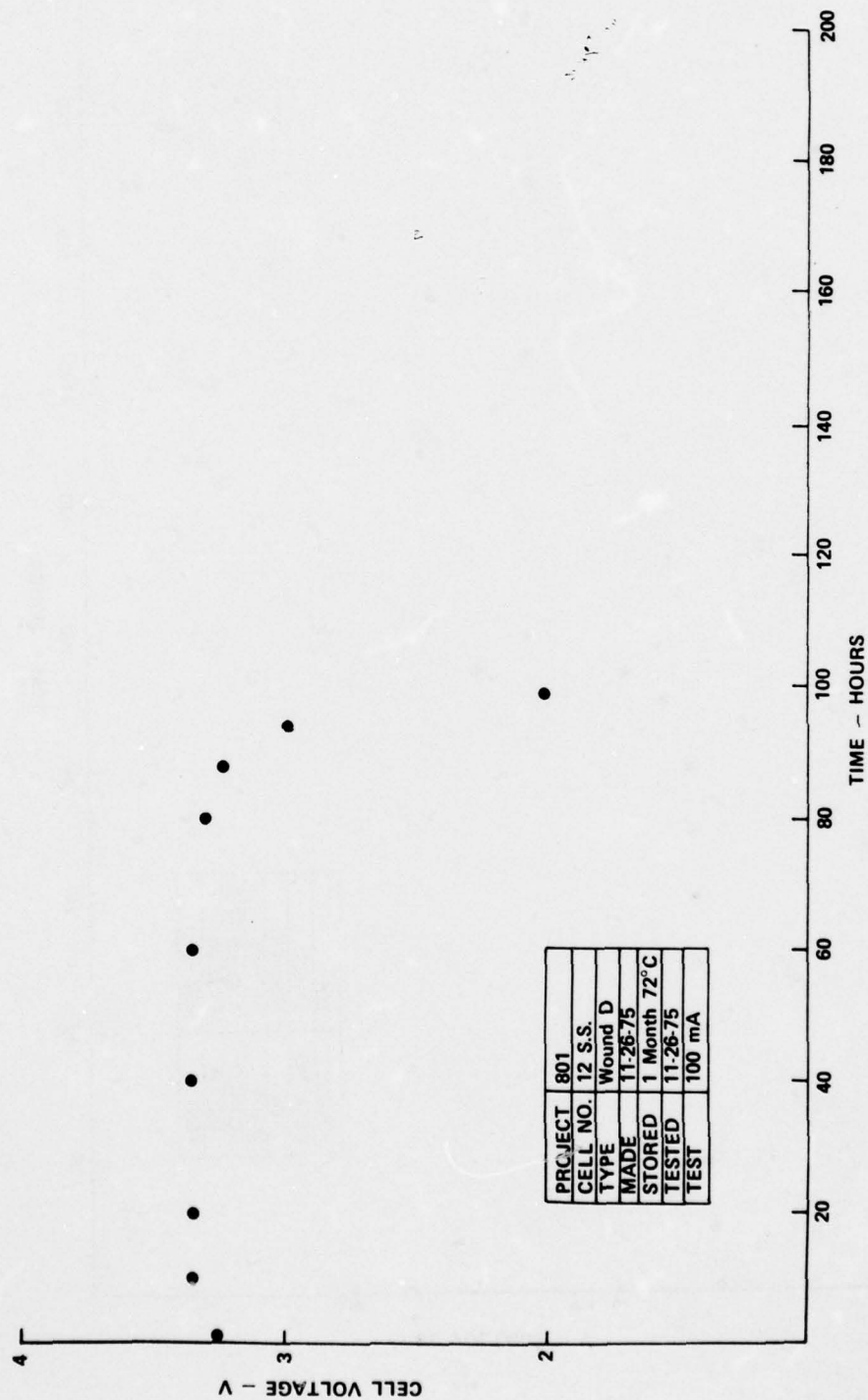


Figure 124. Discharge Curves for Standard Size D Cells after 1 Month Storage at Various Temperatures

The voltage delay data clearly show a superior performance of cells made with stainless steel cans. The cold rolled steel cans show delay effects as soon as they are exposed to temperatures higher than the ambient. This probably is the result of the high rate of corrosion of cold rolled steel with the iron plating out on this lithium anode. The average discharge voltage for these cells, listed in Table 27, also suggest the negative influence of the iron on the cell performance. The cold rolled steel cells have a consistently lower average discharge voltage at the same discharge current and at all three temperatures involved. At high temperatures, more iron is being produced from corrosion and plated out on the lithium, thus increasing the internal impedance of the cell. Since the average voltage in the stainless steel cans are higher than those observed in cold rolled steel, it can be concluded that the stainless steel is subject to less corrosion at the same temperatures. At the storage temperature of 72°C, the cold rolled steel cells are completely passivated. The stainless steel cells at 72°C show somewhat lower capacity and also lower operating voltages than those obtained at 55°C or room temperature. These results suggest that the stainless steel cells might be subject to some degree of corrosion of lithium at 72°C. However, the post mortem analysis showed an excess of lithium to be present in discharged cells. This would mean that the lower cell capacity was not the result of loss of active materials but, rather, the effect of an increased cell impedance, probably associated with the original passive film formed during storage.

Five wound D cells were constructed and stored at room temperature for three months. These cells were not built with the aid of the computer calculations and, therefore, capacity was not optimized. A capacity of 9 Ah to 10 Ah was expected according to the previous experience with this type of cell after storage.

The delay tests were carried out at a current of 300 mA using a high speed strip chart recorder. Of the five cells only one showed a slight delay. All cells retained their full capacity. The results are plotted in Figure 125, 126 and 127 and the capacities listed in Table 28.

It was obvious from this test that three months storage at room temperature had no ill effects on the voltage delay or the capacity of the cell. The delay was not much different from that of a fresh cell and the entire capacity seemed to remain available for discharge. This has generally been the result of most of the test run at room temperature, including the early tests covering one month storage.

TABLE 27

AVERAGE OPERATING VOLTAGES AT 100 mA AFTER STORAGE

CELL NO.	CAN TYPE	STORAGE TEMP.	VOLTAGE - V
1 2	COLD ROLLED STEEL	ROOM TEMP.	3.390 3.438
3 4		55°C	3.210 3.405
5 6		72°C	INOPERATIVE
7 8		ROOM TEMP.	3.438 3.445
9 10		55°C	3.412 3.422
11 12		72°C	3.337 3.340

TABLE 28

CAPACITY AFTER STORAGE FOR THREE MONTHS
AT ROOM TEMPERATURE USING COLD ROLLED STEEL CANS

CELL NUMBER	CAPACITY (Ah)
1	8.6
2	9.2
3	9.5
4	9.1
5	9.2

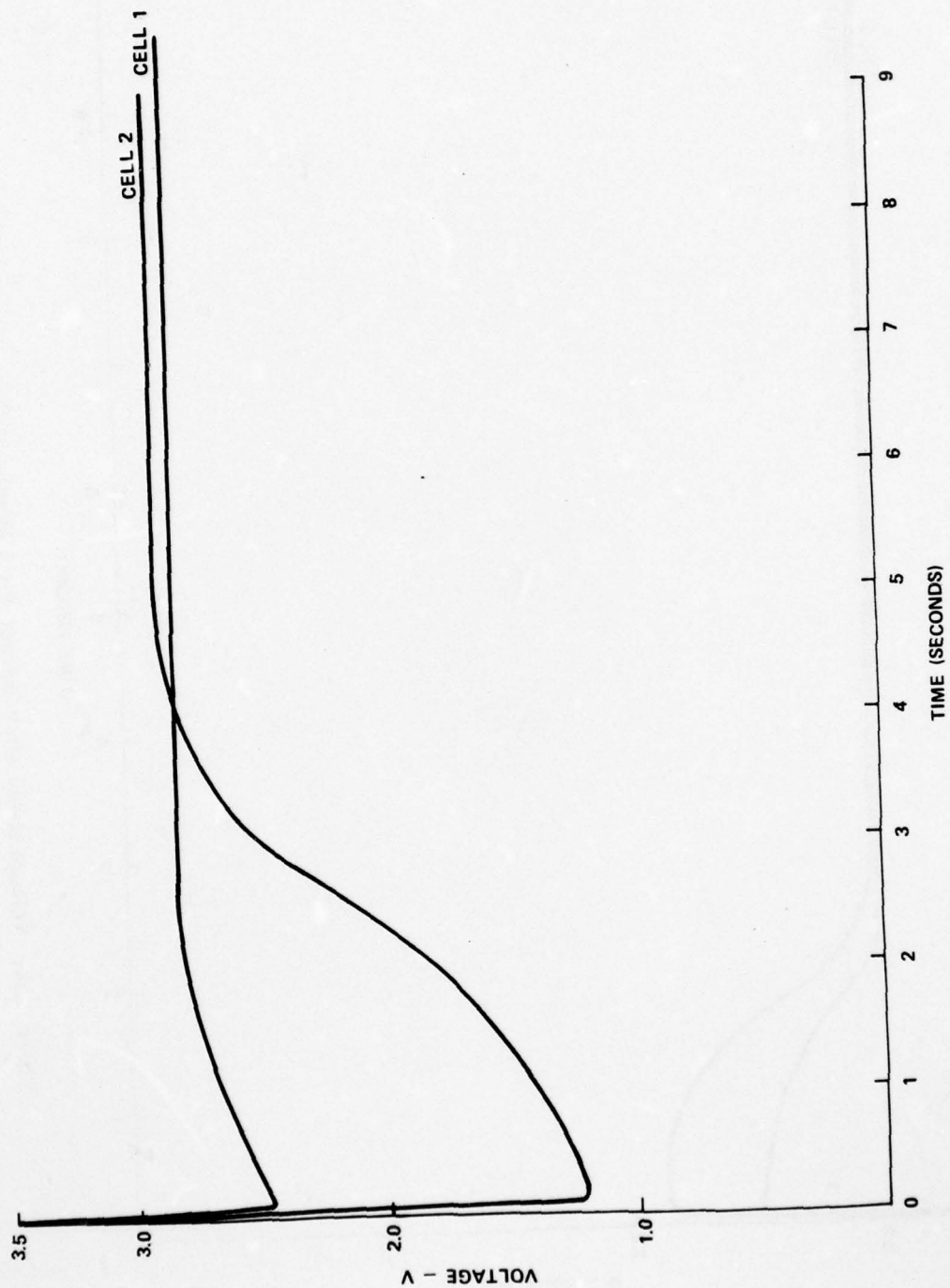


Figure 125. Voltage Delay after Storage for 3 Months at Room Temperature

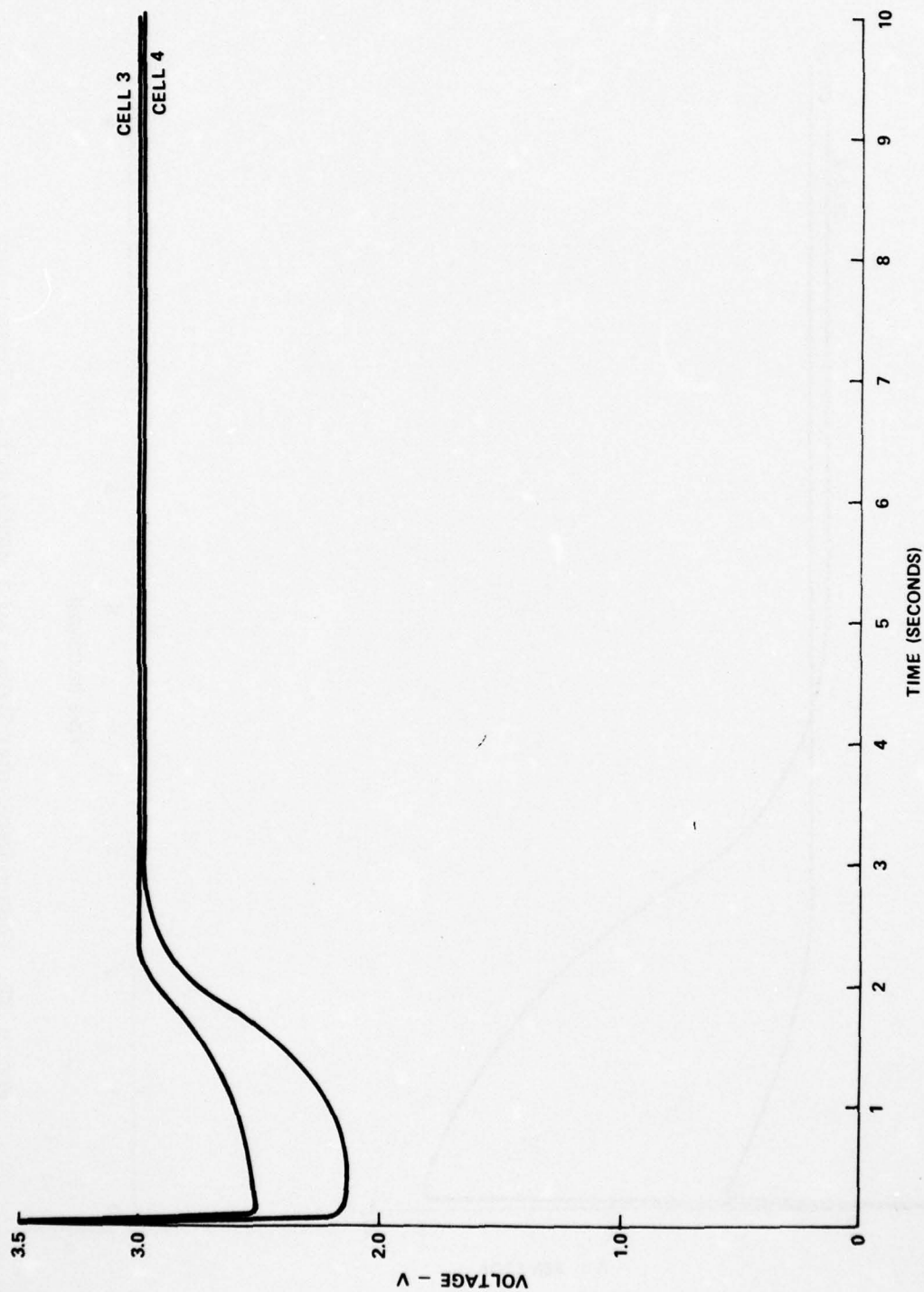


Figure 126. Voltage Delay after Storage for 3 Months at Room Temperature



Figure 127. Voltage Delay after Storage for 3 Months at Room Temperature

11. OPTIMIZATION OF ELECTRODE STRUCTURES

The preliminary cell design, defined at the beginning of the program, has been maintained throughout most of the testing conducted in the program. Although the stoichiometry of the cell discharge reaction did not seem to have been agreed upon between various researchers there was a need to define some of the reaction parameters either by assuming one of the proposed mechanisms or, possibly, by defining the parameters in a general way and then establishing their magnitude applicable for each discharge reaction applied.

A study was made of the design characteristics and optimization procedures leading to an improvement of the maximum cell capacity obtainable with the high power type lithium inorganic batteries. The general relations derived from the low power type cells⁷ have been modified for use in the design of high power type cells. A materials balance was established for the interior components of cylindrical cells made for high discharge rates. The cell design calculations were based on the stoichiometry of one of the proposed cell discharge reactions and also on the experimental work characterizing behavior of porous carbon cathodes used in these cells. Following were the basic parameters established in those studies.

1. Specific cell capacity (k_1) obtained per unit volume of the reaction products formed on discharge was calculated to be 1.079 Ah/cm^3 . This parameter is a characteristic of the lithium/thionyl chloride system and is independent of the cell construction.

2. The maximum specific cell capacity (k_2) obtained per unit of weight of the carbon blend was determined experimentally for cylindrical cathodes operating at low discharge rates and high porosities. This parameter was found to be 2.386 Ah/g for the carbon blend used in this particular electrode configuration. This is a characteristic of the electrode configuration in the cell made with a given electrochemical system. These measurements had to be repeated for high power type electrodes in order to establish the value of this parameter applicable in describing the behavior of the high power cells.

3. The specific volume reduction in the course of discharge (k_3) was calculated from the stoichiometry of the discharge reaction and the densities of the reactants and products. It was found to be $0.5643 \text{ cm}^3/\text{Ah}$. It is another characteristic of the chemical system, independent of the cell construction or the discharge rate.

The new value of the maximum capacity obtained with high power type electrodes, combined with the basic reactions established for the low power electrodes, made possible the development of the design procedures leading to the optimized electrode structures for the high power cells.

The high power type cells are usually made with the wound electrode structure. This is particularly convenient in cases when the cylindrical shape of the cell must be preserved while the surface area of the electrodes is being maximized. The high power type cells must be made with a maximized surface area of electrodes, because of the relatively low conductivity of the electrolytes used. The geometry of the wound electrodes had to be examined before any optimization attempt was made. This study was a part of another program, but its outcome made the most significant impact on the design, optimization and performance of the sealed cells developed for ECOM. The details of the study can be found in the series of publications that resulted.^{7, 8, 9, 10}

AD-A039 336

GTE LABS INC WALTHAM MASS
SEALED LITHIUM INORGANIC ELECTROLYTE CELL.(U)
APR 77 N MARINCIC, A LOMBARDI

F/G 10/3

UNCLASSIFIED

ECOM-74-0108-F

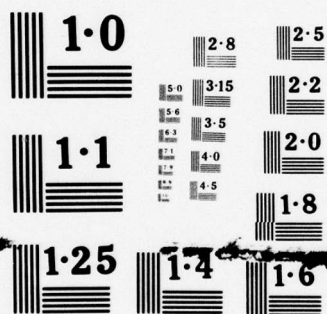
DAAB07-74-C-0108
NL

3 OF 3
ADA
039336



END

DATE
FILMED
5-77



NATIONAL BUREAU OF STANDARDS
MICROCOPY RESOLUTION TEST CHART

12. HERMETIC CELL DESIGN

It has become clear from the tests with the first D cell prototype that a totally hermetic seal is required for the building of lithium inorganic batteries; not so much because of cell performance but because of corrosion of the cell exterior. The compression seals of one sort or another permit the escape of minute amounts of thionyl chloride that decompose on contact with humid air producing highly corrosive acids.

We have developed the hermetic seals for small cells, such as the pacemaker and the electronic watch cell, using a glass to metal feedthrough in conjunction with either the TIG, laser or resistance welding as a final closing step. We have tried to adopt some of these components and procedures in the building of D size cells under this program, in order to avoid large tooling expenditures for the development of D cells at this time. The first prototype seals made are presented schematically in Figure 128.

The D size top was punched and drawn to accommodate our AA hermetic cell feedthrough. The two were laser-welded before the subassembly was mounted on the cell. The cell was closed in a second welding step whereby the top subassembly was welded to the can before the cell was filled with electrolyte. The advantage of this procedure is the absence of corrosive liquids in the welding area during the welding operation. Clean, hermetic welds were easily obtainable every time, once the proper fit was achieved between the can and the cover. The tubular feedthrough was used to dispense the electrolyte. The closing of the tube was done in another welding operation, whereby a head was formed on the pin to be used for making further contacts either to other cells in a battery or to a protective cap for a single cell. The prototypes of this kind of cell were tested for leakage both at elevated temperatures and in a humidity chamber at room temperature. The latter test seemed to be much more sensitive in detecting leakage, since small amounts of thionyl chloride were easily detected at 100% humidity in a closed space by a wet pH paper.

A proper top subassembly for the D size cell should, of course, be made in a different way. A number of on-line welding operations could be reduced by fabricating the subassembly in a separate continuous fusing procedure, or by using a mass produced feedthrough and attaching it to a simple cell top as shown in Figure 129. This could be the least expensive arrangement, provided that the welding of the feedthrough to the cell top is carried out efficiently.

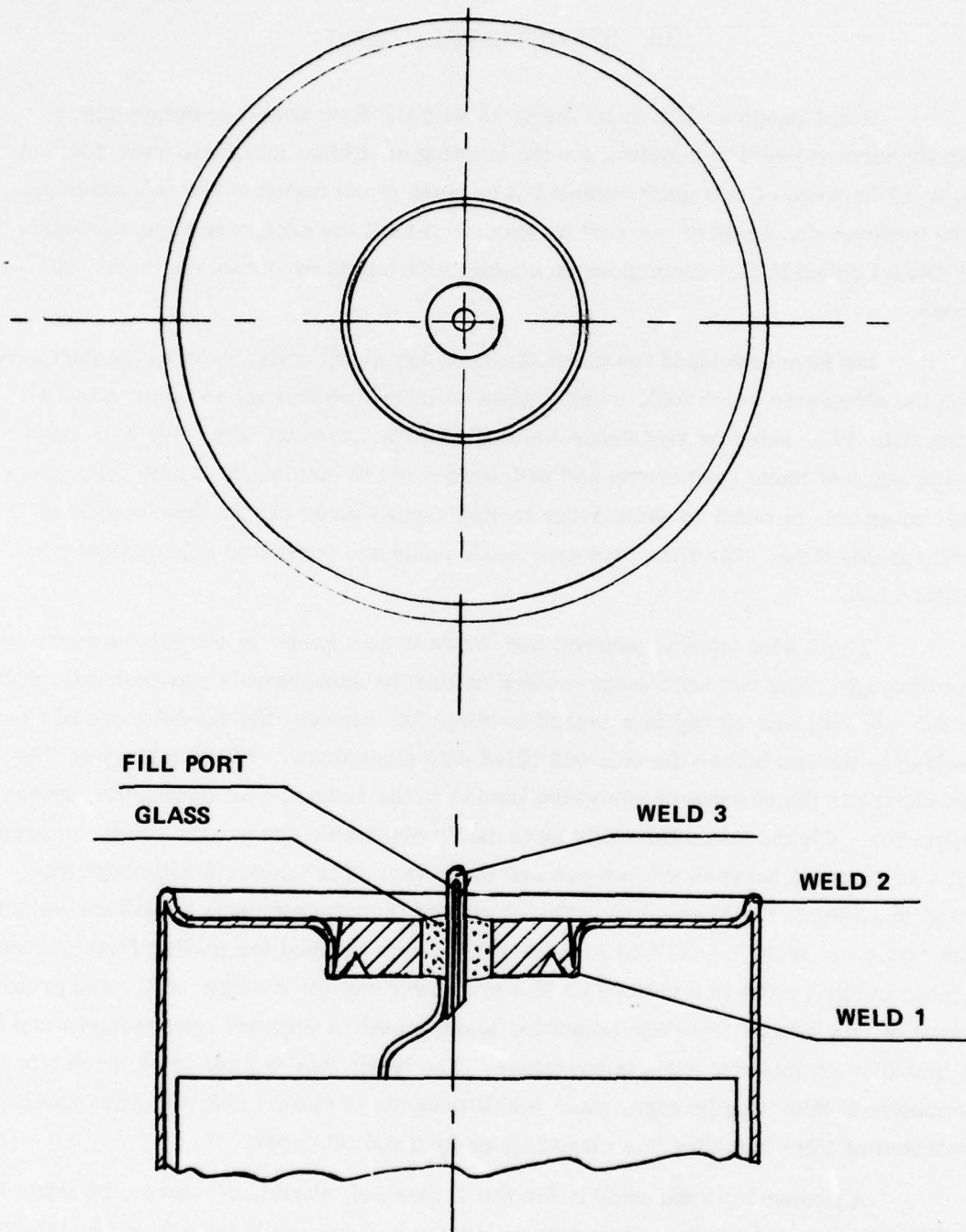


Figure 128. Hermetic D Cell Closure Made With AA Size Subassembly

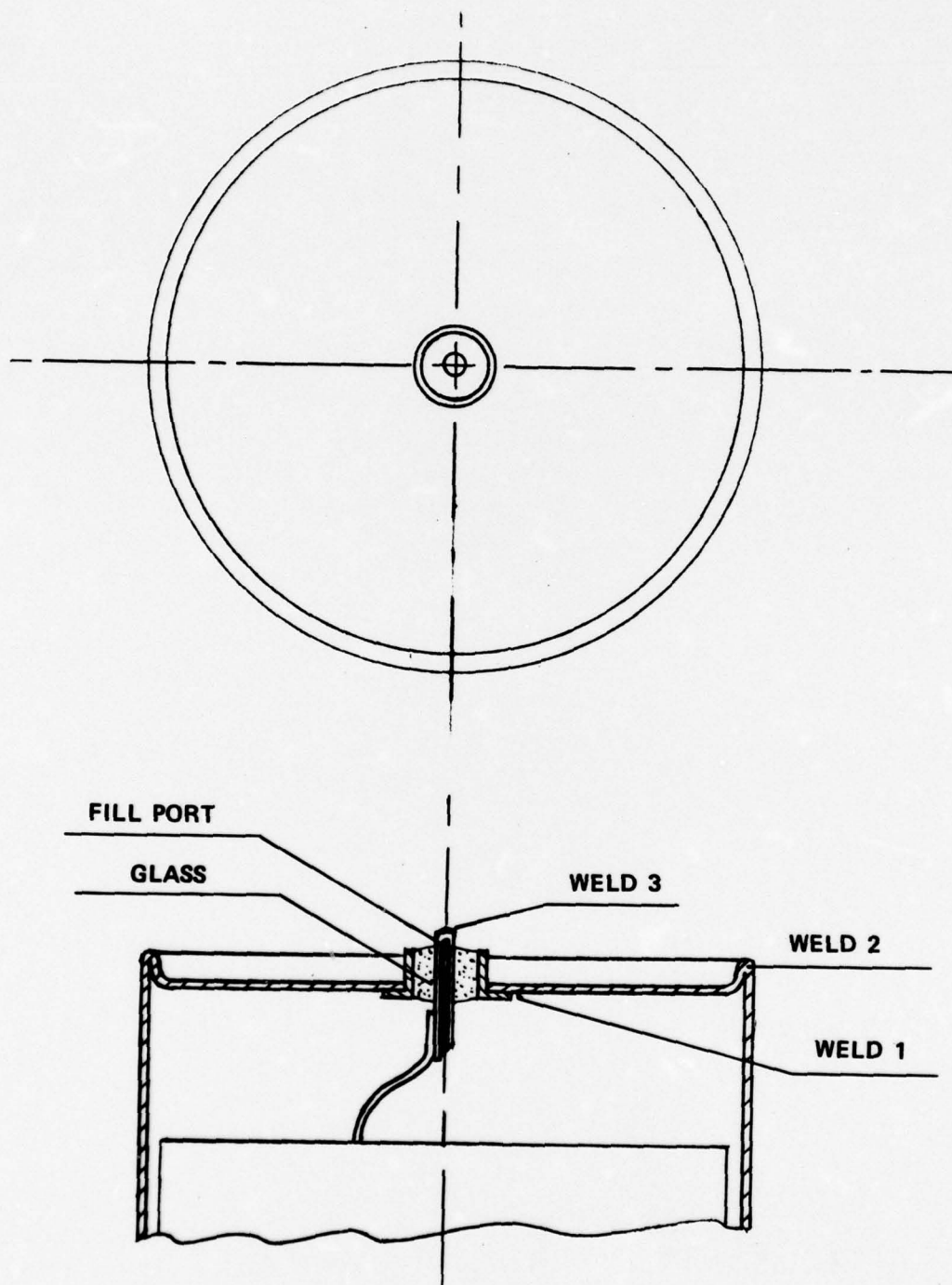


Figure 129. Hermetic D Cell Closure Using Commercially Available Glass to Metal Feedthroughs

13. THERMAL EFFECTS OF BATTERY DISCHARGE

High surface area electrode structures are capable of discharge at a very high rate. Thermal effects accompanying such discharge become significant, particularly during the uncontrolled discharge under conditions approaching a short circuit. A study was made of the discharge conditions leading to thermal runaways,⁸ caused either by the reaction of molten sulfur (112.8°C) with lithium in partially discharged cells or by the reaction of molten lithium (186°C) with SOCl_2 in fresh cells. An expression was derived for a maximum time the cell would take, τ , to reach a certain temperature, t , measured above ambient temperature, during discharge:

$$\tau = \frac{G C (t)}{0.239 \Delta V I - (a + bt + ct^2)} \quad (1)$$

Whereby:

- G = weight of cell
- C = specific heat capacity of cell
- ΔV = voltage drop on discharge
- I = discharge current
- a, b, c = coefficients of the polynomial relating the cooling rate to the cell surface temperature

It has been calculated, for example, that a D size cell discharged with 10 A constant current at 2.0 V will reach the melting point of sulfur in 23 minutes and 39 seconds. In this period of time the cell generates an amount of sulfur which, in an instant reaction with lithium, would increase an average cell temperature by approximately 93°C. Locally however, the temperature increase might be high enough to reach the melting point of lithium starting the thermal runaway. The melting point of lithium is reached under short circuit conditions before a significant amount of sulfur is generated and lithium probably starts the thermal runaway. Sulfur would have a greater role in starting the thermal runaway of partially discharged cells, particularly when discharged at relatively lower rates. The above calculations were experimentally confirmed by A. N. Dey,¹³ demonstrating an explosion of their D size cells at a 10 A discharge rate after 28.49 minutes.

The maximum safe discharge rate has been calculated and experimentally confirmed to be at 4 A for the D size cell, since at this rate the cell reaches the end

of discharge just before its temperature reaches the melting point of sulfur, if the discharge was started at room temperature. For this reason D cells have to be equipped with adequate fuses or they have to be designed so that they are not capable of discharge at rates higher than 4 A. Such cells have been built and operated safely under the most abusive conditions including short circuiting.

Equation (1) is an approximation which expresses time as a function of temperature, but is accurate when the cooling rate is not a significant fraction of the heating rate caused by i^2r power loss inside the cell. We wish to consider here both the case when the cooling rate is significant and include the thermal effect caused by the $T\Delta S$ term in the free energy change of the cell reaction.

We have determined the thermal coefficient of the cell's open circuit potential by measuring this potential at several fixed temperatures between -60° and $+75^\circ\text{C}$. For each temperature, the cell potential was measured as a function of current density for a series of low current levels. Extrapolation to zero current density using least square polynomial curve fitting produced the desired open circuit potentials. Between -20° and $+75^\circ\text{C}$, the open circuit potential is essentially a linear function of temperature, the coefficient being about +1 millivolt per degree centigrade. Since, for the cell reaction, the free energy change is:

$$\Delta G = \Delta H - T\Delta S = -nF\epsilon \quad (2)$$

the difference $\Delta H - \Delta G$ will yield the net thermodynamic heating or cooling effect as energy is withdrawn reversibly (at vanishing low current) from the cell. The difference, $+T\Delta S$, is positive (not positive $\Delta\epsilon/\Delta T$) meaning both that a cell operating under reversible conditions will become cooler (adiabatic operation) or that its entropy will increase (isothermal operation).

A cell operating at high current will be cooled somewhat due to the $T\Delta S$ term, as well as by the convection due to the $(a + bt + ct^2)$ term in the denominator of the right hand side of Eq. (1). Since:

$$T\Delta S = n F T \frac{d\epsilon}{dT} \quad (3)$$

The rate of cooling caused by the thermodynamic effect is:

$$i F T \frac{d\epsilon}{dT} \dots (\text{Kcal. second}^{-1}) \quad (4)$$

where τ is time in seconds, F is the Faraday constant in the appropriate units (2.392×10^{-4} Kcal joule $^{-1}$), i is in amps, and T is in degrees Kelvin. The total rate of heat dissipation is then in Kcal. second $^{-1}$:

$$\frac{dQ_c}{d\tau} = a + bt + ct^2 + i F \frac{d\epsilon}{dT} \quad (5)$$

where t is the temperature in $^{\circ}\text{C}$ measured above ambient. The heating rate is:

$$\frac{dQ_h}{d\tau} = F i (\Delta V), (\text{Kcal. second}^{-1}) \quad (6)$$

where F is 2.392×10^{-4} Kcal joule $^{-1}$, and ΔV is the difference between the open circuit and the operating voltage. The total thermal effect is:

$$\frac{dQ_t}{d\tau} = \frac{dQ_h}{d\tau} - \frac{dQ_c}{d\tau}, (\text{Kcal second}^{-1}) \quad (7)$$

Since $dt/d\tau = dQ/d\tau \times 1/GC$ where G = the weight of the cell in grams and C is the heat capacity in Kcal gram $^{-1}$ degree $^{-1}$:

$$\frac{dt}{d\tau} = \frac{1}{GC} \left[iF (\Delta V) - (a + bt + ct^2) - i F (t + T_o) \frac{d\epsilon}{dt} \right] \quad (8)$$

The value of T_o is 298° , if the ambient temperature is 25°C . If we combine terms so that Eq. (8) takes the form:

$$\frac{dt}{d\tau} = \frac{1}{GC} (a^1 + b^1 t + c^1 t^2) \quad (9)$$

then:

$$a^1 = i F \left[(\Delta V) - T_o \frac{d\epsilon}{dt} \right] - a$$

$$b^1 = -(b + i F \frac{d\epsilon}{dt})$$

$$c^1 = -c$$

To find time as a function of temperature, the following must be integrated:

$$\int_0^t \frac{dt}{a^1 + b^1 t + c^1 t^2} = \int_0^\tau \frac{d\tau}{GC} \quad (10)$$

Under the conditions that the cell current is high enough to cause a net electrical heating effect, and that the temperature t is not above a maximum value determined by the rate of heat loss through convection, the integral takes the form:

$$\frac{-2}{\sqrt{-q}} \tanh^{-1} \frac{2c^1 t + b^1}{\sqrt{-q}} \Big|_0^t = \frac{\tau}{GC} \quad (11)$$

where:

$$q = 4 a^1 c^1 - (b^1)^2$$

Evaluating Eq. (11) under the conditions that $i = 10$ A, $\Delta V = 1.65$ volts, the time necessary to reach the melting point of sulfur (112.8°C) is 40 minutes, 12.2 seconds.

The cell explosion reported¹³ occurred sooner for two possible reasons. The first one must have been the short circuit developed a few minutes before the explosion, indicated by the sudden voltage drop at that point of discharge. The second reason must have been a local overheating for which there was no provision in the above calculations.

14. SAFETY DEVICES FOR HIGH POWER CELLS

14.1 FUSING OF D CELLS

High power type cells with the wound electrode structure are capable of discharge at rates far in excess of the maximum discharge rate at which an equilibrium is reached between the heat generation and the cooling of the cell. As a consequence, there is a steady rise in the cell temperature during discharge, reaching the point where the internal pressure buildup causes an explosion. Calculations present in the preceding chapter established the dependence of the maximum allowable discharge rate on the cell size and geometry. For the purpose of limiting the maximum discharge rate to the values lower than the critical ones, we have developed two types of internal fuses. Accidental short circuit or an intentional attempt to discharge the cell at the rate above the set limit will result in melting of the fuse and breaking the connection between the cathode and the cell positive terminal. Of the two choices given, we have decided in favor of an internally placed fuse with the understanding that an accidental short circuit will mean a loss of the cell. The externally placed replaceable fuse would probably be justified only on larger units, not required to conform to any dimensional standards. Two different types of fuses were developed and tested both satisfactorily. However, only one of them seems entirely feasible.

Preliminary tests were carried out with a simple nickel wire sealed in a glass ampule, as schematically shown in Figure 130. The fuse was connected to the cathode section of the circuit and physically placed in the hollow center of the wound structure. It is approximately 0.1 in. long, with two Kovar leads for connection to the cathode tab and the cell positive terminal. A 0.003 in. diameter nickel wire, for example, will sustain the discharge at 1 A but will melt instantaneously at 1.4 A. The high limits of current are established by heavier gage wires that have to be selected on the basis of experiments in actual cells. The major deficiency of these fuses is a considerable rate of heat generation at values of current slightly below the critical one, due to the high melting point of nickel. Other materials were not applicable in this configuration, since they melted in the process of sealing the glass ampule. For this reason a different design of the fuse has been developed, enabling the use of standard value commercial low melting fuses. This more advanced version of the cell fuse is shown in Figure 131.

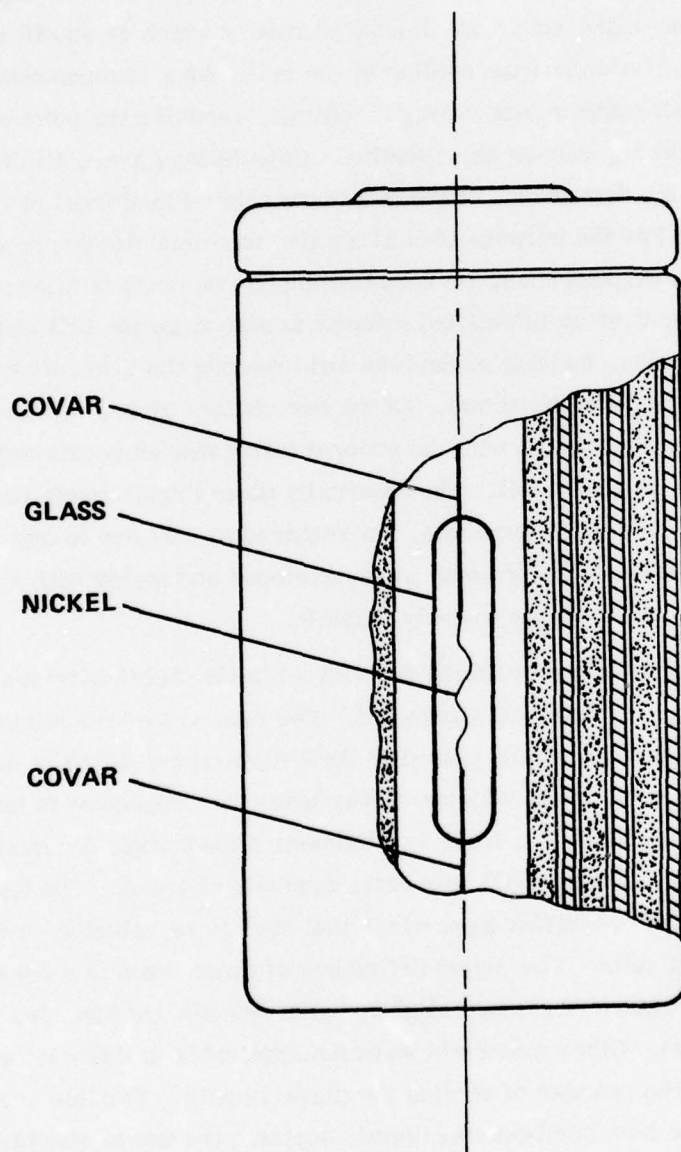


Figure 130. D Cell Fuse-1

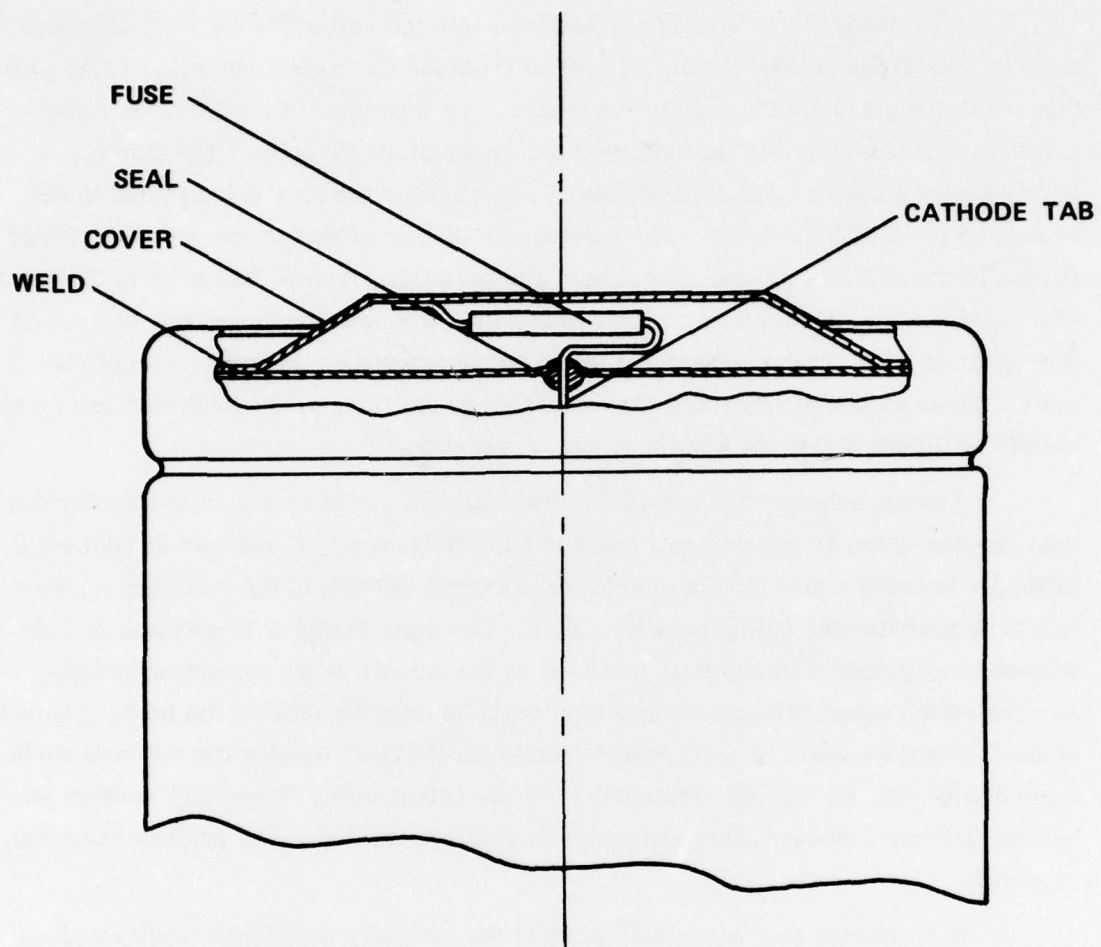


Figure 131. D Cell Fuse-2

The standard 3 A small fuse was built into the cell cover hermetically separated from the electrode compartment, as well as from the outside of the cell. A flat round disc, with the glass feedthrough in the center, was developed for other uses (semiconductor devices) and has been adapted for fusing of single cells. The disc is hermetically welded to the internal side of cover, after the fuse is connected to the cover and the feedthrough pin. The cathode tab is spot welded to the opposite side of the pin in the cell assembling operation. The particular type of fuse used in these tests will sustain a 3 A discharge for 1 hour maximum, will melt in 15 seconds at 4 A and in 5 seconds at 6 A, which seems close to the requirements for the protection of size D cells. Other values of fuses are also available in the same dimensions that can conveniently be placed inside the dimple of our D cell cover.

The top subassembly containing the fuse was tested as a part of the crimped seal version of the D size cell and found to be satisfactory. There was an additional difficulty in using a fuse of this type in the hermetic version of the cell, since a port has to be provided for filling the electrolyte. One such design is illustrated in Figure 132, whereby a separate filling port is provided on the outside of the top subassembly. In this way the entire space between the two tops could be used for placing the fuse. The height of the filling tube would be sufficiently reduced in the final welding operation to avoid its interference with the positive terminal when the cell is being placed into various kinds of battery holders. The cell interconnectors would be attached to the positive terminal, if required.

It is obvious that one could maintain the centrally positioned feedthrough as well, if a sufficiently small size fuse is selected. In this case there would be no need for an extra filling tube, since a tubular pin in the feedthrough can be used for that purpose. However, this design would eliminate the advantage of finishing the top subassembly before the top is welded to the cell can.

A typical heating curve of a fused cell at short circuit is shown in Figure 133.

14.2 VENTING OF D CELLS

A controlled release of gases and liquids must be facilitated, when an unfused cell is discharged at an excessive rate, in order to prevent a violent bursting of the pressurized cell container. Several different types of vents have been considered in the course of this development, but only one has, in fact, been tested. The engineering solution for a similar problem in the building of vented Ni-Cd cells seemed applicable

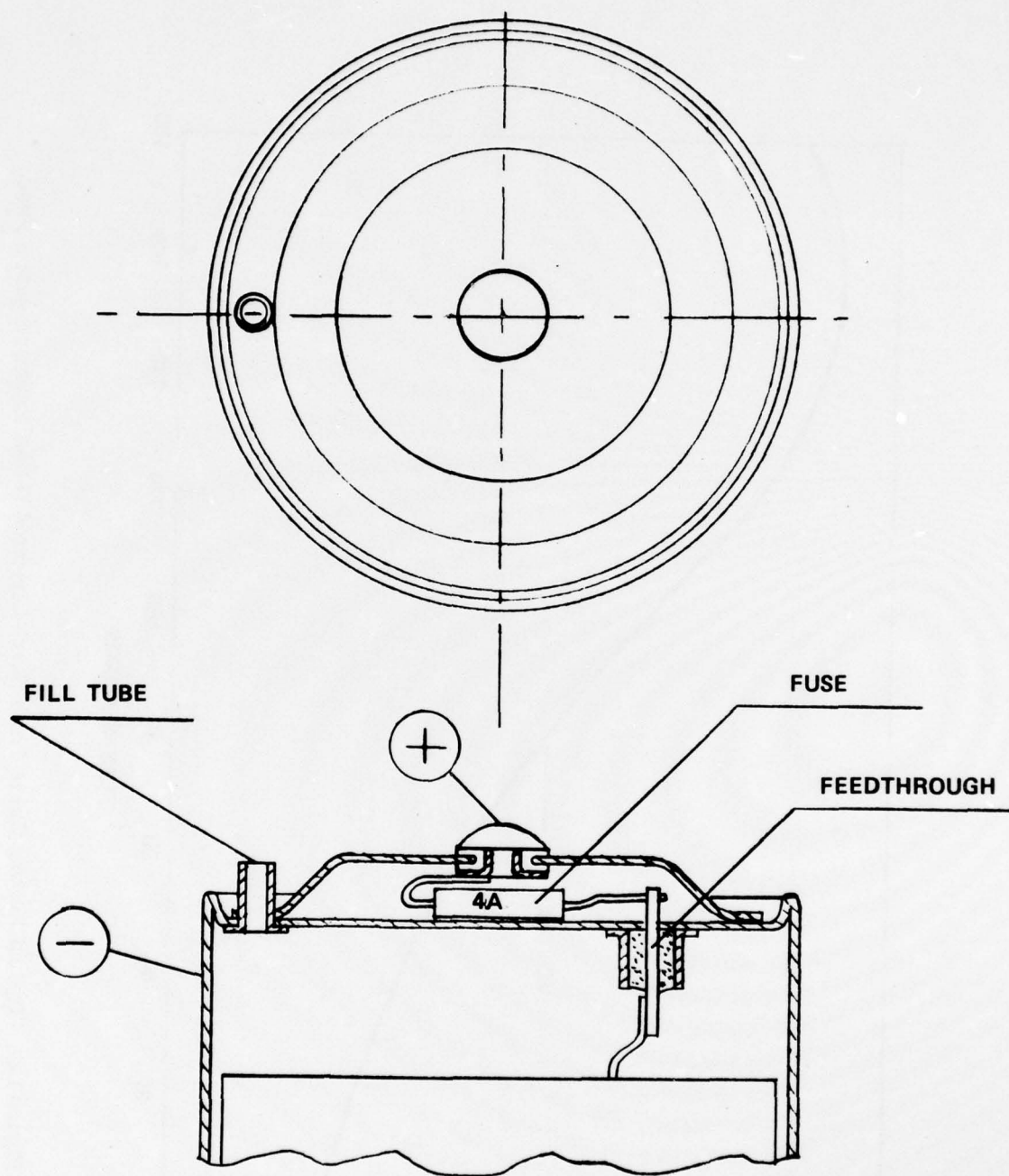


Figure 132. Hermetic D Cell Closure Incorporating a Fuse

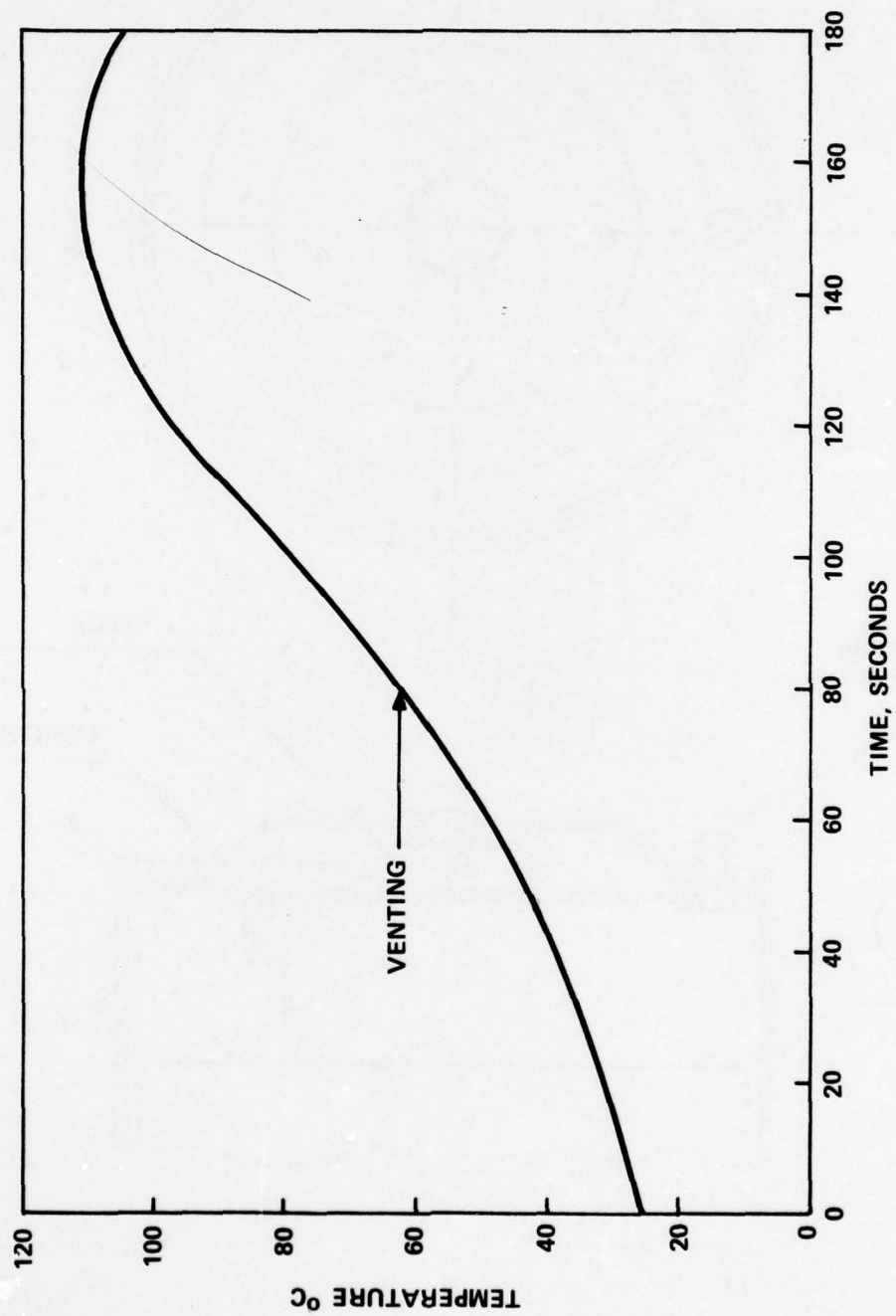


Figure 133. Typical Heating Curve For a Short-Circuited D Cell Equipped With a Fuse

to the lithium inorganic batteries as well. A schematic presentation of the vent construction is shown in Figure 134. A triangular hole is punched in the cell cover from outside, cutting only two sides of the triangle and leaving the spike facing inward. A 0.005 in. nickel membrane was stretched across the cover internal side and crimped over the cover edges. This cover was used to build the cells that were tested under short circuit conditions. Originally, the covers were built to release the gases in the Ni-Cd cells at approximately 150 lb/in.² internal pressure. We have built empty cells using these covers, provided with a welded tube in the bottom of the can for testing under air pressures. A positive release was obtained at the pressures never exceeding 200 lb/in.². Several complete cells, built with these covers were tested under short circuit conditions and the vents operated satisfactorily.

Several types of covers have been used with various vent openings, types of spikes and designs. The cells were tested without labels. The thermocouple junctions were welded to the outside surface of the can and the short circuit was established using a 3 mm solid brass spring loaded clamp. The electric cold junction was installed in the immediate vicinity of the cell, while the thermocouple gage was installed at some distance from the test site. A stop watch was used to measure the time required to reach the venting and/or nonexplosive removal of the cell cover. The results obtained with a series of 16 cells, made with the weakest profile of the cover and the smallest vent opening, are summarized in Table 29. Both the processes of venting and of separating the cover from the case were the results of simple vapor pressure increase rather than violent explosive reaction. In no circumstance was the cell case ruptured, nor were the electrodes expelled from the case.

It is clear from the table that the covers were too weakly joined to the case, in most cases, to be protected by the operation of the vent. It was possible to observe the venting prior to the removal of the cover only on three cells due to a fast rise in pressure and to the proximity of the two events. However, it is interesting to note that the vents would have served as protection against cell explosion if the covers had been rigidly attached. The cover was the only component separated from the cell at the end point accompanied by a cloud of solvent vapors. No displacement of electrodes or separators and no damage has been observed to the can as already noted above. The failure of the operator to read the time for cell number 7 is indicated in the table. Maximum temperatures for cells 5, 8 and 15 were not read since the thermocouple junction welds failed.

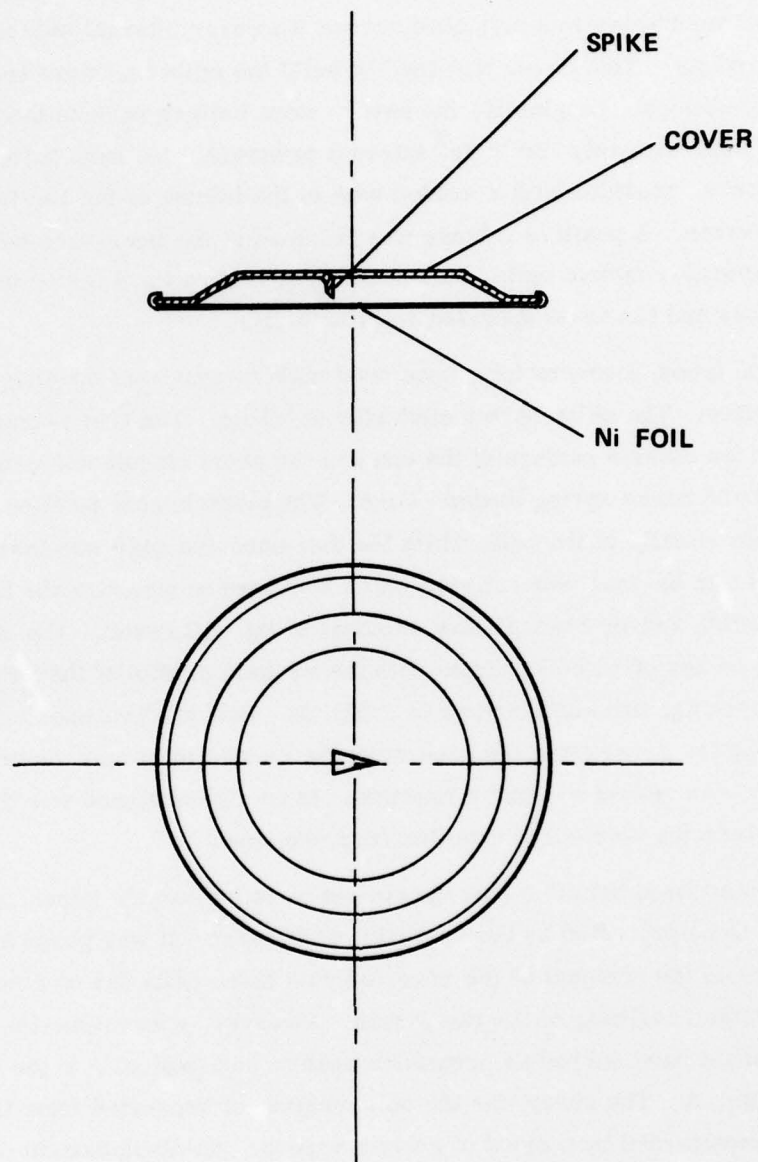


Figure 134. Cell Top with Vent

TABLE 29

VENTING AND COVER BLOW OFF ON SHORT CIRCUIT D CELLS
MADE WITH UNMODIFIED NI-Cd VENTING COVERS

Cell No.	Time to vent (seconds)	Time to cover blow-off (seconds)	Maximum surface temp. (°C)	Age of cells
1	-	40	65	F
2	40	55	59	
3	60	70	48	
4	-	60	56	
5	-	465	-	S
6	-	58	68	
7	65	-	114	
8	-	34	-	
9	-	58	78	H
10	-	93	64	
11	-	64	68	
12	-	45	66	
13	-	50	66	1 WEEK AT ROOM TEMP.
14	-	85	67	
15	-	110	-	
16	-	40	64	

The idea of employing weak covers without special venting mechanisms might be of some value, particularly in building large batteries, where there is no special handling requirement for single cells.

A slight modification to one of the existing covers seems to have provided a good solution to the venting problem of lithium inorganic batteries. This modified venting cover was tested on dummy cells with a back pressure of argon. The pressure was released in the range of 75 to 260 lb/in.², depending on the type of modification made. A batch of cells was made of the type of cover that acts at approximately 150 lb/in.² and they were used in testing. The results obtained shown in Table 30. All four cells vented, one of them somewhat prematurely, but none blew the cover off. The thermocouple junctions remained in place after the venting, so the temperature change was followed until it passed through a maximum.

TABLE 30
VENTING ON SHORT CIRCUIT D CELLS WITH MODIFIED Ni-Cd VENTING COVERS

Cell No.	Time to venting (seconds)	Temp. at venting (°C)	Maximum Temp. (°C)	Time to maximum Temp. (sec.)
1	80	74.5	112	150
2	60	68	106	142
3	85	68.5	116	210
4	50	36	106	180

It is interesting to note that the temperature continued to rise after venting, since a sufficient amount of electrolyte was left in the cell, and its heat generating capability was maintained for another minute or two. The maximum surface temperature of the cells came close to the first possible critical point of explosion (melting point of sulfur); but that did not have any undesirable effect probably due to the short time the temperature of the cell remained in this region. A typical heating curve is shown in Figure 133 for a shorted cell with the modified venting cover.

We believe that this type of vent, used in conjunction with the hermetic cell top, should provide a viable solution to the problem of explosion. However, the venting of the cells is not a complete solution since the cell surroundings would be quickly damaged by the corrosive action of the solvent. As we suggested earlier, some combination of a fuse and a vent might be better, whereby the vent would act only if the fuse failed to break the short circuit. The majority of problems would probably be eliminated with the fuse alone.

The preliminary tests with a low pressure vent, used in combination with a crimp seal were described above. It should be possible to use the same type of vent in combination with the hermetical seal, but this vent, originally developed for Ni-Cd cells, must be modified. A schematic presentation of the assembly is shown in Figure 135.

The cell top had to carry a section of the membrane, hermetically welded to the top and covering the hole that provides access to the spike. It also had to carry the feedthrough with a tubular pin that will also serve as a filling port for the electrolyte. A secondary top would have to be added, carrying a spike and also an insulated button for the second (+) cell terminal.

Each of the two protective devices described above should be adequate to prevent the uncontrolled cell discharge alone. However, the fuse provides the protection only against an external short circuit and is not effective at all in cases of an internal short caused either by an outside damage to the cell or by a vibration of a high amplitude. For this reason one might wish to incorporate both protective devices into each cell, with the understanding that the costs of production would be increased. Such a cell would be sufficiently safe to handle most foreseeable conditions. External shorts, much more frequent than internal shorts, would be protected by fuse action. The vent would act in case of an internal short or in case of an external overheating, relieving the cell pressure long before the cell temperature reaches any of the two possible explosion points (melting points of S or Li). One possible cell design, incorporating both the fuse and the vent, is shown in Figure 136.

It is essential that the vents act at a fairly low pressure, since the pressure buildup is a consequence of temperature rise. The type of vent used in a pressurized SO_2 cell is totally inadequate because it acts at 500 to 600 lb/in.², far too high to vent the cell before it reaches an explosion point. It has been reported recently¹⁵ that these vents were not even effective when used on SO_2 cells. The temperature

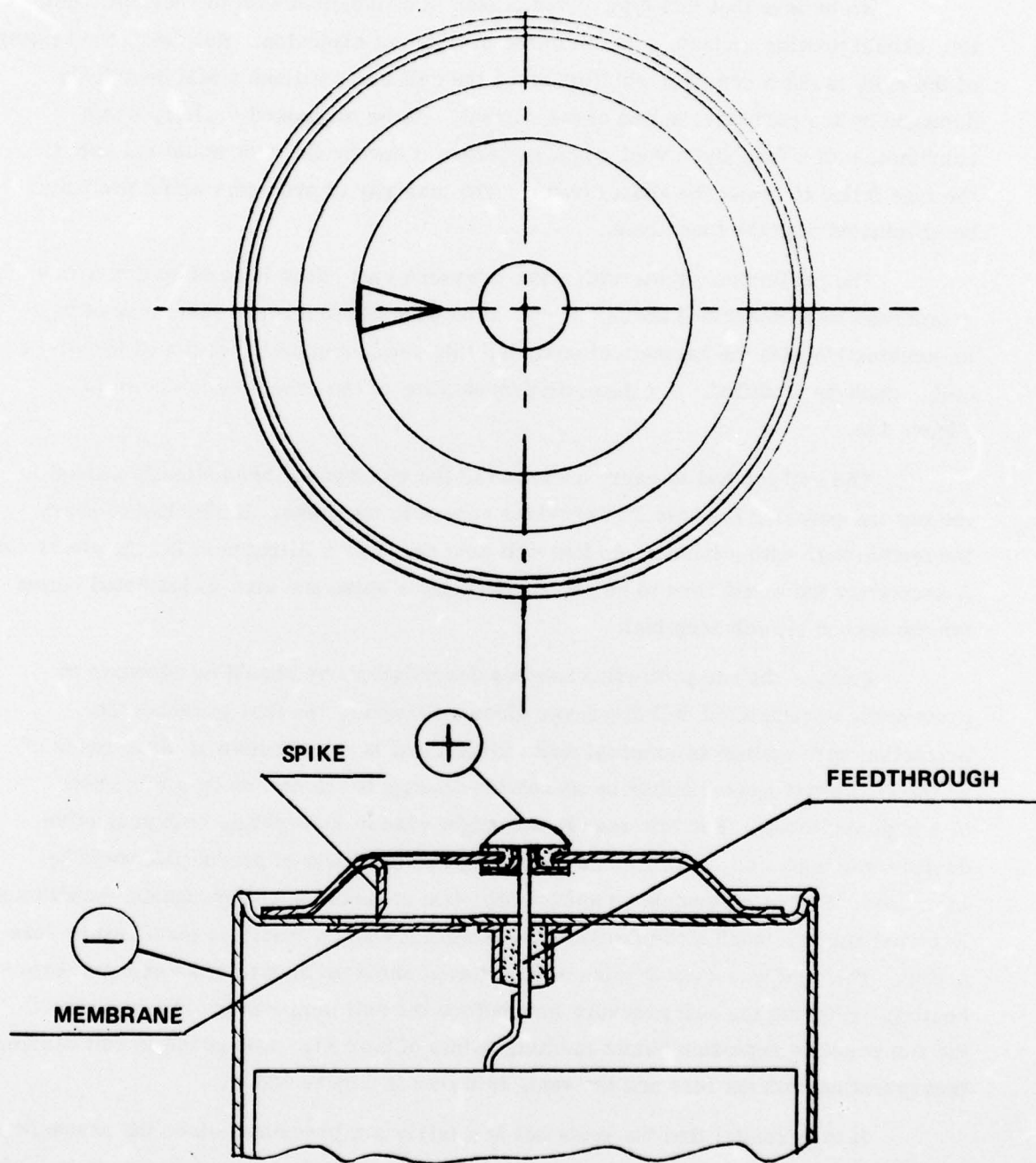


Figure 135. Hermetic D Cell Closure Incorporating a Vent

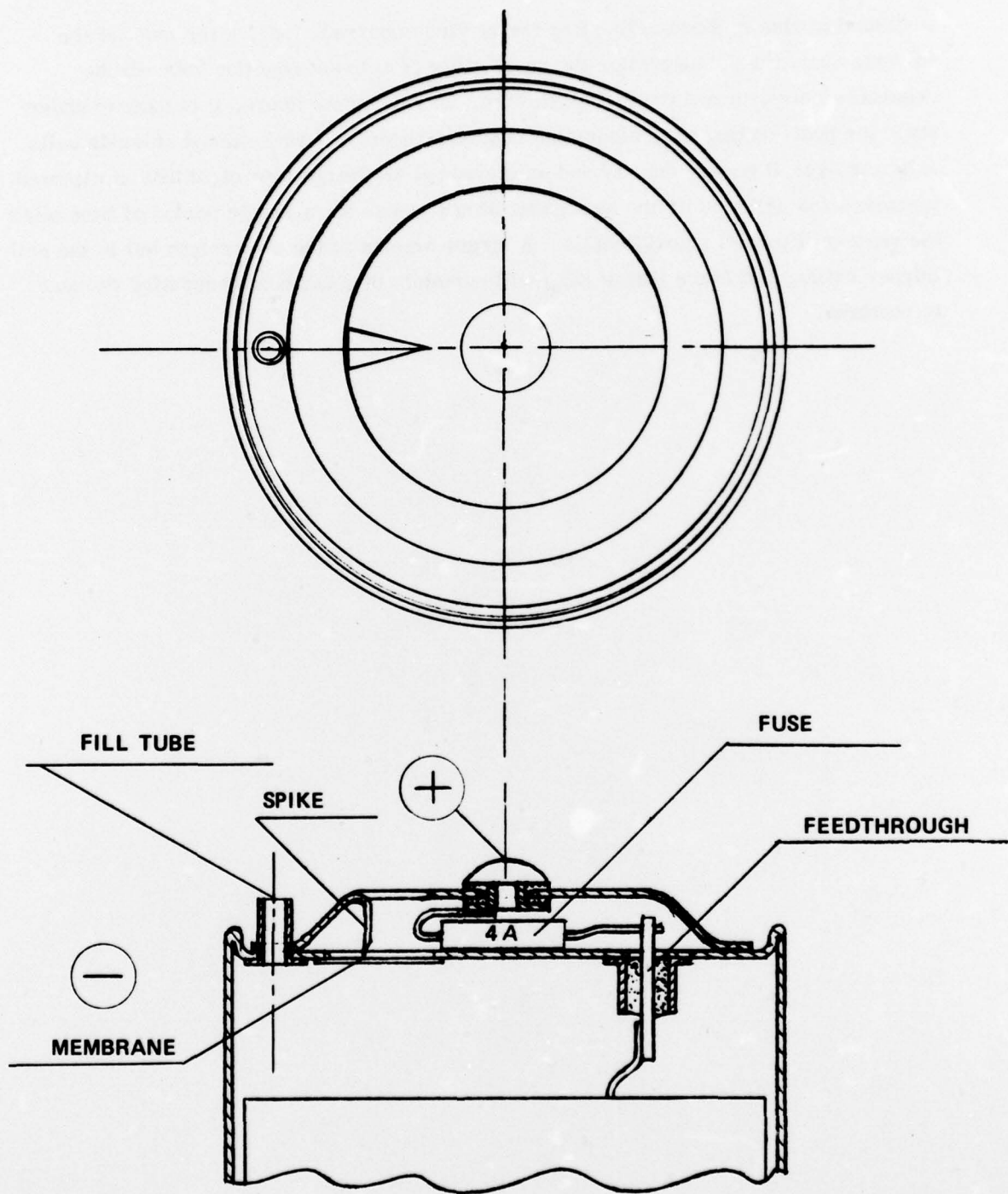


Figure 136. Fuse-Vent Combination in the Hermetic D Cell Closure

continued to rise in those cells after the venting occurred, i.e., after most of the solvents evaporated, suggesting the possibility of a direct reaction between the residual electrolyte and the molten lithium. In view of the above, it is easy to understand the post-venting explosions also reported recently¹⁶ with thionyl chloride cells. A larger overall energy density and an increased discharge rate capability at elevated temperatures will sustain the heat generating process for a longer period of time after the venting of thionyl chloride cells. A larger amount of the electrolyte left in the cell (higher boiling point than that of SO_2) will certainly help the heat generating process to continue.

15. CELLS DELIVERED

15.1 HIGH POWER CELLS

At the conclusion of this program, GTE Laboratories has delivered 50 high power D cells to US Army ECOM for tests and evaluation. The cells represent the state of the art in design and construction of the electrode structure, packaging and the overall performance on discharge. A brief description of the cell is given below, along with the vital design parameters to aid in data processing that will follow the discharge tests.

The can is made of nickel, 0.030 in. wall thickness, by deep drawing with the dimensions of:

O. D.	1.300 in.
I. D.	1.270 in.
Height	2.300 in.

The cans used in building these cells were made by Husdon Tool and Die Company, Newark, NJ.

The top was built with a glass-to-metal feedthrough and also with the venting mechanism that were tested and found to act at the internal pressure of 150 to 200 lb/in². It is made as a double top with two sections welded together. The internal section carries the membrane and the feedthrough, while the external one carries the spike pointing towards the membrane and, also, the contact button as an outside + terminal. An insulating washer is added to prevent an easy outside short between the terminal button and the body of the top.

The electrode parameters were selected from the computer printout shown in Table 31. The particular selection used is underlined. The table shows that the cell could be expected to deliver a maximum capacity of 14.18 Ah under most favorable conditions, i.e., at low discharge rates and room or elevated temperatures. The cathode with the dimensions of $36 \times 4.8 \times 0.084$ cm provided an active surface area of 345.6 cm², while the anode surface area (with the dimensions of $38.60 \times 4.80 \times 0.050$ cm) amounted to 370.5 cm². With the last turn of the anode facing the cathode only on one side, the true active anodes are somewhat smaller, amounting to approximately 330 cm².

The closing of cells, i.e., welding of the cover to the can, was carried out by the TIG welding technique before the electrolyte was added to the cell. The closing of the electrolyte filling port was done by the same technique.

TABLE 31
TYPICAL COMPUTER PRINTOUT FOR D SIZE CELL

L ₁ (cm)	L ₂ (cm)	L ₃ (cm)	L ₄ (cm)	T ₁ (mm)	T ₃ (mm)	T (mm)	D (cm)	Q (Ah)	N
21.00	23.84	24.11	24.37	1.62	0.91	2.83	1.61	18.49	2.80
24.00	26.79	27.09	27.40	1.37	0.78	2.46	1.58	15.92	3.23
27.00	29.73	30.08	30.42	1.19	0.69	2.18	1.56	15.46	3.65
30.00	32.69	33.07	33.46	1.05	0.61	1.96	1.54	14.97	4.09
33.00	35.64	36.07	36.49	0.93	0.55	1.78	1.53	14.55	4.52
36.00	38.60	39.06	39.53	0.84	0.50	1.64	1.51	14.18	4.94
39.00	41.56	42.07	42.58	0.76	0.45	1.51	1.50	13.79	5.39
42.00	44.52	45.07	45.62	0.69	0.42	1.41	1.48	13.46	5.81
45.00	47.48	48.08	48.67	0.63	0.38	1.31	1.47	13.08	6.27
48.00	50.45	51.08	51.71	0.58	0.35	1.23	1.45	12.75	6.70

Can I.D. 3.11 cm

Electrode Width 4.80 cm

Separator Thickness 0.0125 cm

For Other Parameters in the Table see References 8 and 9

15.2 HIGH ENERGY CELLS

Parallel to the ECOM sponsored development of high rate wound cells, efforts were made in GTE Laboratories to develop and optimize cells designed for extremely low discharge rates. Obviously, these cells were designed with a minimal surface of electrodes, and, therefore, the minimal quantities of electrochemically inactive materials. The most advanced among these is the GTE pacemaker cell, produced commercially and implanted routinely since 1974. The scale up of this cell design led to the development of commercial C and D size cells, as well as a Double D size used in specific low rate applications by several companies. The major advantage of this cell design is its safety under conditions of abuse such as short circuit. Whether shorted internally or externally, these cells are not subject to thermal runaway, such as the one experienced with wound cells. For this reason, these cells are not equipped with either of the two protective devices described earlier in this report.

At the request of the US Army ECOM, the size F cell was chosen to represent the state of the art of this technology, having overall cell dimensions of:

O. D	1.300 in.
Height	3.440 in.

The cell can is made of 304 stainless steel with the same diameter of the one used for D cells. The cell top is somewhat simpler, since it does not carry the venting mechanism. Only the terminal button is retained to protect the glass-to-metal feed-through from mechanical abuse from outside.

The electrode structure is the concentric one with two anodes, one in the center and one attached to the interior of the cell can. The cathode is a cylinder formed around a cylindrical current collector and tightly packed between the two anodes, with a layer of a separator on each face. The active surface area of electrodes is estimated to be approximately 90 cm^2 ; the same for the anode and the cathode.

The capacity of the F cell will be established in the course of testing and will show a dependence upon the rate of discharge, for rates in excess of 1 mA/cm^2 . It should be emphasized that the F cell has been produced and tested in limited quantity only. However, since both the smaller size (D) and the larger size (DD) have been under a more extensive test program, and since the geometry of the F cell is different only in the height from the other two, a reasonably predictable performance could be expected of the F cell.

16. REFERENCES

1. J. J. Auborn, et al., J. Electrochem. Soc. **120**, 1613-1619 (1973).
2. A. N. Dey and C. R. Schlaikjer, Proc. of 26th Power Sources Conference, Atlantic City, NJ (1974).
3. A. N. Dey, Proc. of 10th Power Sources Symposium, Brighton, England (1976).
4. N. Marincic, Proc. of 10th Power Sources Symposium (Discussion of paper 32), Brighton, England (1976).
5. W. K. Behl, et al., J. Electrochem. Soc. **120**, 1619-1623 (1974).
6. G. H. Holleck, et al., Report to US Army ECOM-74-0030-4 (January 1975).
7. N. Marincic, J. Applied Electrochem. **5**, 313-318 (1975).
8. N. Marincic and D. M. Koffman, J. Applied Electrochem. **6**, 51-58 (1976).
9. N. Marincic, J. Applied Electrochem. **6**, 263-268 (1976).
10. N. Marincic, J. Applied Electrochem. **6**, 463-468 (1976).
11. N. Marincic, et al., Proc. 26th Power Sources Conference, Atlantic City, NJ (1974).
12. J. J. Auborn and N. Marincic, Proc. 9th Power Sources Symposium, Brighton, England (1974).
13. R. Selim and P. Bro, J. Electrochem. Soc. **118**, 830 (1971).
14. A. N. Dey, Report to US Army ECOM-74-0109-2 (1974).
15. P. Bro, et al., Proc. of 10th Intersoc. Energy Convention Conference, Newark, Del. (1975).
16. A. N. Dey, Report to US Army ECOM-74-0109-5 (1975).

DISTRIBUTION LIST

Defense Documentation Center
ATTN: DDC-TCA
Cameron Station (Bldg 5)
Alexandria, Virginia 22314

Commander
Naval Electronics Lab Ctr.
ATTN: Library
San Diego, California 92152

Commander
Naval Surface Weapons Center
White Oak Laboratory
ATTN: Library, Code WX-21
Silver Spring, Maryland 20910

Commandant, Marine Corps
Hq. US Marine Corps
ATTN: Code LMC
Washington, DC 20380

Rome Air Development Center
ATTN: Documents Library (TILD)
Griffiss AFB, New York 13441

Hq ESD (DRI)
L. G. Hanscom AFB
Bedford, Massachusetts 01731

HQDA (DAMA-ARP/Dr. F. D. Verderame)
Washington, DC 20310

Commander
Harry Diamond Laboratories
ATTN: Library
2800 Powder Mill Road
Adelphi, Maryland 20783

Commander
US Army Research Office
ATTN: DRXRO-IP
PO Box 12211
Research Triangle Park, North Carolina 07709

Commander
US Army Security Agency
ATTN: IARDA-IT
Arlington Hall Station
Arlington, Virginia 22212

Commander
US Army Mobility Equipment R&D Center
ATTN: DRXFB-R
Fort Belvoir, Virginia 22060

Commander
US Army Electronics Command
Fort Monmouth, New Jersey 07703

1DRSEL-TL-DT	1DRSEL-TL-DD
1DRSEL-TL-P	1USMC-LNO
2DRSEL-MS-TI	5DRSEL-GG-AR
1DRSEL-GG-TD	

NASA Sci & Tech Info Facility
Baltimore/Washington International Airport
PO Box 8757, Maryland 21240

SUPPLEMENT TO DISTRIBUTION LIST

Mr. Don Mortel
Director, Aerospace Power Div.
ATTN: AFAPL/PO
Wright-Patterson AFB, Ohio 45433

Mr. E. Cohn
NASA Headquarters
Code RPP
Washington, DC 20546

Institute for Defense Analyses
ATTN: Mr. Robert Hamilton
PO Box 55
Libertytown, Maryland 21762

Commander
US Army Material Development
and Readiness Command
ATTN: DRCRD-FP
5001 Eisenhower Avenue
Alexandria, Virginia 22333

Commander
US Army Material Development
and Readiness Command
ATTN: DRCRD-TC
5001 Eisenhower Avenue
Alexandria, Virginia 22333

Commander
US Army Mobility Equipment R&D Command
ATTN: DRXFB-EE
Fort Belvoir, Virginia 22060

Commander
Harry Diamond Laboratories
ATTN: DRXDO-RDD (Mr. A. Benderly)
2800 Powder Mill Road
Adelphi, Maryland 20783

Commander
Picatinny Arsenal
ATTN: SARPA-FR-S-P (Mr. M. Merriman)
Dover, New Jersey 07801

Power Information Center
University City Science Institute
3401 Market Street, Room 2210
Philadelphia, Pennsylvania 19104

Office of Assistant Director
(Engineering Technology), ODDR&E
Room 3D-1089
ATTN: Mr. R. W. Ziem
Pentagon
Washington, DC 20301

Mr. Richard E. Oderwald
Department of the Navy
Hqs., US Marine Corps
Code LMC 4
Washington, DC 20380

Transportation Systems Center
Kendall Square
Cambridge, Massachusetts 02142
ATTN: Dr. Norman Rosenberg

Foote Mineral Company
Route 100
Exton, Pennsylvania 19341
ATTN: Dr. H. Grady

Honeywell, Inc.
104 Rock Road
Horsham, Pennsylvania 19044
ATTN: C. Richard Walk

Sanders Associates, Inc.
Sonobuoy Division
95 Canal Street
Nashua, New Hampshire 03060
ATTN: Mr. David Dwyer

Eagle Picher Industries
PO Box 47
Toplin, Missouri 64801
ATTN: Mr. E. Broglio

Yardney Electric Company
82 Mechanic Street
Pawcatuck, Connecticut 02891
ATTN: Mr. William E. Ryder

EIC, Inc.
ATTN: S. B. Brummer
Newton, Massachusetts 02158

SUPPLEMENT TO DISTRIBUTION LIST

Exxon Research and Engineering Co.
Corporate Research Laboratory
Linden, New Jersey 07036
ATTN: Dr. R. Hamlen

Argonne National Laboratories
9700 South Cass
Argonne, Illinois 60439
ATTN: Dr. E. C. Gay

GTE Sylvania, Inc.
77 A Street
Needham, Massachusetts 02194
ATTN: Mr. Richard Pabst

General Motors Corp.
Research Laboratories
General Motors Technical Center
12 Mile and Mounds Roads
Warren, Michigan 48090
ATTN: Dr. J. L. Hartman

Union Carbide Corporation
Parma Research Center
PO Box 6116
Cleveland, Ohio 44101

P. R. Mallory & Co., Inc.
S. Broadway
Tarrytown, New York 10591
ATTN: J. Dalfonso

North American Rockwell Corp.
Atomics International Division
Box 309
Canoga Park, California 91304
ATTN: Dr. L. Heredy

General Electric Research &
Development Center
PO Box 8
Schenectady, New York 12301
ATTN: Dr. Stefan Mitoff

University of California
Department of Science & Research
Santa Barbara, California 93100
ATTN: Dr. J. Kennedy

The Electric Storage Battery Co.
Carl F. Norburg Research Center
19 W. College Avenue
Yardley, Pennsylvania 19067
ATTN: Dr. A. Salkind

Gulton Industries, Inc.
Metuchen, New Jersey 08840
ATTN: Mr. S. Charlip

Electrochimica
2485 Charleston Road
Mountain View, California 94040
ATTN: Dr. Eisenberg

Dr. Hugh Barger
Chemistry Department
University of North Carolina (Charlotte)
Charlotte, North Carolina 28223

Energy Storage & Conversion Dept.
T.R.W. Systems
One Space Park
Redondo Beach, California 90278
ATTN: Dr. H. P. Silverman

Sanders Associates, Inc.
24 Simon Street
Mail Stop NSI-2208
Nashua, New Hampshire 03060
ATTN: J. Marshall

Power Conversion, Inc.
70 MacQuesten Pkwy
Mount Vernon, New York 10550
ATTN: Stuart Chodosh

Dr. D. Pouli
Portfolio Manager
Hooker Chemicals & Plastics Corp.
M. P. O. Box 8
Niagara Falls, New York 14302

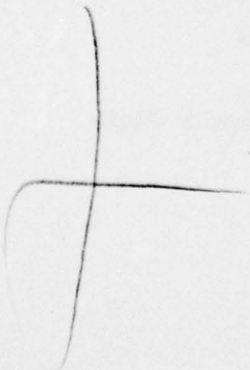
Dr. Leonard Nanis
G207
S. R. I.
Menlo Park, California 94025

SUPPLEMENT TO DISTRIBUTION LIST

Frank Murphy/SB331
Naval Underwater Systems Center
Newport Laboratory
Newport, Rhode Island 02840

NASA Lewis Research Center
Mail Stop 6-1
2100 Brookpark Road
Cleveland, Ohio 44101
ATTN: Dr. Stuart Fordyce

Mr. Joe McCartney
Naval Undersea Center
Code 608
San Diego, California 92132

A large, handwritten plus sign (+) is drawn in the lower-left quadrant of the page. The lines are thin and slightly irregular, suggesting it was drawn with a pen or pencil.